

**Study into Mechanical and Electrochemical Properties  
of Coating Deposits and Welded-Coated Components  
Using the HVOF (High Velocity Oxy-Fuel) Process**

**By**

**Adnan Abdullatif Boudi**

**This Thesis is submitted to Dublin City University as the fulfillment of  
the requirement for the award of the degree of**

**Doctor of Philosophy**

**Supervisors:**

**Professor M.S.J. Hashmi, PhD, DSc  
Professor. Bekir Sami Yilbas, PhD, DSc**

**School of Mechanical and Manufacturing Engineering  
Dublin City University**

**DCU**

**2007**

---

# DECLARATION

---

**I hereby certify that this material, which I now submit for assessment on the program of study leading to the award of Doctor of Philosophy, is entirely my own work and has not been taken from the work of others save and to the extent that such work has been cited and acknowledged within the text of my work.**

Signed: A.A. Bouda I.D. Number: 51161982

Date:

---

# ACKNOWLEDGMENT

---

I would like to thank all those individuals who have assisted me during the course of the present work.

Particularly, I would like to acknowledge the valuable contribution of Professor. M. S. J. Hashmi, my thesis supervisor, Head of the School of Mechanical and Manufacturing Engineering at Dublin City University, for his active supervision, support, and observations during the program of the study.

My sincere thanks and appreciation to Professor B. S. Yilbas of KFUPM (Saudi Arabia), who helped me throughout the study program. Professor Yilbas's encouragement and constructive comments contributed greatly to the completion of the current academic work.

Great appreciation to my parents who have always been a support throughout my life. My parents set an excellent example for me in life and in prospering through education.

Sincere thanks and appreciation go to my wife Asma Boudi, for her love, patience, confidence and support.

---

# ABSTRACT

---

## **Study into The HVOF (High Velocity Oxy-Fuel) Process Mechanical and Electrochemical Properties of Coating Deposits and Weld-Coated Components**

**By  
Adnan A. Boudi**

The present study examines the metallurgical, mechanical and corrosion properties of High Velocity Oxy-Fuel (HVOF) thermal spray coatings of Inconel 625 powders on plain and welded surfaces of mild carbon and stainless steel (304). The research work carried out focused on coating adherence to base substrate, coating integrity and mechanical behavior of coating at the weld-substrate interface when subjected to tensile and fatigue loads. The solid bar and sheet specimens were tested and prepared in accordance with the test standards "Standard Test Method for Adhesion or Cohesion Strength of Thermal Spray Coatings". The specimens were tensile and fatigue tested pre and post exposure to brine. SEM and EDS analysis were carried out to examine the surface morphology and microstructure of the coatings.

The specimens that were subjected to a corrosion environment for an extended period of three weeks failed at a lower tensile load than those that were not exposed to corrosive environment. Shear deformation of the adjacent zones at the coating-substrate interface resulted in the total failure of the coating. However, in some cases, the coating was almost free from voids or pores and was impervious to electrolytic or any other contaminants. This result was observed from tests performed on different sets of specimens to identify brine exposure effects on coating adherence to the substrate. Foreign materials were observed beneath the coating due to improper surface preparation during the specimen preparation prior to coating. From tensile tests results it was observed that the bond strength of the coating reduced due to corrosion effect which caused degradation of the coating adhesion to the specimen's surface. This is probably due to the formation of oxides on carbon steel surfaces during coating. Due to expected progressive oxidation, coating adherence was continuously degraded with lowering bond strength. Fatigue results revealed that an excess of 15 thousand cycles without cracking was demonstrated by the stainless steel coated specimens assuring the fatigue strength. The fatigue life resistance of the stainless steel coated specimens exceeded that of the coated carbon steel specimens. Moreover, the imperfection at the interface resulted during coating could cause early initiation of cracks in the coating, therefore, thus lowering the fatigue strength.

---

# TABLE OF CONTENTS

---

	PAGE
<b>Declaration</b>	<b>I</b>
<b>Acknowledgement</b>	<b>II</b>
<b>Abstract</b>	<b>III</b>
<b>Table of Contents</b>	<b>IV</b>
<b>List of Figures</b>	<b>X</b>
<b>List of Tables</b>	<b>XIII</b>
<hr/>	
<b>CHAPTER 1 INTRODUCTION</b>	<b>1</b>
<hr/>	
<b>CHAPTER 2 LITRATURE SURVEY</b>	<b>15</b>
<hr/>	
2.1 Introduction	1
2.2 HVOF Coating Performance	15
2.2.1 Heat Treatment of HVOF Coatings to Improve Performance	15
2.2.2 Fatigue Performance of HVOF Coatings	16
2.2.3 Electrochemical and Corrosion Behavior of HVOF Coatings	18
2.2.4 Erosion-Corrosion	21
2.2.5 Wear	22
2.2.6 Microstructure of HVOF Coatings	23
2.2.7 Influence of HVOF Spray Parameters on Coating Properties On Mechanical Properties of Coatings	27

2.2.8 HVOF Process Coatings Development and Applications	32
2.2.9 Residual Stresses in HVOF Coatings	33
2.2.10 Laser Process Role in the HVOF Coatings	35
2.2.11 Properties of HVOF Sprayed Coatings	37
2.2.12 Characteristics of HVOF Sprayed Coatings Deposited Onto Welded Steel Surface	39

---

<b>CHAPTER 3</b>	<b>EXPERIMENTAL EQUIPMENT AND PROCEDURES</b>	<b>42</b>
------------------	--	-----------

---

3.1 Introduction	42
3.2.1 Preparation of Flat Specimens	43
3.2.2 Test Specimens and types used in experimental work	43
3.3 Description of Equipment	47
3.3.1 Welding Facility	47
3.3.2 Grit blasting unit for surface preparation of the specimens	48
3.3.3 Fixture for preparation of round specimen for adhesion testing	49
3.3.4 HVOF Thermal Spraying Facility	49
3.3.4.1 High Velocity Oxy-Fuel Facility	50
3.3.5 Spraying Environment	51
3.3.6 Facility Preparation and Description	51
3.3.6.1 Gun Traverse Unit	51
3.3.6.2 Cooling System	52
3.3.6.3 Forced Cooling	52
3.3.6.4 Temperature Measurement and Monitoring Thermometer	52
3.3.7 Corrosion Testing Unit	53
3.3.8 Oven for adhesive curing	54
3.4 Mechanical Properties Testing of Thermally Sprayed Coatings	55

3.4.1 Tensile Testing Preparation	55
3.4.2 Fatigue Testing Preparation	56
3.4.2.1 Control and Data Acquisition System	56
3.5 Metallographic Specimens Preparation	57
3.5.1 Sectioning	57
3.5.2 Mounting	58
3.5.3 Grinding	59
3.5.4 Polishing	59
3.6 Optical Photography	60
3.7 Microscopy	60
3.7.1 Optical Microscopy	60
3.7.2 Environmental Scanning Electron Microscopy (ESEM)	61
3.8 EXPERIMENTAL PROCEDURES	62
3.8.1 Procedure for welding of plane specimens	62
3.9 HVOF THERMAL SPRAYING PROCEDURES	63
3.9.1 Surface Preparation (Grit Blasting)	63
3.9.2 Pre-Heat Treatment	63
3.9.3 Spraying Process	64
3.9.4 Gun Traverse Unit	67
3.9.5 Spraying Process parameters and coating powder	68
3.9.6 Temperature Measurement and Monitoring Thermometer	69
3.10 Preparation of Material and Bonding Surfaces	71
3.10.1 Adhesive Application	71
3.10.2 Adhesive curing	72
3.11 Mechanical Properties Testing of Thermally Sprayed Coatings	72
3.11.1 Tensile Testing Procedure	72
3.11.2 Procedure for tensile testing for the coated flat sheet specimens	73
3.12 Static Corrosion Media Description	74
3.13 Procedure for Characterization Equipments	76

4.1	Introduction	77
4.2	Corrosion and Bond Strength testing of solid round bars (Specimens Selection and distribution)	78
4.2.1	Round Solid Bars (ASTM C-633)	78
4.3	ESEM evaluation of Inconel-625 Thermal Spray Coating (HVOF) onto Stainless Steel and Carbon Steel Post Brine Exposure after Tensile Tests	86
4.4	Tensile Properties of HVOF Sprayed Inconel 625 Coating (Tensile Specimens (in flat sheet form))	101
4.5	Fatigue Testing of Inconel-625 coatings onto Carbon and Stainless Steel	108
4.6	Tensile and Fatigue Properties of Inconel-625 coatings deposited onto Welded Carbon and Stainless Steel Specimens	116
4.6.1	Stainless-Steel Welded-Coated Specimens	116
4.6.2	Carbon-Steel Welded-Coated Specimens	116
4.6.3	Tensile and Fatigue Tests for Welded-Coated Stainless and Carbon Steel Specimens	116
4.6.4	Fatigue Failure on Flat Sheets	117
4.6.4.1	Fatigue failure of welded carbon steel specimens	117
4.6.4.2	Fatigue failure of welded stainless steel (304L SS) Specimens.	118
4.7	Microstructure Characterization	119
4.7.1	Description of the Coating and the Steel-Coating Interface	121
4.7.2	Specimen Observations	125
4.8	Microstructural Examinations using Scanning Electron Microscopy	126
4.8.1	Carbon steel welded-coated specimens	126
4.8.2	304L Stainless steel welded-coated specimens	134

4.9	The Tensile Strengths Behavior of HVOF sprayed Nickel alloy Coatings onto welded Steel Surfaces Exposed to Artificial Sea Water Environment	138
4.9.1	Experimental Work	138
4.9.2	Carbon Steel Welded Coated Specimens	138
4.9.3	Specimens fabrication and distribution	138
4.9.4	Tensile Tests of HVOF Coated Carbon Steel Specimens	140
4.9.4.1	HVOF Coated carbon steel Specimen with no corrosion exposure and exposed coated specimens including coated non-welded and coated welded specimens with weld sizes of 2 mm, 3 mm, and 5 mm	140
4.9.4.2	Stainless Steel Welded Coated Specimens	155
4.9.4.3	Specimens fabrication and distribution	155
4.9.4.4	HVOF coated stainless steel Specimen with no corrosion exposure and exposed coated specimens including coated non-welded and welded specimens with weld sizes of 2 mm, 3 mm and 5 mm.	157
4.10	CONCLUSION	168
4.11	SUMMARY	170

---

<b>CHAPTER 5</b>	<b>CONCLUSIONS AND RECOMMENDATIONS</b>	<b>174</b>
------------------	--	------------

---

5.1	Conclusions	174
5.2	Contributions	176
5.3	Recommendations for Future Work	177

---

<b>PUBLICATIONS RESULTING FROM THE PRESENT THESIS</b>	<b>178</b>
---	------------

---

---

<b>REFERENCES</b>	<b>179</b>
-------------------	------------

---

---

**APPENDICES**

---

Appendix A	I
Appendix B	L

---

# LIST OF FIGURES

---

		PAGE
Figure 1	Flat sheet specimen geometry was used for tensile and fatigue tests with Central Weldment	43
Figure 2	Schematic diagram of the SMAW circuit. As the electric energy melts the base metal and the electrode wire, metal droplets are transferred to the weld and become solidified metal.	48
Figure 3	Grit blasting facility	49
Figure 4	Immersion vessel with ring completely immersed in brine solution	53
Figure 5	A view of the oven and its set-up used to cure the adhesive	54
Figure 6	The Instron Machine specimen set-up assembly	55
Figure 7	A slow motion diamond cut-off wheels saw used to section the specimens	58
Figure 8	A mounting apparatus used for specimen's mounting	58
Figure 9	Grinding equipment used to grind and polish all specimens	59
Figure 10	ESEM/EDS facility used for coating characterization (Philips XL-30)	62
Figure 11	Grit blasted substrate ready for pre-heat treatment	64
Figure 12	Pre-heated treated for flat sheet substrates mounted onto mandrel	64
Figure 13	Round solid bars are fitted onto mandrel prior to spraying	65
Figure 14	Round solid bars being sprayed while mounted onto the mandrel	65
Figure 15	Sprayed round specimens mounted onto mandrel left to cool down	66
Figure 16	Flat sheets specimens fitted onto mandrel and mounted onto lathe machine prior to spraying	66
Figure 17	Active HVOF spraying operation where coating powder is being sprayed onto flat sheets while specimens mounted onto mandrel	67
Figure 18	Flat specimens after been sprayed onto the mandrel left to cool	67
Figure 19	Flat specimens being sprayed using the gun traverse unit on a moving table	68

Figure 20	The Ranger PM Infrared Thermometer was used in measuring specimen and coating temperature.	69
Figure 21	Optical chart showing Thermometer Spot Diameter versus Distance (Sensor to Object)	70
Figure 22	Flat sheet specimen fitted to the fixture ready for tensile testing	72
Figure 23	3 liters, Glass-container test vessel containing 3.5 % sodium chloride	75
Figure 24	Coated specimens fully immersed with equal separation within 3.5 % NaCl.	75
Figure 25	Ring used to hold flat specimens	75
Figure 26	Coating cross-section	79
Figure 27	Coating cross-section micrograph	80
Figure 28	Coating cross-section at the side of the specimen	81
Figure 29	Tensile bond strength of the adhesive	82
Figure 30	Effect of Exposure time on tensile bond strength of 304 L stainless steel	82
Figure 31	Coating cross section with discontinue line at the interface	84
Figure 32	Tensile bond strength of carbon steel	84
Figure 33	The area percent, and EDS spectrum of dark inclusions on top surface of Stainless steel specimen after tensile tests	86
Figure 34	Specimen# 3 is HVOF coated stainless steel surface exposed for 2 weeks original surface examination (not dummy specimen)	88
Figure 35	Stainless steel specimens #9 SS Dummy post 2 weeks exposure Backscattered electron images (BSE) of the top surface of coating after being pulled out from the original SS surface by dummy specimen	89
Figure 36	Sample #9 stainless steel HVOF coated specimen post 2 weeks static corrosion exposure for the original specimen	90
Figure 37	Dummy Stainless Steel Specimen # 9 pulled out from original HVOF coated specimen exposed for 2 weeks.	92

Figure 38	Line-scan of the coating cross section at 2000X magnification on 304L stainless steel exposed for 2 weeks left over on dummy specimen	93
Figure 39	Specimen #7 original carbon steel post static corrosion exposure exposed for 3 weeks	94
Figure 40	Specimen #7 original carbon steel coated specimen (not dummy) exposed for 3 weeks duration. – Top Surface: EDS X-ray spectra of various phases observed on the CS surface.	96
Figure 41	SEM micrographs of carbon steel in cross section and EDS Spectra of the inclusion	97
Figure 42	SEM micrographs of the top surface of the coating after being pulled out from the carbon steel dummy following three weeks of exposure to brine solution	98
Figure 43	SEM micrographs of a coating cross section after being pulled out from a carbon steel dummy	100
Figure: 44	Coating cross-section	102
Figure 45	Micrograph of stringer in the coating. The dark color is the oxides	102
Figure 46	Micrograph of preferential corrosion regions around the splat boundary post three weeks static corrosion tests.	103
Figure 47	Micrograph of a crack site in HVOF coating (15X magnification)	103
Figure 48 A	Tensile test results for HVOF coated 304 L stainless steel specimens prior and post static corrosion exposure	106
Figure 48 B	Tensile test results for HVOF coated carbon steel specimens prior and post static corrosion exposure	107
Figure 49	Fatigue tested stainless steel in 1 week solution of BSE images	109
Figure 50	Fatigue tested stainless steel after 3 weeks in electrolytic solution	111
Figure 51	Fatigue tested carbon steel after 1 Week in electrolytic solution	113
Figure 52	Fatigue tested carbon steel after 3 weeks in electrolytic solution	114
Figure 53	A photograph showing carbon steel smoothly broken specimen posts one week static corrosion exposure in electrolytic solution after fatigue failure	115

Figure 54	A photograph showing coated carbon steel specimen post 3 weeks static corrosion exposure after fatigue failure	115
Figure 55	Entire specimen showing weld and coating	121
Figure 56	SEM micrograph through as-received weld area and coating	122
Figure 57	SEM micrograph through as-received coating above weld area	122
Figure 58	EDS spectrum of bulk steel	123
Figure 59	EDS spectrum of coating in area of boundary with steel	123
Figure 60	Reflected light micrograph showing general roughness of metal surface and thickness of coating	124
Figure 61	Higher magnification micrograph of same area showing voids at interface of coating and steel	125
Figure 62	SEM micrographs for HVOF welded-coated specimen fatigue tested	127
Figure 63	SEM micrographs for HVOF welded-coated specimen post tensile test	128
Figure 64	SEM micrograph for an HVOF coated-welded carbon steel specimen	129
Figure 65	SEM micrographs for HVOF coated-welded carbon steel specimen	130
Figure 66	SEM micrographs for an HVOF coated-welded carbon steel specimen post fatigue test	131
Figure 67	SEM micrographs HVOF coated-welded carbon steel specimen post fatigue test.	132
Figure 68	SEM micrographs for HVOF coated-welded carbon steel specimen post fatigue test	133
Figure 69	SEM micrograph for an HVOF coated-welded 304L stainless steel specimen	134
Figure 70	SEM micrograph for HVOF coated-welded 304L stainless steel specimen	135
Figure 71	SEM micrograph for HVOF coated-welded 304L stainless steel specimen	136
Figure 72	SEM micrograph for HVOF coated-welded 304L stainless steel specimen	137
Figure 73a	Tensile response of the welded and non-welded HVOF coated carbon steel specimens prior to corrosion testing (As received condition).	141
Figure 73b	Tensile response of the welded and non-welded HVOF coated carbon steel specimens in the elastic region prior to corrosion testing	141
Figure 74a	Cross-sections of weld and heat affected zones as well as cross-section of the totally failed zone after the tensile testing	142
Figure 74b	Cross-section of the crack sites in the HVOF coating after the	143

	tensile tests for the specimens subjected to three weeks corrosion environment	
Figure 75a	Tensile response of the welded and non-welded HVOF coated carbon steel specimens after one week corrosion testing	144
Figure 75b	Tensile response of the welded and non-welded HVOF coated carbon steel specimens in the elastic region after one week corrosion testing	144
Figure 76a	Tensile response of the welded and non-welded HVOF coated carbon steel specimens after three weeks corrosion testing	146
Figure 76b	Tensile response of the welded and non-welded HVOF Coated Carbon Steel specimens in the elastic region after three weeks corrosion testing	146
Figure 77a	Tensile response of the non-welded HVOF coated carbon steel specimens in prior and post static corrosion exposure	148
Figure 77b	Tensile response of the non-welded HVOF coated carbon steel specimens in the elastic region prior and post static corrosion exposure	148
Figure 78a	Tensile response of the welded (weld size = 2.5 mm) HVOF Coated Carbon Steel specimens prior and post static corrosion exposure	150
Figure 78b	Tensile response of the welded (weld size = 2.5 mm) HVOF Coated Carbon Steel specimens in the elastic region prior and post static corrosion exposure	150
Figure 79a	Tensile response of the welded (weld size = 3 mm) HVOF coated carbon steel specimens prior and post static corrosion exposure	152
Figure 79b	Tensile response of the welded (weld size = 3 mm) HVOF coated carbon steel specimens in the elastic region prior and post static corrosion exposure	152
Figure 80a	Tensile response of the welded (weld size = 5 mm) HVOF coated carbon steel specimens prior and post static corrosion exposure	154
Figure 80b	Tensile response of the welded (weld size = 5 mm) HVOF Coated Carbon Steel specimens in the elastic region prior and post static corrosion exposure	154
Figure 81a	Tensile response of the welded and no-welded stainless steel specimens prior to corrosion testing	157
Figure 81b	Tensile response of the welded and non-welded HVOF coated stainless steel specimens in the elastic region prior to corrosion testing.	158
Figure 82a	Tensile response of the welded and no-welded stainless steel	159

	specimens after one week corrosion testing	
Figure 82b	Tensile response of the welded and no-welded stainless steel specimens in the elastic region after one week corrosion testing	159
Figure 83a	Tensile response of the welded and non-welded HVOF coated stainless steel specimens after three weeks corrosion testing	160
Figure 83b	Tensile response of the welded and non-welded HVOF coated stainless steel specimens in the elastic region after three weeks corrosion testing	161
Figure 84a	Tensile response of the non-welded HVOF stainless steel specimens prior and post static corrosion exposure	162
Figure 84b	Tensile response of the non-welded HVOF stainless steel specimens in the elastic region prior and post static corrosion exposure	162
Figure 85a	Tensile response of the welded (weld size = 2.5 mm) HVOF stainless steel specimens prior and post static corrosion exposure	163
Figure 85 b	Tensile response of the welded (weld size = 2.5 mm) HVOF stainless steel specimens in the elastic region prior and post static corrosion exposure	164
Figure 86a	Tensile response of the welded (weld size = 3 mm) HVOF stainless steel specimens prior and post static corrosion exposure	165
Figure 86b	Tensile response of the welded (weld size = 3 mm) HVOF stainless steel specimens in the elastic region prior and post static corrosion exposure	165
Figure 87a	Tensile response of the welded (weld size = 5 mm) HVOF stainless steel specimens prior and post static corrosion exposure	167
Figure 87b	Tensile response of the welded (weld size = 5 mm) HVOF stainless steel specimens in the elastic region prior and post static corrosion exposure.	167

---

# LIST OF TABLES

---

		<b>PAGE</b>
Table 1	Composition of 304L Stainless Steel	43
Table 2	Composition of AISI-4140 Carbon Steel	43
Table 3	A matrix for the coated specimens were used for tensile and fatigue testing	44
Table 4	Flat sheet carbon steel welded-coated specimens and testing conditions	45
Table 5	Flat sheet stainless steel welded-coated specimens and testing conditions	46
Table 6	Equipment used during the research study	47
Table 7	Fatigue testing parameters	57
Table 8	Spraying parameters for the deposition of Diamalloy 1005	68
Table 9	Incoenl-625 (Diamalloy 1005) powder constituents by percentage	76
Table 10	Fatigue cycles failure for coated carbon steel	108
Table 11	Fatigue failure coating on welded carbon steel specimens	117
Table 12	Fatigue failure coating on welded stainless steel (304 SS) specimens	118
Table 13	Semi-Quantities analysis for the steel-coating	124
Table 14	HVOF sprayed nickel alloy 625 coatings onto carbon steel specimens	139
Table 15	HVOF sprayed nickel alloy 625 coatings onto 304 stainless steel specimens	156

---

# INTRODUCTION

---

Thermal Spraying is widely used in protecting industrial components from corrosion, wear, abrasion, erosion, surface fatigue and as a thermal barrier to protect substrates from high operating temperatures. Thermal Spray Coatings Processes are classified as follow [1], Cold spraying, Flame Thermal Spray, High velocity oxy fuel (HVOF) spraying, Arc Spray Process, Plasma Spray Process and Detonation Gun Process.

Thermal sprayed metal coatings are depositions of metals, ceramics or polymers that are molten and semi-molten states immediately prior to projection onto the substrate. The thermal spray coating process refers to powder material deposition onto a surface mostly by means of propelled air or other relevant gases. Thermal Spraying involves the modification of a component surface mechanically in the form of a coating providing specialist properties. Alternatively, thermal sprayed coatings are the deposition of thermally sprayed semi-molten materials such as cermets and other powders onto substrates. During thermal spraying, multiple coat material passes are deposited on a substrate surfaces forming a coated surface. Thermal spraying is a group of coating processes in which finely divided metallic or nonmetallic materials is deposited in a molten or semi-molten condition to form a coating. The coating material may be in the form of powder, ceramic-rod, wire, or molten materials [2].

Coating is a layer of material applied by thermal spraying for the purpose of corrosion prevention, resistance to high-temperature scaling, wear resistance, lubrication, or other purpose. Coatings are utilized to protect surfaces from a single effect or multi-effects as well as to provide a functional type coating [1, 2].

Thermal Spraying refer to a wide range of technologies designed to modify the surface properties of metallic and non-metallic components for decorative and/or functional purposes. Thermal Spraying embraces those processes which modify the surfaces of engineering components to improve their in-service performance [3].

The history of thermal spray development is tied to the advancement of what is known as Metalizing (i.e. depositing of a molten metallic material onto another metallic surface). The metal spraying industry has its beginnings early in the 20th century when Dr. M.U. Schoop of Zurich, Switzerland, developed the first process for spraying metal and, subsequently, the first equipment able to spray metal in wire form [1]. The early commercial applications for the "Schoop Process" or "metallizing" took place in Germany, and later in France. Schoop subsequently sold his rights to a German firm known as Metallizator. It was this firm that made and operated the spraying units in Europe, England and the United States beginning in the early 1920's. Among the early U.S. companies to adopt the technology were Metal Coatings Company, Metalweld of Philadelphia and Metallizing Company of Los Angeles [4]. Early applications included the coating of railroad tank cars, U.S. Navy ship tanks, coal barges and the spraying of the emergency gates for the Panama Canal [1].

The earliest commercial applications for thermal sprayed coatings were performed over eighty years ago with first plasma spray coating process introduced by Reinecke in 1939, used for repair and maintenance [1]. Worn or corroded components were coated, machined and returned to service thereby saving the costs of replacement. Coatings for dimensional restoration are selected for their similarity and compatibility to the base metal rather than for their ability to improve wear resistance. Selection is based on likeness in chemistry, metallurgy, mechanical properties, color and performance. [4].

Research and development continued to produce a variety of thermal spray techniques. The High Velocity Oxy-Fuel (HVOF) Thermal Spray Process is among these process techniques. In the early 1980's Browning and Witfield, using rocket engine technologies, introduced a unique method of spraying metal and non-metal powders [1]. The technique was referred to as High Velocity Oxy-Fuel (HVOF). The process utilizes a combination of oxygen with various fuel gases including hydrogen, propane, propylene, hydrogen and even kerosene. In the combustion chamber, combustion by-products are expanded and expelled outward through a nozzle at very high velocities. The process often produces "shock diamonds" exiting the spray gun. METCO developed the Diamond Jet HVOF System in 1988, the technique being studied in the present research work [1].

An engineering component usually fails when it is subjected to an excessive load. The surface material selection, with the appropriate thermal, optical, magnetic and electrical properties and sufficient resistance to wear, corrosion and degradation, is crucial to its functionality [5]. Sometimes technological progress and manufacturing efficiency of the parts may be constrained solely by surface properties. For example, the fuel efficiency and power output of gas turbines or diesel engines are limited by the ability of key components to withstand high temperatures. However, it is often impractical, inefficient or uneconomical to manufacture components from a bulk material simply for their surface properties [1]. It is far better to use a cheaper, more easily formed underlying material and coat it with a suitable high performance film [4]. The resulting product conserves scarce material resources, and may well be cheaper to produce. There are several industrial applications for Thermal Spray Coatings where applying the coating offers an inexpensive alternative and obstacle solver. Another application is coating components operating in high temperature environments where the coating will minimize its original material deterioration and consequently extend equipment working life [4]. Additionally, components operating in extreme corrosive environments can be coated to minimize material loss and extend equipment operating service thereby avoiding un-necessary replacement at high expense [6].

The HVOF coating process finds wide applications in the oil and gas industry where petroleum products are transported through pipelines equipped with valves and pumps. This corrosive and flowing operating service may lead to possible damage by wear and corrosion determining or limiting the practical life or service interval of such components. HVOF process is achieving rapid and active growth in current thermal spray coating research. Whenever applications where deposition of high temperature resistance alloy coatings is required, HVOF spraying can produce coating quality similar to the detonation flow spray process, and exceeding coating quality deposited via air and vacuum plasma spray processes. Such advantage is due to the modest heating of the coating substrate and very high velocities obtained with HVOF [6].

The HVOF process has been able to demonstrate superior characteristics such as high bond strength and lower porosity making this process attractive and easily adaptable by industry [6]. The HVOF process continues to grow and advance through active research in areas

related to spray parameter optimization, control spray system enhancement, post coat treatment and alloy selection. HVOF coating seeks to improve the surface properties of non-metallic and metallic machine parts locally [7]. A coating powder material with the desired properties is mechanically interlocked with a substrate by means of Oxygen, fuel gas, such Propylene, and carrier gas, such as air or Nitrogen [1].

By improving a technical surface locally with an appropriate coating material one can use an ordinary, low cost base material for the body of a component - the part that is not being exposed to high loads. Industrial equipment benefiting from thermal spray coating is wide ranging [4].

Components work better in high-temperature environments with thermally sprayed coatings. These coatings provide heat resistant characteristics and help to retard the destructive effects of chemical corrosion and oxidation. The ability of HVOF thermal spray coatings to insulate and protect substrates disproportionately with regard to their thickness, helps extend the life of mechanical components in aircraft and industrial power turbines, and allows parts to operate and survive in hot, hostile exhaust gas environments. Thermal Spray Coatings such as MCrAlY on the turbine blades of jet engines are crucial to helping retard the effects of oxidation and sulfidation in the 700 to 1200°C operating temperatures of aircraft turbine engines [1, 4]. Zirconium oxide coatings are utilized in the metal casting industry to protect troughs, molds and other components providing practical long-lasting protection against wetting and oxidation. High nickel alloy coating provides excellent shielding for boiler tubing and exhaust fans from the effects of heat and chemical corrosion [8].

Thermal sprayed coatings can beneficially alter the electrical and thermal conductivity of a component. Thermal sprayed coatings exhibit excellent electrical characteristics. The properties of these coatings often differ significantly from those of the materials from which the coating was formed. Thermally sprayed copper, for example, demonstrates exceptional conductivity, so it's a perfect tool for producing highly efficient electrical connections. A thermal sprayed coating of aluminum has 20% greater conductivity compared to wrought aluminum, making it ideal for the manufacture of heating elements

[9]. A coating of thermally sprayed alumina exhibits superior voltage break-down strengths, making it an ideal electrical insulator [9].

Depending on the technique applied, common problems are the combination of a poor bonding of the applied surface layer to the base material, the occurrence of porosity, the thermal distortion of the workpiece, the mixing of the surface layer with the base material and the lack of ability in effecting a very local treatment. Consequently, specific techniques are required in order to match coating to substrates and to allow proper adhesion and ensure superior coating and wear resistance properties. These techniques may include substrate surface preparation, coating material selection to match application and substrate, spray process selection, spray process parameters selection, environment cleanness and substrate pre-coating surface temperature. This is in order to achieve effective metallurgical bonding between the coat and substrate and to maintain the original properties of the coating material [1]

Another frequent phenomena that occurs to surfaces exposed to solids impingement is referred to as erosion defined as the loss of material from a solid surface due to relative motion in contact with a fluid that contains solid particles. Thermally Sprayed Coatings may allow valves and pump pistons used in the treatment of highly abrasive wastewater sludge to last longer. The eroded walls of power generation boiler tubes can be repaired much faster, and have a much longer service life, if thermally sprayed coatings are applied as a protective layer [10].

Initially thermal spray processes were classified according to the type of heat source. For example, processes were classed as flame, plasma or detonation gun spraying. Modifications to the heat source environment further classed these materials into the precise category by which these processes are known today [1].

There are many variations of thermal spraying technology. In flame spraying the combustion of a fuel gas is used to heat the material. In atmospheric plasma spraying (APS) the material is melted and accelerated in a plasma jet [1]. To avoid oxidation of the feed material, spraying can be carried out in an inert gas atmosphere, at a reduced pressure (known as vacuum plasma spraying VPS or low pressure plasma spraying LPPS) [1].

During thermal spraying, particles of 15 to 45 microns are at least partially melted and accelerated to high velocities by a flame [4]. The particles splatter onto a surface and build a layer whose quality is assessed by the oxide content, porosity and bond strength interlocking to the substrate. The sprayed material can be metal, ceramic or polymer [1].

Materials that can be plastically formed either in the solid or liquid state can be deposited. Where heating is involved, only those materials that remain stable upon heating can be sprayed. Instability may lead to oxidation or decomposition of the material. These materials may, however, be deposited in the form of composites where a secondary material is used to protect the unstable or reactive material. Spraying into a special atmosphere, use of a metallic or polymeric binder to form a composite, or encapsulation of these powders are all means of protecting thermally sensitive materials.

Thermal spray feedstock can take several forms which are suited to particular materials such as [1, 4]:

- Powder - plastic, metal, composite, ceramic.
- Wire - metal, composite.
- Rods – ceramic.
- Liquid.

Thermal spraying is used to produce flattened particles, spherical particles (either hollow or dense) and coatings. The most common application of the powder is the production of coatings. Coatings can be deposited to tailored dimensions onto the surfaces [1].

A semi-molten particle or a particle able to deform plastically is transported at high speeds within a heat source towards a surface upon which deposition occurs. The droplet or particle undergoes spreading and may create a chemical bond with the underlying surface. With materials that are not able to produce a chemical bond, the substrate is roughened to create a mechanical bond. Each droplet or particle impacts a roughened surface and mechanically interlocks with the asperities on the underlying surface. Oxidation can be overcome by the use of a shroud placed onto the torch or by placing the thermal spray process into a chamber with a controlled atmosphere. With plasma spraying, the controlled atmosphere most commonly used is a vacuum [1].

Bond strength is dictated by the speed of the particle, temperature within the thermal spray plume, substrate surface roughness and substrate material [1]. Bond strength up to 60-80 MPa is not uncommon for thermally sprayed materials and the bonding ability is material and process dependant [11].

Residual stresses arise from substrate blasting or quenching of the splat on a cool substrate. Residual stress is below 50MPa for ceramics because of micro-cracking but strong alloys could have stresses up to 300MPa [12]. The mismatch in thermal expansion coefficients between surface and spray materials also causes stress which increases with increased temperature difference between spray and ambient and when there are temperature gradients in the sprayed part [1].

The HVOF process with reduced heat effect on the substrate and therefore minimal degradation of fatigue properties is now finding wide application in fatigue critical applications [13]. The critical parameters for process control are residual stress in the deposit and maximum substrate temperature. Both of these methods are technique sensitive particularly in spraying of coupons to evaluate the effect of coating on material properties [14].

With the increased use of thermal spray coatings in more critical applications involving properties like fatigue, the subject of process control is also receiving increased emphasis. This is important where increased heat transfer to the part can affect near surface substrate properties in applications like landing gear fabricated from the family of 4340 materials [15].

Thus, both methods are essential to process control and the production of a final product with the intended properties for the application. The coating temperature must be selected to optimize the required properties as maximum density will occur at a lower temperature than the maximum toughness and hardness [16].

Thermal Spray Process refers to operating conditions or parameters that need to be programmed and followed for each spraying process. These operating parameters will directly affect the produced powder quality. However, the powder type and required deposition control the operating parameters. Essential parameters include spraying

velocity, flow rate, substrate temperature, spraying nozzle distance from the substrate, fuel gas type, inert gas and surrounding gas [6].

High processing temperatures allow deposition of many high melting point materials onto a relatively cold substrate. Extensive use of thermal spray technology has been instrumental in Europe attaining worldwide leadership in the paper and textile industry [12]. Pioneering applications of thermally sprayed wear resistant coatings to blades, rolls and looms have allowed a significant increase in production rates. The aeronautic and space industries have also benefited considerably. Many components in modern aircraft depend on hard, wear resistant coatings which can withstand temperatures of about 850°C [6]. This type of application represents approximately 40% of the total market [12].

The coating adheres primarily through a mechanical anchoring mechanism. Surface roughness plays an overriding role. The adhesion strength of ceramic coating, for example, is a linear function of the average surface roughness [1]. It is unfortunate that there is no generic standard for surface preparation for HVOF coatings.

The type of thermal spraying process will play an important role in determining the characteristics of the coating achieved [17], such as:

- Porosity and oxide levels.
- Performance in wear or corrosion environments.
- Rate of coating deposition.
- Cost to coat a given surface area.

HVOF spraying differs from conventional flame spraying in that combustion occurs at a higher pressure inside the gun, with the resulting flame being accelerated along a nozzle to achieve very high velocities. Gas flow rates and delivery pressures are much higher [4]. This process is the most recent addition to the thermal spraying family and has become established as an alternative to the proprietary detonation flame spraying process and the plasma spraying processes for depositing wear resistant cermet coatings such as tungsten carbide-cobalt and other higher quality metallic coatings [6].

The HVOF process produces dense and with less than 1% porosity coatings that exhibit high bond strengths, some of which exceed 83 MPa (12,000 PSI), low oxides and

extremely fine as-sprayed finishes [6, 18]. The coatings have low residual internal stresses and therefore can be sprayed to a thickness not normally associated with dense, thermal sprayed coatings. Depending on user requirements, propylene, propane, hydrogen or natural gas may be used as the fuel gas [4]. The coating material, in powdered form, is fed axially through the gun, mostly using nitrogen as a carrier gas. The fuel gas is mixed with oxygen in a proprietary siphon system in the front portion of the Diamond Jet gun. The thoroughly mixed gases are then ejected from a nozzle and ignited outside the gun. The ignited gases form a circular flame configuration that surrounds and uniformly heats the powdered spray material as it exits the gun and is propelled to the work-piece surface.

It has always been a challenge to produce a well adhered low porosity deposit coating. This is due to the difficulty of achieving a sufficiently well prepared surface and assuring a well controlled spraying environment free from impurities and with optimized spraying parameters. This, in turn, triggers the need for a thermal spray process that will produce a dense coating with low porosity levels. This need can be met by using the HVOF Process. HVOF processes can be divided into two main groups [1]:

- Surface preparation processes including cleaning and preparing components surface.
- Surface treatments, which give the material the desired properties.

The main process variables are [4]:

- Gas flow rates - fuel, oxygen, and powder carrier gas.
- Powder feed rate.
- Gun temperature and cooling-water flow rate.
- Spray distance.
- Gun traverse rate and spray overlap pattern.
- Combustion chamber size and geometry.

A typical HVOF spray facility will include the following equipment [1]:

- HVOF spraying gun.
- Gas flow control unit.
- Gas delivery system.

- Powder feed unit.
- Heat exchanger for gun cooling.
- Mechanized, automated or robotic spray gun and component manipulation functionality.
- Sound attenuated booth with air extraction and filtration.

The concern in HVOF spraying at lower stand-off distances relates to the substrate and the coating heating up. Although the fundamental temperatures in HVOF are low, the high gas flows involved mean the heat that can be transferred to substrate/coating during spraying at low stand-off distances can be considerable. The proper stand-off distance varies from one type of equipment to another, and the equipment manufacturer should recommend the correct stand-off distance. Thermal spraying practice in general recommends laying down the minimum material in each pass. It is better therefore to rotate the job at the highest possible speeds. However the traverse speed of the gun should be adjusted to synchronize it with the rpm of job rotation to ensure uniform deposits [1].

The main aim in HVOF spraying is to attain as high a velocity as possible. Although it is possible that lower stand-off distances would result in higher particle velocities on impact, but, it becomes meaningless if the substrate is going to be damaged while using low stand-off distance. Thermal Spraying manufacturers usually recommend spraying distance to be maintained between the spraying gun's exit and the sprayed substrate avoiding excessive heat input to substrate and the previously deposited layer. The Gun process has unique features in giving the most consistent and reliable spray. The combustible mixture is fed into the combustion chamber through an array of ports giving a wider flame front and promoting complete burning within the chamber. Powder injection pressures are very low, preventing burned gases from running along the powder feed tube, and a transducer is used to measure the chamber pressure, avoiding inaccurate measurement, due to leaking lines [1].

HVOF process deposited coatings possess outstanding and attractive characteristics. The HVOF process exhibits density, hardness and bond strength coating characteristics that can significantly improve operating components. This is due to HVOF properties including operating at elevated temperature, corrosion resistance, and wear and abrasion resistance.

HVOF coatings have been characterized as having superior density. HVOF coatings are capable of producing deposits with less than 1% porosity [4]. The HVOF coatings process deposits high melting temperature materials offers fast coating deposition and has no volatile organics as is the case with many paints. Also, HVOF has the characteristics of fast heating and cooling, produced in equilibrium phases and therefore avoids decomposition of certain materials [19].

The HVOF Thermal Spray Process has a wide range of advantages. It offers greater thickness capability with no part size restriction. Thermal Spraying Coating can be performed in situ. Thermal spray coating can be used to apply virtually any type of material such as metallic, composites, and ceramics. Thermal Spray Coating can be used to extend useful working lifetimes; or improve economics of production. Thermal Spray Coating minimises corrosion rates to base material. It can reduce frictional energy loss and wear. It acts as a diffusion barrier and provides thermal insulation. It excludes certain wavelengths of radiation and promotes radiation electronic interactions. It increases part and component performance and reduces costs by avoidance of frequent parts replacement. Thermal Spray Coating controls surface properties independently of the substrate and improves component functionality [1].

Thermal Spray Coatings can be considered as a solution to previously insurmountable engineering problems. Thermal Spray Coatings technology may create entirely new products and help in the conservation of scarce material resources. Thermal Spray Coating may reduce power consumption and effluent output. It generates greater particle impact velocities and higher density (lower porosity) coatings. Thermal Spray Coating offers less degradation of carbide phases (for cermet coatings) while the coating hardness is high [19].

HVOF Coating Process has less in-flight exposure time (for metallic coatings) and produces lower oxide content [40, 41]. HVOF Coating Process is known for reduced time at high temperature thereby assisting to maintain the integrity of powder chemistry. HVOF coatings have less residual stresses and thicker coatings are possible [42, 43]. HVOF coatings are characterized by having high impact velocities and use of small powder sizes (producing smoother as-sprayed surfaces) HVOF metallic Coatings demonstrate excellent bond coatings with low oxidation. Such coatings have optimized microhardness

and predictable coating homogeneity. They produce a smooth as-sprayed surface with an excellent machined surface finish. The HVOF Coating Process can be automated. Additionally, HVOF coatings are used in controlling clearance. They are also used to salvage worn components. HVOF Thermal Spray Coating can overcome high temperatures. HVOF Thermal Spray Coatings also enhance electrical properties of the sprayed surface. HVOF Thermal Spray Coating demonstrates high particle velocity with minimal de-carbonization of particles [20].

There are few disadvantages associated with HVOF spraying. Such disadvantages may include powder sizes that are relatively small (around 5 - 45 $\mu$ m) with a need for narrow size distributions resulting in high consumable costs [21]. HVOF Thermal Spray Process requires experienced, qualified personnel to ensure safe operation and the achievement of consistent coating quality. Thermal Spray equipment is also relatively more expensive than other coating facilities.

The manual operation of spray guns is not recommended and automated manipulation is usually required since it produces more reliable coating properties. The deposition of coatings is difficult or impossible on the internal surfaces (diameters) of small cylindrical components as well as on other restricted access surfaces [1]. Instead, this type of process needs line of sight to surface and a spray distance of 150-300mm per [22, 23]. As with all the thermal spraying processes particular health and safety issues should be addressed. HVOF spraying usually needs to be undertaken in a specialized thermal spray booth, with suitable sound attenuation and dust extraction facilities [1].

With HVOF type coatings the mechanical properties of the base metal will be the same after the coating applications as no degradation will occur during the coating operation. Application to alloy steel or other type of non corrosion resistant base metals may result in corrosion as the corrosive medium will diffuse through the coating thickness attacking the base-metal, resulting in corrosion, evolution of hydrogen and finally blistering of the coating [14]. When applied to corrosion resistant base metals that are resistant to the corrosive mediums used, corrosion will not occur and therefore hydrogen as a by product from the corrosion does not exist. Many companies using HVOF process apply a sealant after the coating operation to minimize or eliminate the diffusion of the corrosive medium

attacking the base-metal. This result in the ability to use lower cost, less corrosion resistant base metals [24].

### Objectives of the Current Research:

The objectives of this research are summarized as below:

1. To study the comparative performance of welded carbon and stainless steels due to the application of Inconel 625 coatings deposited using HVOF process.
2. Specifically, to identify appropriate industrial applications of Inconel 625 powder deposited on components of homogenous and welded materials.
3. To investigate the effect of such coatings on mechanical and metallurgical performance under tensile and fatigue loading of such parts/components following exposure to corrosion.

These objectives are based on identifying gaps in the knowledge on this topic, following extensive critical review of literature as outlined later in chapter two of this thesis.

## Structure of the Thesis:

This thesis comprises of five chapters. Chapter Two is a literature survey covering technical articles published in open literature. The literature survey covers HVOF spraying process, coating resistance to wear, mechanical and metallurgical properties of coated surfaces.

Specimen Preparation, Thermal Spray Coating and HVOF processes and equipment used are detailed in Chapter Three. This chapter also addresses the equipment and experimental accessories required and necessary to perform laboratory testing. The tests include coating inspection, tensile quality and fatigue.

Data generated obtained from experimental work is presented in Chapter Four. The influence of brine exposure on the mechanical and metallurgical behavior of coatings is identified. The results of optical microscopy (EDS), Scanning Electron Microscopy (SEM) and Energy Dispersive Spectroscopy examination of various specimens are presented and discussed. Conclusions are presented in Chapter Five. Crack initiation and formation in coating due to tensile and fatigue loadings as well as coating failures due to impurities at the coating-substrate interface are discussed.

---

# LITERATURE SURVEY

---

## 2.1 INTRODUCTION

The present chapter surveys and reviews literature specifically on High Velocity Oxy-Fuel deposited coatings. Literature survey was made through numerous technical papers including those published in academic journals and conferences. The literature review covers work completed on HVOF coating applications for corrosion resistance, spray parameters affecting coat performance, erosion prevention, wear protection, heat treatment of HVOF coatings for residual stress relief, HVOF coatings mechanical properties, fatigue performance of HVOF coatings, microstructure of HVOF coatings, electrochemical behavior of HVOF coatings and particle behavior of HVOF coatings.

## 2.2 HVOF Coating Performance

HVOF Coating performance and function are highly influenced by several factors and parameters. Such affecting parameters can be improved in several ways such as heat treatment, coating sealant application, surface preparation and optimizing coating spraying conditions. In the following sections, literature technical review details HVOF coating properties and achieved work to improve coating performance.

### 2.2.1 Heat Treatment of HVOF Coatings to improve performance

Heat treatment can be defined as heating and cooling a solid metal or alloy in such a way as to obtain desired conditions or properties [25]. Li et al [26] examined effects of heat treatment and its vital role in improving HVOF deposited coating properties by minimizing coating porosity, stress relief, improving coating mechanical properties such as increasing coating adhesive strength, shear strength, Young's modulus and microhardness. Kim and Suhr [27, 28] studied influence of heat treatment in improving HVOF deposited coatings properties affecting the coating performance. The authors concluded that heat treatment is a very effective in improving the coating performance. Lee and Min [29] investigated influence of post heat-treatment in improving coating

performance. The authors concluded that post heat treatment reduces porosity protecting substrate from the corrosion attack through coating pores and voids. Moreover, the authors showed that porosity reduction coupled with improved bonding strength was possible via post heat treatment where porosity reduction could be achieved up to 1%.

The influence of post-coating heat-treatment as an effective approach to improve coating performance including bond strength, erosion and wear resistance, increases hardness and microstructure properties was studied by Rodriguez et al. [30]. These researchers demonstrated improved coating performance, higher bond strength and decreased porosity level achieved during the heat treatment. The post heat-treatment of HVOF tungsten carbides WC-17 wt% Co coatings was also investigated by Stewart et al [31]. The authors demonstrated that as a results of coating exposure to post heat treatment, abrasion wear resistance is can be improved up to 35% compared with the as-sprayed coatings and reduction of coating residual tensile stresses which increased coating working life. Shrestha et al [32] showed that HVOF cermets coating properties were improved by performing coating post heat treatment in vacuum furnace. HVOF coating treatment by vacuum fusion was studied by Shrestha et al [33]. The authors revealed that vacuum fusion treatment minimizes coating porosity, increases coating density and microhardness leading to improved coating corrosion resistance, and enhanced coatings erosion-corrosion characteristic.

The mechanical properties for HVOF MCrAlY coatings were improved by post heat treatment with observed reduced coating residual stresses and less coating porosity as per Itoh et al [34]. Recent studies showed that both porosity of HVOF nickel-based alloys coating was reduced as a result of post heat treatment with improved corrosion resistance according to Gil et al [35]. It was demonstrated by ASI et al [36] that applying heat treatment to the HVOF WC-17Co coatings increases coating metallurgical bonding, reduces fracture toughness and improves coating wear resistance..

### 2.2.2 Fatigue Performance of HVOF Coatings

Fatigue of materials can be defined as the phenomenon that leads to fracture under repeated or fluctuating stresses having a maximum value less than the ultimate tensile strength of the material [25]. Coated components of rotating equipments such as shafts,

turbine blades and rollers as well as valve stems always experience fatigue failure. Accordingly, a thorough study and investigation for the coating fatigue resistance and properties have been progressing where the area of HVOF coating fatigue performance has been investigated widely. Puchi-Cabrera et al [37] investigated fatigue properties of HVOF thermally sprayed coatings. The authors showed that HVOF thermally sprayed Colmonoy 88 coated components exhibit extended fatigue working life after being exposed to NaCl solution and simultaneously subjected to alternating stresses. This coating property provides effective protection against corrosion-fatigue failures.

HVOF coatings are commonly applied to metallic surfaces for protection from high temperature degradation, wear abrasion and corrosion attack. The coating fatigue properties are influenced by several factors such as coating deposition onto weld repaired surface. The coating adhesion onto welded surface may behave differently compared to deposition onto plain surface. According to Al-Fadhli et al [38], fatigue life of welded coated surfaces under short period exposure has similar fatigue life compared to the plain-coated surfaces minimizing the possibility of coating failure due to the presence of weld spots in the substrate. Extended exposure to corrosion environment results in a considerable reduction in the fatigue strength of the coating. Consequently, for the HVOF coating deposited onto welded surface experiences significant fatigue life reduction at extended exposure to corrosive environment.

Research studies showed that carbide coatings applied by HVOF process possess superior properties such as tolerating elevated stress values with observed extended fatigue life offering excellent components protection according to Brandt [39] and Souza, et al [40]. The compressive residual stresses developed within the HVOF tungsten carbide coatings showed increase in the coating fatigue strength life according to Padilla et al [41] and McGrann et al [42]. It was observed that the low level of porosity in the carbide coatings deposited by HVOF process contributes to additional fatigue strength. Generally, parameters affecting fatigue life include substrate surface roughness, coating porosity level, coating bond strength and coating residual stresses according to Nascimento et al [43]. Voorwald et al [44] demonstrated that grit blasting of substrate prior to coating influences fatigue properties. Ahmed and Hadfield [45] found that fatigue failure modes are represented by abrasive, delamination, bulk deformation and spalling. Ahmed [46] showed that HVOF thermally sprayed coatings fatigue life can be controlled via careful and proper selection of coating process, coating

thickness, coating materials and coating tribological parameters. According to Stewart and Ahmed [47], rolling contact fatigue is responsible for the fatigue failure of rolling element bearings, gears and shafts. HVOF thermal spraying coatings provide a cost effective remedy in meeting tribological applications requirements. Research work concluded that an improvement in the HVOF cermets coating fatigue life was achieved by post-treatment using the Hot Isostatic Pressing technique. According to Tipton [48], HVOF martensitic stainless steel coating is an excellent candidate protecting against high cycle fatigue for those metallic operating components in high temperature applications such as turbine blades.

### 2.2.3 Electrochemical & Corrosion Behavior of HVOF Coatings

Corrosion is a very dominant phenomenon in the industry. Corrosion is defined to be the chemical or electrochemical reaction between a material, usually a metal, and its environment that produces a deterioration of the material and its properties [25]. Selection of thermal sprayed coatings material and process for protection of metallic surfaces against corrosion attack depends mainly on the following:

- Substrate metallurgy either a superalloys or low alloyed steel.
- Corrosion mechanism taking place.
- Operating temperature.

Various operational environments may require a careful coating powder material selection where coating microstructure plays a crucial role in determining material behavior. For instance, nickel based alloy 625 coatings deposited via HVOF process are superior corrosion resistance protecting operating components in sea water environment and alkali solutions due where these coatings are dense and with low level of porosity. Moreover, nickel based alloys such as NiCrMoB exhibit corrosion resistance to more sever environments such as  $H_2SO_4$  as was concluded by Sturgeon [49] and Dent et al [50]. According to Tang [51], the oxygen content of the HVOF thermally sprayed NiCrAlY coatings influences the coating performance by limiting its corrosion resistance. Another factor that determines the electrochemical behavior of thermal sprayed coatings is the substrate morphology according to Guilemany et al [52]. Accordingly, a careful proper selection for the coating powder material, thermal spray process, spraying parameters and the substrate roughness will need to be made in advance.

Zhao et al [53] examined corrosion behavior and mechanism using several techniques such as electrochemical polarization, corrosion potential monitoring and cyclic voltammetry to monitor the corrosion resistance of thermal spray coatings. The 316 L stainless steel coatings deposited by HVOF process provide effective coating protection for steel surfaces against corrosion attack in several environments particularly, sea water environment and sulfuric acid  $H_2SO_4$  according to El-Khatib et al [54]. According to [55, 56], HVOF process can deposit AISI 316 coatings with superior corrosion resistance compared to other thermal spraying processes.

Neville and Hodgkiess [57] studied the performance of two HVOF process cermets coatings including WC and nickel based alloys coatings such as NiCr applied onto steel substrates for protection from aqueous corrosion, elevated temperature and varying salinity environments. The two authors concluded that the coating performance relies on the cermets layer porosity. Dense low porosity coating tends to provide improved substrate protection against corrosive media while presence of porosity weakens the cohesive strength within the coating according to Kuroda et al [58]. Non-destructive tests and techniques (NDT) such as fluorescent dye penetration have been found very effective in examining coating-substrate interface for possible corrosion development as was demonstrated by [59, 60]. Ak et al [61] concluded that it is very essential examining the stability of the coating-substrate interface operating in a corrosive environment prior to real life application.

HVOF process deposited coatings are very effective in providing resistance to hot corrosion attack. HVOF process deposited coatings play important role in protecting substrates operating from hot corrosion attack, substrates operating in high temperature applications and those machine parts operate in severe corrosive environments. Hot corrosion usually takes place in high temperature operating environments coupled with high concentration of molten salts. According to ASM Metals Reference Book [25], hot corrosion is defined as an accelerated corrosion of metal surface that results from the combined effects of oxidation and reactions with sulfur compounds and other contaminants, such as chlorides, to form a molten salt on a metal surface that fluxes, destroys, or disrupts the normal protective oxide. Boilers and super-heaters often suffer from hot corrosion, fouling and slagging due to dominant alkali and chlorine contents mandating immediate requirement for protecting operating components from hot

corrosion utilizing protective coatings as was studied by Uusitalo et al [62]. Hearley et al [63] concluded from their studies that thermally sprayed coatings are prone to chlorine attack and during oxidizing conditions. Sidhu et al [64] investigated Nickel based alloy coatings deposited by HVOF thermal spraying process onto alloys operating in high temperatures environments. The authors concluded that these coatings can provide a unique resistance to hot corrosion attack. Sidhu et al [65, 66] investigated properties of NiCrBSi coatings deposited by HVOF process and concluded that these coatings are very effective in protection superalloys from hot corrosion in molten salt environments at 900 °C.

High velocity impact force coating defects such as porosity level and inclusion influences the coating performance in corrosive environments according to Sidhu et al [67]. Zhao et al [68] investigated coating re-melting treatment process for HVOF NiCrBSi coatings to obtain solid surface and optimizing spraying process parameters. The authors concluded that this process could improve the coating resistance to corrosion. Nickel based alloys coatings and Nickel-chromium alloy coatings have been examined for their corrosion resistance by Jokinen et al [69]. The authors concluded that these coatings can provide improved corrosion resistance. The very unique impermeability coating property of the HVOF sprayed Hastelloy C coatings provide excellent corrosion resistant against sea water corrosion according to Kawakita et al [70]. Suegama et al. [71] studied the electrochemical behavior of thermally sprayed coatings and concluded that these coatings can be influenced by gun transverse speed and number of deposited layers while improved corrosion resistance of the coating can be obtained with higher torch speed.

Shrestha and Sturgeon [24] investigated HVOF process metallic coatings and concluded that these coatings offer excellent corrosion protection to process equipments and machine parts. Neville et al [72] investigated the corrosion performance of HVOF-sprayed Inconel 625 coatings. The authors revealed that these coatings are excellent coating candidate for corrosion protection. According to several experimental studies [73, 74], Electrochemical techniques such as AC. & DC have been found by the research community of being very effective in examining corrosion behavior. Tan et al. [75] applied electrochemical potential noise measurement (ENP) technique to examine real time data on the corrosion process occurring on and within an HVOF aluminum-bronze coated carbon steel system using a static corrosion experiment. The authors

found this technique is a very effective measurement tool capable of providing detailed information on corrosion occurring to the substrate.

Due to the fast growing and development of HVOF Thermal spraying process and evolution of powder coatings, Reignier et al [76] investigated suitability of the HVOF sprayed cermets coatings process for protection against wear and corrosion. The authors concluded that this process is believed to be a successful process candidate and alternative to electrolytic hard chrome plating in applications such corrosion and wear are experienced.

#### 2.2.4 Erosion-Corrosion

Erosion resistance of coating to impingement jet is very essential since it adds immunity to the coating against striking solids and increasing the coating performance in protecting the base material from mechanical damage. Erosion can be defined as the following [25]:

- a. Loss of material from a solid surface due to relative motion in contact with fluid that contains solid particles.
- b. Erosion in which the relative motion of particles is nearly normal to the solid surface is called impingement erosion or impact erosion.
- c. Progressive loss of original material from a solid surface due to mechanical interaction between that surface and fluid, a multi-component fluid, and impingement liquid or solid particles.

Operating components always get exposed to dual effects including corrosion and erosion inquiring effective protection to the substrate. HVOF thermal Spraying process has been advancing in depositing coating powders capable of resisting erosion-corrosion effects. According to the ASM Metals Reference Book [25], erosion-corrosion is defined as a condition involving corrosion and erosion in the presence of a moving corrosive fluid joint action leading the accelerated loss of material.

Shrestha et al [8] investigated the erosion-corrosion phenomenon and revealed that operating parts could suffer from erosion-corrosion causing material loss and damage limiting their working life. In marine applications, the erosion-corrosion and jet

impingement erosion are very common phenomena causing deterioration for marine equipments such as ship impellers according to Tan et al [77]. Dallaire [78] demonstrated that arc spray process also can produce excellent erosion resistance at high temperatures. HVOF process deposited coatings find a promised successful and cost effective replacement for current common practice of casting and certainly extending operating component working life. The HVOF coating erosion-corrosion resistance can be improved by high-temperature vacuum-furnace fusion process according to Hjornhede and Olefjord [79]. Wang et al. [80] examined improving the erosion resistance of selected coatings such as NiAl by addition of CeO<sub>2</sub> and Cr.

Several experimental research studies were performed evaluating HVOF process coatings such as work completed by Wang and Lee [81] coupled by similar work produced by Wood and Speyer [82]. The authors demonstrated that these coatings can offer excellent and effective erosion-corrosion resistance at high temperature environments as well as against solids jet impingement at elevated jet velocities. Lee and Wang [83] concluded that the erosion resistance of coatings is related to their composition and microstructure, rather than to their hardness.

Up to date studies investigated various types of coating powders deposited by HVOF process for protection of steel surfaces against high temperature erosion damage, corrosive media and rate of surface material loss according to Wang and Verstak [84]. Wang, and Luer [85] and Scrivani et al [86] studied the erosion influence to HVOF deposited coatings. The authors concluded that erosion effects are influenced by the operating temperature range, particle velocity and impact angle.

### 2.2.5 Wear

Wear is an ongoing phenomenon in industry particularly rotating parts. Wear costs a tremendous loss of materials due to worn parts. Machine parts and components operate in industrial applications and engaged in either sliding motion, rotating bodies and bearing applications are subjected to excessive material loss due to wear [1]. Wear is defined as damage to a solid surface, generally involving progressive loss of material, due to relative motion between that surface and a contracting surface or substrate [25]. Li et al [21] demonstrated based on experimental studies that thermal spraying process coatings provide a very cost effective solution by protecting the operating components

from wear damage. According to Sari and Yilmaz [87], the coating material, mechanical properties and physical properties can determine coating performance in resisting wear damage. Dent et al [88] demonstrated that composite based materials and HVOF sprayed small carbides exhibit excellent wear resistance. Operating components engaged in sliding wear applications usually experience accelerated material loss. This shortcoming could be overcome by HVOF coating these components using coatings containing Teflon-based solid lubricants extending component working life according to Marple and Voyer [89].

Recent studies demonstrate performed by Liu et al [90] showed that sliding wear resistance of thermally sprayed coatings is associated with the coating microstructure, mechanical properties, physical properties, coating defects such as inclusion and porosity. Moreover, the tribological behavior of the sprayed HVOF coating is significantly influenced by the microstructure properties. Therefore, thorough review and understanding for the coating microstructure features that control sliding friction and wear behavior in thermally sprayed coatings are required. The sliding wear resistance of HVOF deposited coatings can be improved with increased coating hardness according to Mohanty et al [91]. According to Staia et al [92], thermal spraying process parameters believed to influence coating wear resistance. Research work performed by Li et al [93] showed that HVOF coating offers excellent wear resistance compared to other coating processes under impact wear. Stoica et al [94] and Toma et al [95] studied influence of the hot Isostatically pressing process applied to the thermally sprayed coatings. The authors concluded that this process influence the sliding wear behavior of HVOF thermally sprayed coatings. The authors revealed that the sliding wear performance of deposited coatings could be improved via post treatment for the coating using such process.

## 2.2.6 Microstructure of HVOF Coatings

Materials are usually characterized through their microstructures. A microstructure is defined as the structure of an object, organism, or material as revealed by a microscope at magnifications greater than 25X [25]. Thermal Spraying processes have been widely utilized in depositing various coating powders including cermets, ceramics and composite materials. These coatings may vary in their structural composition and properties.

Nickel based alloys coating and tungsten carbides are often sprayed using HVOF process for protection against high temperature, wear resistance, erosion and corrosion resistance according to Li and Li [96]. Research work performed by Edris et al [97] concluded that coating microstructure, porosity, oxide contents and microhardness are all influenced by thermal spray procedures. However, according to Guilemany et al [98], coating oxidation is influenced by spraying parameters such as oxygen to fuel gas ratio, combustion chamber length and total gas flow rate. This in turn determines coating performance. The microstructure of the coatings is usually examined using various techniques such as Scanning Electron Microscopy, Transmission Electron Microscopy, Energy Dispersive examination, EPMA and X-ray diffraction methods. Coating microstructure experiences carbon oxidation occurs during spraying being responsible for decarburization while coating oxidation occurs during the splat formation after impact on the substrate according to Verdon et al [99]. Lau and Lavernia [100] studied the oxidation phenomena occurring during HVOF thermal spraying process. The authors concluded that the oxidation directly influence and cause coating microstructure change of nanocrystalline 316-stainless steel coatings deposited by HVOF spray process onto a stainless steel substrate.

Natali-Sora et al [101] investigated the tribological behavior of the coating deposited by HVOF thermal spraying process. The authors concluded that tribological properties are highly influenced by the annealing treatment to the coatings causing microstructural changes. The annealing temperatures range is directly influencing the final coating microstructure since annealing treatment produces enhancement of the oxide content.

Dent et al [102] studied the influence of HVOF thermal spraying parameters to the final coating microstructure. For instance, particle melting affects the microstructure and properties of Inconel 625 produced coatings. The authors concluded that Hydrogen fuel is believed to influence the coating microstructure during the HVOF process. Particle size is usually influenced by particle temperature during spraying where particle size and temperature are both inversely related. The presence of voids in the un-melted particles results in porosity. Particle size range is determined by the particle temperature during spraying where the particle temperature reduces as the particle size increases. However, the feedstock powder microstructure can be retained in the obtained coating under controlled designed spray conditions. Recent studies completed

by He et al [103] showed that the coatings consist of layered morphologies due to the deposition and solidification of successive molten or semi-molten splats.

Metallic coatings are produced using available industrial process for improved performance. For instance, mechanical milling process is used to prepare nanostructured WC-12 pct Co coatings while self-propagating temperature synthesis process is also used to produce cermets coatings. The nanostructured coating has a microhardness average of 1135 HV with superior indentation cracking resistance compared to traditional coatings. These synthesized nanostructured coatings consist of an amorphous matrix and carbides influencing coating performance. The optimization of thermal spray parameters is essential in order to achieve the potential of these coatings according to He et al [104]. Research work completed by Horlock et al [105] demonstrated that HVOF Ni (Cr)-TiB<sub>2</sub> cermets coatings sprayed onto steel substrates are porous compact and dense well bonded. Overall, the advancement in the thermal spraying processes produces improved wear resistant coatings and high hardness.

Tuurna et al [106] studied the performance of the Nickel based alloy coatings deposited by HVOF processes. The authors demonstrated that these coatings are very protective for turbine components. High temperature applications such as power plants and boilers suffer from hot corrosion and oxidation requiring excellent coating protection for the operating components and parts. It was found that controlled spray parameters of the HVOF process produce low oxide well bonded dense coating microstructure allowing enhanced performance where dense coating can be obtained via post heat-treatment. Also, experimental work performed by Wright and Totemeier [107] concluded that HVOF process produces coatings with less residual stresses. In order to improve the performance of the HVOF coatings, research work performed by Hamashima [108] exhibited that post coating annealing produces higher fracture strength. HVOF process produces cermets coatings microstructures with dense uniform layers leading to achieved high bonding strength which can further be improved via post heat treatment. Moreover, these cermets coatings are known of being abrasion resistant at high temperatures. HVOF process compared to other thermal spraying processes is very unique in producing coating microstructures with low oxide level, low porosity and developed dense deposits providing effective wear and corrosion resistance according to Ilavsky et al [109].

Schwetcke and Kreye [110] showed that coating properties including bond strength, hardness, abrasive wears and corrosion resistant are all influenced by the microstructure compositions and properties. HVOF process produces coating of high hardness and improved wear resistance depending on the optimized and selected spray parameters. The coating microstructure and substrate grit blasting play a vital role in determining the substrate-coating adhesion during HVOF spraying. Substrate-coating mechanical and thermal interactions influence significantly the development of the substrate coating adhesion during thermal spraying. Substrate roughness obtained by grit blasting produces excellent bonding mechanism with enhanced adherence of coating onto substrate according to Sobolev et al [111]. HVOF spraying parameters such as fuel type influences coating microstructure formation and corrosion resistance. The fuel type influences the particle melting degree producing coating microstructures with three phases including fully melted particles, partially melted particles area and un-melted particles area, which in turn impacts coating performance. Zhang et al [112] performed research work examining the corrosion resistance of HVOF coatings. The authors concluded that coating produced by high velocity oxy-liquid fuel exhibit improved corrosion resistance compared to those coatings produced by high velocity oxy-gas fuel.

Ji et al [113] studied wear properties of the HVOF coatings. The authors revealed that HVOF coatings are widely used for wear resistance applications and led to that the abrasive wear resistance of HVOF coatings is influenced by the microstructure parameters mainly carbide particle size, carbide content and the bonding of carbide particles. Moreover, NiAl intermetallic coatings deposited by HVOF process exhibit high hardness, improved modulus of elasticity and excellent carburization resistance at high temperature as demonstrated by Wang and Chen [114]. The characteristics of coating microstructures deposited by HVOF process are influenced by particle temperature and velocity prior to impact on the substrate. HVOF process produces dense coating structures with elevated hardness and bond strength and less residual stresses according to Sampath et al [115].

The oxygen content of the HVOF coatings influences its performance. Oxidation tests demonstrate that both the composition and microstructure of the oxide scale formed on the coatings affect the oxygen content in the coating. Low oxygen content in the coating is advantageous for improved coating performance as was investigated by Tang

et al [51]. Gil and Mariana [116] performed research work investigating HVOF coating properties and the influence of HVOF spraying process parameters affecting the coating microstructure. The authors demonstrated that thermal spraying parameters such as spraying distance and feed powder rate affect the coating morphology and microstructure properties including oxygen content. Moreover, coating properties such as porosity, microhardness and corrosion resistance are all influenced by spraying parameters.

Coatings sprayed by HVOF process are manufactured and produced using different techniques and process such as the high-energy ball milling technique producing powders for metal matrix compositions. Powders produced by this process and sprayed using HVOF process are dense coatings with homogenous microstructure providing improved wear resistance and higher microhardness as revealed by Zhao et al [117]. The HVOF spray parameters have great influence on the produced coatings. Mathematical simulation is a useful tool predicting the influence of the HVOF spray parameters on the structural characteristics of the coating. Sobolev et al [118] demonstrated that the mathematical simulation results agreed well with those obtained by direct metallographic methods concluding that the mathematical simulation is an effective tool to study coating microstructure development. Composite coatings find several applications in the industry where HVOF process has been successful in spraying composite coatings. Li et al [119] investigated the impact theory for examining the formation mechanism of HVOF sprayed composite coatings. The authors concluded presence of a chemical bond within the composite coatings influencing coating behavior. Also, the authors were able to observe several findings related to the mechanical properties and biological behavior of the composite coatings from their study.

#### 2.2.6 Influence of HVOF Spraying Parameters on Coating Properties on Mechanical Properties of Coatings

Edris et al [96] studied the influence of HVOF spraying parameters and conditions on produced coatings. The authors investigated several alloy coatings such as nickel-aluminum powders. The authors concluded that HVOF process parameters influence coating microstructure and coating oxygen content. Lugscheider et al [120] studied of influence of the substrate pre-temperature and process fuel type to the final produced

coating. The authors revealed that such factors certainly influence coating deposition mechanism and adherence bond strength. Selection of process parameters such as hydrogen-to-oxygen ration, spray distance, powder feed rate and substrate temperature affect final coating performance. Oxidation tests performed by Varacalle et al [121] demonstrated that HVOF coatings have excellent coating quality. The authors made also studied the combustion process and concluded that the temperature and power dissipated in the gun eventually influences particle melting and oxidation level. Experimental work carried by Arvidsson [122] showed that spray distance and fuel flow were the most significant contributors in lowering porosity and oxide contents. The author showed that coating thickness was controlled by the feed rate while spray distance control deposition efficiency. Wang et al [123] evaluated the influence of HVOF process spray parameters to the coating properties including bond strength, porosity, oxide content, hardness and corrosion resistance and concluded of direct effect to the final coating microstructure. The international thermal spray conference has addressed HVOF thermal spraying process contribution and importance to the industry [124]. Moreover, Thorpe and Kopech [125] performed and published research work examining HVOF coatings properties and how best to be improved meeting industry needs. Power turbines have been receiving attention by applying protective coatings for protection from severe operation conditions such as elevated temperature and corrosive environments. Parker and Kutner [126] performed research work examining how best applying HVOF coatings in providing enhanced protection for power turbines extending their working life. The authors concluded that HVOF coatings exhibit improved corrosion resistance, higher bond strength, low oxide content and low porosity compared to other thermal spraying processes. Moreover, use of HVOF thermal spray technology benefits power utilities through higher efficiencies and extended life for land-based gas-fired turbines. Influence of HVOF process parameters on the composite coating has been investigated by Sturgeon [127]. The author was very successful in promoting HVOF coatings for corrosion protection. Zhao and Lugscheider [128] studied the characteristics and properties of applying high velocity oxy-fuel spraying of a NiCoCrAlY and an intermetallic NiAl-TaCr alloy. The authors revealed that the coating deposited demonstrate promising applications for protecting operating components effectively. Suegama et al [129] showed that the bond strength of HVOF coating correlates well with the effective mass solid phase in spray particle suggesting high density of non-melting phases in a solid-liquid two-phase droplet is required to ensure high bond strength of HVOF coating. The authors concluded that HVOF

process deposited coatings is very corrosion resistant in protecting components operating in corrosive environments. Planche et al [130] studied coatings obtained by HVOF process using different fuels such as propylene and kerosene. The authors demonstrated that fuel flow rate, standoff distance, carrier gas and oxygen flow rate are directly affecting the coating deposition efficiency. Also, the authors concluded that coating obtained by hydrogen fuel HVOF system are very excellent corrosion resistant, dense and low oxides. Carbides coatings matches well with the HVOF process since they do not require high melting deposition forming effective wear resistant surface. Kim and Suhr [131] studied HVOF process details. The authors concluded that revealed that the HVOF process is a well successful process due to its effectiveness in accelerating the particles without overheating them. Also, the authors showed that HVOF process has a major advantage being able in spraying semi-molten particles at high velocities lowering residual stress, higher bond strength, reduced oxide content and very high density. Hearley et al [132] studied HVOF thermal spraying process and concluded that HVOF spraying process can produce coating quality comparable to the detonation flame spray process, and possible superior to air and vacuum plasma spray processes. This is a result of the modest heating and very high velocities obtained with HVOF process. Both oxygen-to-hydrogen ration and the spray distance of the HVOF process could influence the oxygen content of the coating and eventually coating microstructure properties. Lower oxygen-to-hydrogen ratio and longer spray distance lead to a lower degree of oxidation of the spray materials according to Higuera et al [133]. Special attention was paid to the HVOF process gun transverse speed and number of deposited layers. Steffens and Nassenstein [134] showed that coatings obtained with higher torch speed show improved corrosion resistance. Li et al [135] studied influence of the oxygen/fuel ratio on the particle characteristics during their flight in the jet, mainly oxidation content. The authors concluded that combustion process increases the oxide contents influencing coating corrosion behavior while fuel to oxygen ratio influences coating porosity. Also, the authors demonstrated that the higher particle velocities achieved with HVOF spraying lead to less oxidation with improved coating adhesion and lower porosity. Brandt [136] studied the wear resistance of carbide coatings produced by the HVOF process and concluded that the wear resistance can be influenced by process parameters. The author also demonstrated coatings sprayed with a higher chamber pressure yield an increasing wear resistance.

Kawakita and Kuroda [137] studied the phenomenon known to be oxidation of in-flight particles in the HVOF spray process with gas shroud. The authors showed that this oxidation process can be reduced by nitrogen addition to the combustion gas, leading to lowering the temperature of the in-flight-particles while maintaining their high velocity. Oxygen content in the HVOF coatings depend on particle size where decreasing in the particle size leads to increase in the coating oxygen content. Essentially, there are two oxidation mechanisms: an in-flight oxidation and a post-impact one according to Dobler et al [138]. The authors also concluded that spray parameters have great influence on the HVOF coatings oxidations while low particle temperature is necessary for low oxygen content coatings impacting bond and adhesive strength. Consequently, oxygen content can be decreased by controlling the spray parameters. Current research work performed by Hanson et al [139] showed that independent control of HVOF process spray particle velocity and temperature is possible where the particle velocity is related to combustion chamber pressure only. The authors also revealed that particle temperature is related to particle residence time within the nozzle. Such particles control allows the effects of velocity and temperature on coating properties to be assessed and controlled independently. Lih et al [140] investigated the influence of HVOF process parameters including oxygen flow rate, fuel gas flow rate, powder carrier gas flow rate, powder feed rate, nozzle length and stand-off distance on the speed and surface temperature of in-flight molten particles. The authors clearly demonstrated that final coating microstructure is directly influenced by spray parameters. Fillon and Gary [141] studied HVOF process technology in details with performed experimental work. The authors concluded that HVOF process has a potential for commercial applications since it provides well bonded, low porosity, wear resistant and corrosion resistant coatings. Moreover, the authors concluded that applying HVOF coating to operating components increases working life of these components. Additionally, the selection of optimized spray parameters and feedstock will certainly influence coating microstructure properties and performance.

Lau et al [142] investigated the powder particle behavior for during HVOF process spray process. The authors simulated the particle motion during the spray process using mathematical model and predicted the momentum behavior of the micron-sized agglomerates during HVOF spraying process. Joshi and Sivakumar [143] developed several mathematical models representing one dimension to investigate particle behavior associated with the HVOF spraying process. The authors showed from the

calculated particle velocity that the velocity profile depends strongly on the particle thickness. Ait-Messaoudene and El-Hadj [144] demonstrated that the HVOF system is well suited to the spraying of metals and low melting point alloys. Ghafouri-Azar et al [145] developed theoretical models to study the effect of the presence of the substrate on the flow of the exhaust gas. This study was initiated due to the importance of the existence of a boundary-layer zone. The authors concluded from the models that the velocity of the gases is ultimately zero at the substrate surface. Li et al [146] simulated HVOF coating formation using 3-D stochastic model implementing experimental spray parameters used for data input to the model. The authors obtained satisfactory results from the developed model agreed well with those obtained experimentally for coating properties and were found to agree well with coating thickness, porosity and roughness. Sobolev et al [147] investigated feedstock control of the HVOF thermal spraying process coatings using modeling techniques. Also, the authors investigated HVOF flow field and particle dynamics. The authors concluded that particle velocity and melting degree play a vital role in the formation of coating microstructure and can be independently controlled by pressure and oxygen-to-fuel ratio. Chang and Moore [148] developed a mathematical model to study the dynamic process during in-flight motion of the composite powder particles. Also, the authors utilized numerical simulation of gas and particle flow in a HVOF process where a transient two dimensional numerical simulation of Inconel spraying in a HVOF torch barrel was studied. The authors' results showed that the calculated results agree well with the experimental data showing importance of the statistical aspects of particle flow in the torch. Buchmann et al [149] utilized finite element modeling and simulation technique to determine the influence of different process cooling fluids and designs associated with the HVOF process system. The authors concluded that finite element modeling tool was capable in determining the residual stress rising within the thermally sprayed layer composites providing improved understanding of the coating formation. Ghafouri-Azar Mostaghimi [145] performed studies demonstrating finite element modeling abilities in determining residual stress and coating associated properties. Moreover, Lau et al [150] implemented mathematical modeling technique in investigating the particle behavior of Nanocrystalline Ni during high velocity oxy-fuel thermal spray. The authors were successful in utilizing this technique and were found to be very promising predicting particle behavior in comparison with other similar studies and experimental work. Bartuli et al [151] used computational fluid dynamics (CFD) to simulate HVOF process for the optimization of WC-Co protective coatings.

Utilizing the CFD technique, the authors were able also to simulate the thermo-chemical and gas-dynamic properties of the gas flow within an HVOF system torch. The authors concluded that in order to obtain fines coating deposition, proper selection of the spraying operating conditions must be in place by selecting low temperature versus high velocity of particles. Grosdidier et al [152] et al performed analytical examinations for characterizing nanocrystalline iron aluminide coatings prepared by HVOF thermal spraying. The authors implemented analytical instruments including X-rays and transmission electron microscopy (TEM) analyzing coating microstructure. The authors concluded that these instruments are very effective in examining HVOF deposited coatings providing reliable results.

### 2.2.8 HVOF Process coatings Development and Applications

Sartwell et al [15] performed research work comparing the performance of the HVOF thermal spraying coatings to other surface coating processes. The authors concluded that HVOF thermal spraying coatings are very superior in performance and certainly cost effective replacement for hard chrome plating in manufacturing and maintenance usages. HVOF coatings have been found exhibiting superior performance for protecting landing gear, hydraulic actuators and propeller components [1]. Sartwell et al [19] showed that the performance of HVOF coatings exceed that of hard chrome. Also, the authors concluded that HVOF coating possesses excellent fatigue properties; improved corrosion and abrasion wear resistance compared to those for hard chrome plating. Reignier et al [76] showed that HVOF coating demonstrate low porosity level, dense coating and enhanced adhesion property. The authors also showed that coating performance against friction and wear are durable. The authors demonstrated that the HVOF thermally sprayed coatings possess improved superior properties being potential alternative for the commercial hard chrome coatings. Wright and Totemeier [107] performed research work detailing the improved development associated with the HVOF coatings. The authors demonstrated that HVOF coatings can protect aluminum components subjected to dynamic loads against wear stress. Moreover, the authors concluded the new development in producing HVOF equipment enabled the deposition of fine coatings resulting from elevated combustion chamber pressure and reducing particle temperature. Wielage et al [153] showed that cermets coating costs can be reduced through use of ultrafine powders providing improved sliding wear resistance. Zhu et al [154] demonstrated that HVOF process is been able in depositing corrosion

resistance coatings using iron aluminide intermetallic compound  $Fe_3Al$ . The authors demonstrated that HVOF thermal spraying coatings have been widely used in environments to minimize thermal stresses providing oxidation resistance. Tan et al [155] performed research work showed that HVOF process coatings are successful in industrial applications such as components repair by spraying defected parts, build-up worn components, and protection against wear, corrosion and high temperature.

### 2.2.9 Residual Stresses in HVOF coatings

Residual stress refers to the stress existing in a resting body, in equilibrium, and not subjected to external forces. Stress arises in sprayed coatings primarily because the sprayed particles contract on cooling from the liquid to solid state [1]. Various thermal spray processes may influence residual stresses developed in the deposited coatings. The examination of the coating microstructure allows better understanding for the residual stress. Gassot et al [156] demonstrated that HVOF process produces coatings with less residual stresses than Vacuum plasma spraying indicating that the authors concluded that HVOF process is a successful candidate for depositing coatings with less residual stress. Residual stresses arising in thermal spray coatings have been widely investigated through the literature due to its important effects on coating cracking, adhesion and spallation behavior of coatings. Totemeier et al [157] revealed that HVOF process parameters such as spray particle velocity and torch chamber pressure are largely related to the rising of the residual stresses in the coating. Moreover, the authors concluded that the substrate thickness influences the coating residual stress. Watanabe et al [158] performed studied the mechanical properties of the HVOF coatings such as adhesion. The coating performance and working life are directly related to the adhesion level to the substrate. The authors showed that the coating adhesion strength is directly related to the rising residual stresses within the coating.

The residual stresses build up in thick coatings represent a restraining factor for coating performance [2]. Stokes and Looney [159] concluded that careful selection and design for the HVOF thermal spray process parameters has great contribution in limiting the rising of the residual stress in the coatings. Totemeier and Wright [160] performed a comparison measurement for the residual stress rising within the thermally sprayed coatings using two methods including curvature models and X-ray techniques. Wenzelburger et al [161] utilized several methods in determining and analyzing the

residual stress analysis rising within the thermally sprayed and layer composites. The authors concluded that from experimental work that coating thickness is related to the residual stress. Lima et al [162] also evaluated the residual stresses of thermal barrier coating with HVOF thermally sprayed bond coats using the modified layer removal Method (MLRM). The authors concluded that the MLRM was very effective in giving reliable results while measuring the residual stresses rising within the thermally sprayed coatings. Santana et al [163] utilized the incremental hole drilling method in measuring the residual stress in thermal spray coatings. The authors were also successful in adapting this method to measure the residual stress and received reliable results.

In summary, from the aforementioned literature related to the residual stresses arising within thermally sprayed coatings, several available techniques are currently available in estimating residual stresses within thermally sprayed coatings where comparison can be made for accuracy purposes. Also, the authors concluded from their measurements that residual stress in thermal spray coating could be either tensile or compressive. Another conclusion was observed by the authors that residual stresses generate debonding of the thermal barrier coatings deposited by HVOF process leading to collapse of the thermal barrier coating system. Moreover, the above mentioned studies concluded that residual stresses rising within the HVOF deposited Thermal Barrier Coatings (TBCs) are influenced by the thermal history regarding the quenching of individual splats and plastic deformation of ceramic deposits. The authors also concluded that residual stresses forming in HVOF process thermal spray coating can be modeled and studied predicting the coating microstructure behavior. Another conclusion was concluded by the authors that residual stresses formed in the coatings can be generated from substrate pre-treatment, spray particles solidifications, phase transformation during temperature alteration, heat transfer between coating and substrate. The authors also used computational techniques such as modeling and simulation predicting coating residual stress. Among these computation work was a 3-D stochastic model developed to simulate coating formation which was validated though measured values of coating thickness and porosity. Finite element modeling technique was used by the authors to calculate residual stresses rising within the coating where results agreed well with measured values. The above mentioned literature survey all concluded that residual stresses rising within the coatings can be relieved through voids, pores or cracks in the coating. The authors demonstrated that residual stresses

are influenced by spraying temperature and can be decreased by preheating the substrate. Another conclusion was that residual stresses rise due to mismatch between metallic bond coat and ceramic top coat of the thermal barrier coatings. Quenching of individual splats and plastic deformation of ceramic deposits may influence the residual stress in the coatings.

Stokes and Looney [164, 165] studied the properties of WC-Co Components Produced Using the HVOF Thermal Spray Process. The authors also investigated that the HVOF coatings performance with increased coating thickness. The authors showed that residual stress arising during spraying can be minimized by limiting the rise and fluctuation of the die temperature by introducing the carbon dioxide cooling system. This approach was followed by the authors allowed constant deposition at a stable temperature, and eventually produced excellent durable thick-formed WC-Co components. The authors also studied residual stresses and microstructural properties of thick, spray-formed components, produced using the High Velocity Oxy-Fuel (HVOF) thermal spraying process where the forming material used was Tungsten carbide cobalt (WC-Co). The authors targeted examining the effect of production parameters on the formation of thick components where minimizing residual stresses is a must. The authors concluded that residual stresses are very dependence on spraying distance. The authors showed that cylindrical WC-Co components up to a thickness of 9mm can successfully be produced with careful control of the spraying distance representing noteworthy improvement on maximum thickness values.

### 2.2.10 Laser process role in the HVOF Coatings

Corrosion resistance coatings such as Inconel 625 coatings are widely deposited onto industrial parts for corrosion and wear resistance. Thermal spraying processes may produce coatings that require post treatment for improved coating properties. High power laser post treatment and deposition of coatings has been attracting research work recently. Tuominen et al [166] investigated the microstructure and corrosion behavior of high power diode laser deposited Inconel 625 coatings. The authors used one-step powder diode laser for cladding of Inconel 625. The authors observed that the corrosion resistance of laser-clad coatings was found to be superior to HVOF sprayed coatings. Laser post treatment for HVOF coatings plays an important role in improving the coating corrosion and wear resistance by sealing the coating porosity developed during coating deposition. Serra et al [167] demonstrated that electron beam remelting for

HVOF deposited coatings could improve the coating metallurgical bonding, coating cohesive strength and the bond strength between the coating and the substrate. Hamatani et al [168] investigated the optimization of an electron beam remelting of HVOF sprayed alloys and carbides. The authors concluded that coating remelting using the electron beam reduces coating porosity and improves coating morphology. Potzl [169] studied the phenomenon of laser remelting of HVOF coatings for improved coating performance. The author concluded that adhesion and porosity of HVOF coatings always represent a shortcoming that can be eliminated by introducing high power laser heat treatment process of the sprayed coatings. The author also concluded that this laser heat treatment diffuses adhesion of the particles within the coating and to the substrate material resulting in enhanced bond strength and extended coating working life. Tuominen et al [170] using high-power continuous wave Neodymium-Doped Yttrium Aluminum Garnet Laser for improving corrosion properties of high-velocity oxy-fuel sprayed Inconel 625. The authors concluded that laser remelting of HVOF coatings results in a homogenous coating structure, improving coating adhesion performance, increases coating corrosion resistance and protection from high temperature oxidation. Lugscheider et al [171] studied the influence of laser treatment on the coating properties of mcrAlY-alloys. The authors showed that laser remelting for the coating formation produces superior corrosion resistant coatings. Tuominen et al [172] investigated the corrosion behavior of HVOF-Sprayed and Nd-YAG laser-remelted High-Chromium, Nickel-Chromium Coatings. The authors concluded that the corrosion resistance of MCrAlY coatings was improved via laser treatment for the coating material producing improved coating morphology. The authors concluded that laser remelting of the HVOF sprayed coatings is an effective process eliminating coating defects such as porosity, adhesion and cracking. The authors also observed after applying laser surface post-treatment improved coating properties with elevated bond strength of the sprayed coatings. Moreover, the authors revealed that laser remelting process contributed to improved coating against corrosion attack and enhanced corrosion performance in high temperature oxidation resistance. Moreover, the authors revealed that HVOF coatings porosity was reduced using post laser treatment by offering high cooling rates resulting in trapping of the gas in the melt zone.

### 2.2.11 Properties of HVOF Sprayed Coatings

Annealing treatment process of HVOF thermally sprayed coatings has been adapted for improving coating fracture strength due to eliminating internal local residual stresses. HVOF coatings produced at high velocities show zero porosity. Arif and Yilbas [173] performed three-point bend testing of HVOF Inconel 625 coating and finite element modeling associated with experimental investigation. There have been several experimental methods for testing HVOF coating properties mainly adhesion such as scratch testing, Indentation tests and four point bend tests by generating quantitative measures of coating adhesion. The authors concluded that experimental results agree by far with those obtained from simulation work. The mechanical and physical properties of high-velocity oxy-fuel-sprayed iron aluminide coatings have been studied by Totemeier et al [174]. Similarly, tests methods have been conducted evaluating the mechanical properties of HVOF deposited coatings according to Banks et al [175]. High temperature power plants always suffer from thermal fatigue impacting the efficiency of the operating components. Sundararajan et al [176] studied the effect of thermal cycling on the adhesive strength of Ni-Cr coatings. The authors evaluated HVOF coatings sprayed onto operating components for resistant against thermal fatigue. The authors concluded that the adhesive strength of HVOF coatings performed effectively in resisting against thermal cycling tests suggesting that HVOF coatings are a superior candidate for protection from thermal fatigue. Wang et al [177] studied the influence of substrate roughness on the bonding mechanism of high velocity oxy-fuel sprayed coatings. The authors concluded that substrate surface roughness influences adhesive strength of the coating. Moreover, the authors showed that the adhesive strength of the HVOF coatings increases as the substrate surface roughness increases. Also, the authors concluded that the adhesion of HVOF metallic coatings was determined by the mechanical interlocking effects. Lima and Marple [178] studied ductility improvement in thermally sprayed titania coating synthesized using a nanostructured feedstock. The authors concluded that HVOF coatings produced from a nanostructured feedstock powders exhibit a bimodal microstructure containing both semi-molten and fully molten regions. Also, the authors revealed that such bimodal coating demonstrated improved bond strength and enhanced wear resistance compared to those coatings are not synthesized. Celik et al [179] performed assessment of microstructural and mechanical properties of HVOF sprayed WC-based cermets coatings for a roller cylinder. The authors performed coating characterizations using

instrument designated X-ray Diffraction and Scanning Electron Microscopy examinations revealed that HVOF coatings possess high bond to the substrate, low oxide, low porosity and highly dense structure. The authors concluded from their findings that HVOF coatings are promising candidates for industrial applications. In severe working conditions such as internal combustion engines and high temperature power plants, operating parts always suffer from thermal fatigue and components deterioration. Jang et al [180] performed mechanical characterization and studied the thermal behavior of HVOF-sprayed bond coatings for thermal barrier coating (TBCs). The authors concluded from their investigation and tests that thermal barrier coatings are very superior and effective in protecting operating parts in hostile environments. Kwon et al [181] investigated thermal fatigue influence on mechanical characteristics and contact damage of Zirconia-based thermal barrier coatings with HVOF-sprayed bond coatings. The authors concluded that HVOF coatings can tolerate thermal fatigue damage. Also, the authors showed that the coatings demonstrated improved mechanical properties including hardness and modulus of elasticity. Superalloys operating in hostile environments such as steam boilers, furnace equipments and heat exchangers always experience very limited working life and accelerated deterioration. HVOF sprayed Stellite-6 coatings performance deposited onto superalloys operating in high temperature environments have been widely investigated. Sidhu et al [182] conducted research work studying the metallurgical and mechanical properties of high velocity oxy-fuel sprayed Stellite-6 coatings on Ni- and Fe-based superalloys. The authors concluded that such alloys are superior in performance while protecting parts operating in severe environments. Li et al [183] investigated the effect of types of ceramic materials in aggregated powder on the adhesive strength of high velocity oxy-fuel sprayed cermet coatings. The authors performed HVOF coatings characterization using standard analytical equipments resulted in coating low porosity level equal to 2% coupled with high coating hardness. Totemeier et al [183] performed experimental tests evaluating the mechanical and physical properties of high-velocity oxy-fuel-sprayed iron aluminide coatings. The authors concluded that corrosion resistance and mechanical properties of these coatings exhibited improved performance extending superalloys working life. Otsubo et al [184] studied the properties of  $\text{Cr}_3\text{C}_2\text{-NiCr}$  cermet coating sprayed by high power plasma and high velocity oxy-fuel processes. The authors demonstrated that HVOF coatings are very superior while demonstrating improved mechanical and physical properties compared to those coatings obtained by the high power plasma deposition. Also, the authors demonstrated that annealed

coatings exhibit higher fracture strength while increased spray velocity increase the fracture stress. The authors concluded that the adhesion strength of HVOF coatings is higher than the adhesive strength for those coatings deposited by high power plasma spraying. Moreover, the adhesion strength could be improved by heat treatment for elevated values equivalent to 350 MPa. The improvement of the HVOF coating mechanical properties mainly bond strength is receiving great attention in the recent studies. The adhesive strength of HVOF coatings determines coating performance and operating life [1, 4]. The HVOF coating strength was influenced by spraying conditions and annealing time.

#### 2.2.12 Characteristics of HVOF Sprayed Coatings Deposited Onto Welded Steel Surfaces

The behavior and performance of HVOF deposited coatings onto steel surfaces have been widely investigated. However, the characteristics and performance of HVOF coating sprayed onto welded surfaces being dis-similar metallic surfaces have only gained very limited attention. Very often, in the oil and gas industry, parts operating under sever operating conditions get defected requiring immediate repair in order to continue in service safely. For instance, rotating shafts, rollers and valve stems often exposed to erosive-corrosive service and exposed to fatigue where cyclic loadings are applied. One common repair method to repair defects representing material loss is a weld-fill. Such defected parts are always required to be externally coated for protection from erosion and corrosion damage. It was observed that deposition of HVOF coatings onto welded surfaces could experience lack of adhesion, erosion –corrosion lower tensile strength and possible fatigue damage if exposed to sever cyclic loadings. These phenomena have been studied recently by Al-Fadhli et al [185]. Scanning Electron Microscopy (SEM) and Energy dispersive Spectroscopy (EDS) are common analytical techniques to examine coatings and coating-to-substrate interface zone. The authors showed that erosion exposure of coated specimens only affected the non-melted and semi-molten particles. EDS analysis concluded that the coating center have higher Oxygen content than the remaining coating microstructure justified due to extended time required for cooling compared to other remaining coating microstructure. Additionally, analytical techniques showed that coating resistance to erosion-corrosion was lowered due to presence of  $Al_2O_3$  and  $Si_2O_3$  resulted from improper surface preparation. Al-Fadhli et al [186] have utilized the three point bending tests to examine

the mechanical properties of HVOF sprayed Inconel-625 coatings onto steel surfaces and welded-steel surfaces post and prior corrosion exposure in order to realize corrosion influence onto the mechanical properties. The authors also employed analytical equipments for microstructure characterization and surface morphology examinations. Test results revealed that coatings have experienced high stiffness resulted from corrosion attack to both the substrate and the coating with no major impact on the coating elastic behavior as a result of corrosion exposure. The authors observed developed crack within the exposed coating caused coating brittleness. Moreover, it was observed coating porosity minimizing possibility of crack propagation across the coating thickness. Analytical examinations showed that cavitations' presence in between the coating and the substrate believed was the cause of progressive corrosion accelerated the coating-to-substrate failure. Al-Fadhli et al [187] investigated HVOF thermally sprayed inconel-625 coatings onto steel surfaces and spot-welded steel surfaces attempting to understand coating performance onto dis-similar surfaces. The authors studied the erosion-corrosion characteristics of the HVOF thermally sprayed coatings when deposited onto welded steel surfaces. The surfaces understudies were exposed to jet impingement fluid conditions evaluating their corrosion and erosion performance. Analytical instruments such as EDS and SEM were used to examine microstructure and surfaces morphologies. From the test results, the authors concluded that both plain-coated steel surfaces and welded coated surfaces demonstrated comparable level of weight loss as a result to the eroding source being the impingement jet. This fact concludes that proper HVOF coating deposition onto welded steel surfaces can result in reliable part performance compared to the steel coated surface with no weld presence. Consequently, the weld presence did not have any shortcoming to the coating performance. However, test results showed that the exposed coating deposited onto composite surfaces comprising stainless steel carbon steel welded together suffered from excessive metal loss. Moreover, the analytical results demonstrated excessive metal loss from the exposed specimens mainly around the unmelted and semi-molten particles of the coating. Overall, the coating revealed superior erosion-corrosion resistance concluding that the substrate metallurgy did not influence the coating performance. The fatigue and corrosion behavior of HVOF coatings onto steel welded surfaces were investigated by Al-Fadhli et al [38]. The authors demonstrated similar fatigue life for corrosion exposed specimens for both plain steel coated specimens and coated welded steel specimens for exposure periods up to three weeks. However, exposed coated welded specimens for extended periods of four weeks

demonstrated significant decrease in the fatigue strength of the coated welded specimens due to development of fatigue cracks at both the interface between coating and substrate and within the coating.

## **SUMMARY**

It is clear from the review of the literature that although a large volume of works have been reported in the literature on various aspects of HVOF coatings and their performances under mechanical bonding and corrosion etc., there are still gaps on some aspects of the performance of parts coated with Inconel 625 in real industrial applications. In such applications tensile and/or fatigue loading may be involved together with exposure to corrosion during service, especially, for parts having welded joints. In particular, this thesis is directed in investigating the performance of welded carbon and stainless steels due to the application of Inconel 625 coatings deposited using HVOF process. Moreover, to explore current industrial applications of Inconel 625 powder deposited on components of homogenous and welded materials and how these component are performing. This aforementioned observations require investigation of the effect of such coatings on mechanical and metallurgical performance under tensile and fatigue loading of such parts/components following exposure to corrosion where these task will be carried throughout this thesis work.

As such further research is needed to augment the existing state of the art on this topic and the objectives of this study outlined in chapter 1 of this thesis have been formulated accordingly. In order to achieve these objectives detailed experimental research work have been planned and carried out as presented in chapter 3.

---

## EXPERIMENTAL EQUIPMENT AND PROCEDURES

---

### 3.1 INTRODUCTION

This chapter provides details of the experimental work performed, utilized equipment to carry out the experiments and procedures followed to complete the present study.

Thermal spraying process HVOF was employed to deposit Inconel 625 coating powders onto carbon steel and stainless steel substrates. Additional equipment were used to produce the coated specimens and perform experimental work on the as coated specimens. An Instron testing machine was used for performing tensile and fatigue tests on the coated specimens prior and post aqueous corrosive exposures. The objective was to examine the effects of brine exposure on the mechanical properties and the bond strength of the coating. The mechanical properties of the Inconel 625 coating deposited onto welded steel components prior and post corrosive aqueous exposure (adhesion performance on weld-repaired part) were also tested. This was conducted to observe the behavior of the coating on both welded zones and heat affected zones prior and post static corrosion exposure. This phenomenon is common in industry since operating components are always exposed to defects requiring component integrity regain, the avoidance of high component replacement costs and maintaining a component's maximum required strength.

The ASTM C 633-01 [188] standard test method, for evaluating adhesive and cohesive strength of coating was carried out using HVOF coated round solid bars. As per the ASTM C 633-01, the tensile testing was performed on round solid bars. Flat fatigue type specimens were fabricated and HVOF coating for tensile and fatigue testing prior to and post static corrosion exposure. The second major task involved producing weld-repaired components and HVOF coated by Inconel 625 under the same spraying parameters in order to investigate the behavior of the coating onto welded components. Throughout the

experimental work, several equipment were used; these are mainly mechanical properties testing facility (Instron Machine), metallographic equipment and coating characterization equipment (SEM, ESEM and optical microscopy equipment).

### 3.2.1 Preparation of Flat Specimens

Flat sheet specimens were fabricated and prepared from 304L stainless steel and AISI 4140 carbon steel materials for HVOF coating using Diamolloy 1005 coating powder with substrate geometry similar to Figure 1.

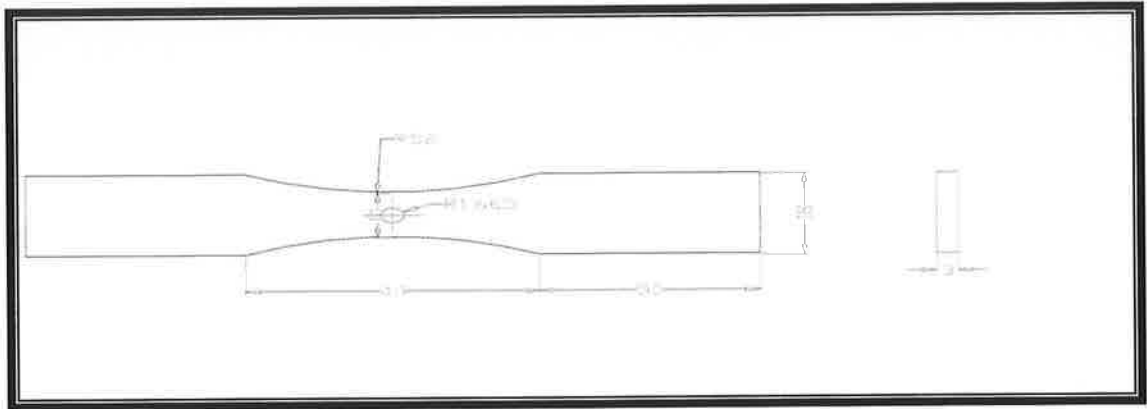


Figure 1: Flat sheet specimen geometry was used for tensile and fatigue tests with Central Weldment.

The composition of the 304L SS is shown in Table 1:

Table 1: Composition of 304L Stainless Steel

Fe	Cr	Ni	Mn	Si	S	C	P	Mo	N	Nb
bal	18.0-20.0	8.0-12.0	0-2.0	0-1.0	0-0.03	0-0.03	0-0.045	...	0-0.03	...

The composition of the AISI-4140 CS is shown in Table 2:

Table 2: Composition of AISI-4140 Carbon Steel

C	Mn	Si	Cr	Ni	Mo
0.36-0.44	0.70-1.00	0.15-0.30	0.80-1.15	...	0.15-0.25

Selected number of these flat sheet specimens was drilled through the center for weld deposition. The complete welded and HVOF coated substrate was tested for tensile and fatigue properties prior and post exposure to corrosion environment. Specimen's substrate specs are as follows: 140 mm length, 10 mm width and 3 mm thickness in accordance with standards ASTM E 466 -96 [189].

### 3.2.2 Test Specimens and types used in experimental work

#### (1) Coated Specimens

The coated specimens including solid round bar and flat sheet ones were used for tensile and fatigue testing are listed in Table 3. The coated round solid bar specimens were used only for tensile testing. Flat sheet specimens were used for tensile and fatigue tests. Tests were carried out to evaluate the mechanical properties of the coatings prior and post exposure to corrosive environment to assess the effect of exposure to corrosive solutions onto the coating properties.

Table 3: A matrix for the coated specimens were used for tensile and fatigue testing.

<b>Material</b>	<b>Type</b>	<b>Number of Coated Specimens</b>	<b>Number of dummy Specimens</b>
Carbon Steel	Round Solid Bars (cylindrical)	6	6
Stainless Steel	Round Solid Bars (cylindrical)	6	6
Carbon Steel	Flat Sheets	6	*N/A
Stainless Steel	Flat Sheets	6	*N/A

\*N/A: No dummy specimen was required to perform the test.

#### (2) Welded Coated Welded specimens

Table 4 lists the carbon steel welded-coated specimens used for tensile and fatigue testing. These welded-coated specimens were tested to evaluate the coating adherence onto welded surfaces and the mechanical properties prior and post exposure to corrosive environment exposure. Flat sheet carbon steel welded-coated specimens tested for fatigue only on the as

received condition and with three weeks exposure to corrosive solution. Due to the limited effects of one week corrosive environment exposure, the fatigue testing for flat sheet specimens was performed for exposed specimens to three week exposure evaluating the effect of corrosive media compared to the as received specimens.

Table 4: Flat sheet carbon steel welded-coated specimens and testing conditions.

<b>Exposure Period</b>	<b>Mechanical Test</b>	<b>Diameter of weldment (mm)</b>
Tested as Received	Fatigue	No weld
Tested as Received	Fatigue	2.5
Tested as Received	Fatigue	3.3
Tested as Received	Fatigue	5.0
3 weeks	Fatigue	No weld
3 weeks	Fatigue	2.5
3 weeks	Fatigue	3.3
3 weeks	Fatigue	5.0
Tested as Received	Tensile	No weld
Tested as Received	Tensile	2.5
Tested as Received	Tensile	3.3
Tested as Received	Tensile	5.0
3 weeks	Tensile	No weld
3 weeks	Tensile	2.5
3 weeks	Tensile	3.3
3 weeks	Tensile	5.0
1 week	Tensile	No weld
1 week	Tensile	2.5
1 week	Tensile	3.3
1 week	Tensile	5.0

Table 5 lists the stainless steel welded-coated specimens tested in a similar scheme as for the carbon steel.

Table 5: Flat sheet stainless steel welded-coated specimens and testing conditions.

<b>Exposure Period</b>	<b>Test</b>	<b>Weld (mm)</b>
3 weeks	Fatigue	No weld
3 weeks	Fatigue	2.0
3 weeks	Fatigue	3.0
3 weeks	Fatigue	5.0
Tested as received	Fatigue	No weld
Tested as received	Fatigue	2.0
Tested as received	Fatigue	3.0
Tested as received	Fatigue	5.0
3 weeks	Tensile	No weld
3 weeks	Tensile	2.0
3 weeks	Tensile	3.0
3 weeks	Tensile	5.0
Tested as received	Tensile	No weld
Tested as received	Tensile	2.0
Tested as received	Tensile	3.0
Tested as received	Tensile	5.0
1 Week	Tensile	No weld
1 Week	Tensile	2.0
1 Week	Tensile	3.0
1 Week	Tensile	5.0

### 3.3 Description of Equipment

The description of equipment is given under the appropriate sub headings. Table 6 lists the main equipment used to coat the specimen and to carry out characterization and testing of coating on test specimens.

Table 6: Equipment used during the research study.

<ul style="list-style-type: none"> <li>• Welding Equipment Facility.</li> </ul>	<ul style="list-style-type: none"> <li>• Optical Photography.</li> </ul>
<ul style="list-style-type: none"> <li>• Corrosion immersion Cell.</li> </ul>	<ul style="list-style-type: none"> <li>• Instron Machine for Tensile and fatigue testing.</li> </ul>
<ul style="list-style-type: none"> <li>• High Velocity Oxy-Fuel facility.</li> </ul>	<ul style="list-style-type: none"> <li>• Environmental Scanning Electron Microscopy.</li> </ul>
<ul style="list-style-type: none"> <li>• Fixture for round solid bar specimen alignment.</li> </ul>	<ul style="list-style-type: none"> <li>• Scanning Electron Microscopy.</li> </ul>
<ul style="list-style-type: none"> <li>• Adhesive Epoxy.</li> </ul>	<ul style="list-style-type: none"> <li>• Optical Microscopy.</li> </ul>
<ul style="list-style-type: none"> <li>• Oven for adhesive curing.</li> </ul>	<ul style="list-style-type: none"> <li>• Energy Dispersive Spectroscopy.</li> </ul>
<ul style="list-style-type: none"> <li>• Specime Metallographic Preparation equipment.</li> </ul>	

#### 3.3.1 Welding Facility

Industrial applications give rise to defects and cavities in components and parts due to impingements, friction, abrasion wear or corrosion attack. Weld filling of such cavities performed in order to regain component integrity and strength. In this research, shielded Metal Arc Welding (SMAW) Process was used to perform the weld fills of the drilled holes. The SMAW is a manual joining process in which coalescence of metals is produced by heat from an electric arc that is maintained between the tip of a covered electrode and the surface of the base metal in the weld joint. A simple schematic of an SMAW welding circuit is shown in Figure 2.

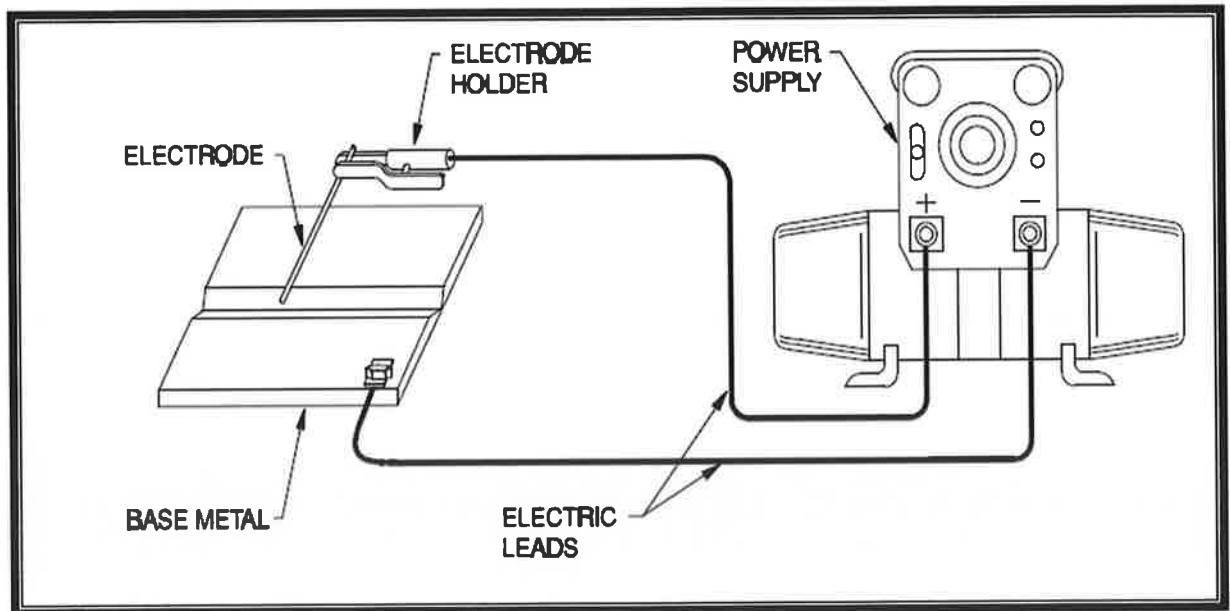


Figure 2: Schematic diagram of the SMAW circuit. As the electric energy melts the base metal and the electrode wire, metal droplets are transferred to the weld and become solidified metal.

### 3.3.2 Grit blasting unit for surface preparation of the specimens

It is essential to maintain a clean surface already grit blasted and with proper surface profiles in order to secure required adherence of coating-to-substrate. Such surface properties are required for all thermal spray coatings applications. Utilizing a harsh material such as sand via grit blasting will provide the required surface preparation. Grit blasting was used to create eroded steel surface using dry particles to create a rough surface for mechanical inter-locking between the substrate and the sprayed coating. The grit blasting facility and equipment were used to grit blast all specimens are shown in Figure 3. Inadequate surface preparation is the single greatest cause of surface treatment (coating) failure. All specimens were grit blasted using in-house equipment called EMPIRE model-PF-4848 made by EMPIRE Abrasive Equipment Company [190].



Figure 3: Grit blasting facility, Courtesy of [190].

### 3.3.3 Fixture for preparation of round specimen for adhesion testing

In order to perform tensile bond strength tests for measuring bond strength as per ASTM RP C 633-01 [188], an alignment fixture or loading device was designed and fabricated. In preparation for bond strength testing, the coated solid bar is adhered using adhesive epoxy against a non coated dummy solid bar. The test platform arrangement includes a specimen fixture to accommodate the coated and dummy specimens being glued in place using an adhesive of high tensile strength and cured in an oven. Since the coated and dummy specimens are solid round bars, the loading fixture must be circular for proper alignment. The fixture length must be greater than the total length of the two specimens (coated and dummy) for proper alignment, adhesive thickness application and force application. A suitable fixture was fabricated from aluminum material using a V angle bar with a total length of 127 mm. This fixture was equipped with a threaded bolt from one end to provide alignment and balance.

### 3.3.4 HVOF Thermal Spraying Facility

The HVOF thermal spraying facility consists of several units. These units were inspected, tested and approved for operation prior to the spraying of the components. The entire thermal spray facility including all the associated units is available at Saudi Aramco Mechanical Shops facility. Below is a description for the operating HVOF facility components:

### 3.3.4.1 High Velocity Oxy-Fuel Facility

The HVOF coating facility was utilized in producing coated substrates and comprises the following units:

- HVOF spraying gun.
- Gas delivery and storage (gas cylinders)/ Gas flow control unit.
- Consumable powder delivery equipment.
- Spraying system.
- Support system.
- Controlling system.
- Heat exchanger for gun cooling using treated water.
- Mechanized automated spray gun and component manipulation.
- Sound attenuated booth with air extraction and filtration.

The main process variables for spraying were:

- Gas flow rates – fuel (Propylene), oxygen, and powder carrier gas (Nitrogen).
- Powder feed rate.
- Spray distance.
- Gun traverse rate and spray pattern.
- Gun temperature and cooling-water flow rate.
- Combustion chamber size and geometry.

The HVOF spraying system was utilized in performing the coating, used oxy-fuel combustion to heat a coating material, in powder form, and to accelerate the heated particles to very high velocities prior to impacting with the substrate. The sprayed coating powder was nickel based alloy powder Inconel 625 commercially known as Diamalloy 1005, which has a particle size in the range of 15-45  $\mu\text{m}$  [4]. All the units comprising the spraying system were integrated to function jointly in order to produce an end product and a well controlled spraying operation. The spraying system equipment, support system and controlling systems were all supplied by Sulzer METCO [191]. The system comprises an automatic ignition system and a remote control accessory allowing the operator to work

with flexibility either inside or outside the booth whilst spraying. The operator is capable of remotely controlling the powder feeder. The gun can be operated manually or mounted on a fully programmable computer-controlled, high speed traverse.

### 3.3.5 Spraying Environment

In order to achieve a safe operation and the completion of acceptable work completion, a well designed spraying facility work space was necessary in order to accommodate the thermal spraying equipment unit. The facility operator was equipped with safety materials and equipments. The spraying space was also provided with exhaust ventilation and fire extinguishers. The work space was regularly inspected for safety precautions while the spraying equipment system was also frequently checked to assure that it met required spraying operations and parameters as instructed by the vendor.

### 3.3.6 Facility Preparation and Description

The manual mode involves a hand held gun spraying. This mode leads to non-uniform coating deposit thickness where residual stresses are developed. Moreover, the specimen could experience overheating due to lack of distance control. Usually, manual coating is only applied to those components and parts operating in non-critical environments or machines. There is also a multidirectional gun system that allows coating deposition in multiple directions that may be necessary due to the complexity of the coated part shape. In the current research, an automatic controlled spraying distance system was employed to deposit the coating powders onto the substrates.

#### 3.3.6.1 Gun Traverse Unit

This sub-system component allows for mounting specimens for coating spraying offering several advantages including avoidance of parts overheating and eliminating undesirable increased coating thickness resulting in development of residual stresses. This unit is integrated to a programmable controller that adjusts and controls directional speed. Elements that can be controlled with this unit are traverse distance, speed and acceleration. This control assures a secured kinematics path of the spraying gun with a guaranteed end product. Based on the nature of the specimen being coated, acceleration must be controlled in order to achieve the required coating product. This will allow a perfect avenue of

movement of the gun during spraying. The system manufacturer has provided a tailored prepared computational program capable of controlling the system set-up and geometry.

### 3.3.6.2 Cooling System

Due to the high combustion temperature and the high flame temperature, it was necessary to introduce a cooling system such as treated water into the HVOF system. The cooling system protects the nozzles, gun and combustion chamber from overheating which leads to total burn out and damage. The HVOF gun mount was attached to double treated cooling water solenoid consoles and nozzles. The cooling water flowed from a tank-heat exchanger arrangement through a pump with a line pressure of 3.44738 bars. During the spraying process, treated water was flowing through the hose providing cooling effect for the gas chamber and associated gun assembly.

### 3.3.6.3 Forced Cooling

Sulzer METCO HVOF thermal spraying system manufacturer requires forced cooling media associated with the gun assembly such as compressed air. The compressed air provides the HVOF spraying system with a cooling environment controlling and maintaining constant spraying temperature at the required setting. Forced cooling using compressed air minimizes the thermal expansion mismatch between the specimen and the deposited coating leading to lower residual stress build-up. A hose arrangement was tied to the gun assembly at one end while the other end was hocked up to an air compressor for air receiving.

### 3.3.6.4 Temperature Measurement and Monitoring Thermometer

Ongoing temperature measurement and monitoring of the deposited coating and the specimen surface temperature are crucial for the coating process. Temperatures of both the specimen and the deposited coating must be measured and controlled during spraying. The purpose is to protect the specimen's surface from overheating and monitor the deposited powder temperature. In the present study, a portable infrared non-contact hand controlled thermometer was continuously used for measuring the coating deposition and base material temperatures. The Ranger PM Infrared Thermometer Model referenced Ranger PM 20 made by Raytek [192] was used for measuring specimen and coating temperatures. The

deposition temperature of the coating was measured with slight fluctuation within range of  $\pm 2$  °C. The Raytek infrared thermometer offers a slightly more compact package and features a laser sight that illuminates the surface being measured. The thermometer is equipped with a screen display for reading and monitoring measured temperature.

### 3.3.7 Corrosion Testing Unit

For corrosion testing purposes, selected coated specimens were tested in an artificial sea water environment using a 3-liters glass container filled with treated water and 3.5% NaCl salt. The container was always kept sealed and covered maintaining clean corrosive liquid. The brine solution glass container which was used for specimens' immersion is shown in Figure 4. Static corrosion immersion tests are convenient means for laboratory simulation of many service environments for the purpose of evaluating the corrosion resistance of materials and for determining the effects of metallurgical, processing, and environmental variables on corrosion processes. The reason for such tests was to more closely recreate the operating conditions commonly occurring in commercial or industrial processes.

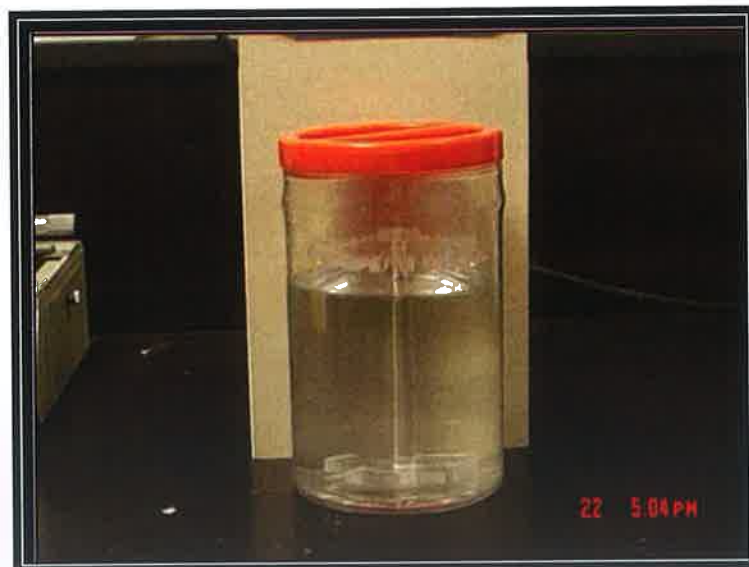


Figure 4: Immersion vessel with ring completely immersed in brine solution

### 3.3.8 Oven for adhesive curing

The curing oven made by Lab Line Instruments [193] shown in Figure 5 was used to cure-treat the adhesive gluing the round solid specimens due to adhesive manufacturer requirement. The adhesive was required to bond the coated specimens to uncoated round solid specimen for bond strength testing as per the ASTM C 633-01 [188]. The specifications of the used oven are:

- Model: 3471 MT.
- Temperature: ambient +10°C up to 270°C.
- Digital temperature display for convenient temperature monitoring.
- Hydraulic thermostat controller with temperature range from ambient +5°C to 270°C with  $\pm 1.0^\circ\text{C}$  control.

The oven temperature was set constant at 176 °C since this temperature was required to cure the adhesive in accordance with the adhesive manufacturer requirements.



Figure 5: A view of the oven and its set-up used to cure the adhesive.

### 3.4 Mechanical Properties Testing of Thermally Sprayed Coatings

#### 3.4.1 Tensile Testing Preparation

The INSTRON 8501 Dynamic Materials Testing System [194] shown in Figure 6 was used to perform tensile and fatigue tests on coated specimens including both round solid bars and fatigue type flat sheets. This system has a load capacity of  $\pm 100$  kN and actuator displacement of  $\pm 75$  mm. Tensile tests were carried out utilizing dedicated software called Wave Maker, Max. The tensile tests were performed to obtain stress-strain plots for all the coated specimens examining the bond strength of the coating, tensile strength of the coating and effects of exposure of the corrosive environment on the cohesive coating strength. The INSTRON machine was programmed to run the tensile tests under load associated to a displacement rate of 0.08 mm/sec. The strain data was determined using an extensometer attached to the specimen. By converting the plotted force (load) data to engineering stress-strain, an engineering stress-strain curve could be developed. Tests were performed at room temperature. The software provides the load and displacement characteristics of the tested specimens  $25\text{ }^{\circ}\text{C} \pm 2\text{ }^{\circ}\text{C}$ .

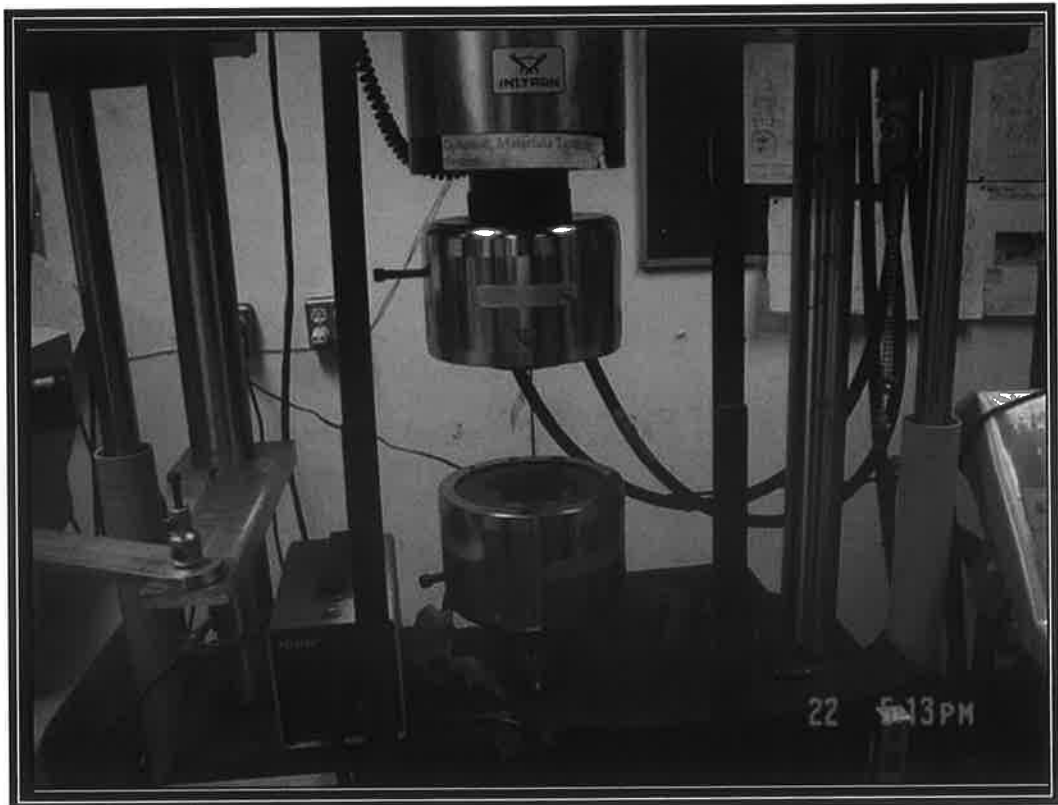


Figure 6: The Instron Machine specimen set-up assembly.

### 3.4.2 Fatigue Testing Preparation

The Instron 8501 Dynamic Material Testing System [194] was used to carry out fatigue tests on coated specimens examining coating fatigue properties under cyclic loadings. This dynamic system is capable of testing all kinds of metallic, polymeric and composite materials. The servo-hydraulic material testing systems was rated at 1000-kN and provided a broad range of material testing capabilities. A spectrum of optional accessories including load cells, fixtures, extensometers, software, and related peripheral equipment enables this system to be readily tailored to meet various testing needs. The fatigue tests were carried out utilizing special purpose software application named Wave Maker FLAPS, Series IX. The displacement was set to  $\pm 75$  mm while the strain at  $\pm 25\%$ . The maximum frequency applied was 100 Hz while the software application was ramped to a mean load level with a sinusoidal loading of a frequency of 20 Hz at a stress ratio  $R = 0.1$ . The maximum cyclic stress ranged approximately from 70% to 90% corresponding to the material's tensile strength. All tests were carried out at room temperature of  $25\text{ }^{\circ}\text{C} \pm 2\text{ }^{\circ}\text{C}$ .

#### 3.4.2.1 Control and Data Acquisition System

During each load cycle, the control and data acquisition system prompted to measure the displacement of the flat specimen, computes the strain in the specimen and adjusting the load applied by the loading device such that the specimen experiences a constant level of load on each cycle. In addition, the control and data acquisition system records load cycles, applied loads, measuring strain and computing and recording the maximum tensile stress and maximum tensile strain at load cycle intervals specified by the user. The fatigue testing parameters are shown in Table 7.

Table 7: Fatigue testing parameters

Load Capacity	1000 kN
Cyclic Wave Forms	Sine, Triangle, Square, HSine, HTriangle and HSquare
Ramp Wave Forms	Single, Dual and Trapezoidal
Frequency Range	1 - 10 Hz
Space Between Columns	562 mm
Testing Type	Cycle Fatigue, Tension and Compression
Drive Unit	Hydraulic System

### 3.5 Metallographic Specimens Preparation

Thermal sprayed coatings are usually examined and observed using microscopy instrumentation. The specimens were prepared to fit for microscopy examination. Four stages were required to prepare coatings for microstructural evaluation. The metallographic process comprises four distinct areas including sectioning, mounting, grinding and polishing.

#### 3.5.1 Sectioning:

The mechanically tested and corrosion exposed specimens were sectioned in area equivalent to 25mm<sup>2</sup>. This size enables observing extended specimen area and fits into the microscopy instrumentation in use. A slow motion diamond cut-off wheel saw was used to section the specimens as shown in Figure 7. The diamond cut-saw was an ISOMET model 1000 made by BUEHLER [195]. During sectioning the specimens, lubricant oil was introduced providing a cooling medium.

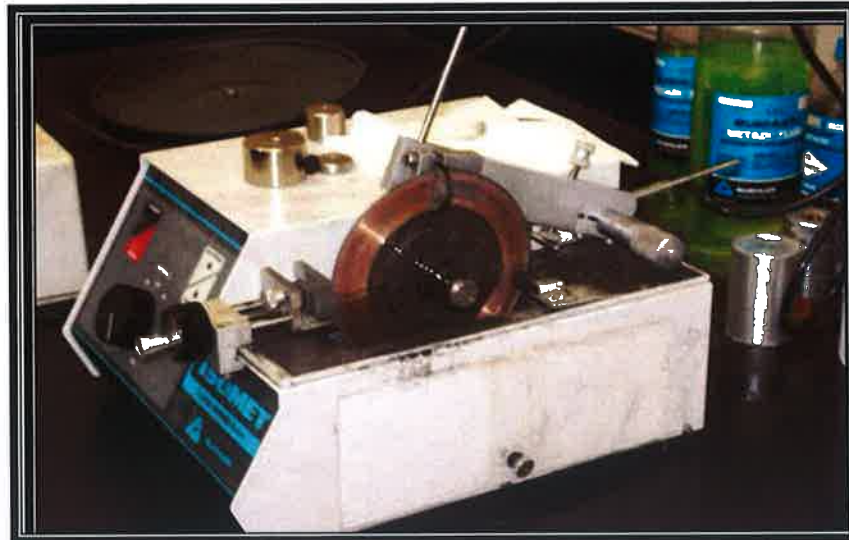


Figure 7: A slow motion diamond cut-off wheels saw used to section the specimens

### 3.5.2 Mounting

Mounting was the second process requirement for specimen preparation once the specimen had been sectioned to the required size. All specimens were mounted using a common technique known as hot-compression mounting as shown in Figure 8. This process involved setting a specimen in a thermoplastic or thermosetting resin, subjected to temperature of  $200^{\circ}\text{C}$  and high pressures of 40 MPa for 7 to 10 minutes. A laboratory available hot mounting equipment SIMPLIMET 2000 manufactured by BUEHLER [195] was used to mount all the coated specimens.



Figure 8: A mounting apparatus used for specimen's mounting.

### 3.5.3 Grinding

Grinding is defined as the removal of undesired materials. The grinding process was performed as per [199]. Grinding can be performed either manually or automatically comprising two steps: plane grinding and fine grinding. Fine grinding was applied to all specimens to remove any deformation experienced during the plane grinding step using silicon-carbide paper A P60 (very coarse SiC abrasive paper) to fine grind a specimen and leveling the resin holder to plane level. Fine grinding also machines away the excess damaged surface. Grinding was performed for all specimens using grinding equipment manufactured by BUEHLER [195] set to the automatic mode as shown in Figure 9.



Figure 9: Grinding equipment used to grind and polish all specimens.

### 3.5.4 Polishing

There were two steps involved in the polishing process including diamond polishing and oxide polishing. All specimens were polished in two steps process including diamond polishing and oxide polishing. Diamond abrasives were very effective during the polishing stage. The most common diamond particle sizes are 6, 3, and 1 micron, however other variables also influenced the final results, such as the polishing cloth, lubricant, force, revolutions per minute and time. The oxide polishing step was completed in just one minute at a low force on a medium to high nap polishing cloth. This nap cloth was soft and secured the abradable specimen during the polishing process.

### 3.6 Optical Photography

Optical camera made by Sony featured Cyber-Shot with 2.0 mega pixels was used to photograph equipments used for experiment5al procedures, prepared specimens and materials characterizations equipments. The camera model was DSC-P31 with precision digital zoom 3X.

### 3.7 Microscopy

#### 3.7.1 Optical Microscopy

Various materials such as coatings and welds could be too large to be observed under the microscope. The coating and weld microstructure can be examined effectively using an optical microscope. The optical microscope provides useful information about the microstructure, porosity/voids in the coating or weld, heat affected zone, coating adherence, coating or weld cracking, weld porosity and interface line between coating and base material. Semi-molten or un-molten coating particles fraction and size, deformation (thermal and mechanical) of the substrate near the coating, distribution of phases in the coating, presence of particles that have reacted in the flame (reduced or oxidized) in the coating can also be observed. LEICA [196] optical microscopy examinations revealed porosity levels in the coating microstructure. Optical microscopes will provide quantitative data. In order to receive complete quantitative data about a coating or weld being analyzed microscopically, the computer connected to the microscope had an automatic image analyzer (computer program system). Coating thickness measurement was a procedure performed to evaluate coating microstructure. This procedure was required to relate coating thickness to corrosion rate, coating mechanical properties and adherence level. Optical microscopy was employed to measure coating thickness using integrated software and camera with the optical microscopy. Using such techniques, additional data and information about the coating microstructure were identified and reported.

### 3.7.2 Environmental Scanning Electron Microscopy (ESEM)

#### Methods and Materials:

Materials characterization and elemental composition was observed utilizing ESEM (Electron Scanning Electron Microscopy) and EDAX (Energy dispersive X-ray microanalysis (EDS) system) made by FEI Company [197]. Coating microstructure examinations and elemental composition identification are essential functions that could be performed using SEM and EDAX microscopy examinations. The coating microstructure and the interface between the coating and the base metal could be imaged using backscattered electrons (BSE) and analyzed using the EDAX energy dispersive X-ray microanalysis (EDS) system. Both the EDAX and ESEM were capable of identifying the microstructure composition of each individual coated specimen as well as weld integrity since the coating comprises several phases. The specimens were prepared for metallographic examination—through saw cutting, resin mounting, grinding and polishing. Coating defects, failures, de-lamination, cracks and porosity were detected using available optical techniques.

In the current research study, an ESEM manufactured by the FEI-Philips Field-Emission XL30 (ESEM-FEG) was used to characterize the coating microstructure. The resolution of the ESEM can approach a few nanometers ( $\times 10^{-9}$ ) and it can be operated at magnifications from 10X to 300,000X. In the present study, an environmental scanning electron microscope (ESEM) was used shown in Figure 10 to characterize the coatings on stainless and carbon steels after tensile and fatigue testing. Both coating porosity level and coating thickness were determined and measured. The ESEM is a low-pressure scanning electron microscope, which allows direct imaging of dry or wet specimens with little or no preparation. This is particularly useful for minimizing damage to artifacts or destruction of the original characteristics of delicate specimens. The ESEM consists of a differentially pumped vacuum system and a gaseous secondary electron detector (GSE). The GSE detector, unlike the conventional Everhart-Thornley (ET) secondary electron detector commonly used in a high-vacuum SEM, was capable of operating under low partial pressures (down to 13 mbar) of gases such as water vapor, oxygen or carbon dioxide in the specimen chamber. In addition to GSE imaging, the ESEM also allows backscattered

electron (BSE) imaging with a solid state detector or a new gaseous BSE detector that can operate in both high-vacuum and gaseous modes of imaging. The backscattered electron images provide atomic number contrast (shades of gray) which help to quickly identify chemical differences in a specimen.



Figure 10: ESEM/EDS facility used for coating characterization (Philips XL-30).

As in the conventional SEM, elemental analysis could also be performed in the ESEM using an Energy dispersive X-ray spectrometer (EDS). Elements from carbon to uranium could be identified using the light element solid state X-ray detector, and also their spatial distribution can be plotted or mapped directly on the image using the advanced Linescan and X-ray mapping capabilities of the instrument.

### 3.8 EXPERIMENTAL PROCEDURES

#### 3.8.1 Procedure for welding of plane specimens

A selected number of specimens consisting of flat fatigue specimens from both metallurgy types (Stainless steel and carbon steel) were shop drilled using increasing drill sizes and controlled by the specimen cross sectional area. Hallow sizes included 2, 3 and 5 mm through the complete specimen thickness of 3 mm. The complete hallow created through the center of the specimen was filled with weldemnt using an electrode of the same substrate. A consumable electrode is one that is consumed in the heat of the welding arc and adds metal to the weld. Consumable electrodes are considered to be filler metal. The

specification for the welding rod was used to deposit all the weldments was an AWS No **ER309L** with a rod size of 2.4 mm.

### 3.9 HVOF THERMAL SPRAYING PROCEDURES

Below sub-headings detail all the steps were executed in performing the HVOF thermal spraying process was utilized in depositing Inconel 625 coating powder onto steel substrates included welded specimens. The complete HVOF process coating includes surface preparation, pre-heat treatment and spraying process.

#### 3.9.1 Surface Preparation (Grit Blasting)

Prior to powder spraying the specimens, all specimens were cleaned, degreased and prepared through three steps. This preparation phase was required to eliminate any contaminants or grease that might have settled on to the specimen surface.

- Specimen surfaces were manually cleaned using fresh tissues and rags.
- Surfaces were cleaned and degreased using degreaser/cleaner spray termed LPS ZeroTRI made by LPS Laboratories, Inc. USA.
- All specimen surfaces including the welded surfaces were grit blasted using the grit blasting equipment available at the shop made by Empire Company.

#### 3.9.2 Pre-Heat Treatment:

Pre-heat treatment process for the specimens prior to coating spraying is an essential process as per recommendation of the Sulzer-Metco Manufacturer. This pre-heat treatment will eliminate any surface humidity, moisture or condensates settled onto the specimen. Consequently, specimen pre-heating can lessen or promote thermal stresses. The exposure period dictates how thermal stresses may behave. Prior to spraying the specimens, the gun was ignited, producing flame where the torch was used to heat-up the specimens to a degree of 93 °C. Both Figure 11 and Figure 12 demonstrate grit blasted specimen ready for pre-heat treatment and after preheat treatment completion for a flat sheet specimens mounted onto a mandrel respectively.



Figure 11: Grit blasted substrate ready for pre-heat treatment.



Figure 12: Pre-heated treated for flat sheet substrates mounted onto mandrel.

### 3.9.3 Spraying Process

Propylene fuel gas and oxygen are mixed in the gun before entering the combustion chamber where the gases are burnt. Since the HVOF thermal spraying process was used utilized a Sulzer METCO facility, the manufacturer has provided recommended spraying conditions for deposition of Diamalloy 1005, Inconel 625. The HVOF thermal spraying system used Nitrogen as an inert carrier gas in order to feed the powder directly into the center of the combustion chamber, where rapid heating and acceleration of the particles take place. The combination of a fuel gas pressure of over 6 bar and gas flow rates of several hundred liters per minute can produce a flame speed of 2000 m/sec and a particle velocity of 800 m/sec [191]. The stand-off distance between torch and substrate was 304

mm. In the current research the automated mode was selected during specimen coating. In this mode the automated system moves in one or two directions (traverse units) simultaneously. The coating was deposited onto cylindrical components and flat specimens using two different geometries of prepared tailored mandrel. The specimens were fitted onto the mandrel for spraying as shown in Figure 13.



Figure 13: Round solid bars are fitted onto mandrel prior to spraying.

Round solid bars are grit blasted and fitted onto the mandrel having speed of 300 mm/sec for spraying with the coating powder. The HVOF spraying facility is programmed according to spraying parameters and the spraying process takes place until required coating thickness deposition is maintained and completed. Figure 14 shows round solid bars being HVOF sprayed while mounted onto the mandrel.

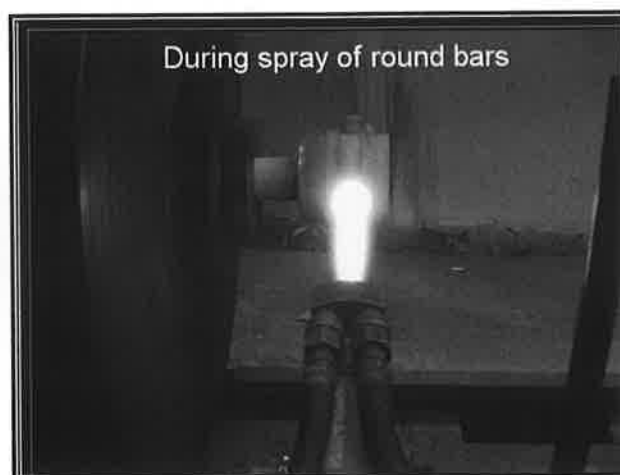


Figure 14: Round solid bars being sprayed while mounted onto the mandrel.

Once round solid bars have been HVOF sprayed to the required coating thickness, the coated specimens are left to cool down prior to removing them from the mandrel as shown in Figure 15.



Figure 15: Sprayed round specimens mounted onto mandrel left to cool down.

Figure 16 shows a complete set-up for HVOF spraying flat sheet specimens fitted onto a mandrel and mounted onto a lathe machine ready for spraying the coating powder.

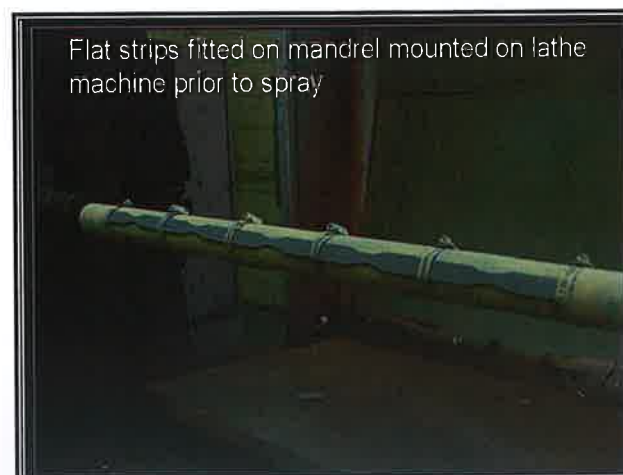


Figure 16: Flat sheets specimens fitted onto mandrel and mounted onto lathe machine prior to spraying.

Figure 17 shows a spraying process onto flat sheets while mounted onto mandrel. The mandrel speed was 300 mm/second.

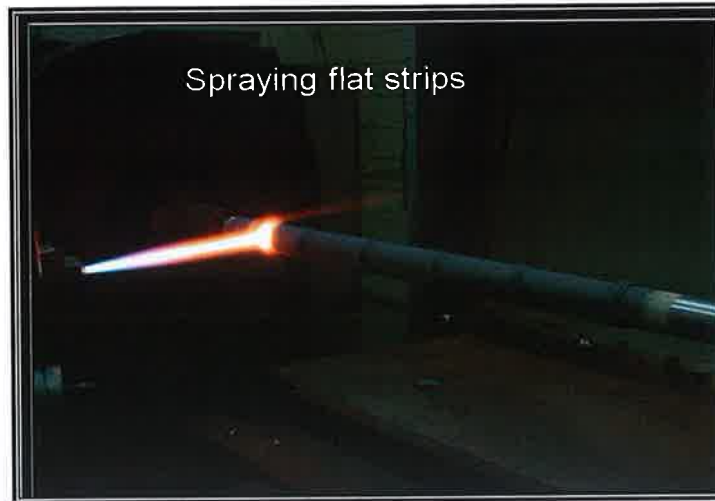


Figure 17: Active HVOF spraying operation where coating powder is being sprayed onto flat sheets while specimens mounted onto mandrel.

After the spraying process is complete for the mounted specimens, specimens are left on the mandrel until to cool down prior to removing them from the mandrel. Figure 18 shows flat specimens just sprayed with the coating powder.



Figure 18: Flat specimens after been sprayed onto the mandrel left to cool.

### 3.9.4 Gun Traverse Unit

A single axis (X-plane) in which the gun will traverse from left to right, is believed to be suitable for the HVOF process. A second axis (Y-plane) allows the gun swell, forcer and platen to be predetermined at different spraying distances depending on the required final coating properties. This correct predetermination of distance is fixed prior to the spraying process and coating deposition. Figure 19 shows flat specimens being sprayed using the gun traverse unit and moving table.



Figure 19: Flat specimens being sprayed using the gun traverse unit on a moving table

### 3.9.5 Spraying Process parameters and coating powder

The HVOF spraying parameters recommended by Sulzer-METCO are listed in Table 8.

Table 8: Spraying parameters for the deposition of Diamalloy 1005 [191].

Spray Parameters	Nickel/Chromium/ Molybdenum Alloy
Oxygen Pressure (Bar)	10.3
Oxygen flow (S.L.P.M*)	309.7
Propylene pressure (Bar)	6.1
Propylene flow (S.L.P.M*)	74.9
Air Pressure (Bar)	7.2
Air Flow (S.L.P.M*)	345.5
Nitrogen pressure (Bar)	17
Nitrogen Flow*	345.5
Spray distance (mm)	305
Powder feed rate (gm/min)	150
Air Vibrator (Bar)	1.4
Lathe Speed (RPM)	300
Gun Temperature (F)	300
Cooling Water Pressure (Bar)	3.40
Traverse Feed Rate (mm/sec)	300
S.L.P.M* = Standard Liters Per Minute	

In order to obtain the required end product, proper controlled safe operation of the spraying facility must be achieved. Consequently, safety equipment including masking, glasses, clothing, ventilation exits, and fire extinguisher were in place prior to the start of work. The spraying facility was inspected prior to equipment operation. Required equipment operator training certification was assured. A quick procedure needs to be followed prior to starting the spraying operation. Utilizing the powder feed assembly chamber, the Nickel/Chromium/Molybdenum Alloy powder was added. The powder spraying nozzles were inspected and ensured to be debris free. The associated nozzles along with the HVOF gun were checked prior to spraying starts. The spray parameters must be followed as described in Table 8.

### 3.9.6 Temperature Measurement and Monitoring Thermometer

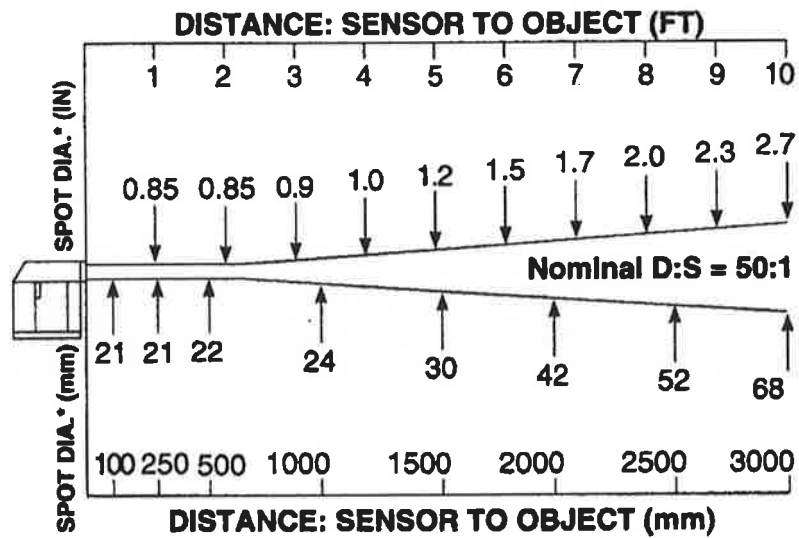
An infrared thermometer was used to monitor the coating deposition temperature [192]. This is to ensure that the substrate is not being overheated by thermal spraying stream during spraying which may cause substrate deterioration. While spraying the substrate, the thermometer is hand held with infrared beam directed directly towards the specimen being thermally sprayed measuring its temperature. The accuracy is  $\pm 1\%$  of the reading or  $\pm 1.0$  °C ( $1.5$  °F) which ever is greater, at  $23 \pm 5$  °C. The temperature monitoring using the thermometer is shown in Figure 20.



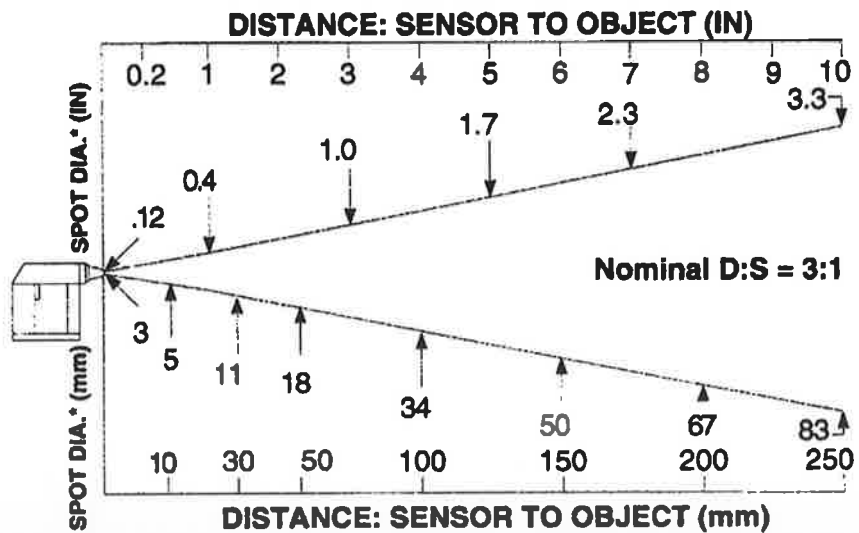
Figure 20: The Ranger PM Infrared Thermometer was used in measuring specimen and coating temperature.

Details of the spot size and range of the temperature are demonstrated in the below schematic of Figure 21.

### Optical Chart for Basic, Standard, Extended Performance and Data Logger Models



### Optical Chart for Close Focus Model



\*Nominal spot diameter at 90% energy.

Figure 21: Optical chart showing Thermometer Spot Diameter versus Distance (Sensor to Object). Courtesy of [192]

### 3.10 Preparation of Material and Bonding Surfaces

The bonded surfaces for adhesion testing were carefully cleaned, degreased and dried in order to obtain the maximum bond strength. Using a standard chemical etching solvent such as acetone, the bonding metal (coated and un-coated) surfaces were etched. A mechanical abrasion for the metal surface would roughen the bonding area using sand blasting, sandpaper or emery paper. Also, for some specimens, emery paper was used to roughen the metallic bonding surface. A simple yet effective test for surface cleanliness was to place few drops of cool water on the surfaces to be bonded. Parts were sufficiently clean if the water spread over the area in a continuous film.

#### 3.10.1 Adhesive Application

As per ASTM RP C 633-01 [188] recommendation and in order to perform tensile bond strength tests for the coated specimens, a high tensile strength adhesive is required for bonding the coated surface to the un-coated dummy specimen. The tensile strength of the adhesive material used must be higher than the expected bond strength of the coating deposited onto the specimen. A single component heat curing epoxy with high tensile strength was selected. The polymer epoxy system used was made by Master Bond [198] with a reference number of EP15 was rated for the tensile strength in excess of 82,737.08 kilopascal (kPa) exceeding the anticipated coating tensile strength. It was mainly designed and prepared for a high tensile strength. This EP15 adhesive epoxy was formulated to cure at temperatures from 148.89 °C to 176.67 °C for 60-90 minutes. This epoxy referenced EP15 forms rigid and dimensionally stable bonds with minimal shrinkage upon cure. It is 100% reactive and does not contain any solvents or diluents. Its service temperature range is -51.11°C to 121.11 °C. The manufacturer recommended that less adhesive thickness should be applied, but since the HVOF was a porous surface, it was necessary to apply more adhesive to fill the coating voids. This adhesive thickness was concluded to be appropriate after experimentation with several dummy specimens glued with much lower adhesive thickness. It was necessary to test the adhesive tensile strength and determine the suitable adhesive thickness necessary to be applied. The bonded parts were clamped together with sufficient pressure to maintain intimate contact during cure. Thicker glue lines do not increase the strength of a joint and do not necessarily give lower results - as the EP15 adhesive system does not contain any volatiles. Five millimeters of thickness

adhesive was applied in between the two specimens and wrapped with an aluminum foil and sealed with a high temperature tape keeping the liquid glue in place between the two specimens avoiding any escape or leakage and maintaining the required adhesive thickness.

### 3.10.2 Adhesive curing

The oven was started allowing the temperature to reach a stable of 176.67 °C. The test fixture arrangement including the aligned two glued round solid specimens were placed inside the oven for adhesive curing treatment for a period of ninety (90) minutes. Then, the fixture assembly was removed from the oven and left to cool down prior to performing bond strength testing. After that, the two glued specimen were removed from the fixture and uploaded into the tensile testing machine for tensile testing.

## 3.11 Mechanical Properties Testing of Thermally Sprayed Coatings

### 3.11.1 Tensile Testing Procedure

The Instron Machine specimen set-up assembly is shown in Figure 22.



Figure 22: Flat sheet specimen fitted to the fixture ready for tensile testing.

The mechanical tests carried out in this thesis research work were according to fatigue and tensile tests industrial standards mentioned below:

- **ASTM E-739:** Standard Practice for Statistical Analysis of Linear or Linearized Stress-Life ( $S-N$ ) and Strain-Life ( $\epsilon-N$ ) Fatigue Data.
- **ASTM E8:** Standard Test Methods for Tension Testing of Metallic Materials.

Following is the procedure for the tensile testing:

- The Instron Machine 8501 to be set-up was connected to data acquisition system and selected displacement load.
- Static tensile load was applied to the dummy specimen pulling it out where the coated specimen was stationary.
- While the tensile load continued pulling the specimen, a tensile-stress curve was being generated.
- Under increasing tensile load and until reaching the plastic region, an adhesive-coating layer was pulled out representing the coating bond strength where the tensile test stopped. The time required to complete the test was dependent on the coating bond strength. So, for higher coating bond strengths, elevated tensile load strengths were required with consequent additional time required by the Instron machine to reach the required load level.
- A constant rate tensile load was applied with of cross-head travel of between 0.030 in./min (0.013 mm/s) and 0.050 in./min (0.021 mm/s). Utilizing an associated data acquisition system and monitor connected to the machine, the monitoring device registers coating curve behavior until rupture. Once the adhesive was broken and the coating pulled out from its base material, the coating bond strength was indicated and that is where the tensile test stopped.
- A repetition for similar tests will indicate individual specimen's bond strengths. An identified base line is established after repeating each experiment for three times.

### 3.11.2 Procedure for tensile testing for the coated flat sheet specimens

- The Instron 8501 machine to be set-up was connected to the data acquisition system and selected displacement load. A displacement load of 3 mm/min. was selected.

- The flat specimens were prepared and coating thickness maintained at one (1) millimeter deposited onto 3 millimeters thick flat sheets (CS and SS specimens).
- Using the Instron 8501 machine, the specimen was attached to the testing device.
- Static tensile load was applied to the specimen pulling it upward where the lower part was held stationary.
- While the tensile load continued pulling the specimen, a tensile-stress curve was being generated.
- Under increasing tensile load and until reaching the plastic region, the coating starts cracking and eventually breaks. This is represented by a curve indicating the force required to break the coating in a tensile mode. The tensile test continued until the base material broke. Two curves were generated on graph paper showing the loads required to break the coating and the base material respectively. Of course, the time required to complete the test was dependent on the coating bond strength. So, for higher coating bond strengths, elevated tensile strength loads were required with a consequent additional time being required by the Instron machine to reach the required load level.

### 3.12 Static Corrosion Media Description

In the current research, a test vessel containing a 3.5 % sodium chloride (NaCl) brine solution dissolved in 3 liters of distilled water was used as shown in Figures 23 to Figure 25. The sodium chloride selected was NaCl iodized salt. The test solution was changed once every seven (7) days. The coated specimens selected for corrosion tests, were completely immersed within the artificial sea water solution inside the glass container. The specimens were immersed for different periods including one week, two weeks and three weeks. The specimens were attached to a ring with complete immersion in the water maintaining equal separation distance allowing complete interference within the brine solution as shown in Figure 24. The immersion period was variable to simulate lengthened exposure to the critical conditions that are suspected to cause corrosion damage.



Figure 23: 3 liters, Glass-container test vessel containing 3.5 % sodium chloride.



Figure 24: coated specimens fully immersed with equal separation within 3.5 % NaCl.

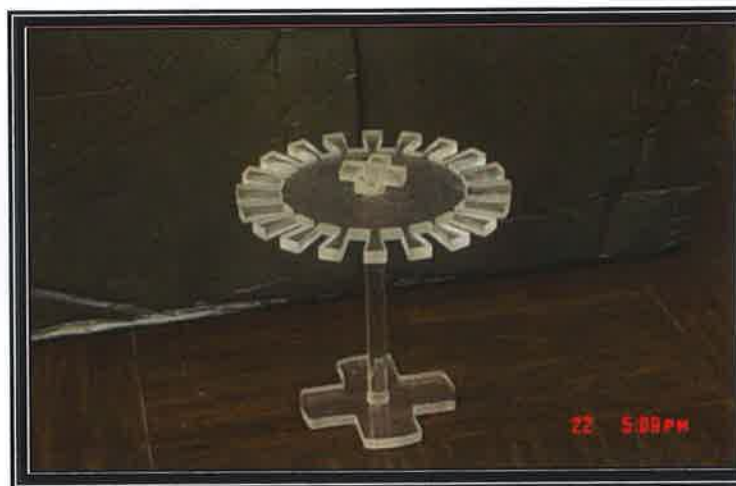


Figure 25: Ring used to hold flat specimens.

### 3.13 Procedure for Characterization Equipments

Materials characterization and elemental composition was observed utilizing ESEM (Scanning Electron Microscopy) and EDAX (Energy dispersive X-ray microanalysis (EDS) system). Mounted specimen was placed into a testing unit associated with the optical microscopy and ESEM for examination at the following zones:

- Coating-Substrate interface for disbonding and corrosion products.
- Coating microstructure including porosity level, oxidation and coating defects.
- Examination for the specimen at left edge, right edge and at the substrate middle.

By analyzing the chemical composition of the coating powder Diamalloy 1005 deposited onto the specimens, it was found that it comprises the following alloy fractions as shown in the Table 9.

Table 9: Incoenl-625 (Diamalloy 1005) powder constituents by percentage.

<b>Powder Material: Inconel-625</b>				
Ni (%)	Cr (%)	Mo (%)	Fe (%)	Co (%)
66.5	21.5	8.5	3	0.5

---

## RESULTS AND DISCUSSION

---

### 4.1 INTRODUCTION

The results of mechanical tests, metallurgical examinations and the surface morphology of the coating prior and after exposure to a corrosive environment are presented in this chapter. The findings are discussed to provide an insight into coating responses to mechanical and corrosion tests. In this chapter the experimental results of the HVOF thermal spraying process are presented and analyzed as follows:

- Results and discussion of the mechanical and metallurgical properties of Inconel 625 deposits onto cylindrical solid bars tested as per the ASTM C-633 standard prior and post static corrosion tests.
- Results and discussion of the mechanical and metallurgical properties of Inconel 625 deposits onto tensile specimens (in flat sheet form) prior and post static corrosion tests.
- Results and discussion of the mechanical and metallurgical properties of Inconel 625 deposits onto fatigue specimens (in flat sheet form) prior and post static corrosion tests.
- Results and discussion of the mechanical and metallurgical properties of Inconel 625 deposits onto welded tensile and fatigue specimens (in flat sheets form) prior and post static corrosion tests.

## 4.2 Corrosion and Bond Strength Testing of Solid Round Bars: (Specimen Selection and Distribution)

Specimens are selected in accordance with international standards governing testing procedures. Throughout the study, the testing procedures follow international standards including ASTM C-633-01.

### 4.2.1 Round Solid Bars (ASTM C-633-01)

A combination of solid round bars as specified by ASTM C-633-01 was prepared from carbon steel and 304L Stainless Steel specimens. Coated bars and dummy bars were used in combination for performing the tensile strength tests. A total of 120 coated solid bars were prepared consisting of 60 specimens' carbon steel and 60 specimens' 304L stainless steel. Only 10% of the total number (120) of coated specimens was selected as a statistical representation for the complete set. This selection representation is anticipated to yield similar results and performance behavior for the remaining specimens. The number of tested specimens was twelve (12) coated specimen. Dummy non coated specimens were prepared in accordance to the standard requirement. These dummy specimens are glued using the adhesive recommended for the coated surfaces. Random tensile tests were performed prior to and post static corrosion exposure.

HVOF coating of stainless and carbon steel surfaces was carried out. Inconel 625 powders were used during the thermal spraying. Static electrochemical testing of the specimens was carried out prior and post tensile testing of the coated surfaces.

Cross sections of the coatings (Inconel 625) deposited onto substrate were examined. They demonstrated a layered structure consisting of well consolidated metallic layers separated by a darker contrast phase believed to be oxide. It is believed that these layers represent the individual gun spray passes during specimen spraying. The oxide content was observed in addition to noticeable coating porosity. Microscopic examination revealed that limited occurrence of un-melted and partially melted powder particles. Examinations of coating cross-section showed the presence of oxide traces. Due to the

observed partially deformed particles of the deposited coatings, it was concluded that these coatings are compactly layered thus producing limited porosity level. The nickel alloy coating in particular appears fully dense with almost no visible porosity. The bond of the HVOF coating to a substrate is attributed primarily to the mechanical interlocking with asperities on the surface of the substrate material. In order to enhance the bonding strength, roughening of the substrate surface was required. Due to very high particle velocities, some fractured powders on the impacted surface were observed. This in turn partially reduced the bond strength of the coating. Oxidation of coating occurs during the spraying process due to oxygen gas associated with the process. This in turns creates oxide layers causing reduced coating bond strength. The formation of oxides can be categorized into three spatial zones. The first zone starts at the point of particle ejection within the nozzle and extends to the end of the jet case. In this zone, particles are exposed to high temperature flame as well as the combustion products. Zone two refers to the time from the moment the transported atmosphere reaches the centerline of the flame until the particles impact upon the substrate material. The third zone refers to the time the particles spend on the substrate after impact until the next layer covers them. During this period, the individual splats are still exposed to the oxidizing effects of the flame and may undergo some oxidation. Moreover, the contribution of the different oxidation mechanisms to the oxygen content of a coating depends not only on the spray parameters, but also on the spray powder feedstock. The porosity of the coating varies within 1.5% - 4.5 % for Inconel 625 coating. Consequently, results indicate that the coating was prepared with relatively low levels of porosity. Optical microscopy micrographs of coating cross-section are shown in Figure 26. However, the coating cross section was examined using Scanning electron microscopy (SEM) shown in Figure 27.

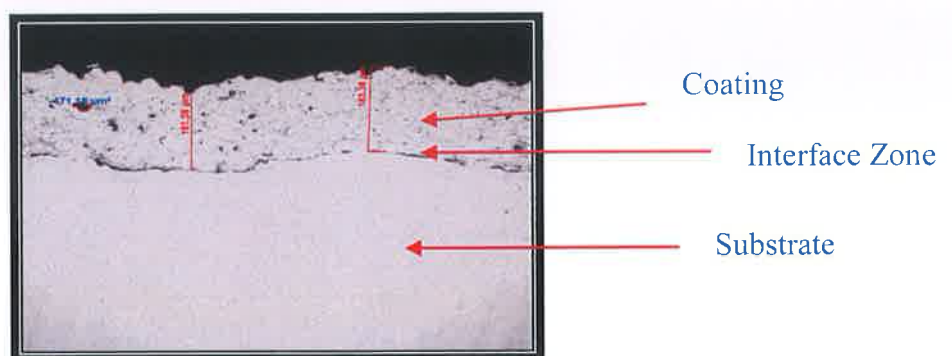


Figure 26: Coating cross-section.

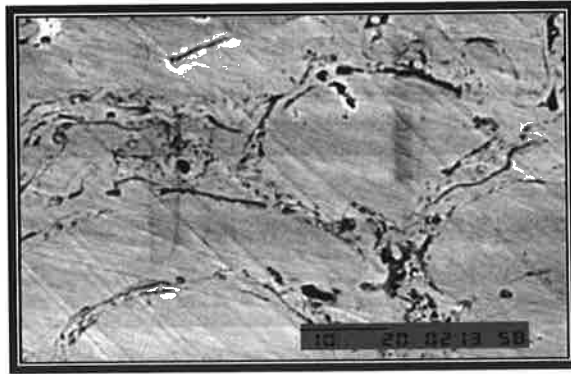


Figure 27: Coating cross-section micrograph.

The SEM and optical microscopy generated micrographs demonstrated that the powder was melted during the spraying process to give a lamella type microstructure with oxide strings aligned parallel to the substrate surface. The coating has a noticeable layered structure, with the layers parallel to the substrate surface and segregated by a slightly darker contrast phase presumed to be oxide. Each layer is considered to represent one pass of the spray over the surface. Moreover, the microstructure obtained for the coating of stainless steel surface has higher amounts of porosity than that corresponding to carbon steel. The microstructure obtained appears to consist predominantly of well stacked, partially deformed particles. This indicates that the powder particles were at a lower temperature on impact with the substrate below the melting point. Smaller powder size range (20 to 35 microns) gave coatings with a slightly less porosity.

With a microstructure consisting of well stacked partially deformed particles, the surface appears to be more resistant to corrosion. In this case, pit formation at the surface is not observed. Moreover, lamella type microstructure with higher oxide prevents the corrosion solution from reaching the base substrate. In the case of a porous structure, it is possible that some of the porosity will be interconnected. This phenomenon and coating defect substantially reduce coating bond strength as demonstrated in the following bond strengths tests. As a result of interconnected porosity a corrosion media may penetrate the coating and attack the substrate causing reduction in the bond strength of the coating and accelerated coating dis-bonding from the substrate. This observation is explained in the below bond strengths tests, even though the coating is itself resistant to the particular corrosive environment. It should be noted that most steel specimens are highly susceptible to surface corrosion, particularly in a chloride containing aqueous media. As a

result, the substrate may be corroded beneath the coating, causing the coating to blister and spall as shown in the upcoming experiments. In the current experiments, the surface of one of the specimens suffered from the corrosion effect. It was observed that due to a gap between the coating and the substrate surface on the side of the specimen shown in Figure 28, corrosion solution entered through the gap and resulted in crevice corrosion beneath the coating.

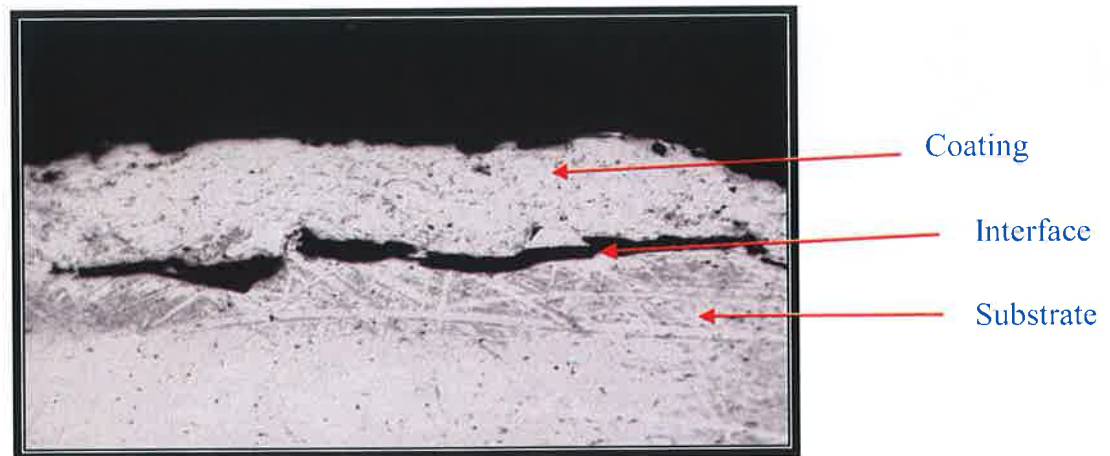


Figure 28: Coating cross-section at the side of the specimen.

The adhesive selected to perform the bond strength for the coated specimens round solid bars as per ASTM C-633-01 standard was made by Masterbond, USA model type EP-15. This adhesive is rated for bond strength in excess of 82 MPa (12000 psi) as indicated by the manufacturer. The adhesive tensile strength was tensile tested for varied adhesive material thicknesses using dummy non-coated specimens to determine proper required adhesive thickness to be applied between the coated surface and the dummy specimen to assure proper complete bonding for bond strength testing. Various adhesive thicknesses were applied and tensile tested representing three thicknesses as shown in Figure 29. It can be observed that the tensile bonding strength of the adhesive is in the range 45-60 MPa. This is; however, lower than the normal bond strength of the nickel based alloy coating similar to the Inconel 625 as indicated by the powder manufacturer which is 69 MPa. Consequently, bonding strength beyond 40 MPa is considered as satisfying the condition for sound bonding.

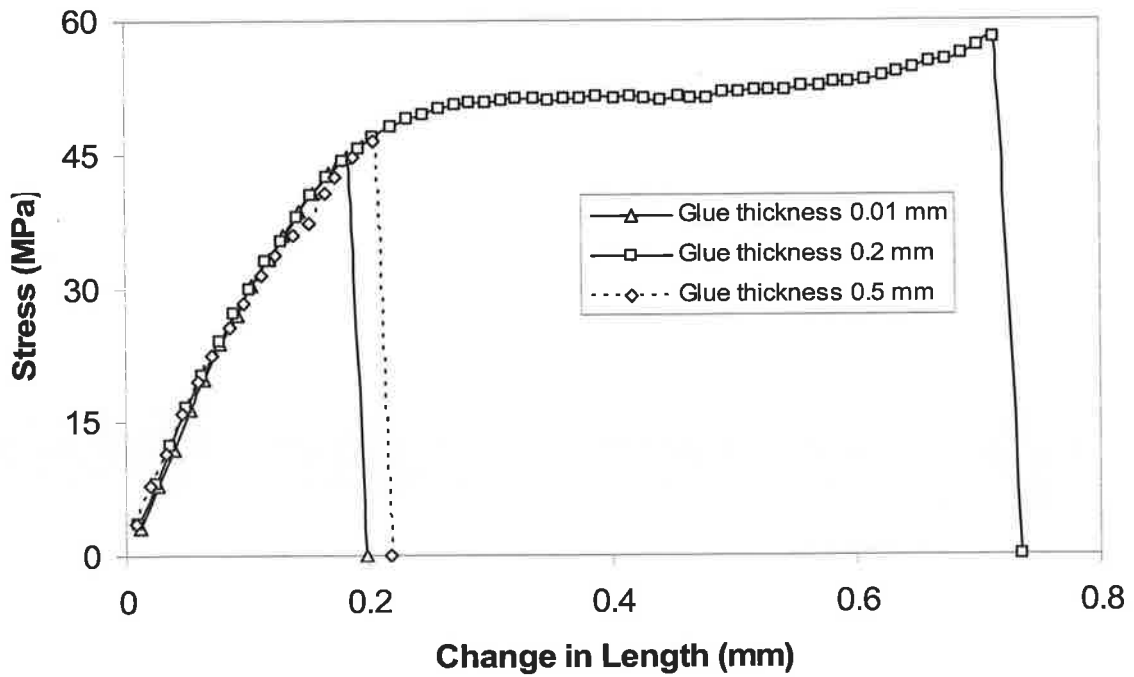


Figure 29: Tensile bond strength of the adhesive.

The tensile bond strength for HVOF coated 304L stainless steel specimen exposed to three different durations is shown in Figure 30. The specimen was exposed to one week immersion into a 3.5% NaCl solution showed high tensile bond strength close to 35 MPa.

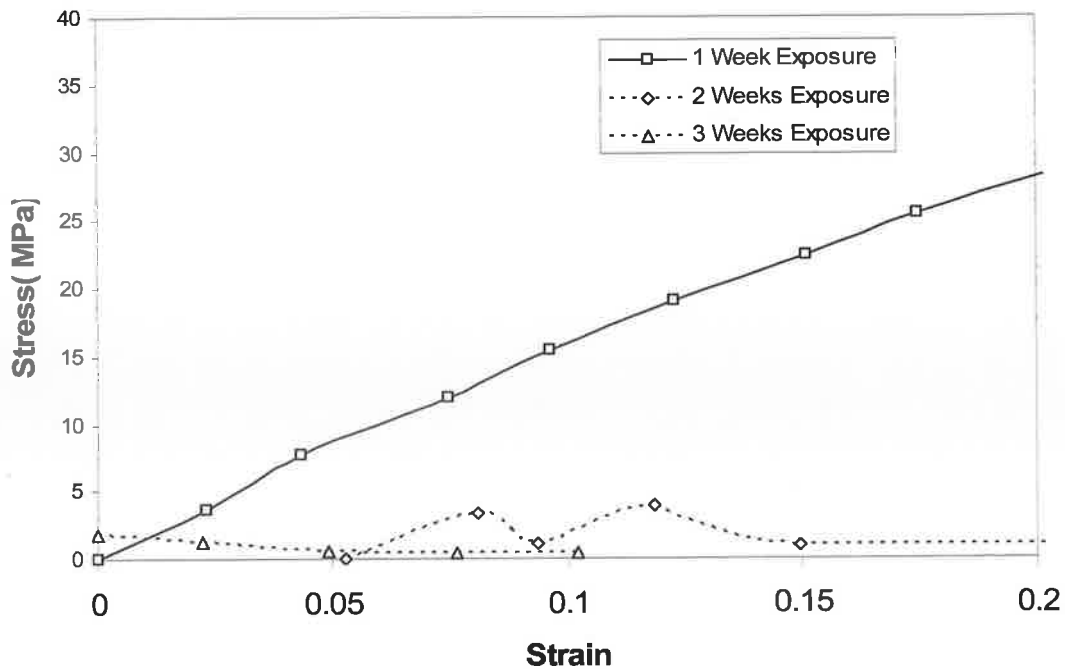


Figure 30: Effect of Exposure time on tensile bond strength of 304 L stainless steel

This measured tensile bond strength indicates that the corrosive solution had a limited influence and effect to the coating-substrate due to short period of exposure. However, for a specimen exposed for duration of two weeks, a significant reduction in bond strength was observed where the bond strength measured was 3.4 MPa. The coating film deposited onto the stainless steel substrate was examined by SEM and showed porosity distribution throughout the coating surface, coating dis-bonding and gap presence between the coating and the substrate. All these channels allowed for the corrosive solution penetrating through to the substrate causing accelerated corrosion attack to the mechanical bonding between the coating and the substrate. Finally, the specimen was exposed to three weeks corrosion solution demonstrated further bond strength reduction down to 1.86 MPa. This dramatic bond strength reduction is justified to extended corrosion exposure permitting corrosive solution reaching the substrate causing corrosion to the substrate and the mechanical bonding resulting in accelerating corrosion. Also, localized general surface and pitting corrosions were observed. The presence of gap between the coating and the substrate apparently allowed flow of the corrosive solution to the substrate causing crevice and local corrosion. Consequently, the coating-substrate bonding was affected by the corrosive solution lowering the coating bond strength. This may suggest that the porous structure of the coating permits the corrosion solution to reach the substrate surface therefore reducing the bonding strength of the coating. The aforementioned assessment is supported by the SEM micrograph shown in Figure 31 demonstrating the low bonding strength of the coating where a long discontinuity line along the coating-substrate interface occurs. This in turn lowers the bonding strength substantially. This may suggest that the porous structure of the coating permits the corrosion solution to reach the substrate surface reducing the bonding strength of the coating. Moreover, it is highly likely that the corrosive media penetrated through the discontinuity line causing crevice corrosion at the interface zone. This in turn lowers the bonding strength substantially.

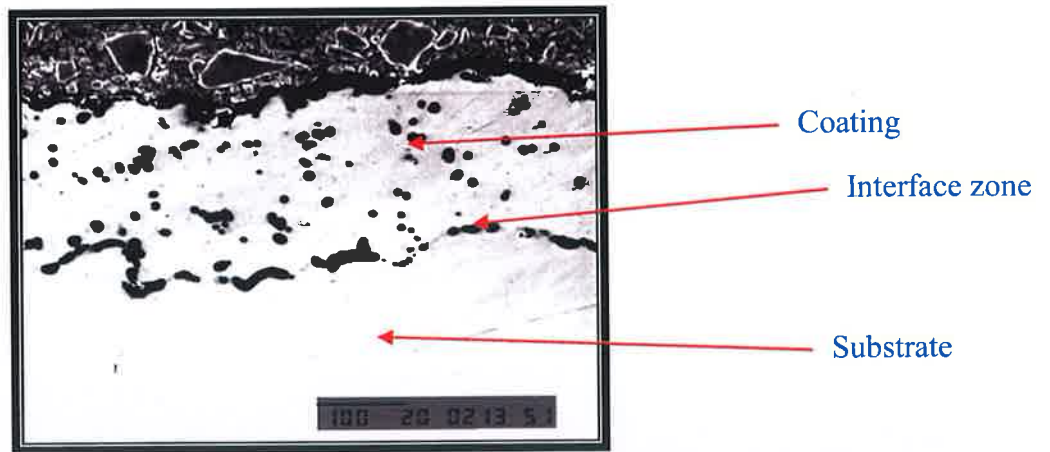


Figure 31: Coating cross section with discontinue line at the interface

The tensile bond strength for HVOF coated carbon steel specimen exposed to three different durations is shown in Figure 32.

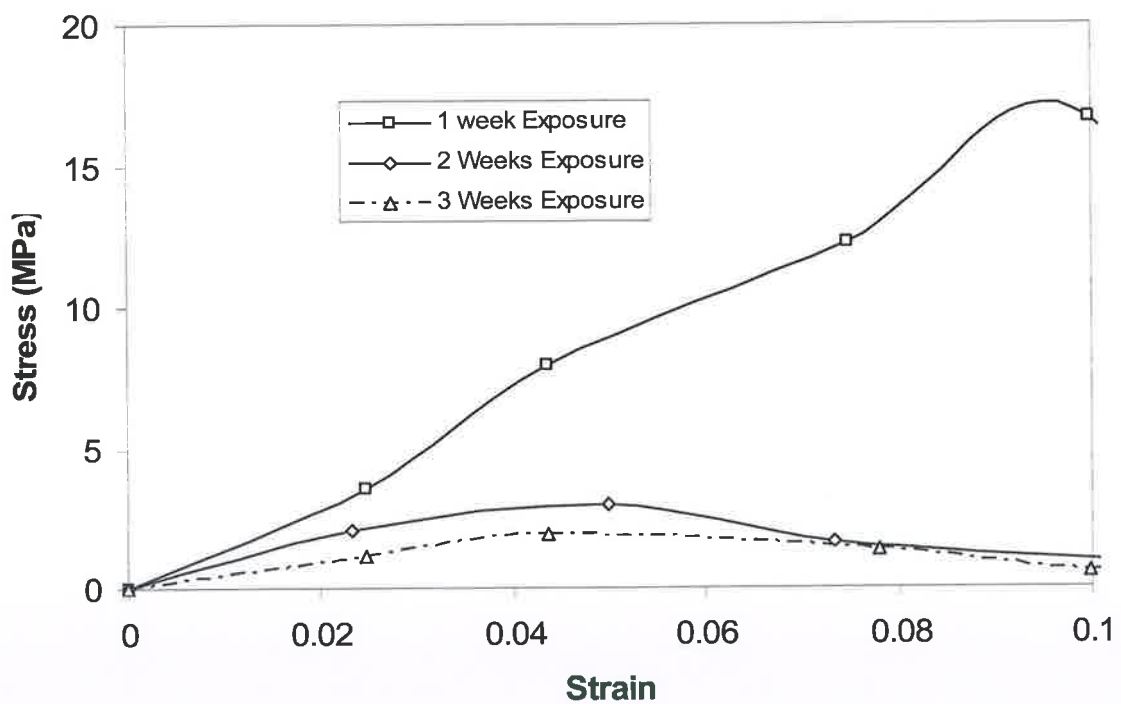


Figure 32: Tensile bond strength of carbon steel.

The specimen was exposed to one week immersion into a 3.5% NaCl solution showed high tensile bond strength close to 16.7 MPa indicating acceptable measured bond strength post one week exposure. However, for the specimen exposed for two weeks duration, a considerable reduction in bond strength was observed to be 2.96 MPa. The

coating film deposited onto the stainless steel substrate was examined by SEM and showed coating porosity level indicating possible corrosive solution penetration through the coating to the substrate. Also, coating boundaries showed clear lack of coating adherence onto the substrate could be due to un-melted coating particles and improper surface preparation permitting corrosive solution to cause coating surface corrosion and local pitting. Also, the substrate suffered from accelerated corrosion due to corrosive media settlement for two weeks lowering the bond strength. Finally, the specimen exposed to three weeks corrosion solution demonstrated further bond strength reduction down to 1.86 MPa. This dramatic decrease in bond strength due to extensive corrosion exposure permitting corrosive solution reaching the substrate causing local corrosion, pitting and surface general corrosion. Moreover, it is also possible that the corrosion solution penetrates through the discontinuity line, resulting in crevice corrosion at the interface. This in turn lowers the bonding strength substantially. The interfacial discontinuity here is not considerable. This may suggest that the porous structure of the coating permits the corrosion solution to reach the substrate surface reducing the bonding strength of the coating.

In the current case of the carbon steel specimens, a similar situation to that observed from the 304L stainless steel was noticed despite the fact that interfacial discontinuity was not considerable. This observation suggests that the porous coating structure permits the corrosion solution reaching the substrate surface. Consequently, the bonding strength of the coating is reduced.

#### 4.3 ESEM Evaluation of Inconel-625 Thermal Spray Coating (HVOF) onto Stainless Steel and Carbon steel Post Brine Exposure after Tensile Tests

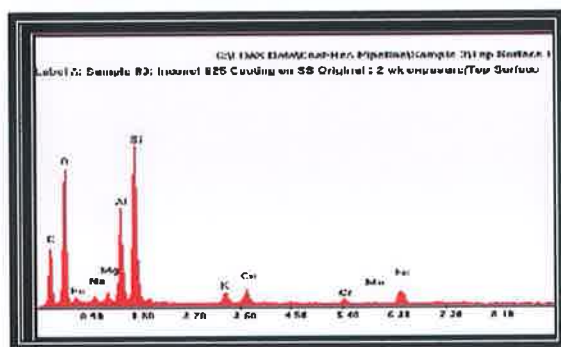
Elemental composition and microstructure of HVOF coating at the base material-coating interface was investigated after the tensile tests. Specimens were subjected to up to 3 weeks of exposure. Since all the specimens were sprayed under the same spraying conditions, exposure solution and tensile testing conditions, only the two weeks exposed specimen was selected for ESEM examinations. The backscattered electron images of the top surface of the stainless steel (SS) were subjected to two weeks in brine solution. The results after the tensile tests are shown in Figure 33. These images show some amount of silicate impurities (dark) on the original surface (bright) suggesting that the metal surface may have been contaminated during surface preparation prior to coating application due to time delay between surface preparations and coating spraying operation. The area percent of silicate impurity covering the surface is approximately 20% of the coated base material surface.



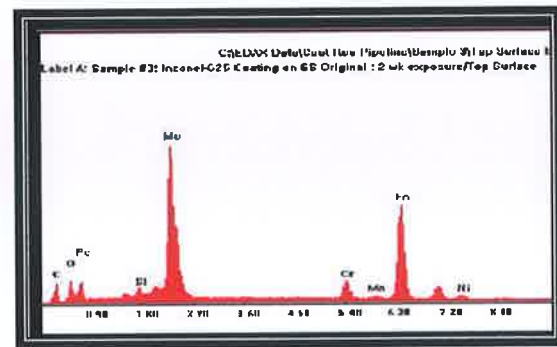
Inclusions on stainless steel surface



Dark inclusions on stainless steel surface



EDS Spectrum of dark inclusions

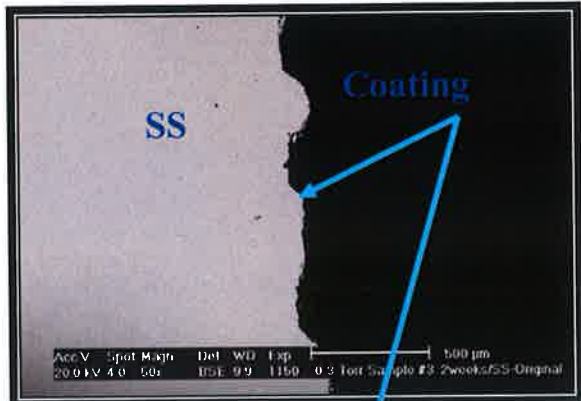


EDS Spectrum of a molybdenum-rich area of retained coating on the original stainless steel surface.

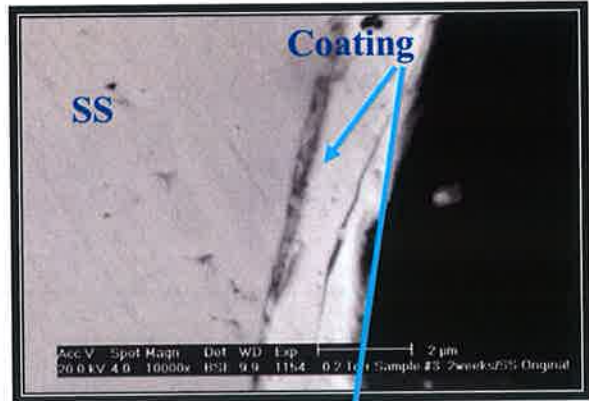
Figure 33: The area percent, and EDS spectrum of dark inclusions on top surface of Stainless steel specimen after tensile tests.

The cross-sectional images of the metal surface after the tensile tests are shown in Figure 34. Image A shows a low-magnification back scattered electron (BSE) image of the HVOF coated stainless steel surface post 2 weeks corrosion exposure. This image shows the cross-section nearly complete pullout of the coating by dummy. Images B through E demonstrate cross-sectional images of a 2  $\mu\text{m}$  wide coating fragment on the stainless steel surface at successive higher magnifications. Note presence of dark gray material at the stainless steel/coating interface and faint dark lines in the coating. Image F shows EDS x-ray spectrum indicating the presence of silicon and carbon at the stainless steel/coating interface. The observed Fe, Ni, Cr and Mo peaks in the spectrum are both from the coating and the stainless steel substrate. In these images a small fragment of the coating appears to be attached to the base material surface. From these images it can be noted that there exists a 0.25  $\mu\text{m}$  wide impurity layer between the coating and the base metal. Presence of this impurity certainly lowers the coating-substrate bond strength. The EDS analysis of this interfacial layer indicates that it is most likely iron-oxide and, since the specimen surface would be relatively inert to oxidation, the source of this layer appears to be iron-rich impurity in the Inconel-625 powder. The images of the top surface of the coating post the tensile test after being pulled-out by a dummy are shown in Figure 35 and Figure 36 respectively. The inset in the top image shows EDS X-ray elemental analysis of the coating. Following are revealed observations from Figure 36:

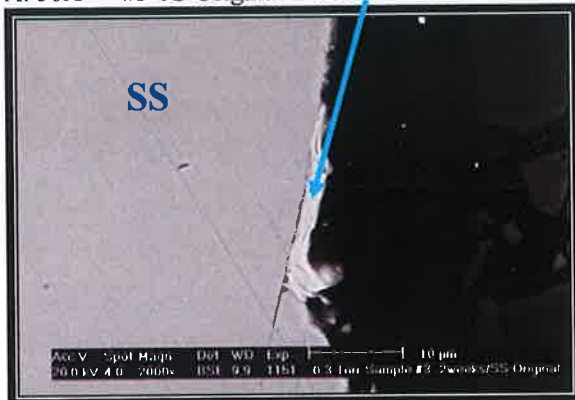
- Images A & B are backscattered electron images of Top Surface of the coating.
- Images C & D are for area percent of dark inclusions: ~16% at 57X magnification, and 24% at 200X magnification.
- Images E & F are for EDS X-ray spectra of dark inclusions in circled areas showing compositions similar to surface preparation material, Si-C in image A and K-Ca-Al-silicate in image B.
- These images also show considerable amounts of silicate-rich material, which is embedded in the coating matrix. The area percentage of this material ranges from 16 to 24%, and is analogous to the top surface of the metal substrate as shown in Figure 33.



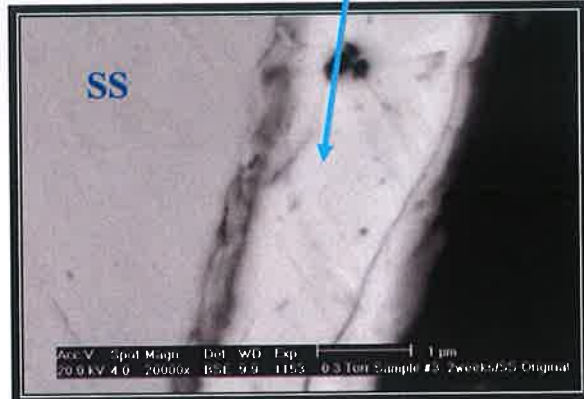
A: 50X #3 SS-Original 2 weeks cross-section



D: 10000X #3 SS-Original 2 weeks cross-section



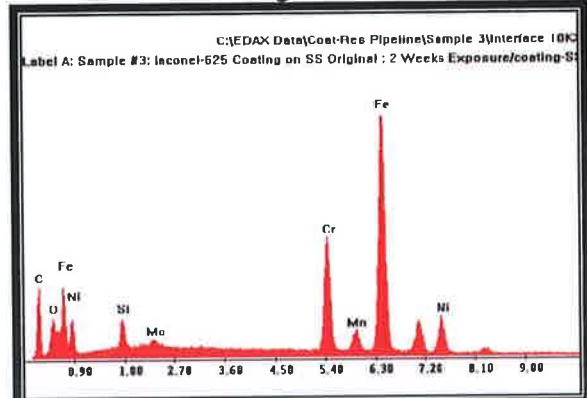
B: 2000X #3 SS-Original 2 weeks cross-section



E: 20000X #3 SS-Original 2 weeks cross-section

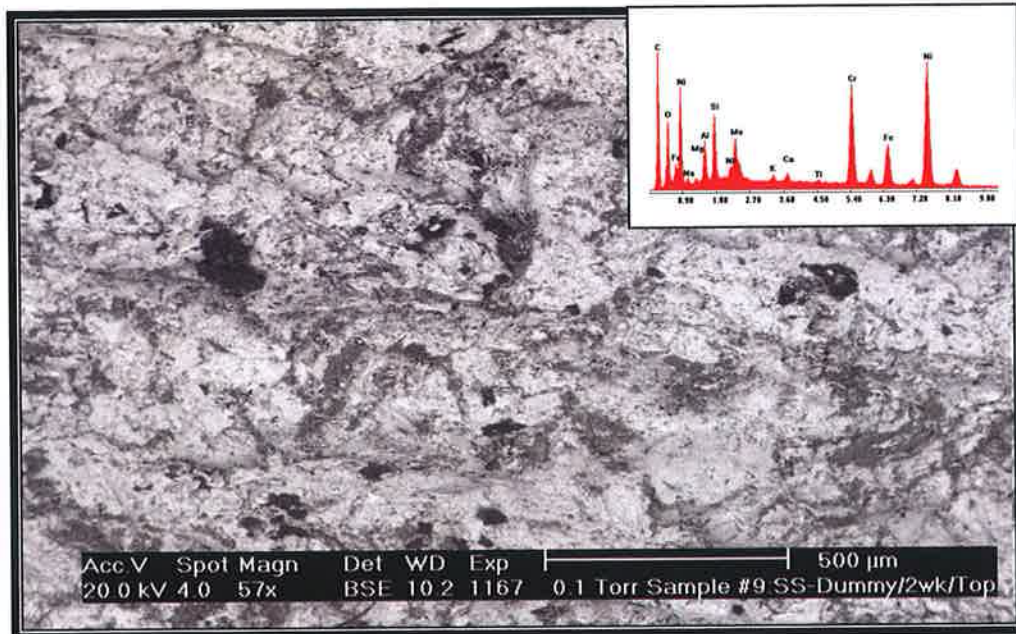


C: 5000X #3 SS-Original 2 weeks cross-section

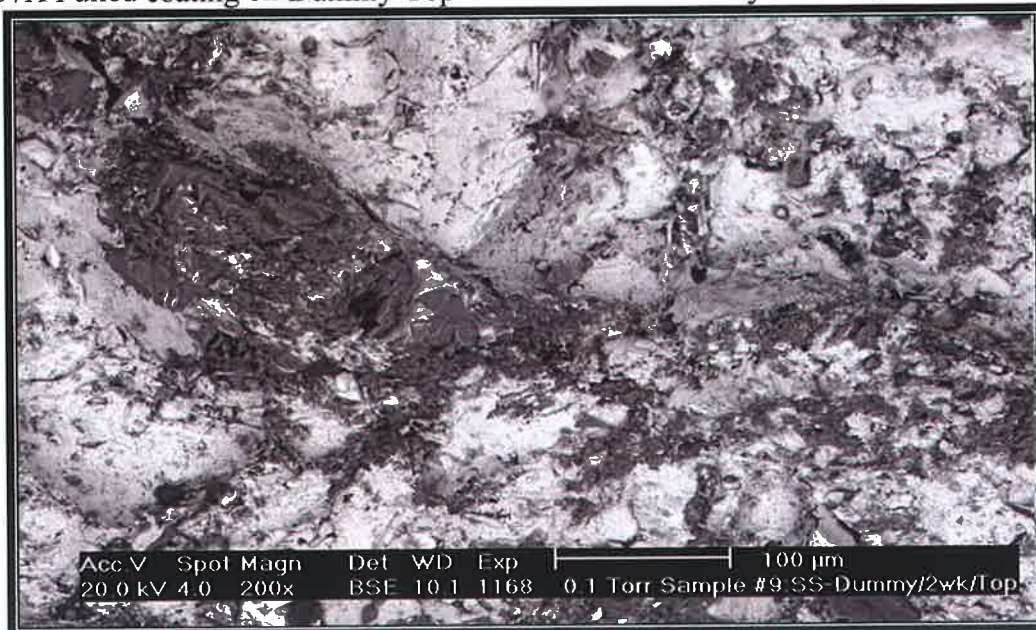


F: EDS X-ray Spectrum of interface material in D

Figure 34: Specimen# 3 is HVOF coated stainless steel surface exposed for 2 weeks original surface examination (not dummy specimen).



57X Pulled coating on Dummy-Top Surface #9 SS-Dummy-2 weeks.



200X Pulled out coating on Dummy-Top Surface #9 SS-Dummy-2 weeks.

Figure 35: Stainless steel specimen #9 SS Dummy post 2 weeks exposure Backscattered electron images (BSE) of the top surface of coating after being pulled out from the original SS surface by dummy specimen.



A: 57X Coating Top Surface on Dummy #9 SS Dummy 2/W



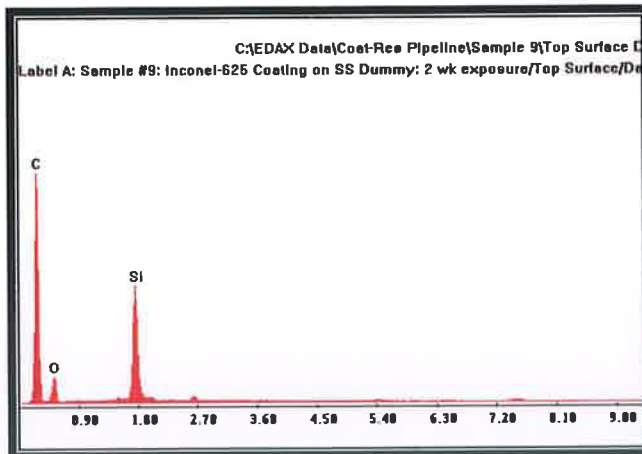
B: 200X Coating Top Surface on Dummy #9 SS Dummy 2/W



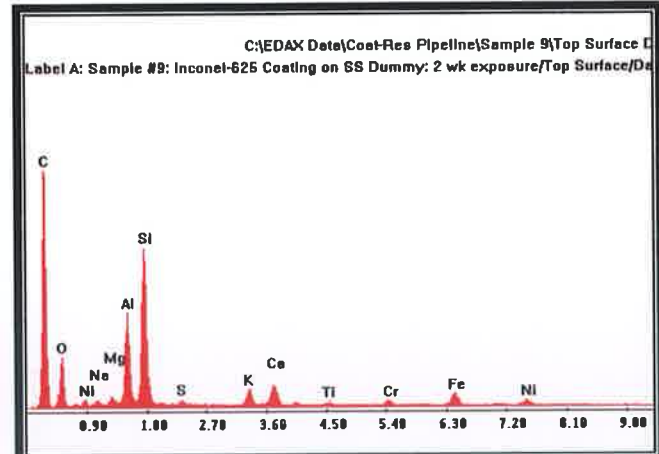
C: 57X Dark Area Fraction in A 16%



D: 200X Dark Area Fraction in B 24%



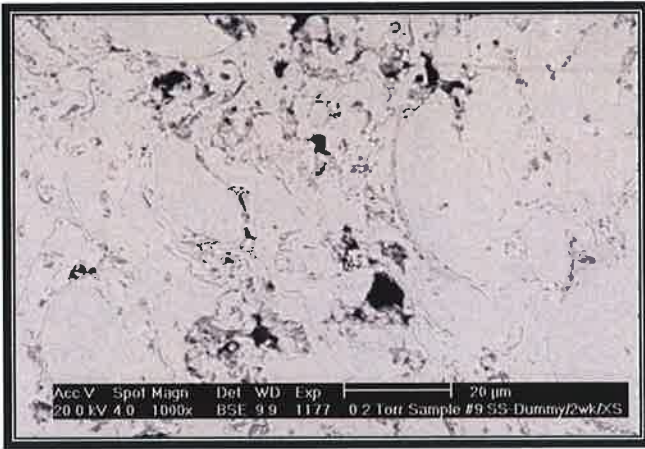
E: EDS-X-ray spectra.



F: EDS-X-ray spectra.

Figure 36: Sample #9 stainless steel HVOF coated specimen post 2 weeks static corrosion exposure for the original specimen. The above examinations are for pulled out coating onto a dummy specimen.

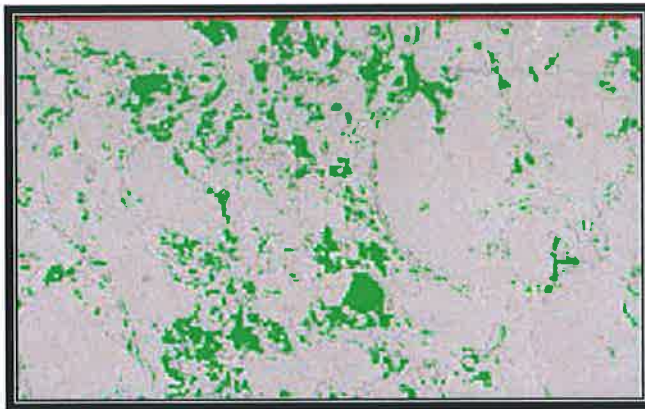
Figure 37 shows dummy stainless steel specimen after pull out from HVOF coated specimen exposed for two weeks. Figure 37 shows the backscattered electron images (BSE) of the top surface of coating after being pulled out from the original stainless steel surface by a dummy following two weeks of exposure to salt solution. Note dark inclusions in the bright coating matrix. The inclusions are most likely surface preparation material embedded in the original stainless steel surface prior to HVOF coating deposition. Images A and B represent coating cross section. Images C and D show the area percent of dark inclusions in A and B being approximately 8% at 1000X magnification, and 18% at 5000X magnification. Image E shows EDS X-ray spectrum of dark inclusions indicating they are mainly Cr-Nb oxide. Image F demonstrates EDS X-ray spectrum of the coating showing strong Ni, Cr and Mo peaks. Careful examination for the Figure 35, it is obvious that the cross-sectional image of the coating indicates that it was not affected by two weeks of exposure to brine. However, the images showed that it contained numerous process related inclusions and thin dark lines. The EDS analysis indicates that the inclusions are primarily oxides of Cr and Nb. It was also observed that the area percent increased with increasing magnification of the image. This suggests that there is significant variation in coating composition at the micron-scale.



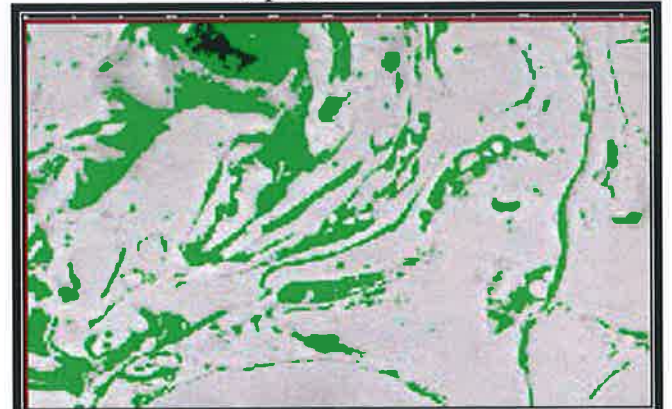
A: 1000X Coating Cross section on Dummy-SS after two weeks exposure to brine solution.



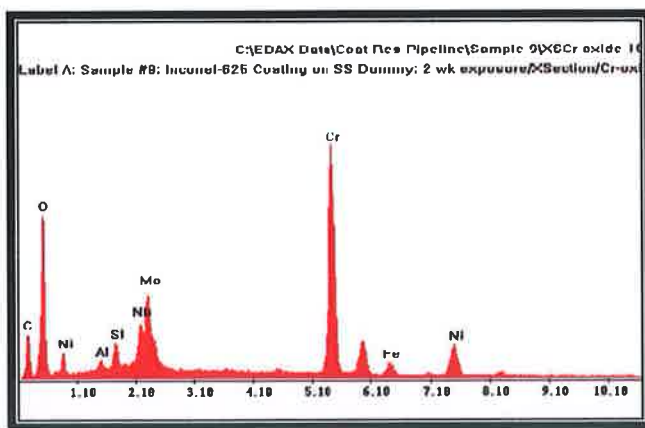
B: 5000X Coating Cross section on Dummy-SS after two weeks exposure to brine solution.



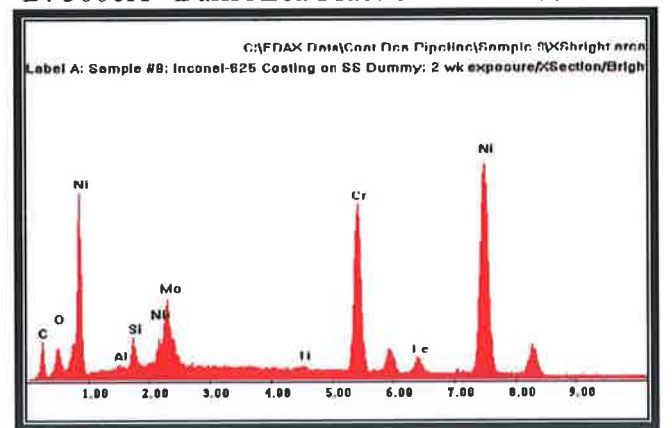
C: 1000X Dark Area Fraction in A 8%



D: 5000X Dark Area Fraction in B 18%



E: EDS X-ray spectrum of dark inclusions.



F: EDS X-ray spectrum of the coating.

Figure 37: Dummy Stainless Steel Specimen # 9 pulled out from original HVOF coated specimen exposed for 2 weeks.

The concentration profiles of Ni, Cr, Mo, Nb, Fe, O and C, as shown in Figure 35 which reveal that there is approximately 5-10% variation in the Ni content of the coating matrix, but more importantly the dark inclusions and lines show very high concentrations of Cr, Nb and O and concomitant decrease in Ni and Mo. This indicates that Cr and Nb are segregating out of the matrix as they are oxidized during the high-temperature coating

process causing brittle coating causing the coating to crack. The line-scan, ESEM images and EDS spectrum of the coating on the carbon steel specimen after three weeks of exposure to brine after the tensile test are shown in Figure 38 to Figure 40 respectively. The images show a significant amount of silicate impurity and iron-oxide and mild-rich contamination underneath the coating. The composition of the silicate suggests that it could be the material which was left on the specimen surface during surface preparation prior to coating. In contrast, the presence of iron-oxide together with small amounts of NaCl indicates that salt water must have penetrated through the coatings microscopically and corroded the base material (carbon steel). Figure 38 shows X-ray linescan of the coating cross section at 2000X Magnification. This linescan represents consecutive 128 analysis points on an arbitrary line A\_\_\_\_\_B on the coating. At each of the 128 analysis points on the line concentrations of seven elements (Ni, Cr, Fe, Mo, Nb, O and C) are measured. The data are then superimposed on the original image as color-coded scatter plots for each element. The plots show variations in elemental concentrations as line traverses from bright to gray to dark areas on the image. For example as the line traverses the dark inclusion in the center (red dots), Ni Wt% (red) decreases while Cr (yellow), O (blue) and Nb (brown) increases. This indicates that dark areas in the bright Ni-rich matrix are inclusions of Cr- Nb oxide or holes from defect in the coating or pulled out inclusions.

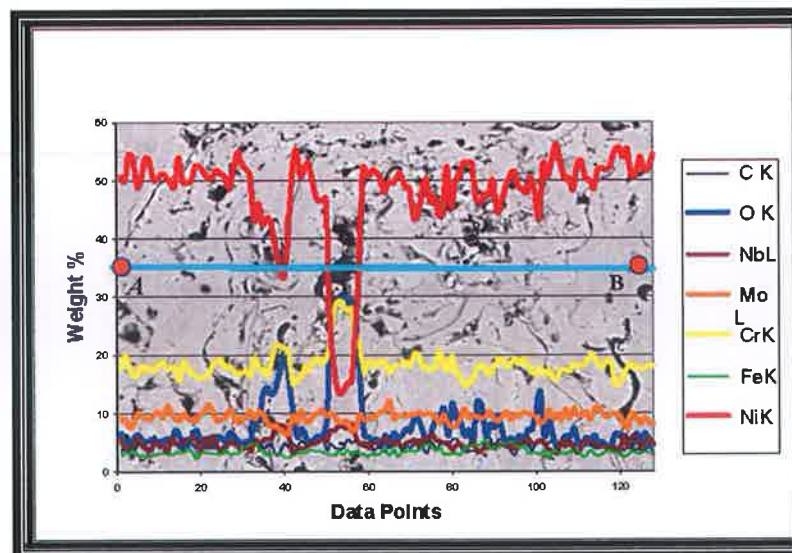
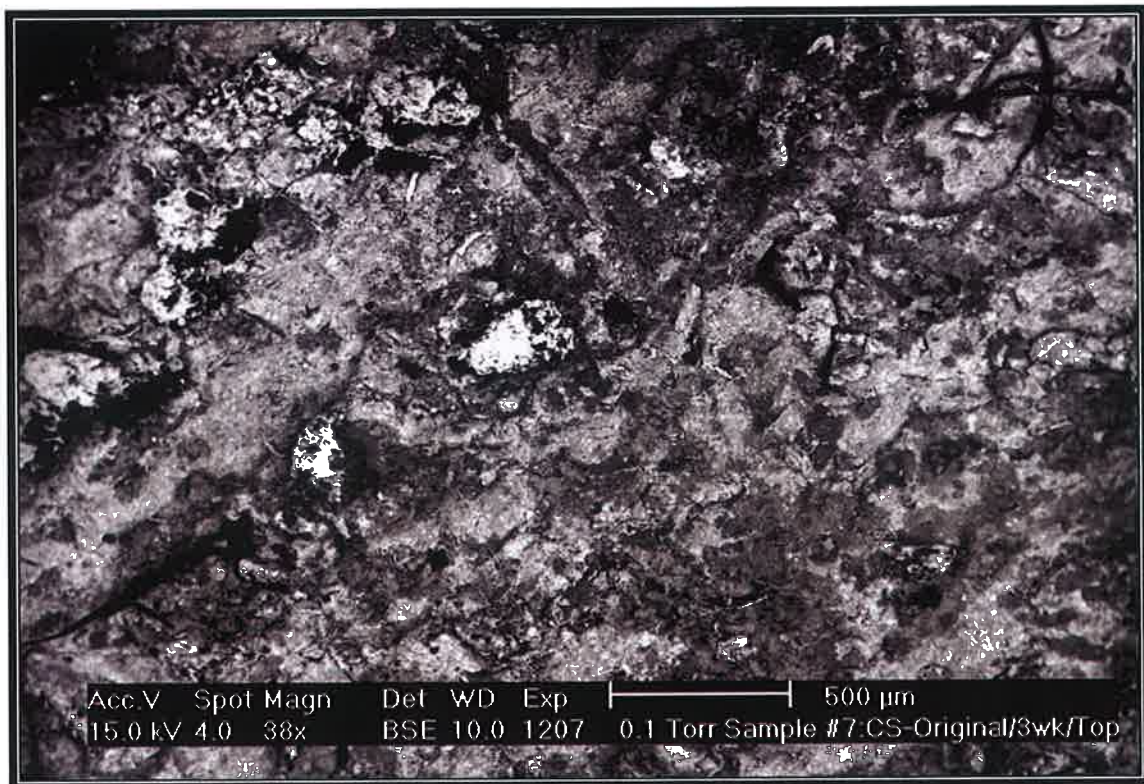


Figure 38: Line-scan of the coating cross section at 2000X magnification on 304L stainless steel exposed for 2 weeks left over on dummy specimen.



**A: 38X Original CS surface after coating pull out #7 CS-Original 3 weeks exposure.**



**B: 304X Original CS surface after coating pull out #7 CS-Original 3 weeks exposure.**

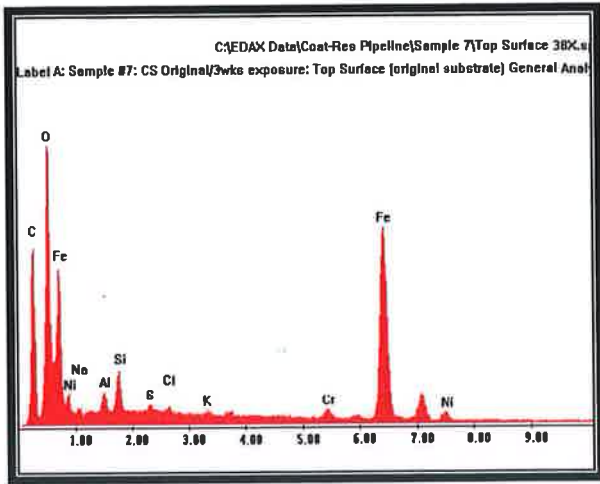
Figure 39: Specimen #7 original carbon steel post static corrosion exposure exposed for 3 weeks.

Figure 39 demonstrates backscattered electron images (BSE) of the top surface of the original carbon steel after the coating was pulled out following three weeks of salt water exposure. Image A is a low magnification image showing significant oxidation of the surface (gray matrix) and small amounts of retained coating (bright). Image B represents a surface preparation material (dark) and iron oxide corrosion products (bottom right) at 304 X magnifications. Carbon steel coated specimen was exposed for three weeks in brine solution. Below are revealed observations:

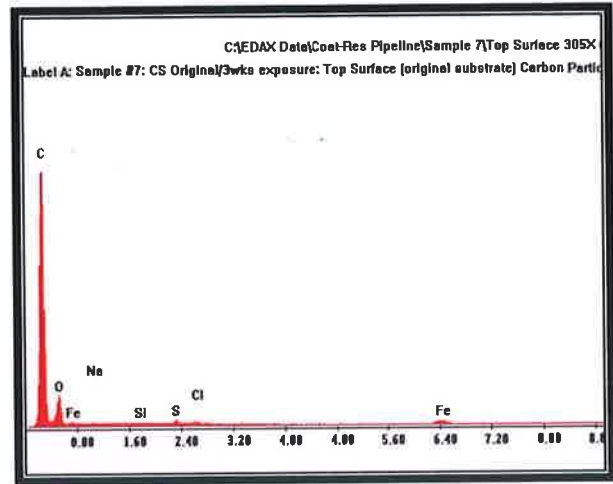
- Image A is a low magnification image showing significant oxidation of the surface (gray matrix) and small amounts of retained coating (bright).
- Image B refers to surface preparation material (dark) and iron oxide corrosion products (bottom right) at 304 X magnifications.

In Figure 40, several observations are concluded from the EDS spectra of the various elements observed from carbon steel top surface as follow:

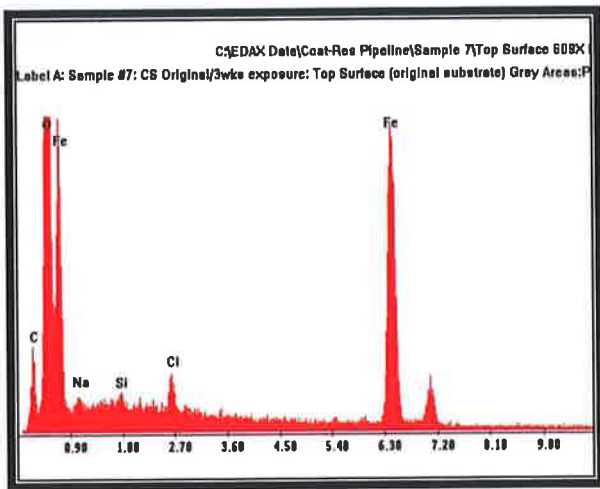
- Image A is for a CS surface after coating pull out showing strong O and C peaks.
- Image B is for an Oxide-rich area shown in Figure 39(B). Note presence of sodium and chlorine peaks.
- Image C Carbon-rich dark area at top left of the image in Figure 39(B).
- Image D is for Aluminum silicate inclusions (gray areas) in the center of the image in Figure 39(B). The spectra indicate water seepage through the interface between the coating and the base metal due to poor adhesion. The coating is not affected by salt-water exposure.



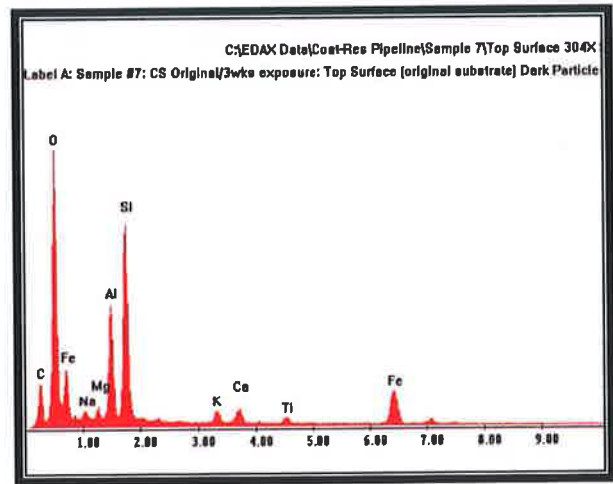
A: CS surface composition after coating pull out



C: Carbon-rich area



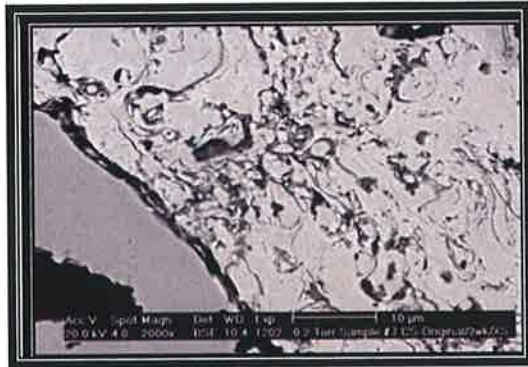
B: Iron oxide corrosion product



D: Silicate inclusions

Figure 40: Specimen #7 original carbon steel coated specimen (not dummy) exposed for 3 weeks duration. – Top Surface: EDS X-ray spectra of various phases observed on the CS surface.

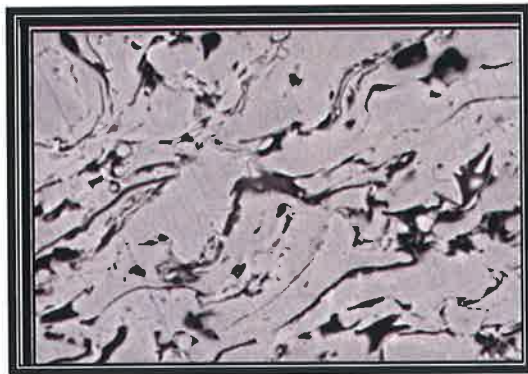
Figure 41 shows cross-sectional images of a small fragment of the coating attached to the base metal. The numerous dark inclusions seen on the micrograph are similar to those seen on stainless steel. The area percent of these inclusions is determined to be approximately 9%.



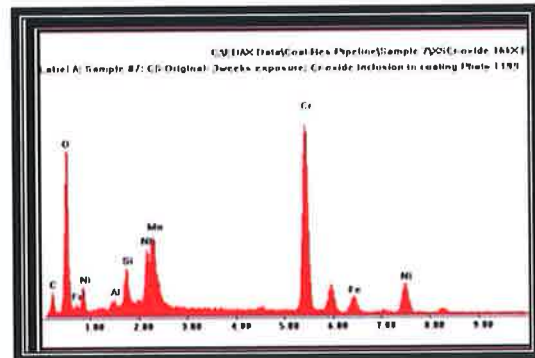
Cross section of coating on a carbon steel specimen after three weeks exposure to brine solution.



Cross section of coating on a carbon steel specimen after three weeks exposure to brine solution.



Cross section of coating on a carbon steel specimen after three weeks exposure to brine solution.



EDS spectrum of the inclusion.

Figure 41: SEM micrographs of carbon steel in cross section and EDS Spectra of the inclusion.

The EDS spectrum of the inclusion in Figure 41 indicates that it is primarily a chromium-oxide inclusion in which niobium or niobium oxide particles are dispersed as sub-microscopic inclusions (bright dots). The discrete nature of Cr and Nb suggests that, even though these elements are associated together, only Cr might be undergoing preferential oxidation during the high-temperature coating process.

Figure 42 shows the top surface of the coating that was in contact with the base metal

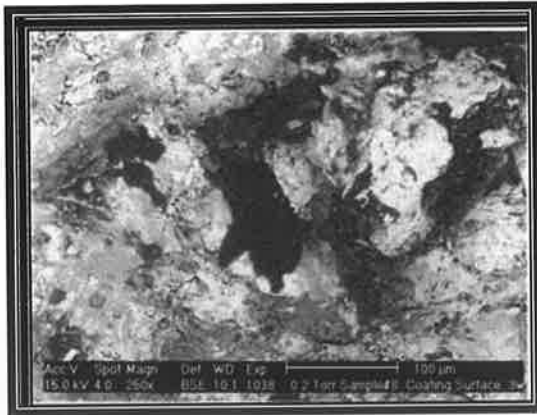
before being subjected to the tensile test. The surface shows numerous impurities and iron-oxy hydrate similar to that observed on the mating carbon steel substrate. These images reveal evidence that the coating was not completely fused with the base metal owing to the presence of impurities and iron-oxide on the surface of the metal. The images also indicate that water must have entered the interface between the coating and the base metal through microscopic openings surrounding the impurities, thus resulting in the corrosion of the metal and weakening of adhesion between the coating and the base metal.



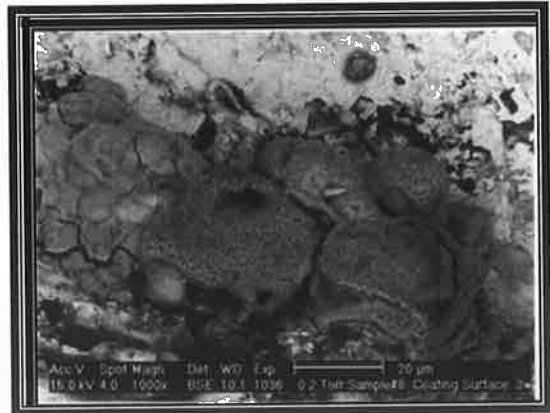
Coating remained on top surface of carbon steel dummy after three weeks exposure to brine solution.



Coating remained on top surface of carbon steel dummy after three weeks exposure to brine solution.



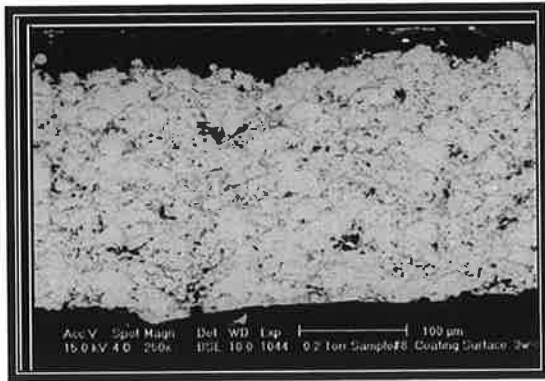
Coating remained on top surface of carbon steel dummy after three weeks exposure to brine solution.



Coating remained on top surface of carbon steel dummy after three weeks exposure to brine solution.

Figure 42: SEM micrographs of the top surface of the coating after being pulled out from the carbon steel dummy following three weeks of exposure to brine solution.

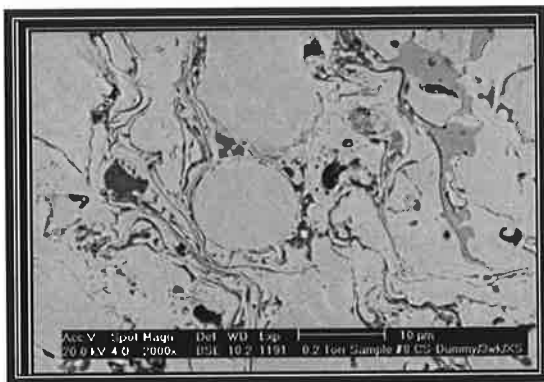
The cross-sectional images of the coating on carbon steel after being pulled out from a carbon steel dummy are shown in Figure 43. In the micrographs the coating has a composition and microstructure similar to those observed on stainless steel. The coating contains numerous dark inclusions and lines which, as before, are segregated areas of chromium-oxide in the nickel-rich matrix.



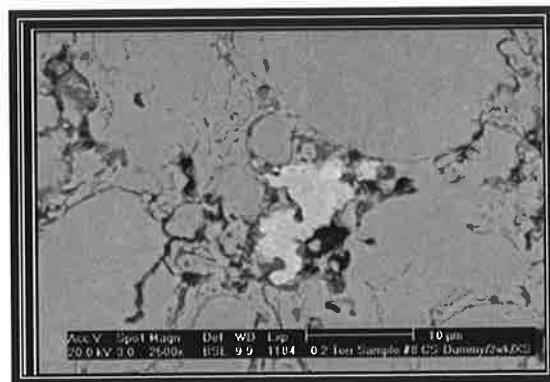
Coating cross-section on a carbon steel dummy after three weeks exposure to brine solution.



Coating cross-section on a carbon steel dummy after three weeks exposure to brine solution.



Coating cross-section on a carbon steel dummy after three weeks exposure to brine solution.



Coating cross-section on a carbon steel dummy after three weeks exposure to brine solution.



Coating cross-section on a carbon steel dummy after three weeks exposure to brine solution.



Coating cross-section on a carbon steel dummy after three weeks exposure to brine solution.

Figure 43: SEM micrographs of a coating cross section after being pulled out from a carbon steel dummy.

Certain zones demonstrated about 5% porosity while other zones in the microstructure demonstrated 15% to 20% porosity level. The coating does not appear to have any pores or voids except for minor pull-out of chromium-oxide inclusions. The coating will therefore be impervious to water or any other corrosive agents and should protect the base metal from corrosion. However, this does not seem to be the case with this specimen since the base metal appears to have undergone corrosion - even though it is well protected by the coating. The reason for this inconsistency is attributed to the significant presence of impurities on the metal surface prior to the application of the coating. Since these impurities do not bond properly to either the metal or the coating, they would leave microscopic void space at the interface through which water can enter and corrode the surface. The consequence of such corrosion will be premature failure of the coating.

#### 4.4 Tensile Properties of HVOF Sprayed Inconel 625 Coating (Tensile Specimens (in flat sheet form))

A combination of coated tensile specimens (in flat sheet form) was prepared from carbon steel and 304 stainless steel alloy. A total of twelve (12) coated specimens were selected for tensile testing. Selected specimens were exposed to a static corrosion environment. Tensile tests were performed on all the twelve specimens prior and post static corrosion testing. The tensile properties of HVOF sprayed Inconel 625 coatings were examined. The influence of aqueous corrosion on the mechanical and interface properties of HVOF coatings was studied. Figures 44 to Figure 46 represent micrographs of an HVOF coated stainless steel specimen cross-section and preferential corrosion regions around the splat for three weeks corrosion test duration exposure. Figure 44 shows a micrograph of the coating cross-sections indicating slight porosity in the coating. Also, it is visible that the coating is in the form of a layered structure typical of thermally deposited powders. The dark and the light regions shown in the coating are due to oxide and metallic phases.

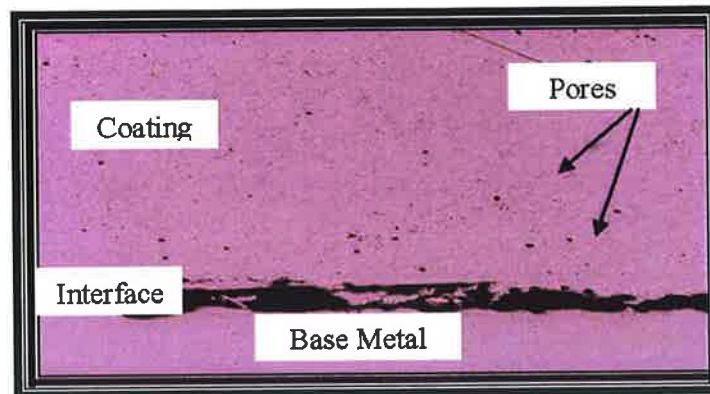


Figure: 44: Coating cross-section

The local presence of oxide stringers is apparent from Figure 45. Stringers contain a high amount of oxygen and are often rich in Cr, Nb, and Mo. In addition, some small numbers of un-melted powder particles are identified. Some slight porosity is observed in the coating and the cavitations in the coating-base metal interface appear to be small and scattered locally.

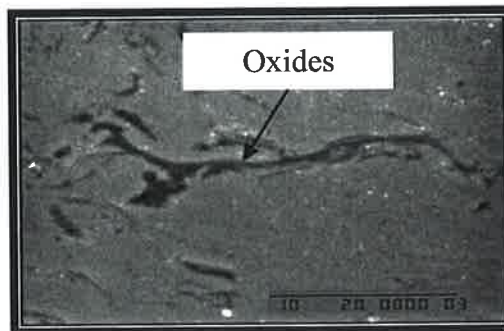


Figure 45: Micrograph of stringer in the coating. The dark color is the oxides.

In the case of specimens subjected to static corrosion exposure testing as shown in Figure 46, a network of pores within the coating provides a path for the electrolyte to pass through the coating. This results in preferential corrosion around the splat boundaries. Consequently, corroded splats have higher oxide contents. However, lateral cracking of the splats due to oxide induced expansion is not observed in the coating. The corrosion occurs when the electrolyte reaches the coating-base material interface. The local cavitations at the interface accelerate the corrosion rate, particularly on the steel surface. This in turn causes local de-lamination at the interface.

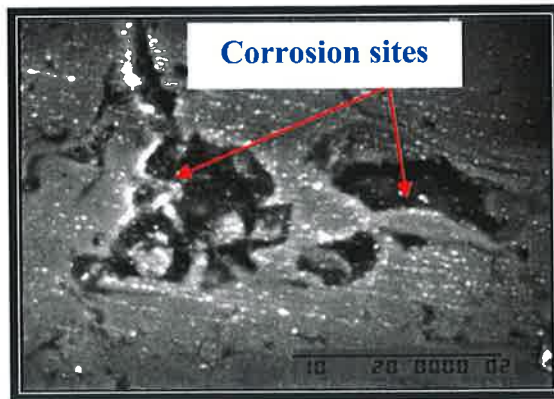


Figure 46: Micrograph of preferential corrosion regions around the splat boundary post three weeks static corrosion tests.

Figure 47 shows micrographs of the coating surface and crack site. When the crack site is examined closely the coating edge de-lamination under the action of stress above the plastically deformed region is observed. Shear failure in the surface region can be related to the differences in coating and substrate material elastic module. When the local critical stress for crack propagation is reached, an elongated crack along the coating surface occurs. In this instance, coating does not conform to the plastic deformation produced along the crack sites. This in turn initiates splitting separation between layered columns in the coating. Consequently, shear deformation of the columns is responsible for cracking and the total failure of the coating. It should be noted that when the coating is fractured the internal stresses in the coating interface are relaxed.



Figure 47 - Micrograph of a crack site in HVOF coating (15X magnification).

If the energy used to propagate these cracks is dissipated the effect of crack propagation on the specimen diminishes, which in turn increases the magnitude of rupture stress as seen from Figure 47. Similar investigations were performed by Al Fadhli et al [186, 187, 200]. The authors studied the tensile properties and corrosion performance of HVOF sprayed Inconel 625 coatings. The authors concluded that the coating was deteriorated due to presence of oxides and cavitations accelerated the corrosion attack to the substrate. Also, the authors observed crack formation in the coating layer that helped in relieving the stress levels avoiding spalling or buckling of the coating. Apparently, the current study and previous studies agreed with each other in their findings. Tensile tests have been carried out on HVOF coated specimens comprising 304L stainless steel and carbon steel prior and post static corrosion exposure. All the tensile tests and corrosion exposure were performed under standard conditions. The tensile results for the 304L stainless steel specimens are shown in Figure 48 A while those tensile results performed on the carbon steel are shown in Figure 48 B. Figure 48 A shows the tensile stress for 304 L stainless steels specimens prior to static corrosion exposure and for specimens exposed to one week and three weeks static corrosion respectively. The broad tendency for the curves in the elastic region is similar. Minor variations are observed in the elastic region for all the tested specimens beyond the tensile 12.2 KN. However, the maximum load was achieved by the coated non exposed (as received condition) specimens. It is obvious that the tensile tested coated non exposed specimen showed improved elastic-plastic properties. The one week exposed specimens' demonstrated enhanced elastic-plastic properties than the three weeks exposed specimens. The plastic deformation for both the one week and three weeks exposed coated specimens shows negligible variation associated with the exposure period where eventually they behave similarly. While the tested coated non exposed specimens showed improved plastic properties than all the exposed specimens. The specimens exposed to three weeks static corrosion demonstrated lower elastic and plastic stress levels compared to the non exposed in the as received coated specimens and the one week exposed specimens. Apparently, the one week exposure to static corrosion has a negligible effect to the elastic-plastic properties of the coating while the extended exposure period decreases the coating resistance to the corrosion lowering tensile stresses. From microscopic examinations including SEM and optical microscopy, those

specimens were exposed to three weeks exposure to static corrosion demonstrated surface cracks developed within the coating at a distance away from the region where the total failure of the material occurred. The corrosion effect in the surface region causes failure of the coating through early crack formation during the tensile testing. The plastic deformation of the specimens subjected to the three weeks corrosion testing shows the corrosion effect extends to the substrate material influencing the plastic deformation on the contrary where three weeks exposure to corrosion shows minor effect on the elastic response of the specimens. The yielding limits for all the tested specimens differ little indicating excellent coating resistance to the corrosion exposure. It should be noted that tensile tests are terminated if either the coating or the substrate material fail. The elastic deformation of the coated specimen tested with and without corrosion is similar. However, in the region of initiation of the plastic zone there considerable differences are observed. In this case a coated specimen subjected to three weeks of static corrosion fails at a lower load than the non exposed coated specimens. In this case the stiffness of the coating changes due to corrosion effect and results in early failure. It is also possible that micro-cracking due to the impact of some un-melted powder particles results in residual stress sites, particularly at the coating-base material interface. Poor bonding adds to this effect at the interface. These defect sites can act as stress risers and contribute to sub-surface crack initiation and propagation. The differences in the elastic modulus between the coating and the base material accelerate crack initiation and propagation. The tensile cracking in the coating accelerates through crack propagation in the shear mode. This increases with tensile load. In this case the elastic flow of substrate material and plastic flow of the coating leads to conformity of interface. Increasing the tensile load further causes the coating to flow in the plastic region and the substrate material can no longer support the coating. This results in the cracking of the coating. Once this stage is reached de-lamination failure and spalling occurs due to the extensive crack propagation along the subsurface and to the interface defects. Spalling is therefore triggered at the boundaries of the microstructural defects in the coating.

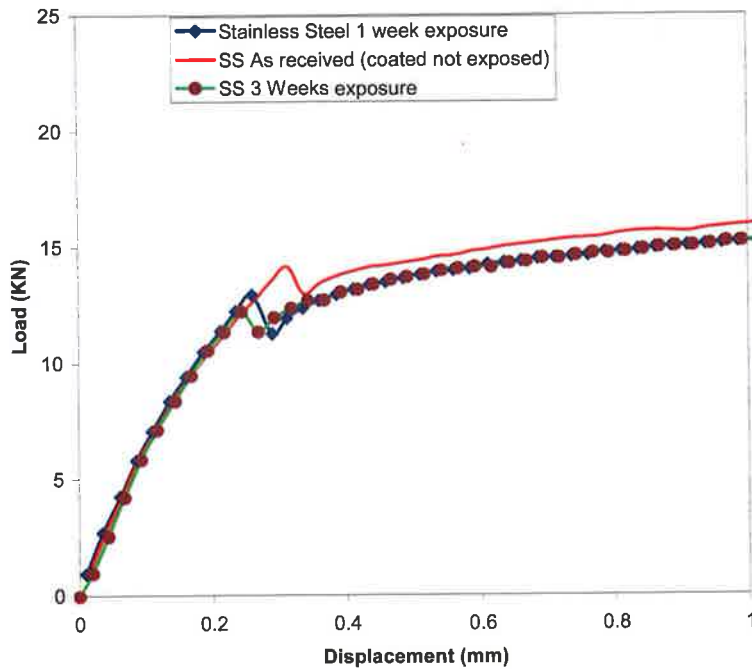


Figure 48 A: Tensile test results for HVOF coated 304 L stainless steel specimens prior and post static corrosion exposure.

Figure 48 B shows the tensile stress for carbon steel specimens prior to static corrosion exposure and for specimens exposed to one week and three weeks static corrosion respectively. In the elastic region, all the tested specimens (including exposed and non exposed) response to the tensile load is similar with exception to minor variations could be related to experimental errors. Similar situation is observed for the plastic behavior of the substrate indicating good coating resistance. Minor variations are observed in the elastic region for all the tested specimens beyond the tensile 11 KN. However, the maximum achieved load at yield was 13 KN. It is evident from the curves that all the specimens are yielding almost at the same magnitude indicating influence of the static corrosion exposure. The minor variations observed from both the elastic and plastic regions are associated with the errors related to the experiments repetition. The tested non exposed specimens' showed improved elastic plastic properties compared to others. Additionally, the one week exposed coated tested specimens still showing enhanced elastic plastic properties than the three weeks exposed tested specimens. It is obviously

concluded the gradual effect of the static corrosion in lowering the bonding strength of the specimens depending on the exposure period.

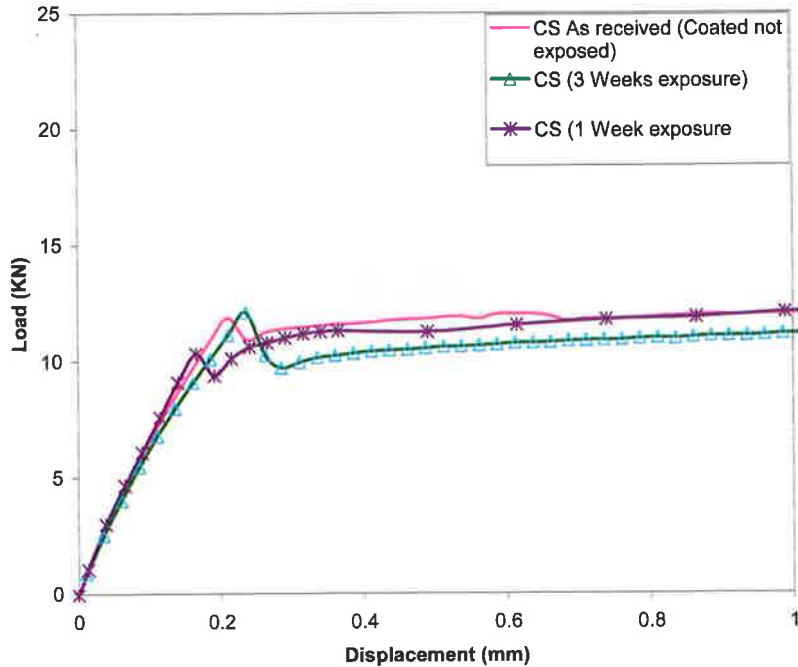


Figure 48 B: Tensile test results for HVOF coated carbon steel specimens prior and post static corrosion exposure.

Al-Fadhli [200] conducted tensile tests examining the elastic and plastic properties of the HVOF Sprayed Inconel 625 Coating onto steel surfaces. The author performed several tests examining the influence of static corrosion exposure on the tensile properties of HVOF coated specimens with Inconel 625 powder coating. Overall, the results obtained by the author showed similar behavior mainly in the elastic regions to those examined in this current research work.

#### 4.5 Fatigue Testing of Inconel-625 Coatings onto Carbon steel and Stainless Steel Flat Sheet Surface

The inconel-625 coatings on flat sheets stainless steel and carbon steel specimens were examined after exposure to an electrolytic solution for 1 and 3 weeks prior to fatigue testing. The averages cycles to failure for those specimens exposed to one week and three weeks corrosion environment are shown in table 10. The one week exposure of carbon steel demonstrated a life of 17000 cycles while three weeks exposure showed a life of 15720 cycles as given in Table 10. This average was made based on fatigue testing of five specimens each. However, the fatigue response of coated stainless steel specimens exposed to electrolytic solutions is found to be more resistant and resulted as a run out compared to corresponding carbon steel specimens.

Table 10: Fatigue cycles failure for coated carbon steel.

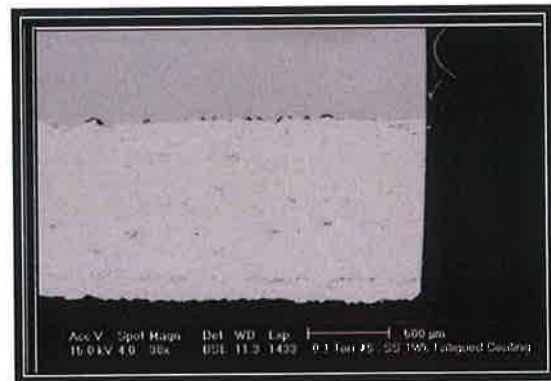
<b>Exposure Period (Weeks)</b>	<b>Cycles to Failure</b>	<b>Number of Coated Tested Exposed Specimens</b>
1	17000	5
3	15720	5

Figure 49 shows SEM micrographs and EDS spectrum of coating on Stainless Steel flat sheet specimens subjected to electrolytic solution for one week prior to fatigue testing. The low-magnification images of the left edge, right edge and centre of the coating show virtually no effects on the integrity and adhesion of the coating. However, at the interface between the coating and the specimen surface numerous impurity particles are locally observed. The presence of these particles, which are presumably the impurities left over from the surface preparation process, appears to have no significant effect on the integrity of the adhesion of the coating to the base metal. This finding clearly indicates the improved adherence of coating onto the flat sheets steel surfaces compared to the early round solid bars where the presence of impurities had a significant effect on the integrity of the adhesion of coating onto the substrate. Left and rights edges are shown in A and

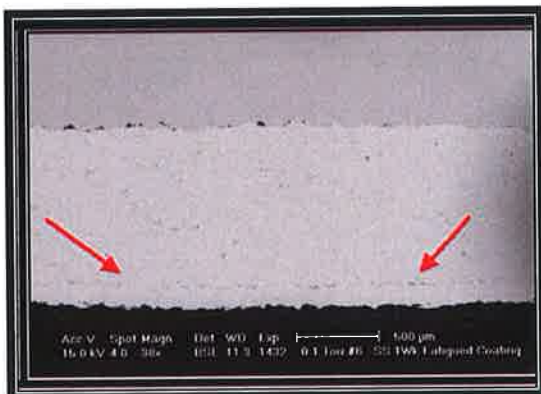
B respectively. The middle zone is shown in C. Bottom edge is shown in D demonstrating inclusions presence. Image E shows coating/Stainless Steel interface while image F shows EDS X-ray spectrum of coating. Note the absence of any fatigue induced major or minor cracks in the coating, and a faint line of inclusions in the coating about 150  $\mu\text{m}$  from the bottom edge (arrows in A& C).



A: 38X Left Edge (See arrows explanations)



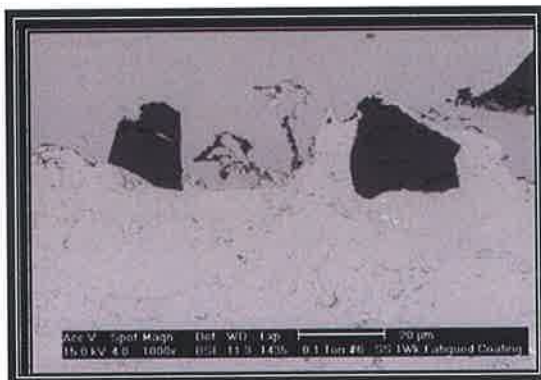
B: 38X Right Edge



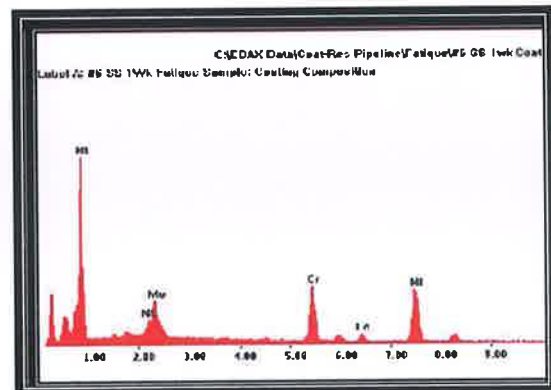
C: 38X Middle (See arrows explanations)



D: 250X Bottom Edge



E: 1000X Interface



F: EDS X-ray Spectrum of Coating

Figure 49: Fatigue tested stainless steel in 1 week solution of BSE images.

SEM examinations for the coating on a stainless steel specimen with three weeks exposure to the electrolytic solution reveals that there is no significant effect on the integrity and adhesion of the coating to the base material as shown in Figure 50. Consequently, fatigue induced stresses do not have undue influence on the microstructure at the interface between the coating and the specimen surface. BSE images showing (A) left edge, (B) right edge (C) middle, (D) bottom edge. (E) coating/Stainless Steel interface and (F) EDS X-ray spectrum of coating. Note the absence of any fatigue induced major or minor cracks in the coating, dark impurities at the coating/Stainless Steel interface in (E), and a line of iron oxide inclusions 150  $\mu\text{m}$  away from the bottom edge of the coating in C and D.

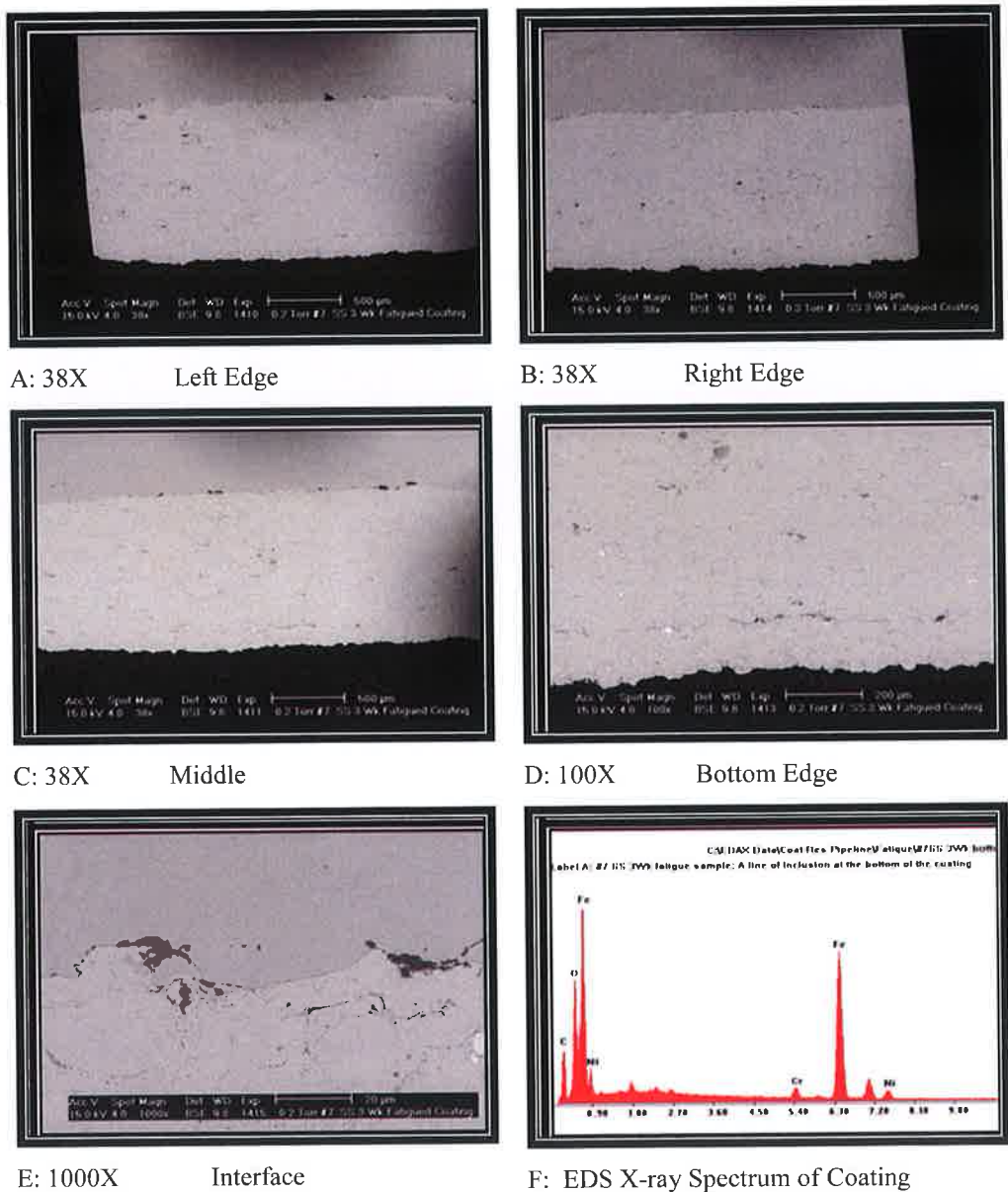


Figure 50: Fatigue tested stainless steel after 3 weeks in electrolytic solution

The images of the coatings on carbon steel after one and three weeks of fatigue through SEM examination are shown in Figure 51 and Figure 52 respectively. The images show no detrimental effects of fatigue induced stresses on the integrity of the coating. Moreover, the coating/specimen interfaces of both specimens show significant gaps or lack of adhesion to the base metal. This lack of adhesion is more pronounced for the specimens exposed to solution for three weeks. This may be related to the presence of oxide compounds at the interface. However, the amount of oxide compound in the coating depends on the flight-time and temperature of the

splats. In this case, high velocity and short flight-time results in less oxygen content of the splats. However, it was reported that lowering the splat temperature might avoid the oxidation, but it would also reduce the adhesion of the splats onto the specimen surface. Figure 51 shows fatigue tested carbon steel after 1 week in electrolytic solution. The BSE images show (A) being the left edge, (B) right edge, (C-D) middle, and (E) coating/Carbon steel interface and (F) EDS X-ray spectrum of coating. Note the absence of any fatigue induced major or minor cracks in the coating. Figure 52 shows fatigue tested carbon steel after 3 weeks in electrolytic solution. The BSE images show (A) being the left edge, (B) right edge, (C) middle, (D) coating/carbon steel interface and (F) EDS X-ray spectrum of coating. Note absence of any fatigue induced major or minor cracks in the coating, but significant separation at the coating/metal interface. The dark spots in (A, B and C) are droplets of oil, presumably from improper cleaning after polishing the surface. The high oxygen content observed from an EDS graph (Figure 51 and Figure 52) indicates that the splat temperature was high. In addition, the possible formation of the oxide compound at the coating-specimen interface enhances the brittleness of the interface. Moreover, due to high speed impact of the splats, the specimen surface hardens.





Figure 53. Figure 54 shows that the coating has peeled-off from the specimen surface particularly at the fractured ends. Al Fadhli et al [38, 200] studied the fatigue and corrosion behavior of stainless steel specimens HVOF coated with Inconel-625 alloy. Similar conclusion was observed by the authors where the a considerable reduction in the fatigue strength of the coating when subjected to long period static corrosion exposure. Also, the authors observed from SEM examinations that fatigue cracks were formed at both the interface between the coating and substrate as well as within the coating. Moreover, presence of non melted particles and voids within the coating and alumina particles on the substrate beneath the coating contributed to crack initiation within the coating and the coating-substrate interface. Accordingly, the coating microstructure enhanced the fatigue behavior of the coated surfaces.



Figure 53: A photograph showing carbon steel smoothly broken specimen posts one week static corrosion exposure in electrolytic solution after fatigue failure.



Figure 54: A photograph showing coated carbon steel specimen post 3 weeks static corrosion exposure after fatigue failure. Peeling-off coating from the base material is evident.

## 4.6 Tensile and Fatigue Properties of Inconel-625 Coatings Deposited Onto Welded Carbon steel and Stainless Steel Specimens

### 4.6.1 Stainless Steel Welded-Coated Specimens

A combination of 304 stainless steel welded specimens was HVOF coated using Inconel 625 powder. A total of twenty (20) coated specimens of variable weld size were selected of variable weld size for tensile and fatigue testing. Partial selection of those welded coated specimens was exposed to a static corrosion environment prior to performing the mechanical testing. The mechanical property tests were performed on (i) as received welded coated specimens with no exposure to corrosive media and (ii) welded-coated specimens exposed to corrosive media.

### 4.6.2 Carbon Steel Welded Coated Specimens

A combination of carbon steel welded specimens was HVOF coated using Inconel 625 powder. A total of twenty (20) coated specimens of variable weld size were selected for tensile and fatigue testing. Partial selection of those welded-coated specimens was exposed to a static corrosion environment prior to performing the mechanical testing. The mechanical properties tests were performed on the HVOF coated welded specimens prior and post corrosion exposure.

### 4.6.3 Tensile and Fatigue Tests for Welded-Coated Stainless and Carbon Steel Specimens

Tensile and fatigue tests were performed on selections of the welded-coated and coated specimens prior and post exposure to brine solution representing a static corrosion environment at different exposure durations. Stainless steel specimens survived higher tensile loads compared to those of carbon steel.

#### 4.6.4 Fatigue Failure on Flat Sheets Specimens

##### 4.6.4.1 Fatigue failure of welded carbon steel specimens

Table 11 shows fatigue failure of carbon steel specimens in cycles for as received coated specimens (no exposure to corrosive media) and for exposure to static corrosive media of 3 weeks along with associated stresses and weldment sizes. The inconel-625 coatings on welded flat sheets carbon steel were examined after exposure to an electrolytic solution post one and three weeks prior to fatigue testing. The averages cycles to failure for those coated specimens non-welded and non exposed to corrosion in the as received condition was 104620 cycles while for those coated non welded and exposed to three weeks static corrosion was 72356 cycles. Obviously, the exposure to static corrosion reduces fatigue life for those coated non welded specimens. Similar observation was found for those coated welded specimens when compared their fatigue life in the as received condition with no exposure to static corrosion and for those coated welded specimens exposed to three weeks static corrosion. Overall, it is concluded that static corrosion exposure reduces fatigue life for coated specimens either welded or non-welded. On the other hand, it is concluded that coated welded specimens demonstrate shorter fatigue life compared to the non welded coated specimens in both scenarios with corrosion exposure and without corrosion exposure. Additionally, it is concluded that increased weld size also shorten the fatigue life of the coated welded specimens in both cases exposed and non exposed specimens.

Table 11: Fatigue failure coating on welded carbon steel specimens.

As Received Life (Cycles)	3 Week-Life	Stress to failure of coating (MPa)	Weldment Size
104620	72356	197.45	This specimen has no weldment
73552	43658	197.04	Welded: 2.5 mm
25436	17569	216.75	Welded: 3.3 mm
5560	4896	177.34	Welded: 5 mm

#### 4.6.4.2 Fatigue failure of welded stainless steel (304 SS) specimens.

Table 12 shows fatigue failure life of stainless steel (304L SS) specimens in cycles for as received specimens (no exposure to corrosive media) and for exposure to static corrosive media of 3 weeks together with associated stresses and weldment sizes.

The inconel-625 coatings on welded flat sheets 304L stainless steel specimens were examined after exposure to an electrolytic solution post one and three weeks prior to fatigue testing. The averages cycles to failure for those coated specimens non-welded and non exposed to corrosion in the as received condition was 25000 cycles while for those coated non welded and exposed to three weeks static corrosion was 19635 cycles. Obviously, the exposure to static corrosion reduces fatigue life for those coated non welded specimens. Similar observation was found for those coated welded specimens when compared their fatigue life in the as received condition with no exposure to static corrosion and for those coated welded specimens exposed to three weeks static corrosion. Overall, it is concluded that static corrosion exposure reduces fatigue life for coated specimens either welded or non-welded. On the other hand, it is concluded that coated welded specimens demonstrate shorter fatigue life compared to the non welded coated specimens in both scenarios with corrosion exposure and without corrosion exposure. Additionally, it is concluded that increased weld size also shorten the fatigue life of the coated welded specimens in both cases exposed and non exposed specimens. Literature search identified similar work was performed evaluating fatigue properties of HVOF coated welded steels surfaces.

Table 12: Fatigue failure coating on welded stainless steel (304 SS) specimens.

<b>As Received Life (Cycles)</b>	<b>3 Week-Life</b>	<b>Stress to failure of coating (MPa)</b>	<b>Weldment Size</b>
25000	19635	256.9	No weldment (HVOF coated only)
19568	15658	220.6	Welded: 2 mm
7256	6958	228.2	Welded: 3 mm
2598	2787	256.7	Welded: 5 mm

Al-Fadhli et al [38, 200] performed experimental work studying the corrosion-fatigue behavior of Inconel 625 thermally sprayed using HVOF coating process. The authors found that the fatigue strength decreases as the period of coating exposure to corrosive environment increases.

#### 4.7 Microstructure Characterization

Examinations of the microstructure and the bonding of a welded sample of a HVOF coating applied to stainless steel were performed using an SEM facility. The examinations performed are summarized as follow:

- Topographic examination using SEM (secondary and backscattered electron at high magnification): this is to determine the nature, defects and characteristics of bonding between the thermal spray coatings, adhesion to base metal, to the welded zones and the heat affected zones.
- Micro-chemical analysis using the energy dispersive (EDS) X-ray analyzer in performing semi-quantitative analysis of the thermal spray coatings adhesion to base metal to the welded zones and to the heat affected zones.
- Optical examination to determine bonding between the thermal spray coatings adhesion to base metal, to the welded zones and to the heat affected zones.

A specimen of stainless steel was coated with Inconel 625 using the HVOF Thermal Spray Coating Process. The coating was deposited onto a weld and the heat affected zone (HAZ). SEM instrument was employed in characterizing the bonding of the coating, including any differences in the bonding over the weld, the heat-affected zone and the base metal. The specimen was examined after it had been polished and etched. The etching at the bond was quite deep in the area over the weld, suggesting that the coating was actually de-bonded in this area. The bonding zone was observed being completely bonded further away from the weld zone. Exactly, when the de-bonding occurred is not known. A single specimen was an already-polished-and-etched cross section of thermal-spray-coated steel. The specimen was examined to determine the nature of the bonding of the coating and the steel in the weld zone, the heat-affected zone and the bulk steel. Scanning electron microscopy, energy-dispersive spectroscopy and light microscopy were used to characterize the bonding in these areas. The original etch

showed that the specimen contained a two-sided weld through a sheet of steel approximately 3 mm thick. The coating was slightly over 1 mm thick. The as-received specimen was heavily etched and showed several spots where residual fluids from polishing had leaked out from the interface. It was re-polished with only a very shallow re-grind. Since the specimen thickness was not known in the opaque mount we wanted to avoid grinding entirely through the sample. Evidence of the original etch still remained in the coating after the polish, suggesting that the original etch had been quite deep. Once again after etching the specimen to bring out the structure of the metal in the weld, the coating was again found to be quite heavily etched. The specimen was examined using the scanning electron microscope (SEM) under the conditions described above. The deep etch made interpretation of the surface and the porosity difficult, so the specimen was once again polished with a shallow grind to remove most of the evidence of etching. The specimen received the bulk of the attention in its now-as-polished state. The welded coated specimen still showed considerable evidence of the grain/particle boundaries and the inter-particle phases and/or porosity.

#### 4.7.1 Description of the Coating and the Steel-Coating Interface

Scanning electron microscopy examinations were performed on the steel-coating interface for the specimen as-received with the original etches, showing the complexity of the interface structure. The sample was made from two sheets of steel that were butt-welded from both sides of the sheets. The weld area is somewhat thicker than the rest of the original sheet. The general appearance of the sample is shown below in Figure 55. Note the swell in the sheet in the center of the weld. The base steel shows a strong rolling texture from the original formation of the sheet. The heat-affected zone (HAZ) is only a few grains wide around the weld, separating it from the elongated grains showing the rolling texture. Thus the HAZ did not have a significant effect on the bonding of the coating to the steel.

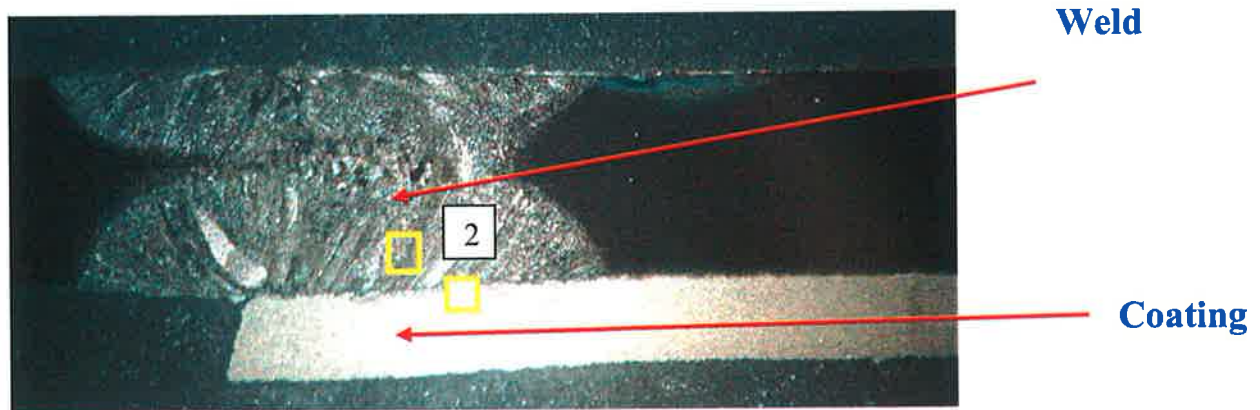


Figure 55: Entire specimen showing weld and coating

Figure 56 is a scanning electron micrograph of the steel-coating interface in the sample as-received with the original etches, showing the complexity of the interface structure. The dark areas were not well-defined at this point, being either original porosity or having been created by the etching process.

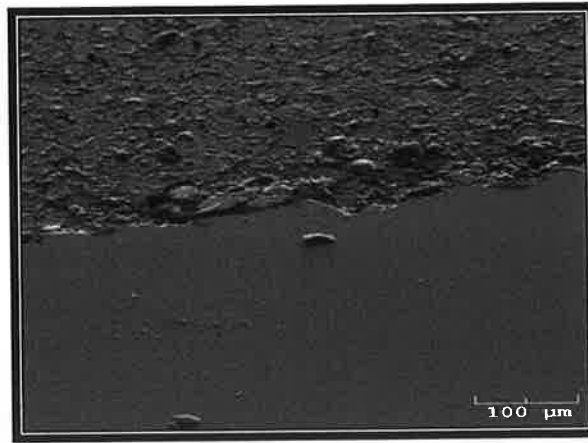


Figure 56: SEM micrograph through as-received weld area and coating

Figure 57 is an SEM micrograph of the coating in the same condition, showing the as-received etched structure, with well-defined particles of metal and undefined inter-particles phase.

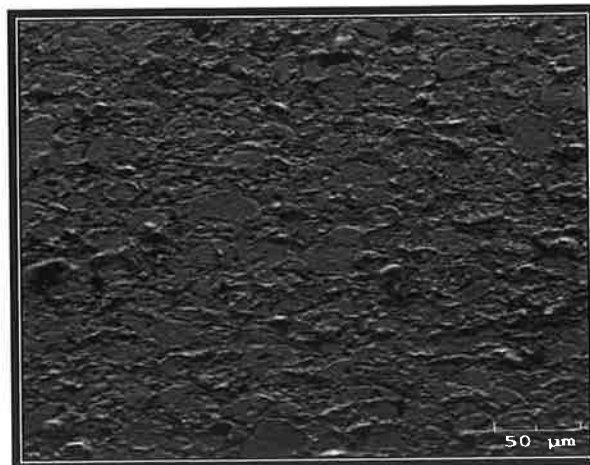


Figure 57: SEM micrograph through as-received coating above weld area

Figures 58 and 59 are energy-dispersive x-ray spectra showing the compositions of the steel and the coating in these two areas. Semi-quantitative analyses based on these spectra are shown in Table 13. The dark areas were not well-defined at this point, being either of original porosity or having been created by the etching process. SEM examinations showed well-defined particles of metal and an undefined inter-drop phase for the as-received etched structures.

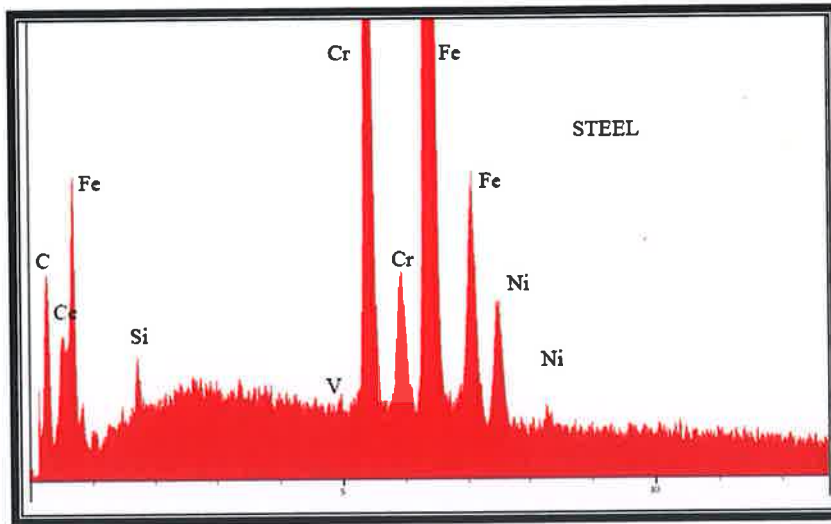


Figure 58: EDS spectrum of bulk steel.

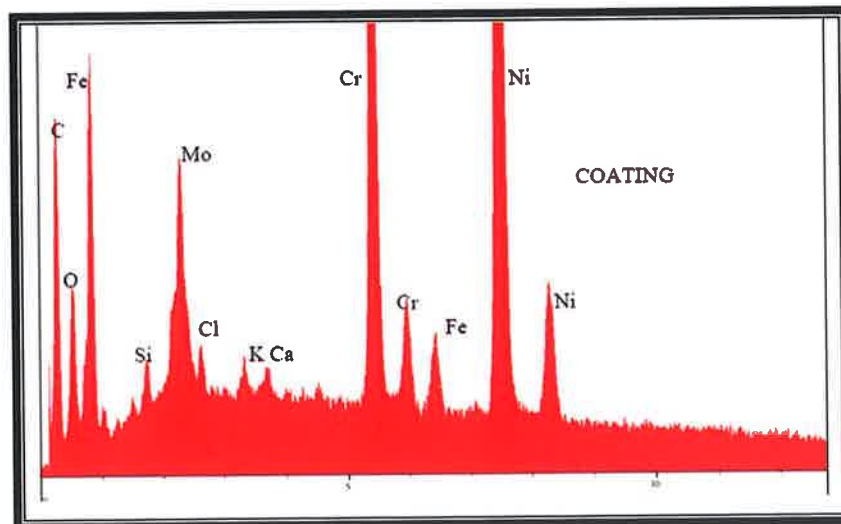


Figure 59: EDS spectrum of coating in area of boundary with steel. Note Cl peak in addition to normal coating constituents, plus minor to trace K and Ca.

Table 13: Semi-Quantities analysis for the steel-coating

Element	Steel	Coating
Cr	19	23
Fe	72	3
Ni	8	61
Si	1	N/A
Mo		9
Nb		3
Ta		Not detected
O		<31
Cl		1

Energy-dispersive spectra examinations were performed to examine the compositions of the steel and the coating. The presence of Cl in the coating analysis was unexpected but appeared to be pre-existing in this area. Note that this analysis is taken from a small, randomly selected area and is not taken to be representative of the whole coating.

Figures 60 through 61 are a series of light micrographs showing many aspects of the coating. The specimen at this point had been originally polished and etched, re-polished and re-etched. Development of appropriate etching techniques is a matter of trial and error, depending on what information is needed from the specimen. Etching by definition involves solution and removal of some of the specimen material.

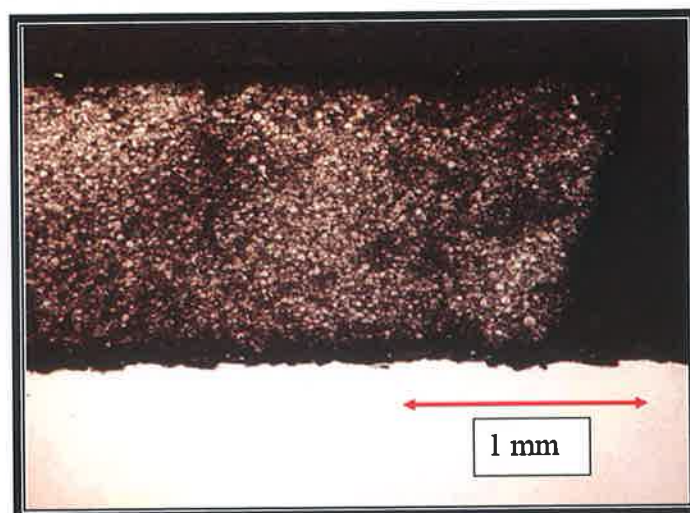


Figure 60: Reflected light micrograph showing general roughness of metal surface and thickness of coating.

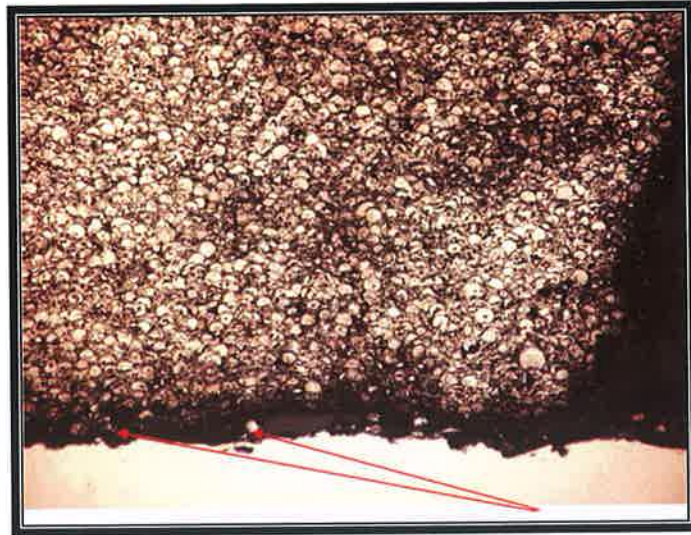


Figure 61: Higher magnification micrograph of same area showing voids at interface of coating and steel.

#### 4.7.2 Specimen Observations

- This specimen exhibited a prominent de-bonding of the coating from the steel. Whether this happened prior to original specimen preparation or was actually caused by the mounting process was unknown.
- The boundary between the steel and coating was topographically quite rough. Grains of residual grinding or blasting media were located along the boundary or were embedded in the steel. There was also considerable carbon in the boundary area and in the “porosity” in the coating. This was suspected to be cutting oil or some other hydrocarbon, not original to the specimen manufacturing/coating process.
- Particles in the coating range from 5 to as much as 80 micrometers. The particles were generally flattened, with the long dimension parallel to the steel. The drops themselves were relatively rich in Mo and O; while the inter-drop area was richer in Ni and Cr. Significantly, some of the particles at the boundary were not metallurgically bonded.
- The specimen exhibited a fairly high level of apparent porosity in the as-etched state. This porosity appeared to be the sum of inherent inter-particle/inter-granular

pore space plus space created by the etching process. This porosity could be quantified provided an accurate pre-definition of the total porosity was established.

- Elemental mapping showed what the general chemistry of the coating might be. However, de-bonding interfered the performance of this type of semi-quantitative analysis directly at the boundary.
- Non-bonded powder particles were located above the steel, suggesting that the substrate had been cold when coated.
- Alumina particles were embedded in the steel surface, probably residual from grit-blasting the steel surface. Contamination of the bonding surface may have been part of the cause of the de-bonding.
- Porosity in the coating was in the 17% range, but this included both “real” original porosity and areas dissolved out by etching.

#### 4.8 Microstructural Examinations using Scanning Electron Microscopy

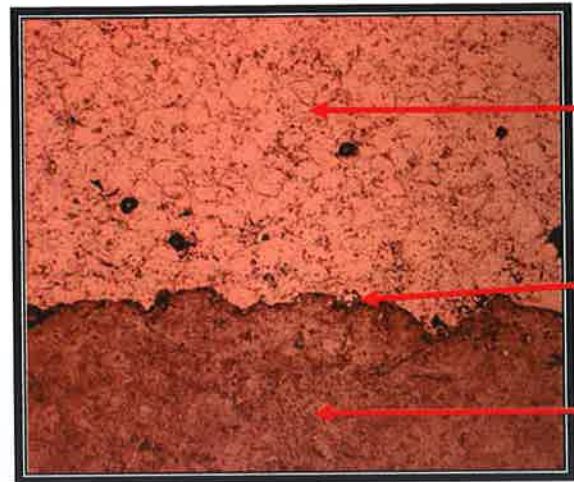
Microstructure examinations play a vital role in determining and identifying corrosion products, imperfection of substrates, coating structure, porosity level, coating adherence and weld to coating adherence. In the current work, selected welded-coated and exposed specimens were sectioned, mounted, prepared and examined under SEM to determine coating and weld defects.

##### 4.8.1 Carbon steel welded-coated specimens

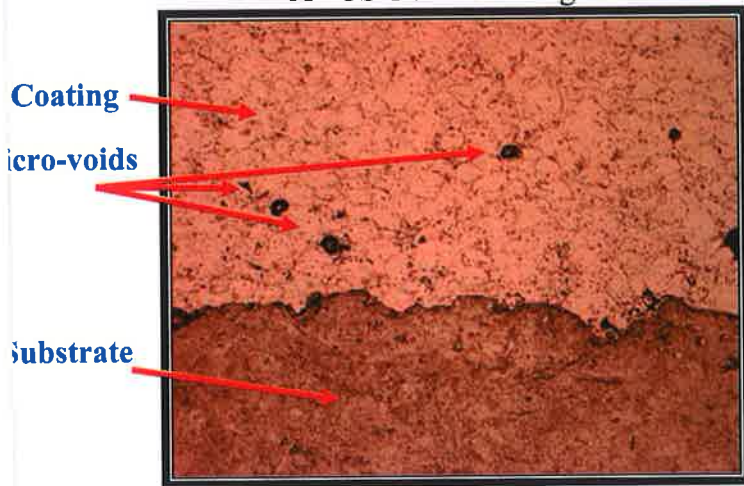
Figure 62 shows SEM micrographs demonstrate SEM obtained image for a single specimen HVOF welded-coated by powder similar to Inconel 625 and fatigue tested. The micrographs show right side, left side and the middle interface. Also, the EDS analysis of the deposited coating powder compositions is shown.. The micrograph A shows right edge side indicating no overlay at the top of the weld. The micrograph B shows the left edge side indicating good adhesion. The middle interface is shown in micrograph C showing minor micro-voids. It is clear that only a very low percentage silicate is detected represented by 0.49%.



A- CS-1-FT-25X-Right-side



B- CS-1-FT-200X-Left-side



C- CS-1-FT-200X-Mid interface

Element	Weight %
Al	0.44
Si	0.49
Ti	0.25
Cr	17.88
Fe	15.88
Ni	59.96
Mo	5.11

Figure 62: SEM micrographs for HVOF welded-coated specimen fatigue tested.

Figure 63 shows SEM micrographs demonstrate SEM obtained image for a single specimen welded and HVOF coated by powder similar to Inconel 625 and tensile tested. The micrographs show right side, left side and the middle interface. The micrograph A shows the right edge side indicating crack initiation transfer at the overlay. The micrograph B shows the left edge side indicating excellent adhesion of the HVOF coating onto the steel surface. The micrograph C shows middle interface indicating micro-voids. The EDS analysis of the thermal spray coating is given below. It is clear here that the silicate material is of high percentage approximate by 3.51%.

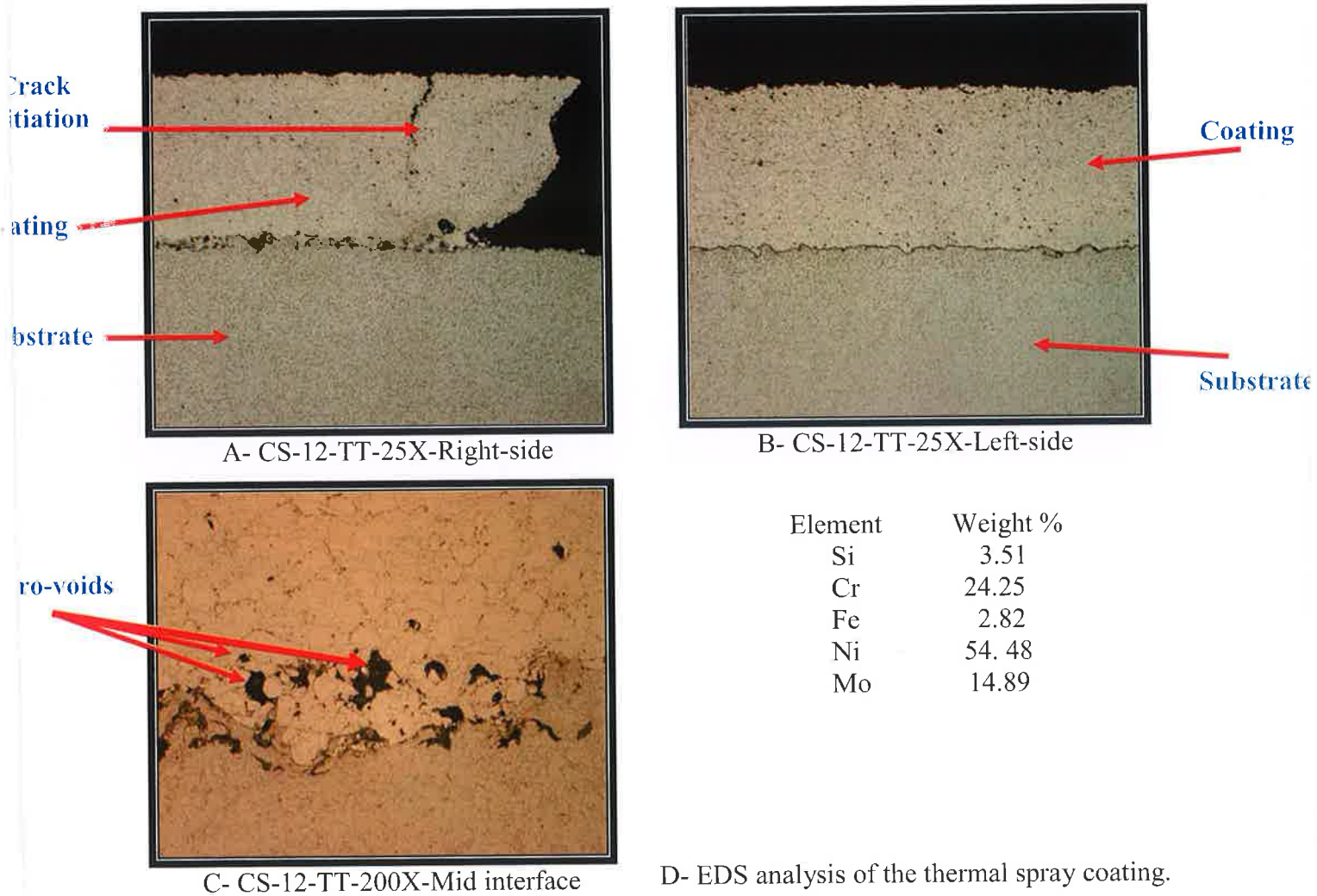
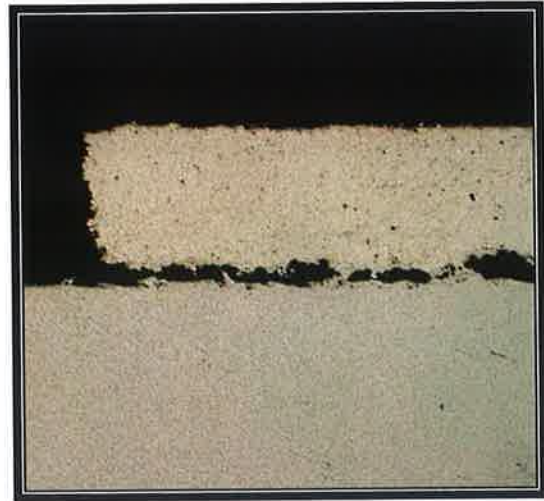


Figure 63: SEM micrographs for HVOF welded-coated specimen post tensile test.

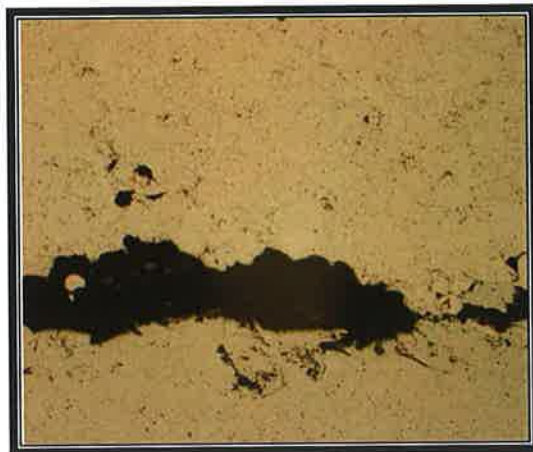
Figure 64 shows SEM micrograph for an HVOF coated-welded carbon steel specimen. The micrographs A shows the right edge side shows indicating superior adhesion with no observed discontinuity between the coating and the substrate. The micrograph B shows the left edge side shows no overlay on the top of the weld and poor adhesion between the substrate and the overlay. The micrograph C shows the middle interface indicating lack of bonding between the thermal spray coating and the substrate. The EDS analyses of the thermal spray coating are given in D.



A- CS18-25X-Right side



B- CS18-25X-Left side



C- CS18-25X-Mid interface

Element	Weight %
Si	8.49
Ti	0.28
Cr	17.24
Fe	11.12
Ni	57.80
Mo	5.08

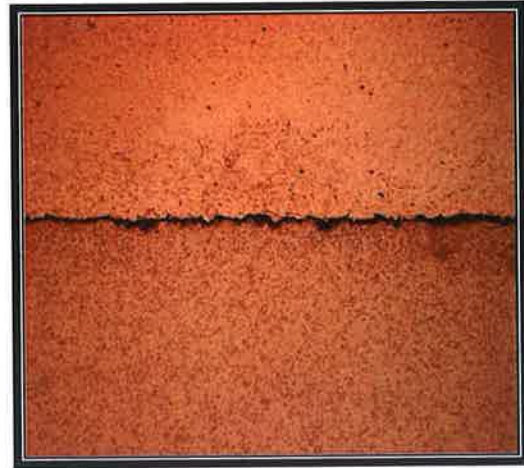
D- EDS Analysis of the thermal spray coating

Figure 64: SEM micrograph for an HVOF coated-welded carbon steel specimen

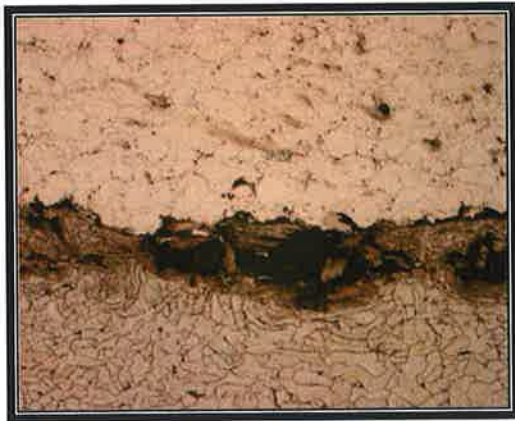
Figure 65 shows SEM micrographs for HVOF coated-welded carbon steel specimen. The micrograph in A shows the right edge side indicating no overlay at the top of the weld. The micrograph in B shows the left edge side indicating oxidation layer between the overlay and the base metal. The micrograph shown in C shows the mid interface indicating presence of micro-voids. The EDS analyses of the thermal spray coating are given in E.



A- CS14-25X-Right side



B- CS14-25X-Left side



C- CS14-25X-Mid interface

Element	Weight %
O	6.28
Si	4.08
Cr	15.86
Fe	17.75
Ni	51.50
Mo	4.53

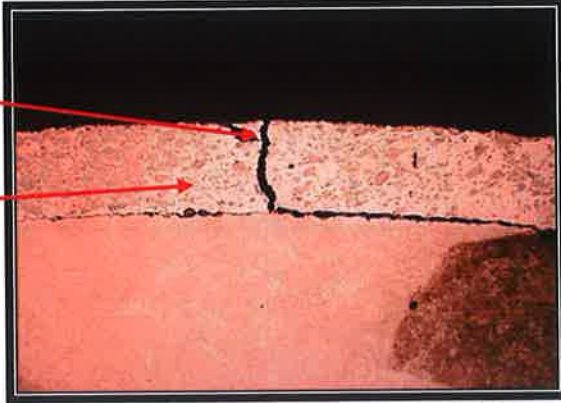
D- EDS analysis of the thermal spray coating

Figure 65: SEM micrographs for HVOF coated-welded carbon steel specimen

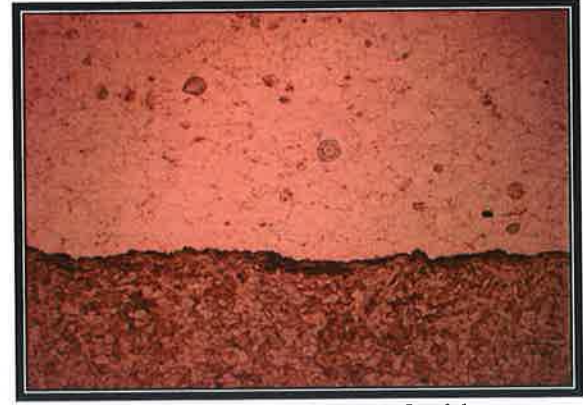
Figure 66 shows SEM micrographs for an HVOF coated-welded carbon steel specimen post fatigue test. The micrograph shown in A indicates a transverse crack at the top of the weld. The two micrographs shown in B and C demonstrate the left edge and right edge respectively showing good adhesion. The EDS analyses of the thermal spray coating are given in D.

Transverse  
Crack

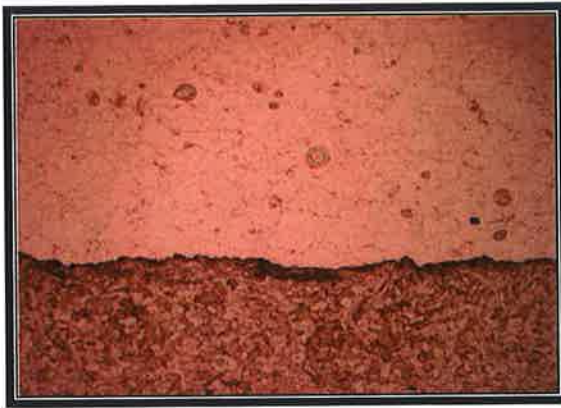
Coating



A- CS-4-FT-16X-top of the weld



B- CS-4-FT-200X-Left-side



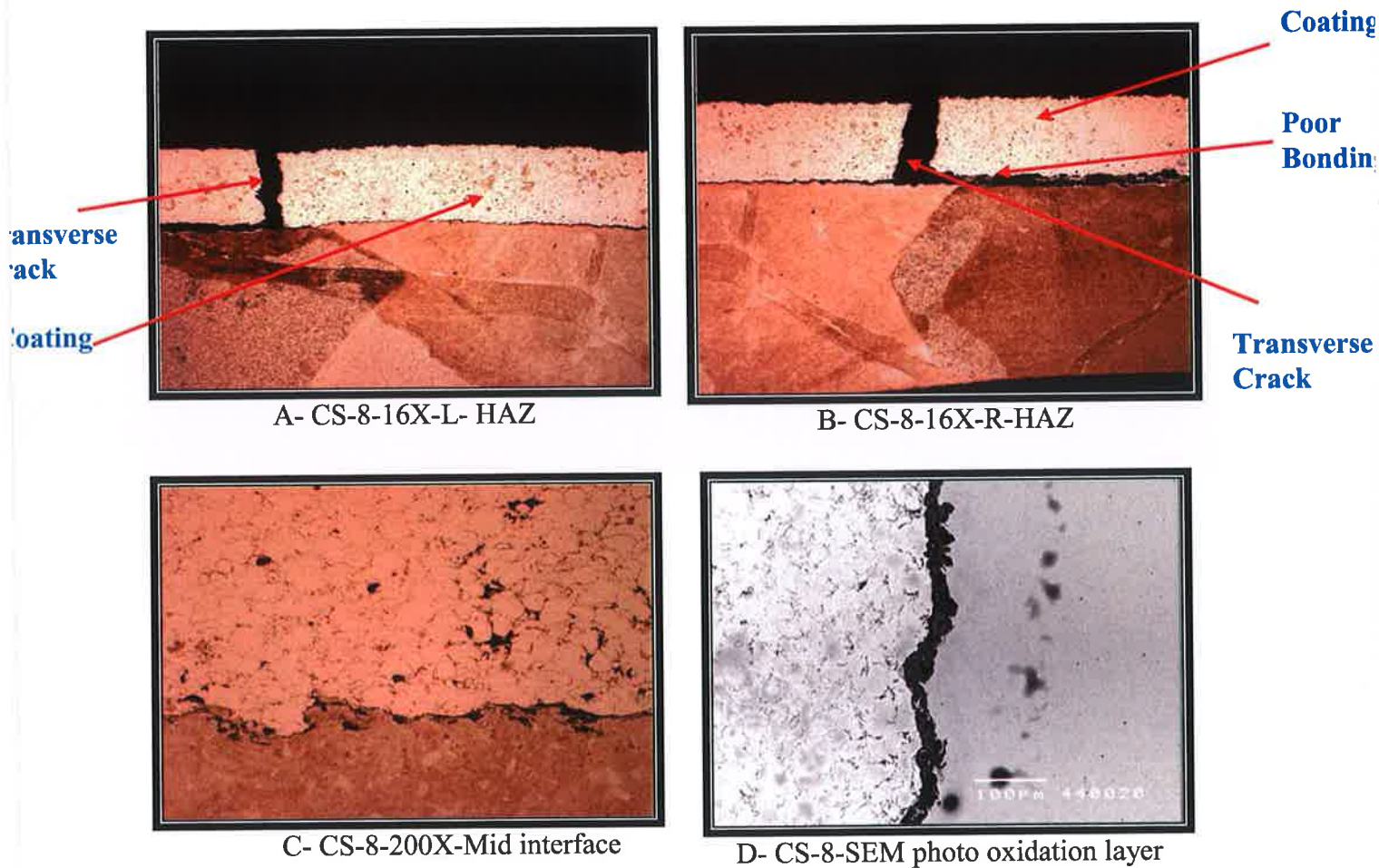
C- CS-4-FT-200X-Right-side

Element	Weight %
Si	0.54
Cr	21.49
Fe	3.27
Ni	68.33
Mo	6.38

D- EDS analysis of the thermal spray coating

Figure 66: SEM micrographs for an HVOF coated-welded carbon steel specimen post fatigue test

Figure 67 shows SEM micrographs HVOF coated-welded carbon steel specimen post fatigue test. The micrographs shown in A and B are for left and right edges respectively. Both micrographs of the edges indicate a presence of transverse crack, poor bonding at the top of the Right & Left heat affected zone. The micrograph shown in C indicates is for the mid-interface indicating a good adhesion with observed micro-voids within the coating.. The micrograph depicted in D indicates presence of an oxidation layer at the interface. The EDS analyses of the thermal spray coating are given in E. The EDS analyses of the oxidation layer are given in F.



Element	Weight %
O	4.16
Si	0.38
Ti	0.35
Cr	19.17
Fe	2.43
Ni	66.71
Mo	6.27

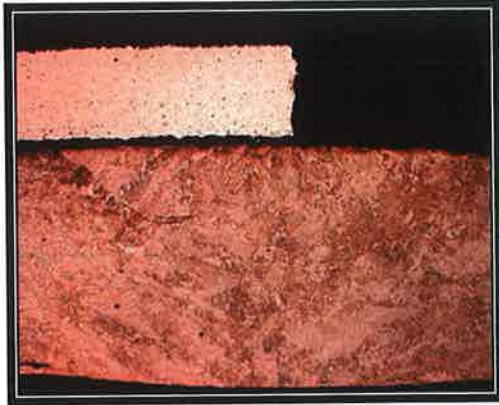
Element	Weight %
O	39.41
Al	2.60
Cl	2.15
Cr	0.51
Fe	55.33

E- EDS analysis of the thermal spray coating interface (Figure D- CS8)

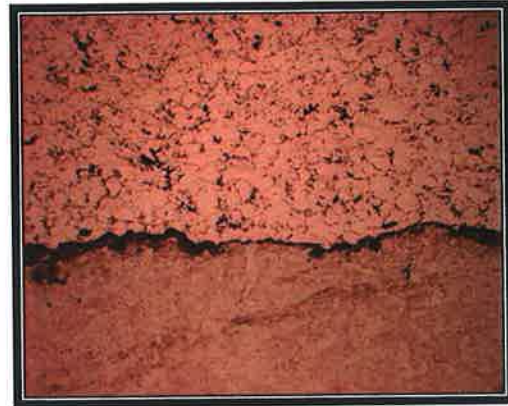
Figure 67: SEM micrographs HVOF coated-welded carbon steel specimen post fatigue test.

Figure 68 shows SEM micrographs for HVOF coated-welded carbon steel specimen post fatigue test. The micrograph shown in A is for the left edge to the HAZ indicating poor bonding at the HAZ and no overlay on the top of the weld. The micrographs shown in B and C are for the right and left edges respectively showing oxidation layer at the

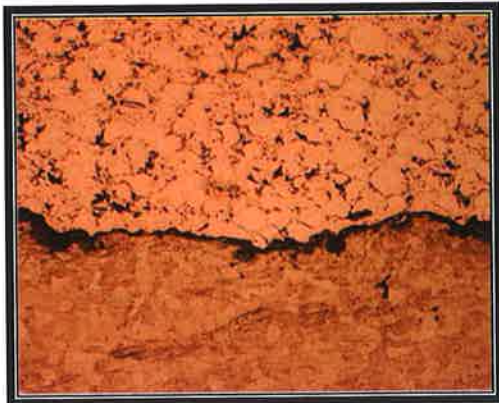
interface. The micrograph in D indicates to the oxide layer at the interface. The EDS Analysis of the thermal spray is given in E. The EDS analyses of the oxide layer (Figure D-CS-5) are given in F.



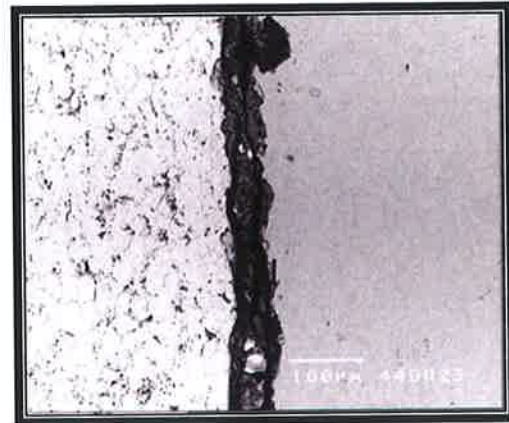
A- 5-16X-Left - HAZ



B-CS-5-200X-L-Side



C- CS-5-200X-Mid interface



D- CS-5 SEM Photo Oxide layer

Element	Weight %
O	6.12
Si	4.03
Cr	19.19
Fe	3.07
Ni	61.41
Mo	6.17

Element	Weight
O	25.43
Fe	74.57

E- EDS Analysis of the thermal spray interface (Figure D-CS-5)

F- EDS analysis of the Oxide layer at the interface (Figure D-CS-5)

Figure 68: SEM micrographs for HVOF coated-welded carbon steel specimen post fatigue test

#### 4.8.2 304L Stainless steel welded-coated specimens

Figure 69 shows SEM micrograph for an HVOF coated-welded 304L stainless steel specimen. Micrograph A represents the right edge side showing porosity & poor adhesion. Micrograph B shows the left edge side showing no overlay on the top of the weld, poor adhesion and oxidation layer between the substrate and the overlay. Micrograph C shows the mid interface with observed porosity & oxidation layer between the overlay and the substrate. The EDS analysis of the oxide layer and the coating are given in (E).



A- SS52-25X-Right side



B- SS52-25X-Left side



C- SS52-200X-Mid interface

Element	Weight %
Si	11.47
Ti	0.16
Cr	19.08
Fe	7.95
Ni	55.99
Mo	5.36

D- EDS Analysis of the thermal spray coating

Element	Weight %
C	72.01
O	26.67
Si	1.25
Fe	0.07

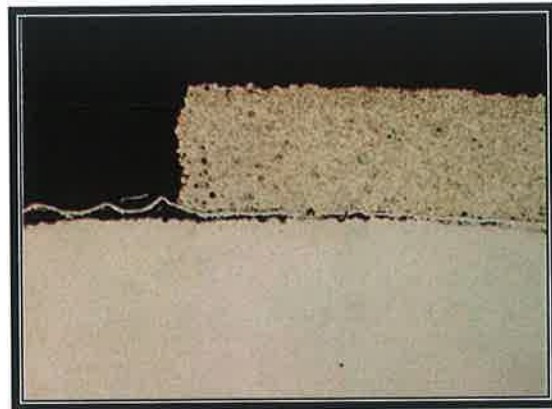
E- EDS analysis of the oxidation layer

Figure 69: SEM micrograph for an HVOF coated-welded 304L stainless steel specimen.

Figure 70 shows SEM micrograph for HVOF coated-welded 304L stainless steel specimen. The micrograph in A shows the right edge side indicating a good adhesion. The micrograph shown in B is for the left edge side indicating no overlay on the top of the weld and poor adhesion between the base metal and the overlay. The micrograph shown in C is an indication of a transverse crack & micro-voids at the top of the HAZ. The micrograph depicted in D is for the mid section of interface between the base metal and overlay indicating presence of non-metallic inclusion. The EDS analyses of the thermal spray coating are given in E. The EDS analyses of the non-metallic inclusions are given in F.



A- SS50-25X-Right side



B- SS50-25X-Left side



C- SS50-25X-HAZ



D- SS50-500X- interface

Element	Weight %
O	5.22
Cr	19.19
Fe	7.58
Ni	61.63
Mo	5.66

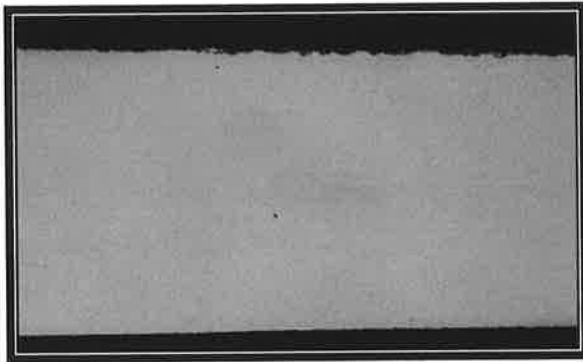
E-EDS analysis of the thermal spray coating

Element	Weight %
O	45.16
Al	54.84

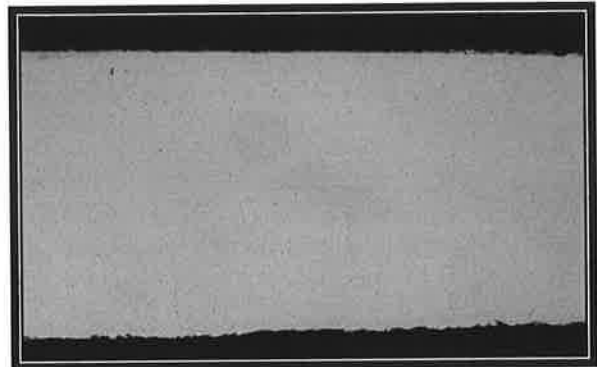
E-EDS analysis of the non-metallic inclusion shown in photo (D)

Figure 70: SEM micrograph for HVOF coated-welded 304L stainless steel specimen.

Figure 71 shows SEM micrographs for HVOF coated specimens deposited onto plain 304 stainless steel surfaces with no weld overlay or deposition (not metallurgically affected steel surface). It is apparent from the SEM examinations and micrographs that the two micrographs indicate spalled thermal spray coating layer from the surface indicating poor adhesion.



A-SS47-25X



B- SS48-25X

Figure 71: SEM micrograph for HVOF coated-welded 304L stainless steel specimen.

Figure 72 shows SEM micrograph for HVOF coated-welded 304L stainless steel specimen. The micrograph shown in A represents the left side to the weld indicating a transfer crack and porosity at thermal spray layer (top of the weld). The micrograph shown in B is for the left edge showing excellent adhesion with some micro-voids at the thermal spray layer. The micrograph shown in C indicates the mid interface area between the coating and the substrate indicating superior adhesion. The EDS analyses of the coating are given in D.

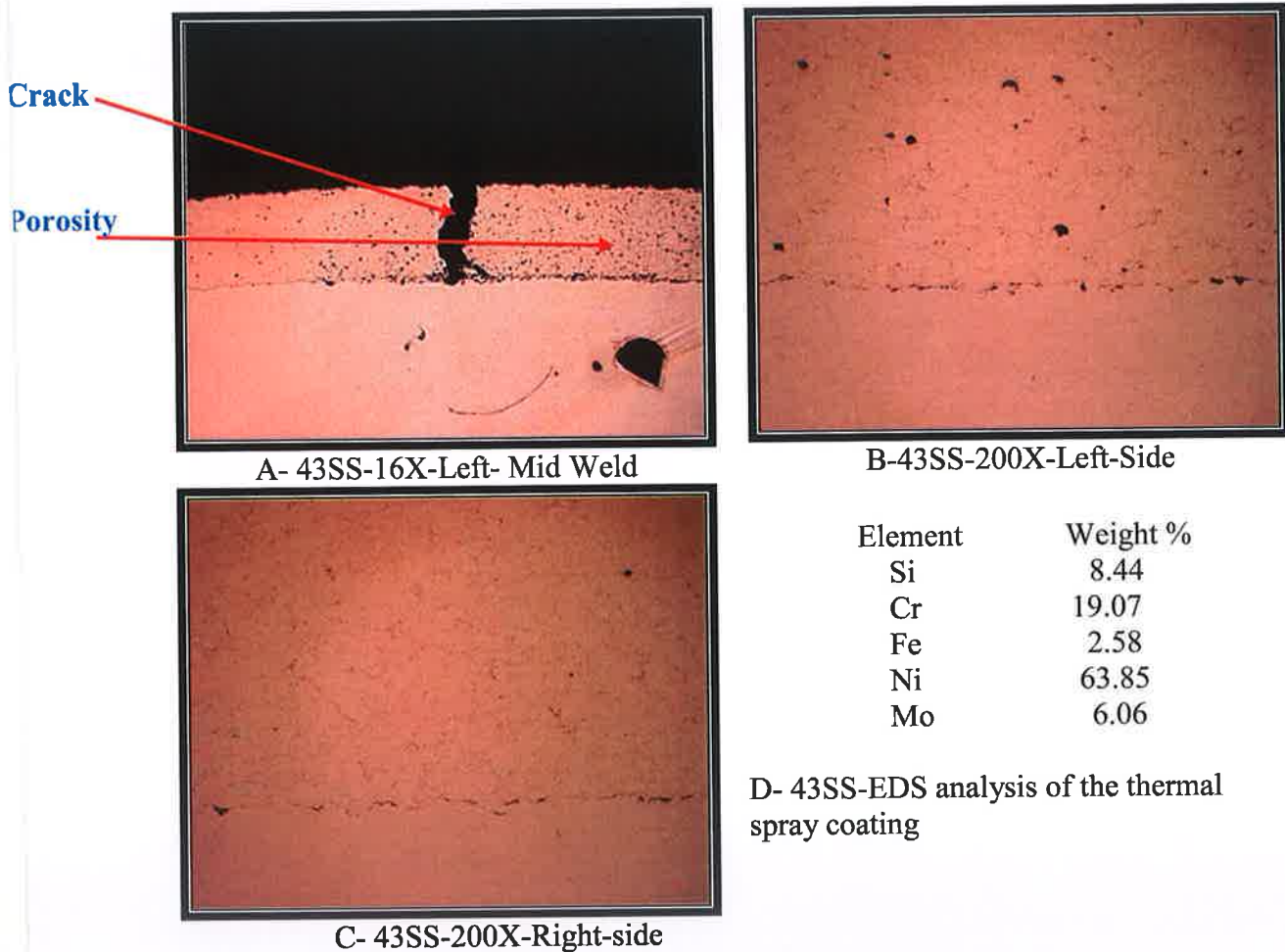


Figure 72: SEM micrograph for HVOF coated-welded 304L stainless steel specimen

## 4.9 The Tensile Strengths Behavior of HVOF sprayed Nickel alloy Coatings onto welded Steel Surfaces exposed to Artificial Sea Water Environment

### 4.9.1 Experimental Work

This experiment investigates the tensile strength and corrosion properties of HVOF sprayed coatings of nickel based alloys similar to Inconel 625 deposited onto steel plain surfaces and welded steel surfaces were investigated. All the steel specimens used throughout the experimental work are HVOF coated selectively welded with different weld diameters. The experimental work includes the following:

- Exposure of welded coated specimens to static corrosion environment examining the effect of corrosion exposure onto the tensile strength of the coating onto plain steel surfaces and onto welded steel surfaces.
- Examination of the influence of the weldment size onto the coating-substrate tensile strength properties.

### 4.9.2 Carbon Steel Welded Coated Specimens

Carbon steel specimens were HVOF coated using Inconel 625 powder. A total of 24 specimens were machined of carbon steel selectively welded and all coated using HVOF process. The welds included sizes of 2 mm, 3 mm and 5 mm. All the coated and coated-welded specimens were tensile tested with and without corrosion exposure examining effect of corrosion onto tensile properties.

### 4.9.3 Specimens fabrication and distribution:

Test specimens were machined and prepared in accordance with standards ASTM E 466 - 96. All specimens were made to dimensions of 10 mm W x 140 mm L and thickness of 3 mm. All the specimens were coated to a thickness of 1000  $\mu\text{m}$ . All specimens including coated and welded coated specimens were tensile tested, prior and post corrosion exposure and compared to those tested without corrosion exposure. All tensile tests were

carried out using lab standard Instron Machine model 8501. Table 14 demonstrates all tested coated carbon steel specimens.

Table 14: HVOF sprayed nickel alloy 625 coatings onto carbon steel specimens

<b>Sample#</b>	<b>Exposure Period</b>	<b>Weld Size</b>
1	No exposure	No weld.
2	No exposure	2.5 mm
3	No exposure	3 mm
4	No exposure	5 mm
5	One week	No weld.
6	One week	2.5 mm
7	One week	3 mm
8	One week	5 mm
9	Three weeks	No weld.
10	Three weeks	2.5 mm
11	Three weeks	3 mm
12	Three weeks	5 mm
13	No exposure	No weld.
14	One week	No weld.
15	Three weeks	No weld.
16	No exposure	2.5 mm
17	One week	2.5 mm
18	Three weeks	2.5 mm
19	No exposure	3 mm
20	One week	3 mm
21	Three weeks	3 mm
22	No exposure	5 mm
23	One week	5 mm
24	Three weeks	5 mm

#### 4.9.4 Tensile Tests of HVOF Coated Carbon Steel Specimens

##### **4.9.4.1 HVOF Coated carbon steel Specimen with no corrosion exposure and exposed coated specimens including coated non-welded and coated welded specimens with weld sizes of 2 mm, 3 mm, and 5 mm.**

Figure 73.a shows tensile stress for welded and non-welded HVOF coated carbon steel specimens prior to the static corrosion exposure tests (HVOF coated in the as received specimens condition) while Figure 73.b shows the stress strain curves close to the elastic region. It should be noted that Figure 73.b is the expansion of Figure 73.a in the elastic region (up to the strain 2.5). The general trend of the curves is similar in the elastic region, where minor variation in the elastic behavior of the specimens is observed beyond the tensile stress of 125 MPa. The minor variation in the elastic behavior of specimens is attributed to the heat affected zone and welding conditions. In this case, the elastic limit becomes lower for specimen with 5 mm diameter than the others. Moreover, the non-linear variation of the elastic limit of the specimens with the size of the heat affected zone is observed. This can also be associated with the error related with the experiments, which is in the order of 5.7%. It should be noted that the error is estimated from the repeatability of the experiments, i.e. each experiment is repeated five times. However, the effect of weld size on the tensile stress levels after necking is significant. The plastic deformation of the specimen varies with the weld size such that reduction in the weld size results in sharp decay of the strain after the necking. This behavior is because of the increase in the size of the welded zone. Since the hardness of the welded section is higher than the base material, the material flows in the region next to the welded zone under the tensile load before the failure. This situation is observed from Figure 74a and 74b in which the micrographs of the weld section after the tensile tests are shown. The corrosion effect in the surface region causes failure of coating through early crack formation during the tensile testing. In this case, it is observed that the surface cracks are developed in the coating at a distance away from the region where the total failure of the material occurs. This is more pronounced for the specimens subjected to three weeks corrosion environment.

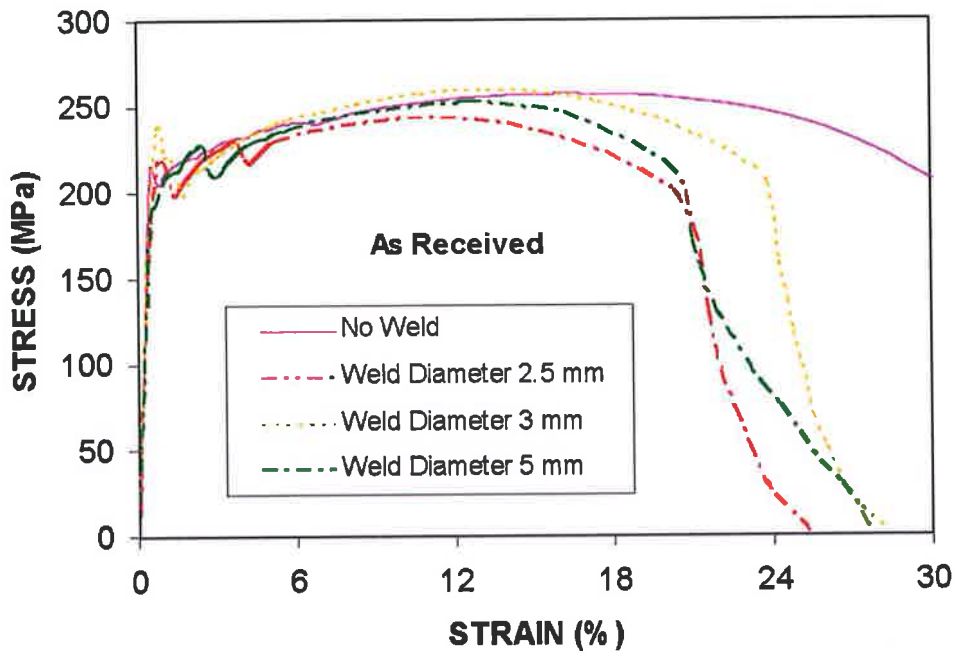


Figure 73a: Tensile response of the welded and non-welded HVOF coated carbon steel specimens prior to corrosion testing (As received condition).

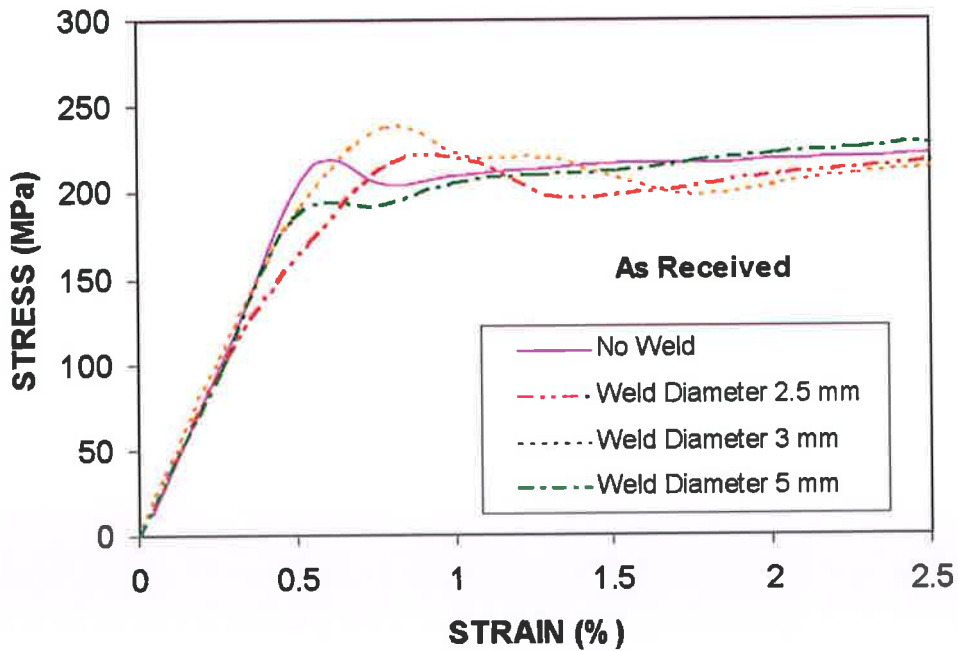


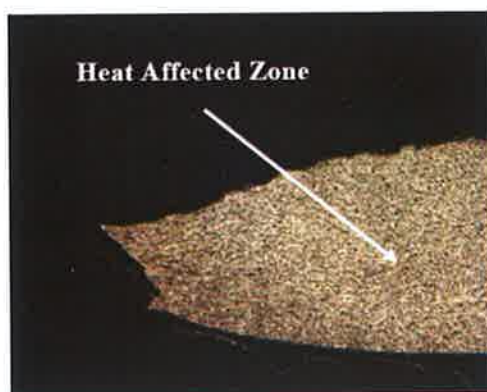
Figure 73b: Tensile response of the welded and non-welded HVOF coated carbon steel specimens in the elastic region prior to corrosion testing.



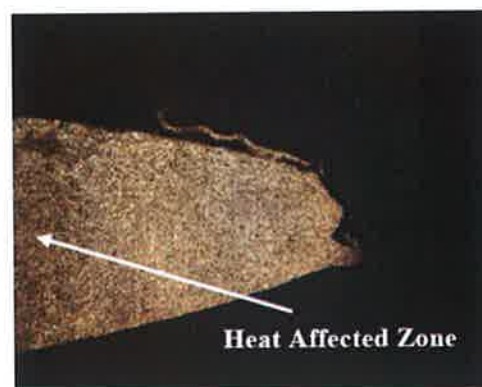
Coating is peeled off from the weld surface.



Material flow next to the weld zone.



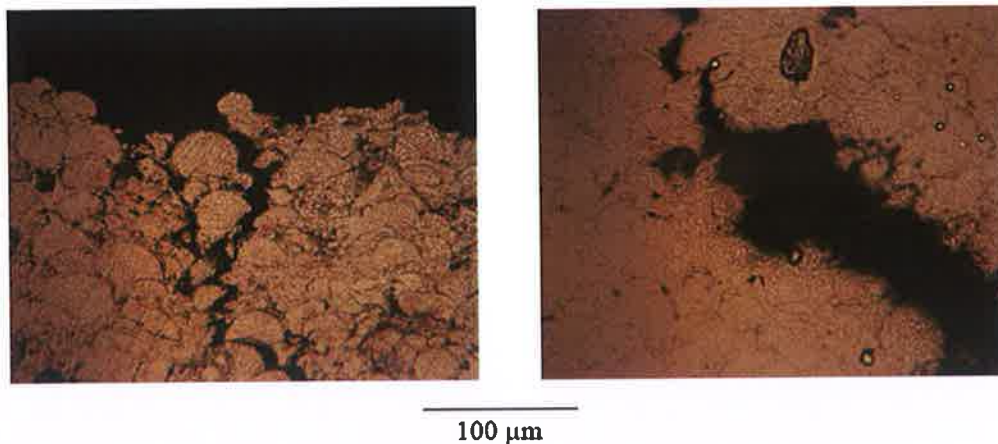
Failure of the specimen after tensile test



Failure of the specimen after tensile test

Figure 74a: Cross-sections of weld and heat affected zones as well as cross-section of the totally failed zone after the tensile testing.

For the coated welded carbon steel specimens; there is an effect on the plastic stress. However, the effect of welding (which creates higher strength in the “Heat Affected Zone”) may show less effect for larger weld size due to larger HAZ in the specimen. Al-Fadhli et al [200] showed that welded coated specimens that are no exposed to static corrosion demonstrate improved elastic and plastic properties compared to HVOF coated welded specimens exposed to static corrosion environment.



**Corrosion induced failure in the coating**

**Corrosion induced failure in the coating**

Figure 74b: Cross-section of the crack sites in the HVOF coating after the tensile tests for the specimens subjected to three weeks corrosion environment.

Figure 75a shows tensile test results for the HVOF coated welded specimens of three weld sizes subjected to one week corrosion testing while Figure 75b shows the tensile properties in the elastic region of Figure 75a. Tensile properties are the same for all the specimens subjected to the corrosion testing. However, it is observed that the elastic limit of each specimen changes slightly. The effects of electrolytic solution on the specimens are evident when Figure 73b is compared with Figure 75b. This effect is not linear on the elastic behavior of specimens because of the coating response to the electrolytic solution. In this case, the coating is affected by the electrolytic solution almost equally regardless of the weld size. The plastic deformation of the specimens subjected to the corrosion testing shows different behavior to the specimens without corrosion testing after the occurrence of necking (Figure 75a). The presence of coatings on welded specimens appears to give some level of protection so that plastic stresses are slightly greater than the non-welded specimens. This indicates that the corrosion effect extends to the substrate material influencing the plastic deformation of the substrate material. The plastic stress level of the coated non-welded carbon steel specimens is affected more to longer exposure than shorter period or no exposure. For the coated welded carbon steel specimens; there is an effect on the plastic stress. However, the

effect of welding (which creates higher strength in the “Heat Affected Zone”) may show less effect for larger weld size due to larger HAZ in the specimen. Al-Fadhli et al [38, 200] showed that presence of weld and HAZ reduces coating resistance to corrosion.

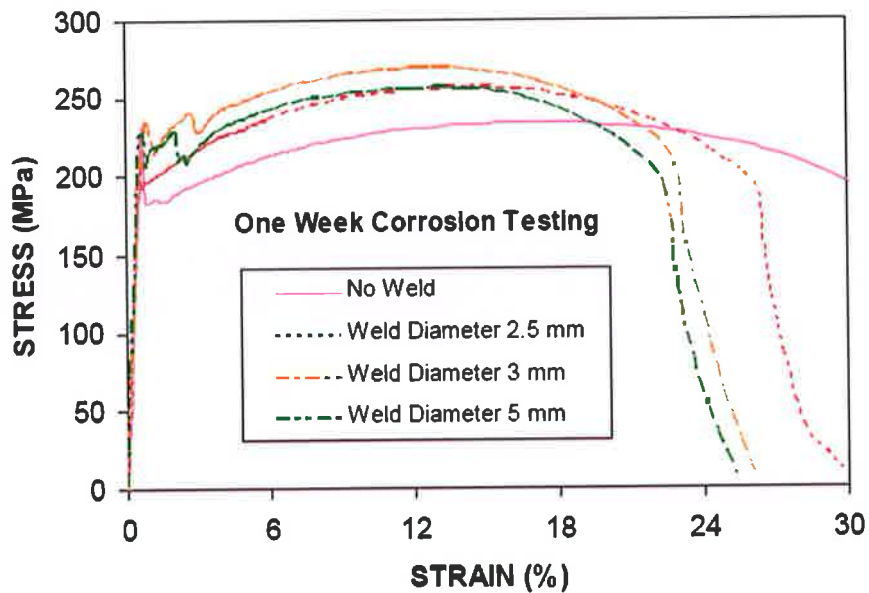


Figure 75a: Tensile response of the welded and non-welded HVOF coated carbon steel specimens after one week corrosion testing.

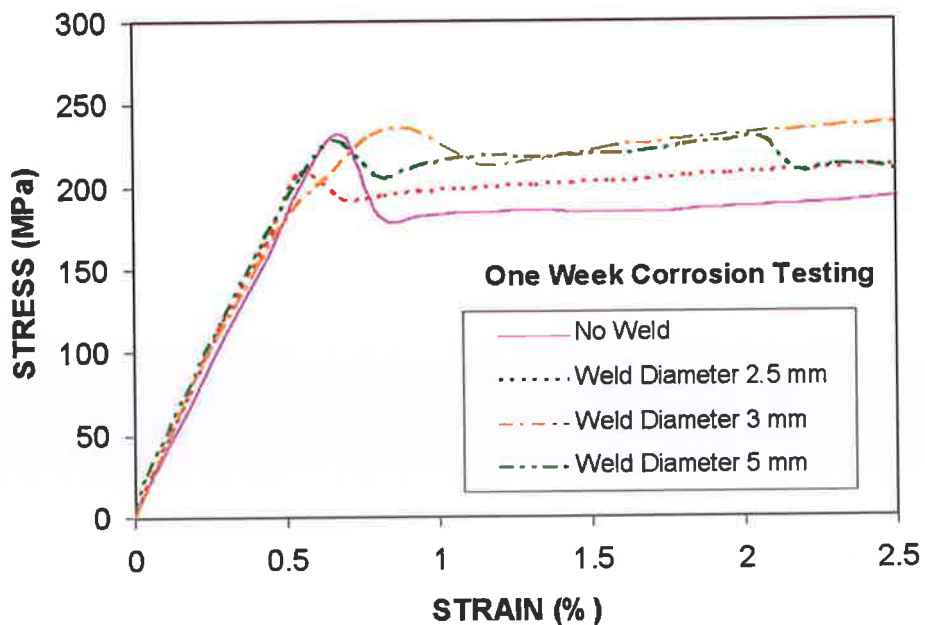


Figure 75b: Tensile response of the welded and non-welded HVOF coated carbon steel specimens in the elastic region after one week corrosion testing.

Figure 76 a and Figure 76 b show tensile stress for the welded and non-welded HVOF coated carbon steel specimens after three weeks of corrosion testing. It can be observed that in the elastic region Figure 76 b, tensile stress behaves similarly for all the specimens. This is because of the corrosion effect was similar to that described earlier for Figure 75 b. Consequently, three weeks duration in the static corrosion environment has little effect on the elastic response of the specimens. The corrosion response of the heat affected zone alters the plastic deformation of the base material after the necking. The yielding limit of the specimens differs slightly from those tested for one week in the static corrosion vessel Figure 75 b. This is attributed to the non-linear effect of the corrosion process in the welded and the heat affected zone of the specimens. The coating on welded specimens increases the plastic stresses compared to the non-welded specimens. There is a very little difference in stresses for specimens with 2.5 mm and 3.0 mm weld sizes. The 5.0 mm weld size demonstrates higher stress values compared to the others. This is due to the increased heat affected zone (HAZ). The plastic stress level of the coated non-welded carbon steel specimens is affected more to longer exposure than shorter period or no exposure. For the coated welded carbon steel specimens; there is an effect on the plastic stress. However, the effect of welding (which creates higher strength in the "Heat Affected Zone") may show less effect for larger weld size due to larger HAZ in the specimen. It is obvious that when comparing results for different weld sizes for no exposure, one week exposure and three weeks exposure, the results clearly more influenced for larger weld size specimens for three weeks exposure to static corrosion exposure. Al-Fadhli et al [38, 200] examined the effect of static corrosion exposure on the elastic and plastic properties of the coated welded specimens. The authors concluded that weld presence decreases coating resistance to corrosion exposure. Also, the authors concluded that the HAZ presence decreases corrosion resistance.

The current experimental work and corrosion testing demonstrated weld presence improves enhances corrosion resistance.

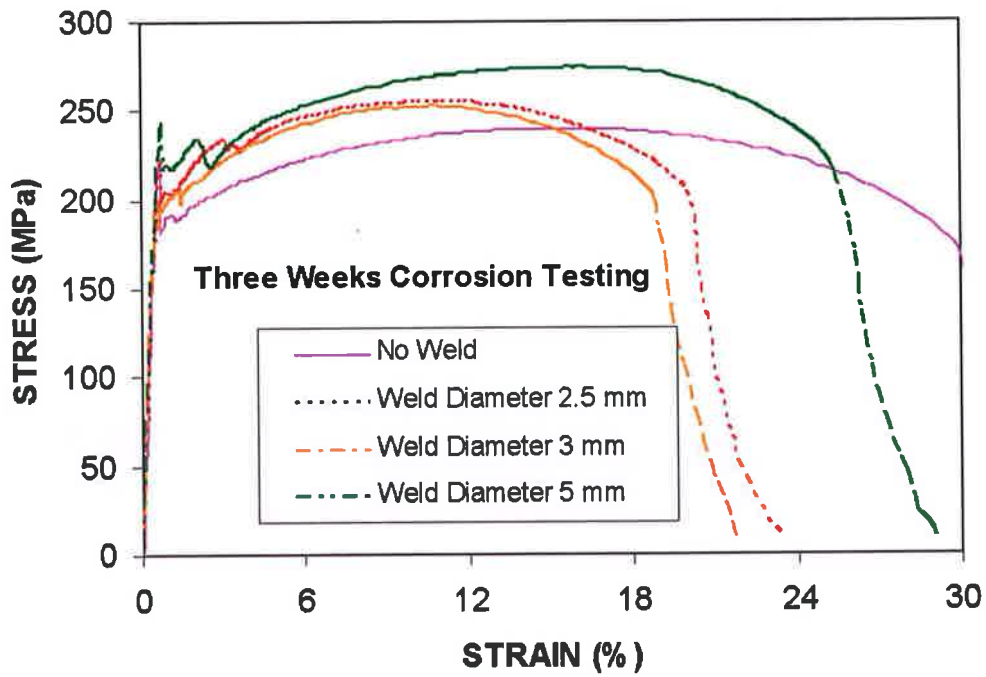


Figure 76 a: Tensile response of the welded and non-welded HVOF coated carbon steel specimens after three weeks corrosion testing.

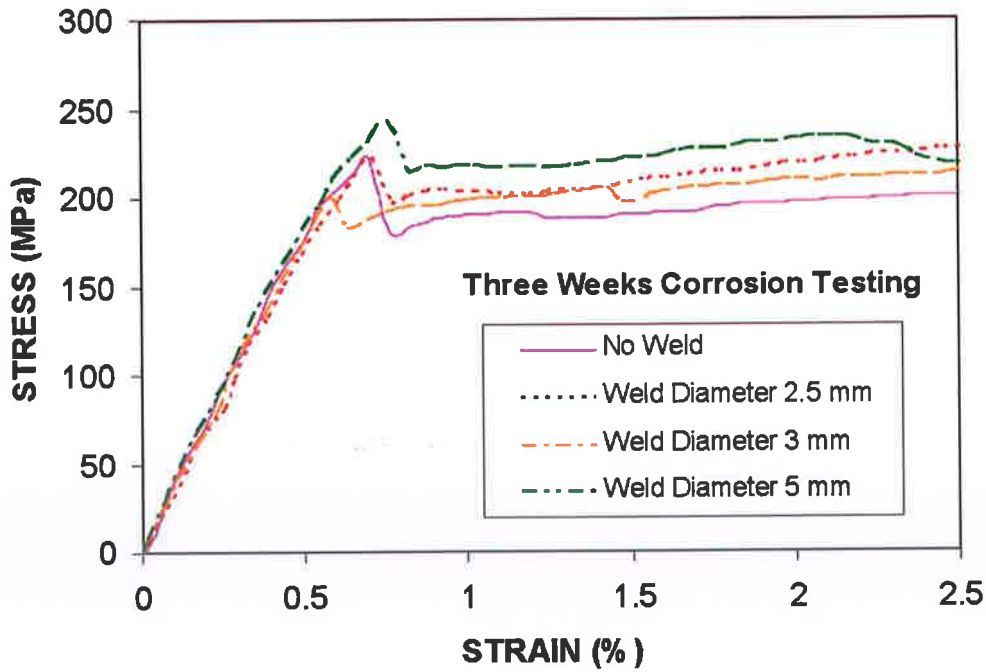


Figure 76 b: Tensile response of the welded and non-welded HVOF Coated Carbon Steel specimens in the elastic region after three weeks corrosion testing.

Figure 77 a shows tensile stress for non-welded HVOF coated carbon steel specimens prior and post static corrosion exposure while Figure 77 b shows the stress strain curves close to the elastic region. It can be observed that in the elastic region Figure 77 b, tensile stress behaves similarly for all the specimens. This is because of the corrosion effect was similar to that described earlier for Figure 76 b, 75 b, 73 b for the coated non-welded specimens. It should be noted that Figure 77 b is the expansion of Figure 77 a in the elastic region (up to the strain 2.5). The general trend of the curves is similar in the elastic region where minor variation in the elastic behavior of the specimens is observed beyond the tensile stress of 150 MPa. Moreover, the non-linear variation of the elastic limit of the specimens for tensile stresses exceeding 150 MPa are observed. This can also be associated with the error related with the experiments, which is in the order of 5.7%. It should be noted that the error is estimated from the repeatability of the experiments, i.e. each experiment is repeated five times. The plastic deformation of the specimen varies depending on the exposure and no exposure in the as received condition. This situation is observed from Figure 77 a, in which the yielding value and the plastic behavior are shown. Specimens exposed for three weeks duration in the static corrosion environment demonstrate slight effect on the plastic response of the specimens. The yielding limit of the specimens differs slightly depending on the exposure period where the non exposed specimen demonstrated improved plastic properties concluding that exposure to static corrosion slightly reduces plastic stress.. Overall, there is a very little difference in stresses for specimens with and without static corrosion exposure. The plastic stress level of the coated non-welded carbon steel specimens is affected more to longer exposure than shorter period or no exposure.

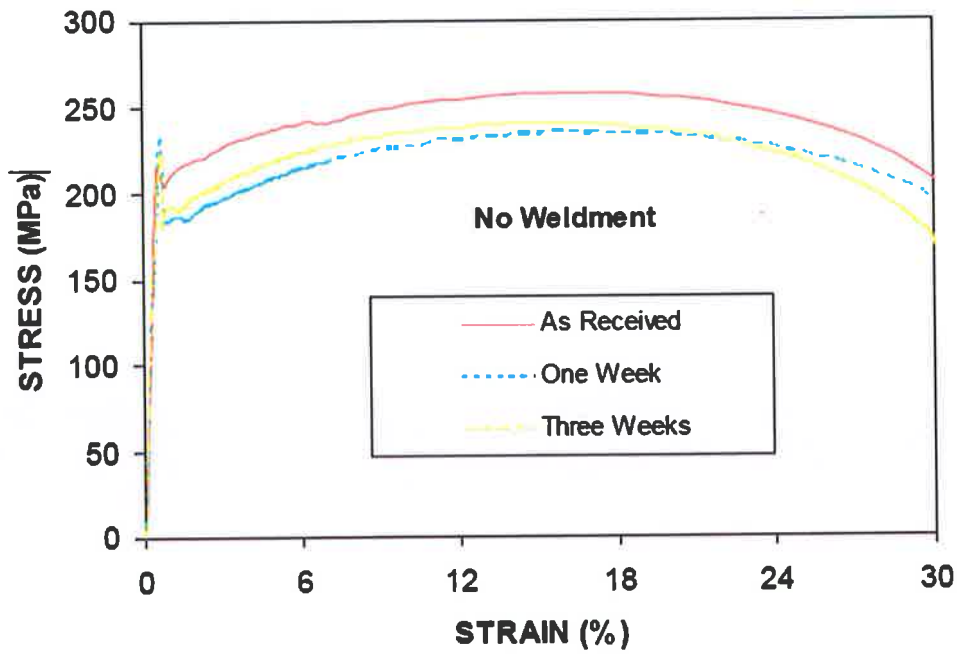


Figure 77 a: Tensile response of the non-welded HVOF coated carbon steel specimens in prior and post static corrosion exposure.

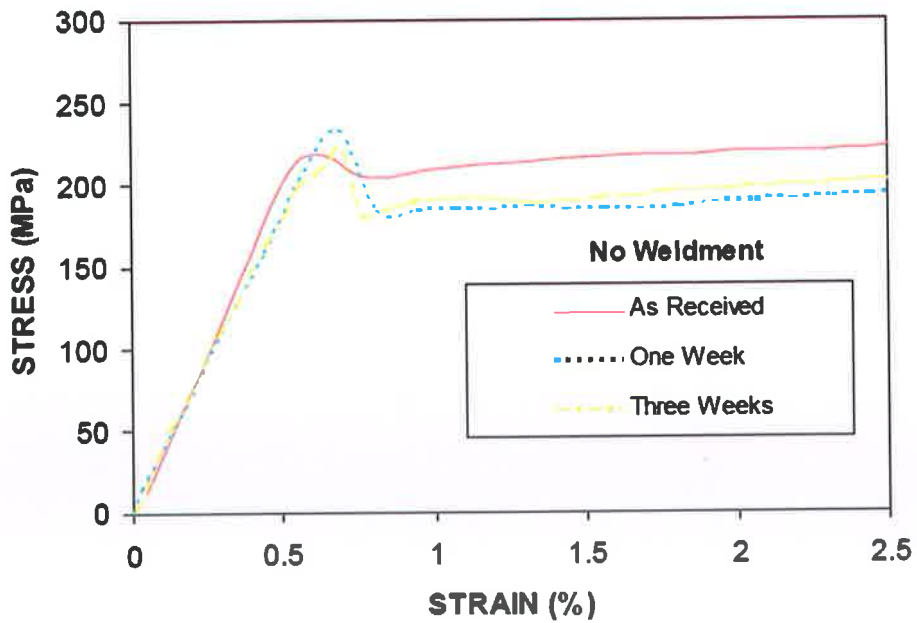


Figure 77 b: Tensile response of the non-welded HVOF coated carbon steel specimens in the elastic region prior and post static corrosion exposure.

Figure 78 a shows tensile stress for welded of size 2.5 mm HVOF coated carbon steel specimens prior and post static corrosion exposure while Figure 78 b shows the stress strain curves close to the elastic region. It can be observed that in the elastic region Figure 78 b, tensile stress behaves similarly for all the specimens up to a tensile stress of 150 MPa. This is because of the corrosion effect was similar to that described earlier for Figure 77 b, Figure 76 b, Figure 75 b and Figure 73 b. It should be noted that Figure 78 b is the expansion of Figure 78 a in the elastic region (up to the strain 2.5). The general trend of the curves is similar in the elastic region where minor variation in the elastic behavior of the specimens is observed beyond the tensile stress of 150 MPa. Moreover, the non-linear variation of the elastic limit of the specimens for tensile stresses exceeding 150 MPa are observed. This can also be associated with the error related with the experiments, which is in the order of 5.7%. The non exposed welded coated specimen demonstrated improved tensile properties compared to the exposed specimens. It should be noted that the error is estimated from the repeatability of the experiments, i.e. each experiment is repeated five times. The corrosion effect in the surface region causes failure of coating through early crack formation during the tensile testing as was observed from earlier performed SEM examinations. In this case, it is observed that the surface cracks are developed in the coating at a distance away from the region where the total failure of the material occurs. This is more pronounced for the specimens subjected to three weeks corrosion environment. Specimens exposed for three weeks duration in the static corrosion environment demonstrate slight effect on the elastic response of the specimens. Overall, there is a very little difference in stresses for specimens with and without static corrosion exposure.

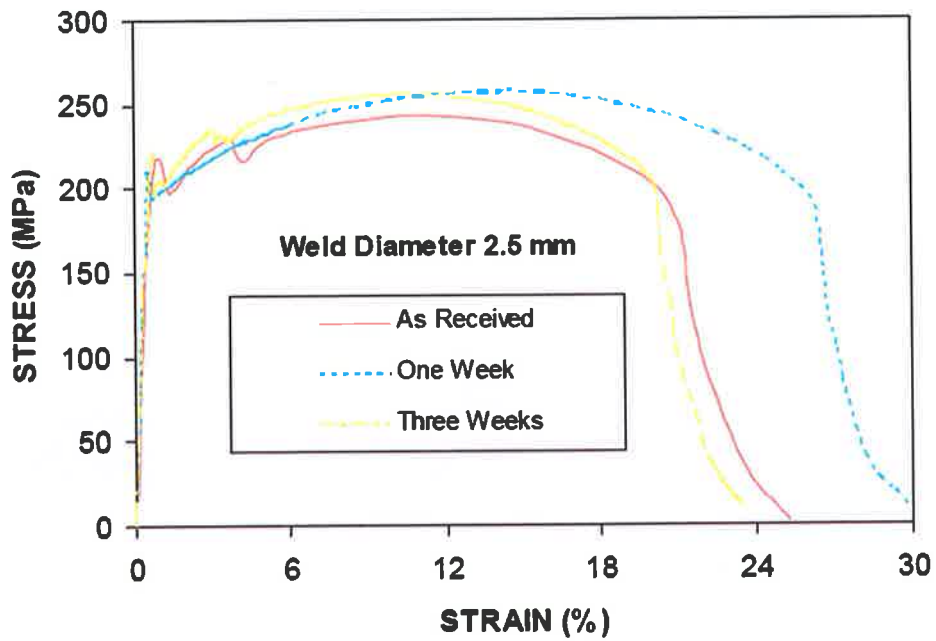


Figure 78 a: Tensile response of the welded (weld size = 2.5 mm) HVOF Coated Carbon Steel specimens prior and post static corrosion exposure.

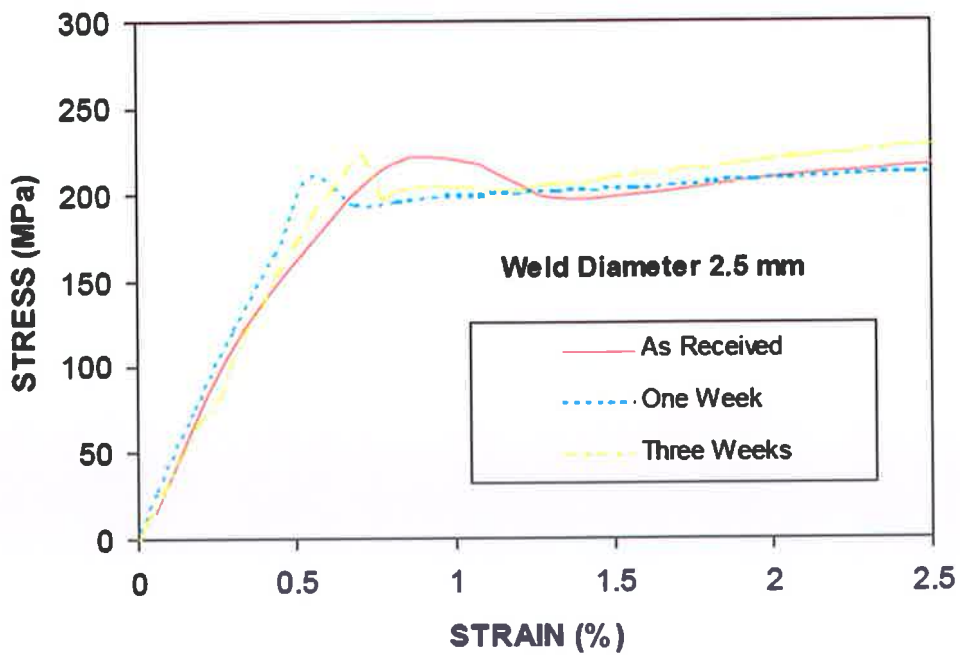


Figure 78 b: Tensile response of the welded (weld size = 2.5 mm) HVOF Coated Carbon Steel specimens in the elastic region prior and post static corrosion exposure.

Figure 79 a shows tensile stress for welded of weld size 3 mm HVOF coated carbon steel specimens prior and post static corrosion exposure while Figure 79 b shows the stress strain curves close to the elastic region. It can be observed that in the elastic region Figure 79 b, tensile stress behaves similarly for all the specimens up to a tensile stress of 200 MPa. This is because of the corrosion effect was similar to that described earlier plots. It should be noted that Figure 79 b is the expansion of Figure 79 a in the elastic region (up to the strain 2.5). The three weeks exposed specimen shows lower tensile strength compared to others which is expected. The non exposed specimen demonstrated improved elastic and plastic properties. The general trend of the curves is similar in the elastic region where minor variation in the elastic behavior of the specimens is observed beyond the tensile stress of 200 MPa. Moreover, the non-linear variation of the elastic limit of the specimens for tensile stresses exceeding 200 MPa are observed. This can also be associated with the error related with the experiments, which is in the order of 5.7%. It should be noted that the error is estimated from the repeatability of the experiments, i.e. each experiment is repeated five times. The corrosion effect in the surface region causes failure of coating through early crack formation during the tensile testing as was observed from earlier performed SEM examinations. Specimens exposed for three weeks duration in the static corrosion environment demonstrate slight effect on the elastic response of the specimens. Overall, there is a very little difference in stresses for specimens with and without static corrosion exposure.

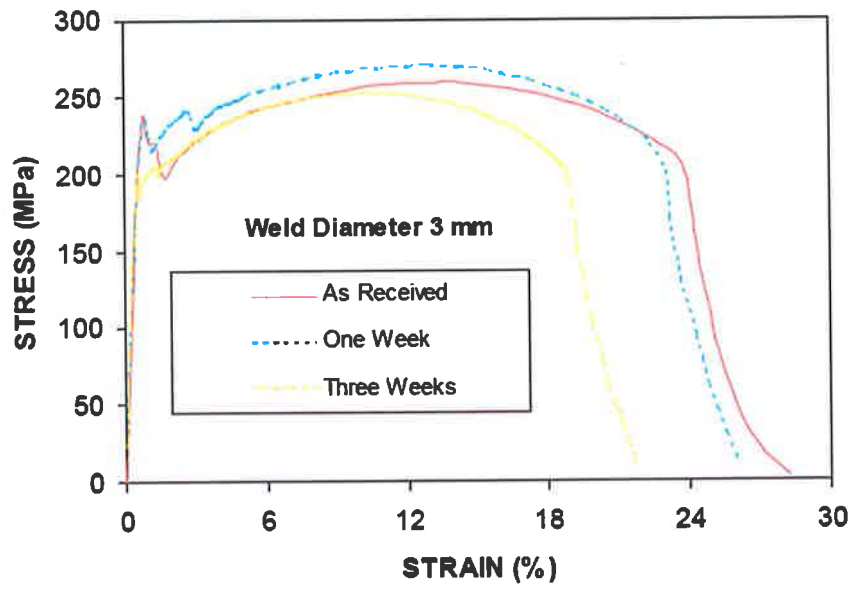


Figure 79 a: Tensile response of the welded (weld size = 3 mm) HVOF coated carbon steel specimens prior and post static corrosion exposure.

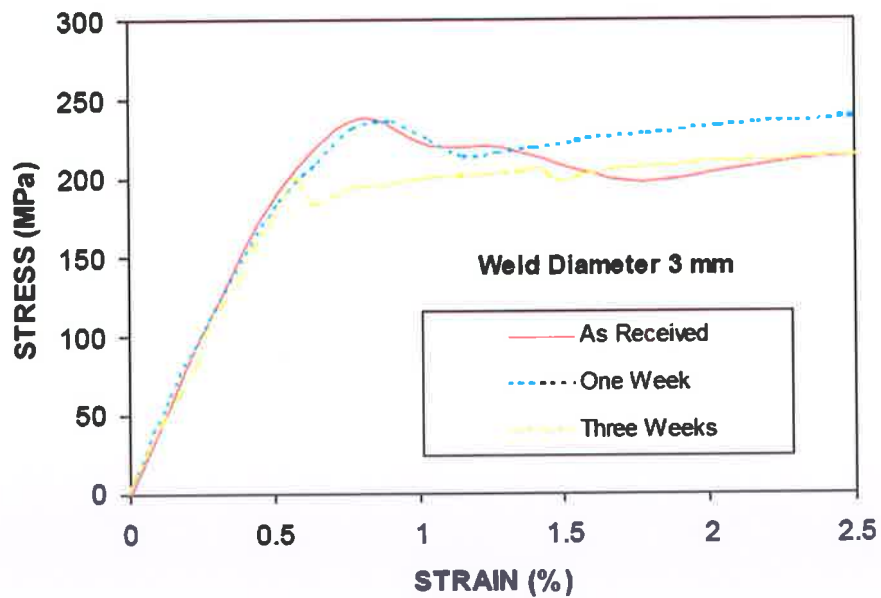


Figure 79b: Tensile response of the welded (weld size = 3 mm) HVOF coated carbon steel specimens in the elastic region prior and post static corrosion exposure.

Figure 80 a shows tensile stress for welded of weld size 5 mm HVOF coated carbon steel specimens prior and post static corrosion exposure while Figure 80 b shows the stress strain curves close to the elastic region. It can be observed that in the elastic region Figure 80 b, tensile stress behaves similarly for all the specimens up to a tensile stress of 180 MPa. This is because of the corrosion effect was similar to that described earlier plots. It should be noted that Figure 80 b is the expansion of Figure of 80 a in the elastic region (up to the strain 2.5). The general trend of the curves is similar in the elastic region where minor variation in the elastic behavior of the specimens is observed beyond the tensile stress of 180 MPa. Moreover, the non-linear variation of the elastic limit of the specimens for tensile stresses exceeding 180 MPa are observed. This can also be associated with the error related with the experiments, which is in the order of 5.7%. It should be noted that the error is estimated from the repeatability of the experiments, i.e. each experiment is repeated five times. Overall, there is a very little difference in stresses for specimens with and without static corrosion exposure. For the coated welded carbon steel specimens; there is an effect on the plastic stress. However, the effect of welding (which creates higher strength in the "Heat Affected Zone") may show less effect for larger weld size due to larger HAZ in the specimen. It is obvious that when comparing results for different weld sizes for no exposure, one week exposure and three weeks exposure, the results clearly more influenced for larger weld size specimens for three weeks exposure to static corrosion exposure.

It is observed that the influence of weld presence, weld size and exposure to static corrosion. It is occasionally observed that there exist experimental variations in the obtained results provided these experiments are repeated several times. Such variations could be due to material inconsistency and experimental errors within a range of  $\pm 10\%$ .

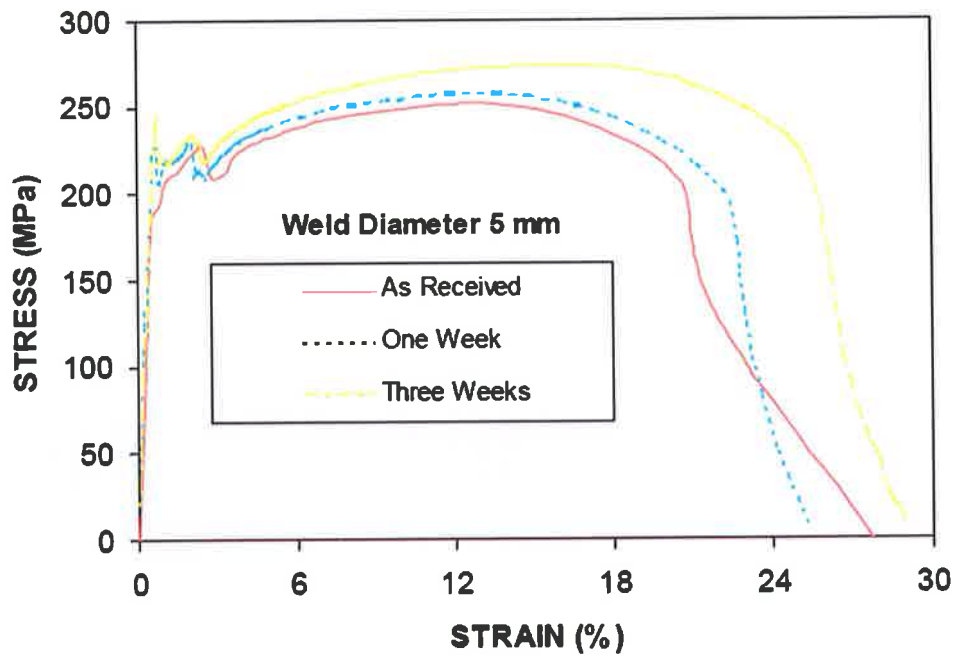


Figure 80 a: Tensile response of the welded (weld size = 5 mm) HVOF coated carbon steel specimens prior and post static corrosion exposure.

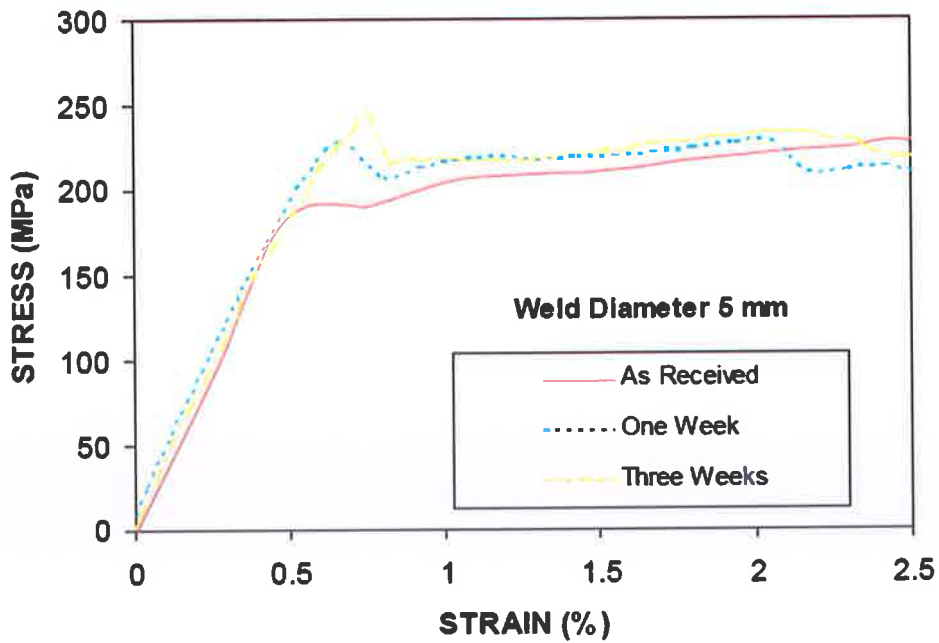


Figure 80 b: Tensile response of the welded (weld size = 5 mm) HVOF Coated Carbon Steel specimens in the elastic region prior and post static corrosion exposure.

#### 4.9.4.2 Stainless Steel Welded Coated Specimens

Stainless steel welded specimens were HVOF coated using Inconel 625 powder. A total of 24 specimens were HVOF coated onto both welded and non-welded steels surfaces. The welded specimens included weld size were selected for tensile testing.

#### 4.9.4.3 Specimens fabrication and distribution

Test specimens were machined and prepared in accordance with standards ASTM E 466 - 96. All specimens were made to dimensions of 10 mm W x 140 mm L and thickness of 3 mm. All the specimens were coated to a thickness of 1000  $\mu\text{m}$ . All specimens including coated and welded coated specimens were tensile tested, prior and post corrosion exposure and compared to those tested without corrosion exposure. All tensile tests were carried out using lab standard Instron Machine model 8501. Table 15 demonstrates all tested coated carbon steel specimens.

Table 15: HVOF sprayed nickel alloy 625 coatings onto 304 stainless steel specimens

<b>Sample#</b>	<b>Exposure Period</b>	<b>Weld Size</b>
25	No exposure	No Weld
26	No exposure	2.5 mm
27	No exposure	3 mm
28	No exposure	5 mm
29	One week	No Weld
30	One week	2.5 mm
31	One week	3 mm
32	One week	5 mm
33	Three weeks	No Weld
34	Three weeks	2.5 mm
35	Three weeks	3 mm
36	Three weeks	5 mm
37	No exposure	No Weld
38	One week	No Weld
39	Three weeks	No Weld
40	No exposure	2.5 mm
41	One week	2.5 mm
42	Three weeks	2.5 mm
43	No exposure	3 mm
44	One week	3 mm
45	Three weeks	3 mm
46	No exposure	5 mm
47	One week	5 mm
48	Three weeks	5 mm

#### 4.9.4.4 HVOF coated stainless steel Specimen with no corrosion exposure and exposed coated specimens including coated non-welded and welded specimens with weld sizes of 2 mm, 3 mm and 5 mm.

Figure 81 a shows tensile test results of HVOF coated welded and non-welded stainless steel specimens prior to the static corrosion exposure tests (in the as received condition) while Figure 81 b shows the tensile test results close to the elastic region. In the elastic region, the specimens' response to the tensile load is similar, except small discrepancies, which can be related to the error (which is 5.7%) and the non-linear effect of the welding and heat affected zone on the tensile properties. This situation is also observed for plastic behavior of the base material which differs from the carbon steel Figure 73 a. Consequently the combined effect of the weld and the heat affected zone size on the tensile response of the specimens is in the non-linear form. It should be noted that the error is estimated from the repeatability of the experiments.

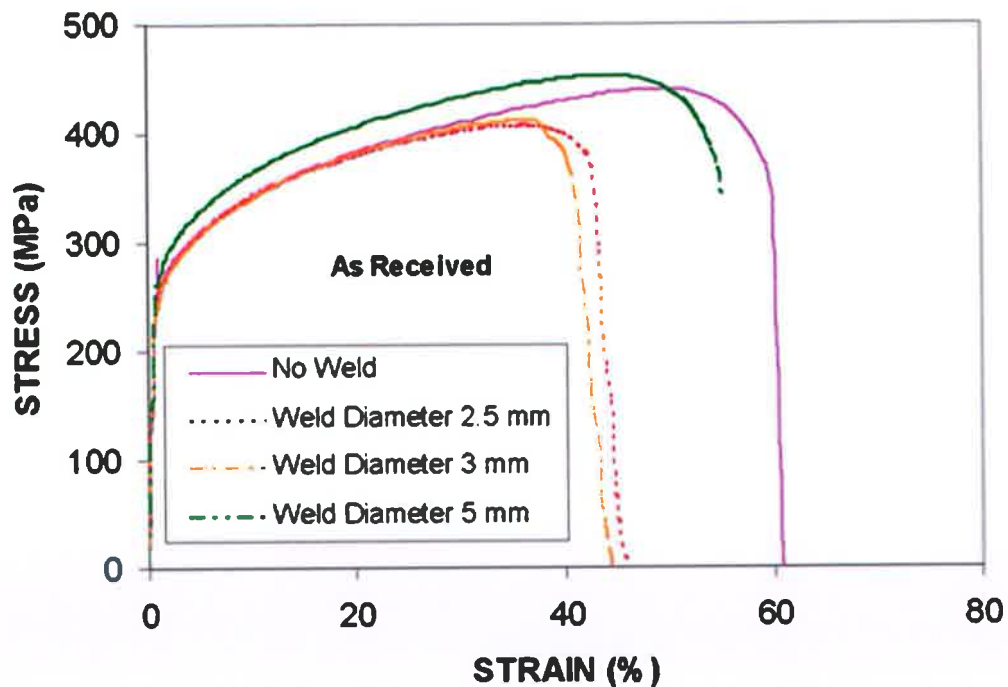


Figure 81 a: Tensile response of the welded and no-welded stainless steel specimens prior to corrosion testing.

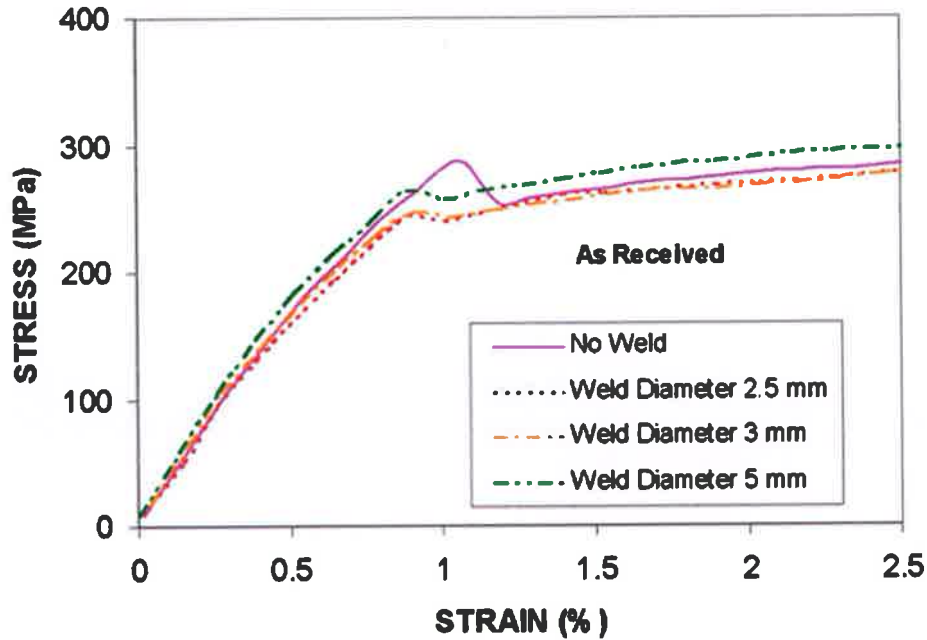


Figure 81 b: Tensile response of the welded and non-welded HVOF coated stainless steel specimens in the elastic region prior to corrosion testing.

In the case of one week duration static corrosion exposure shown in Figure 82 a and Figure 82 b, a similar situation is observed, that in the elastic region, the specimen response to tensile load differs slightly from each other. This is attributed to the nonlinear effect of the weld and heat affected zone sizes on the tensile response of the specimens. For the coated stainless steel specimens, the effect of exposure to corrosion may be less on plastic stress. The effect on plastic stress may be reduced for larger diameter of welds for no exposure or for the same duration of exposure to corrosion.

For the coated stainless steel specimens, the effect of exposure to corrosion may be less on plastic stress. The effect on plastic stress may be reduced for larger diameter of welds for no exposure.

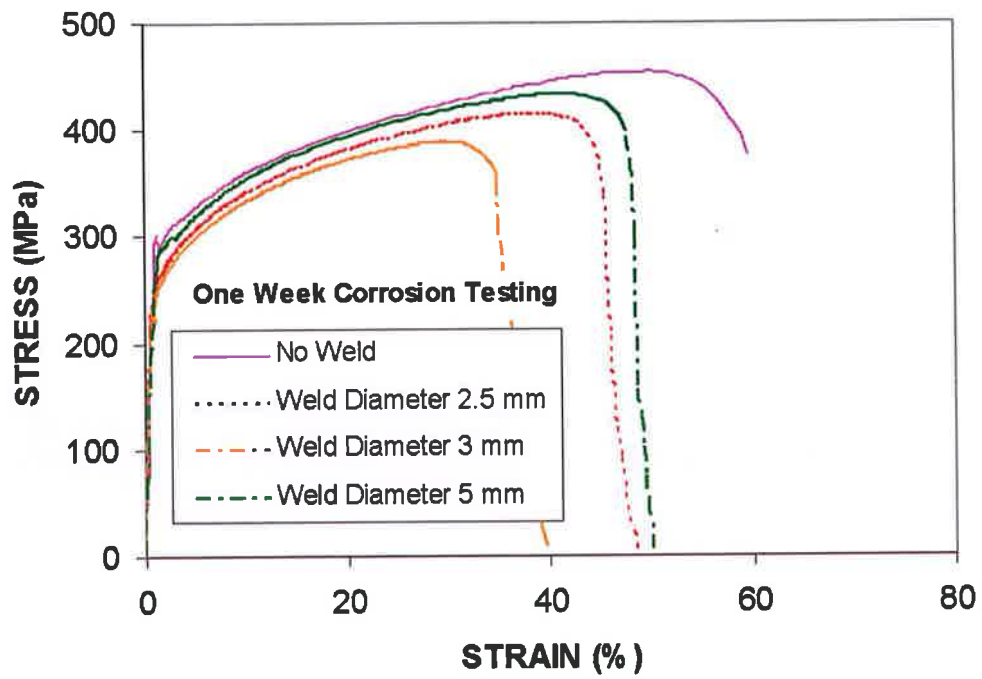


Figure 82 a: Tensile response of the welded and no-welded stainless steel specimens after one week corrosion testing.

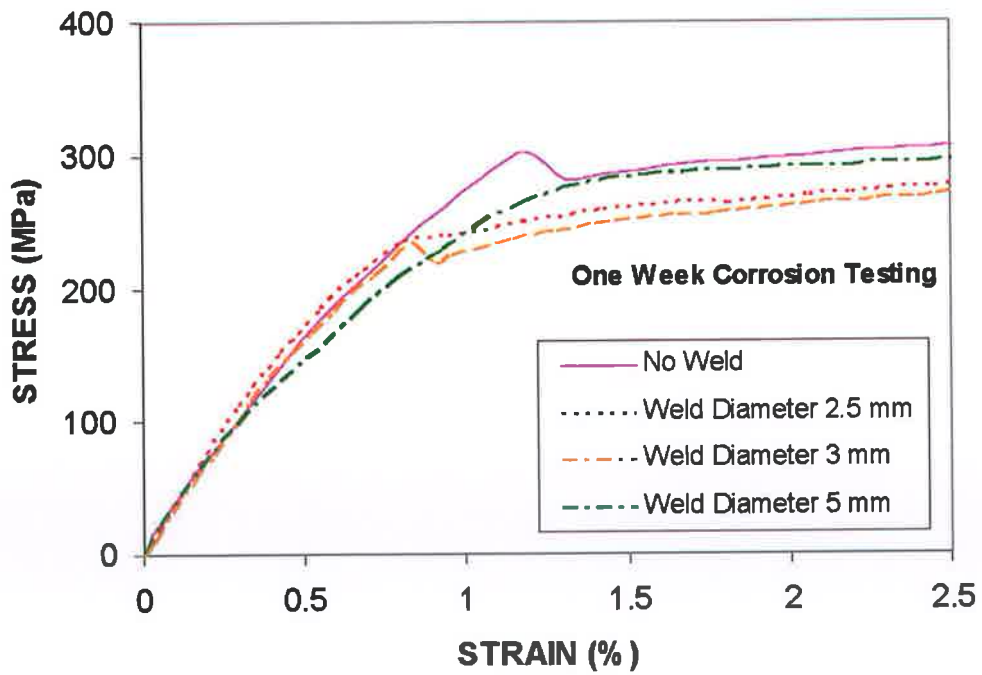


Figure 82 b: Tensile response of the welded and no-welded stainless steel specimens in the elastic region after one week corrosion testing.

Moreover, similar situation is observed for three weeks corrosion durations Figure 83.a and Figure 83 b. When comparing Figures (81.b), (82.b),and (83.b), it can be observed that there is no clear pattern of the tensile behavior due to different weld sizes and corrosion durations, provided that the yielding limit of the non-welded specimen remains higher as compared to that of the welded specimens including all the corrosion duration considered. Consequently, specimens' welding reduces the elastic limit of the specimen regardless of the weld diameter. This situation is slightly modified for corrosion duration of three weeks; in which case, the elastic limit reduces slightly for all the specimens after three weeks of corrosion testing. For stainless steel coated specimens, the corrosion protection after one week exposure is more evident in the non-welded specimens compared to the welded specimens. While specimens with 5.0 mm weld sizes provide almost similar protection. For the coated stainless steel specimens, the effect of exposure to corrosion may be less on plastic stress. The effect on plastic stress may be reduced for larger diameter of welds for no exposure or for the same duration of exposure to corrosion.

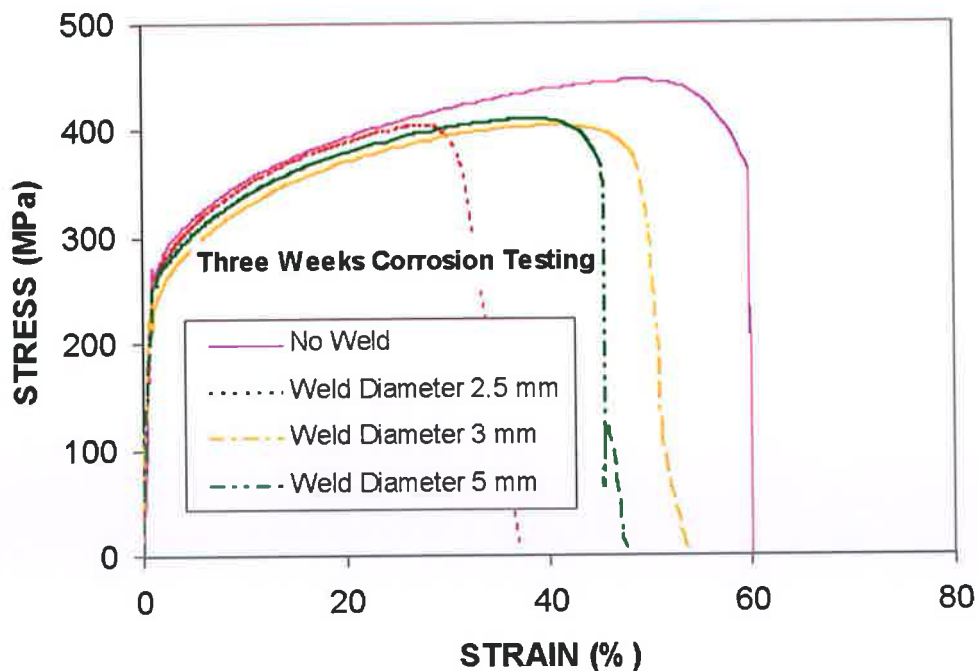


Figure 83.a: Tensile response of the welded and non-welded HVOF coated stainless steel specimens after three weeks corrosion testing.

However, for 3 weeks exposure, larger weld size shows a detrimental effect on plastic stress levels than the non-welded and smaller diameter welded specimens.

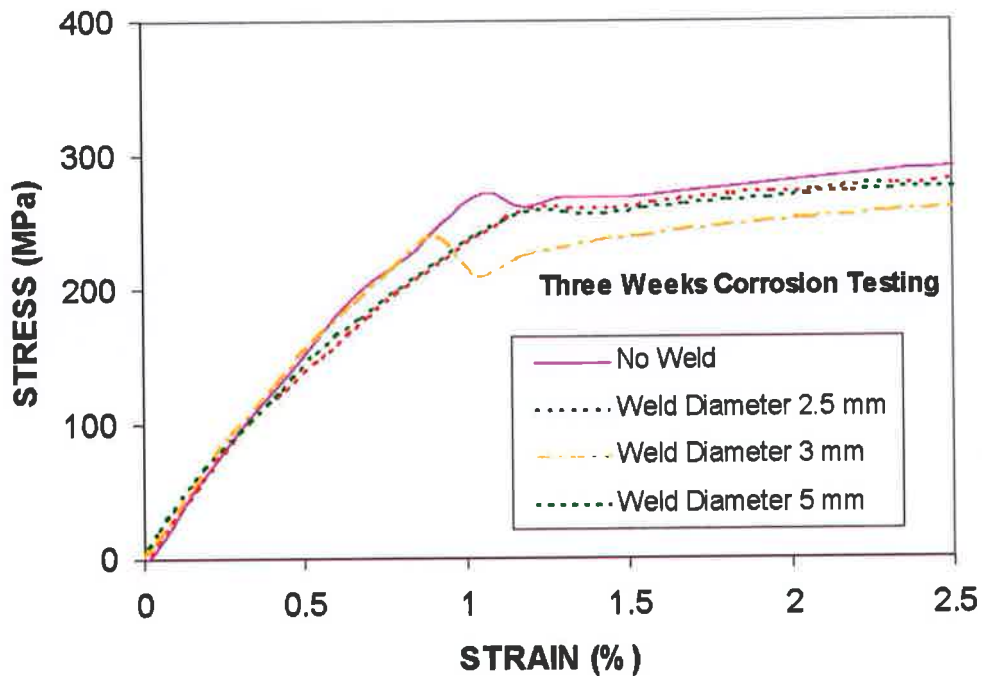


Figure 83 b: Tensile response of the welded and non-welded HVOF coated stainless steel specimens in the elastic region after three weeks corrosion testing.

Figure 84 a shows tensile test results of HVOF coated non-welded stainless steel specimens prior and post to static corrosion exposure while Figure 84 b shows the tensile test results close to the elastic region. In the elastic region, the specimens' response to the tensile load is similar, except small discrepancies, which can be related to the error (which is 5.7%) and exposure period affecting the tensile properties. This situation is also observed for plastic behavior of the substrate material which differs from the carbon steel Figure 77 a. Consequently the effect of the exposure period is very similar in both elastic and plastic regions. It should be noted that the error is estimated from the repeatability of the experiments.

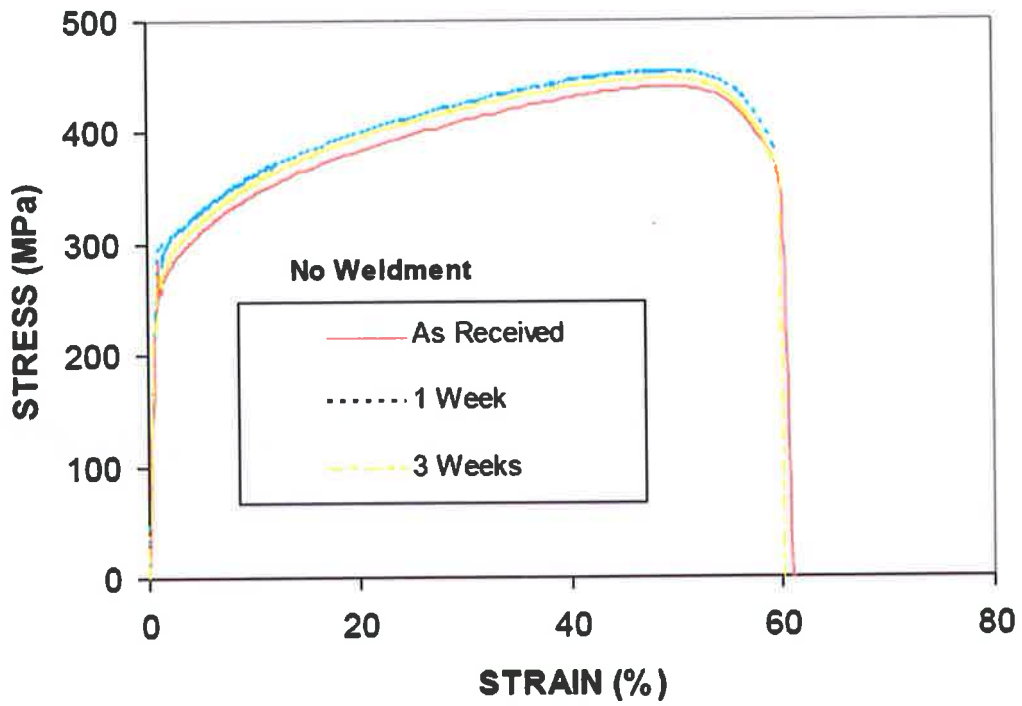


Figure 84 a: Tensile response of the non-welded HVOF stainless steel specimens prior and post static corrosion exposure.

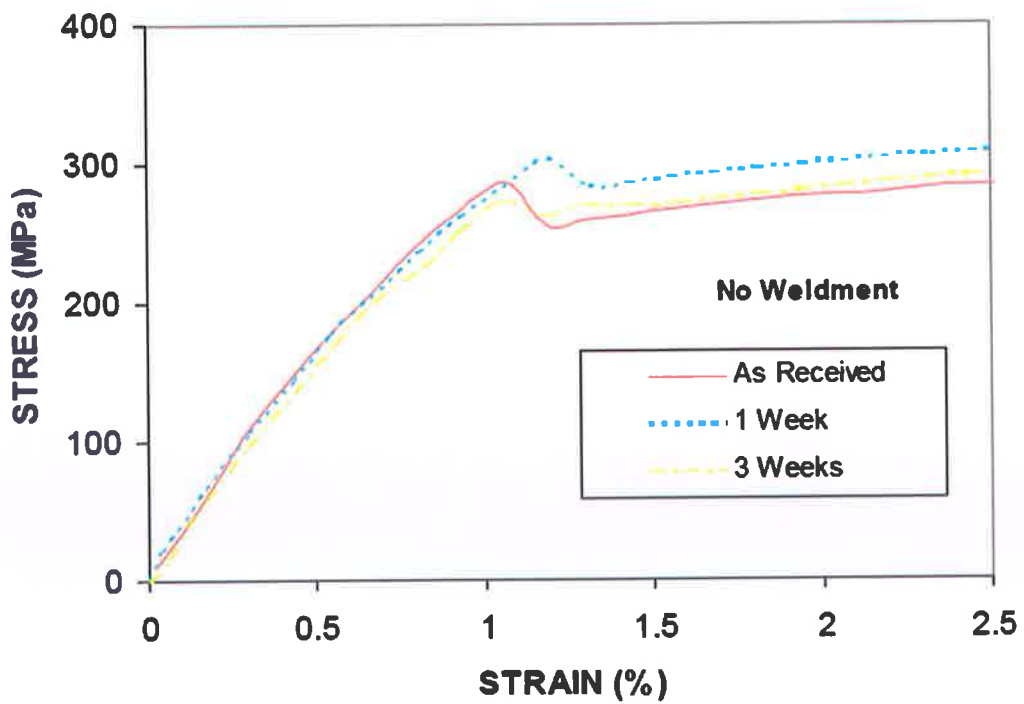


Figure 84 b: Tensile response of the non-welded HVOF stainless steel specimens in the elastic region prior and post static corrosion exposure.

Figure 85 a shows tensile test results of HVOF coated welded (weld size = 2.5mm) stainless steel specimens prior and post to static corrosion exposure while Figure 85 b shows the tensile test results close to the elastic region. In the elastic region, the specimens' response to the tensile load is similar, except minor variations, which can be related to the error (which is 5.7%) and exposure period affecting the tensile properties as well as the effect of the non-linear effect of the welding and heat affected zone on the tensile properties. This situation is also observed for plastic behavior of the base material which differs from the carbon steel Figure 78 a. In the plastic region, the effect of the exposure period is observed. The three weeks exposed specimen showed lower plastic stress level compared to the one week exposed and non exposed specimens. It should be noted that the error is estimated from the repeatability of the experiments. The corrosion protection after one week exposure is more evident in the non-welded specimens compared to the welded specimens as shown earlier. For the coated stainless steel specimens, the effect of exposure to corrosion may be less on plastic stress. The effect on plastic stress may be reduced for larger diameter of welds for no exposure or for the same duration of exposure to corrosion.

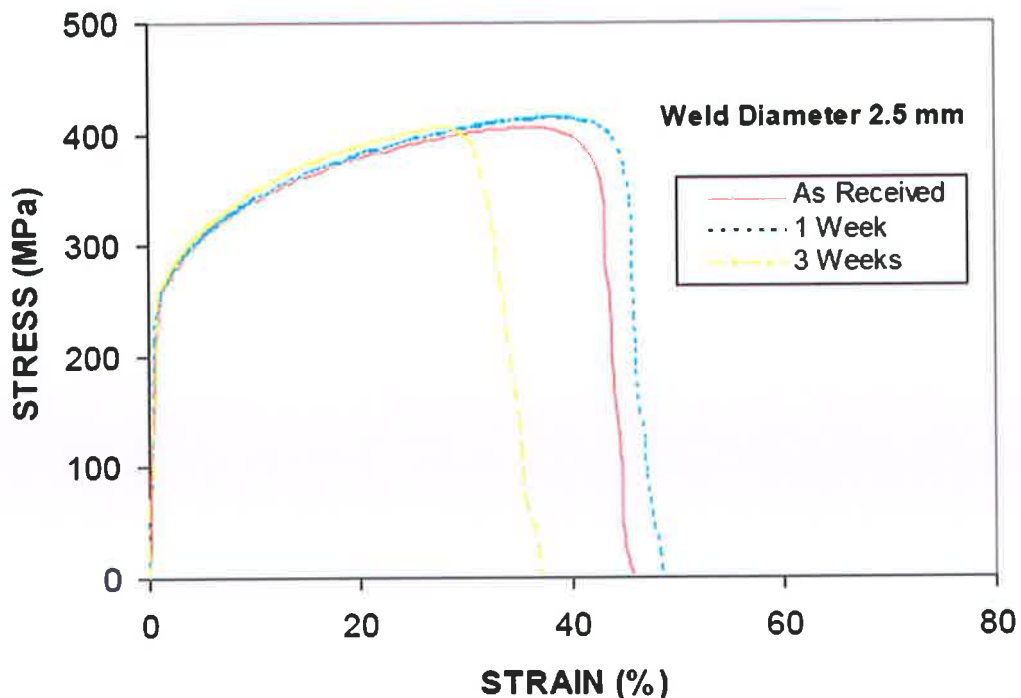


Figure 85 a: Tensile response of the welded (weld size = 2.5 mm) HVOF stainless steel specimens prior and post static corrosion exposure.

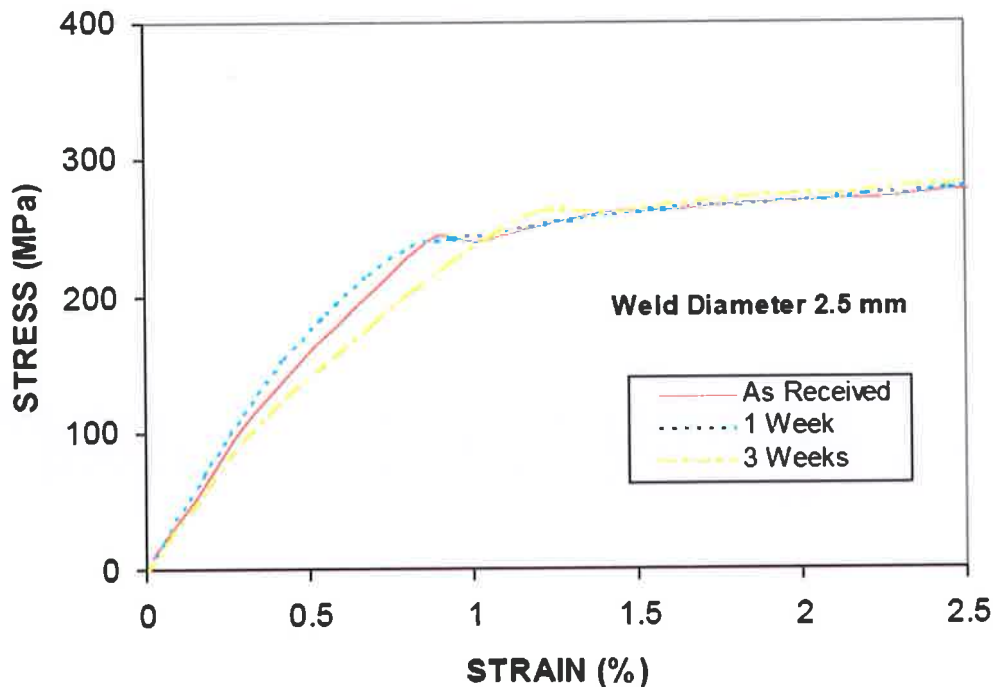


Figure 85 b: Tensile response of the welded (weld size = 2.5 mm) HVOF stainless steel specimens in the elastic region prior and post static corrosion exposure.

Figure 86 a shows tensile test results of HVOF coated welded (weld size = 3 mm) stainless steel specimens prior and post static corrosion exposure while Figure 86 b shows the tensile test results close to the elastic region. In the elastic region, the specimens' response to the tensile load is similar, except small discrepancies, which can be related to the error (which is 5.7%) and the non-linear effect of the welding and heat affected zone on the tensile properties. Consequently the combined effect of the weld and the heat affected zone size on the tensile response of the specimens is in the non-linear form. It should be noted that the error is estimated from the repeatability of the experiments. It can be observed that there is no clear pattern of the tensile behavior due to different weld sizes and corrosion durations, provided that the yielding limit of the non-welded specimen remains higher as compared to that of the welded specimens including all the corrosion duration considered. Consequently, specimens' welding reduces the elastic limit of the specimen regardless of the weld diameter. For the coated stainless steel specimens, the effect of exposure to corrosion may be less on plastic stress. The effect on plastic stress may be reduced for larger diameter of welds for no exposure

or for the same duration of exposure to corrosion.

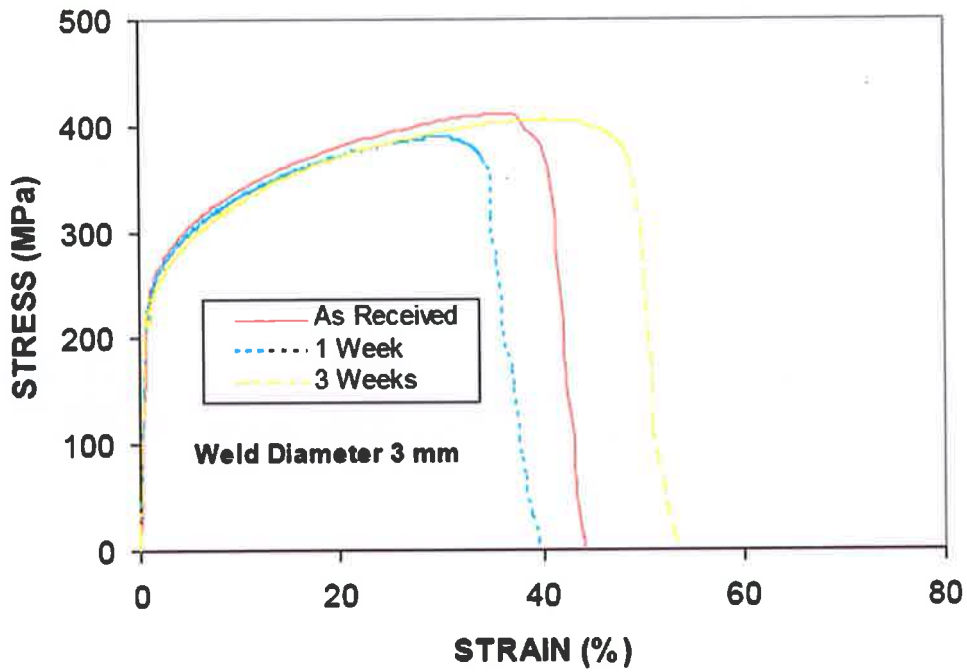


Figure 86 a: Tensile response of the welded (weld size = 3 mm) HVOF stainless steel specimens prior and post static corrosion exposure.

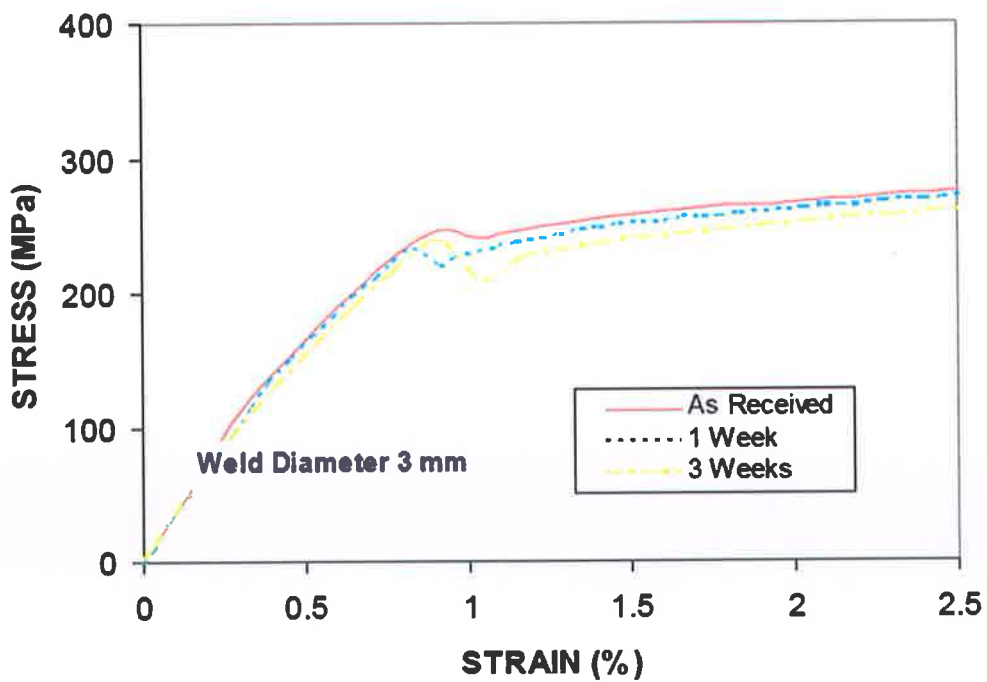


Figure 86 b: Tensile response of the welded (weld size = 3 mm) HVOF stainless steel specimens in the elastic region prior and post static corrosion exposure.

Figure 87 a shows tensile test results of HVOF coated welded (weld size = 5 mm) stainless steel specimens prior and post static corrosion exposure while Figure 87 b shows the tensile test results close to the elastic region. In the elastic region, the specimens' response to the tensile load is similar, except small discrepancies, which can be related to the error (which is 5.7%) and the non-linear effect of the welding and heat affected zone on the tensile properties. The three weeks exposure was very evident in affecting the elastic and plastic properties compared to the one week exposure and the non exposed specimen. Consequently the combined effect of the weld and the heat affected zone size on the tensile response of the specimens is in the non-linear form. It should be noted that the error is estimated from the repeatability of the experiments. Consequently, specimens' welding reduces the elastic limit of the specimen regardless of the weld diameter. For the coated stainless steel specimens, the effect of exposure to corrosion may be less on plastic stress. The effect on plastic stress may be reduced for larger diameter of welds for no exposure or for the same duration of exposure to corrosion. In conclusion and after analyzing all the generated plots, and comparing influence of weld presence, weld size and exposure to static corrosion, it is occasionally observed that there exist experimental variations in the obtained results provided these experiments are repeated several times. Such variations could be due to material inconsistency and experimental errors within a range of  $\pm 10\%$ .

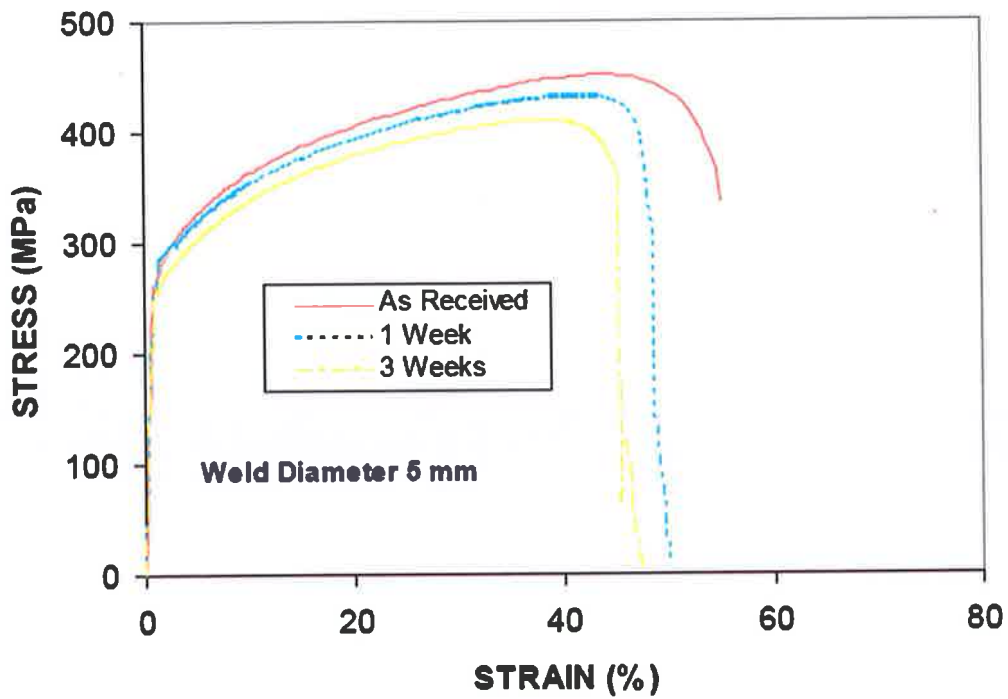


Figure 87 a: Tensile response of the welded (weld size = 5 mm) HVOF stainless steel specimens prior and post static corrosion exposure.

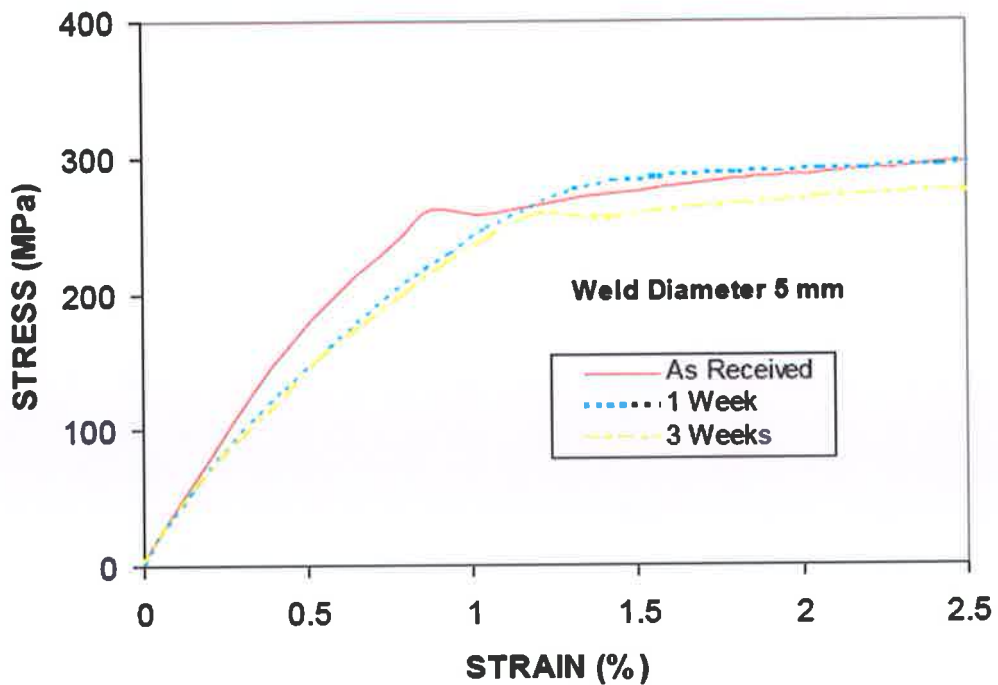


Figure 87 b: Tensile response of the welded (weld size = 5 mm) HVOF stainless steel specimens in the elastic region prior and post static corrosion exposure.

#### 4.10 CONCLUSION

The effect of the weld size and weld size related heat affected zone on the tensile properties of the specimens is more pronounced for carbon steel specimens. In this case, welding size and related heat affected zone modify the elastic response of the specimens. However, after the corrosion exposure for periods of one and three weeks, tensile response in the elastic region of the specimens becomes almost similar. The weld size and the related heat affected zone influence the plastic behavior of the specimens. Increasing weld diameter modifies this situation. The influence of weld size and related heat affected zone on the tensile properties is very observed for the stainless steel specimens. For coated non-welded carbon steel specimens, the plastic stress level is affected and influenced more to longer exposure than shorter period or no exposure to static corrosion. Though, for the coated carbon steel welded specimens there was slight effect on the plastic stress. However, the effect of welding (which creates higher strength in the "Heat Affected Zone" showed less effect for larger weld size due to larger HAZ in the specimens. The coated welded carbon steel specimens are influenced more for larger weld sizes specimens for 3 weeks exposure to static corrosion. The coated welded carbon steel specimens are influenced more for larger weld sizes if exposed for three weeks exposure to static corrosion. The coated stainless steel specimen demonstrated less effect to static corrosion exposure in the plastic stress region. The coated stainless steel specimens showed reduced stress effect on the plastic stress for larger weld sizes for non-exposed coated welded specimens and those welded coated specimens exposed for short period to static corrosion. The coated welded stainless steel specimens demonstrated improved and higher resistance to static corrosion exposure provided that the presence of HAZ has enhanced corrosion resistance. Generally, for those coated welded specimens with weld size of 5 mm, the HAZ is greater leading to increase in the strength of the welded zone of the material.

The influence of weld presence beneath HVOF coating onto steel surfaces has gained only limited attention. Al Fadhli et al [200] investigated effect of weld presence and UVOF coating onto the corrosion resistance. The author found that Inconle-625 coating

protects substrate and welds from corrosion effects. The author also concluded that the elastic behavior was similar for examined coated-welded specimens prior and post corrosion exposure which agree with the current concluded results of this study. Both the current research study and Al Fadhli et al [200] research concluded that the Inconle-625 powder coating improves the corrosion resistance of exposed stainless steel coated welded specimens. Additionally, the two studies observed that the extended static corrosion exposure for the HVOF coated specimens reduces coating resistance. Al Fadhli et al [200] demonstrated that the corrosion resistance of coated welded stainless steel specimens decreases compared to the plain stainless steel specimens. This is due to the corrosion exposure reducing the coating resistance. Also, the author showed that the presence of weld decreases the corrosion resistance. The current research study concluded that the weld presence increases coating resistance to static corrosion exposure. For coated non-welded carbon steel specimens, the plastic stress level is affected and influenced more to longer exposure than shorter period or no exposure to static corrosion. The current research study showed that the coated welded specimens with weld size of 5 mm, the HAZ is greater leading to increase in the strength of the welded zone of the material, consequently, improved mechanical properties and corrosion resistance. Al Fadhli et al [200] concluded that presence of weld reduces coating resistance to the corrosion exposure.

The current study examined the fatigue properties of coated welded stele surfaces exposed to static corrosion having different weld sizes. The experimental work performed in this study concluded that length of exposure to static corrosion decreases coating resistance to fatigue compared to the non exposed specimens. Also, the presence of weld decreases the fatigue life of the coating with further decrease to fatigue life associated to extended static corrosion exposure. Al-Fadhli et al [38, 200] performed experimental work studying the corrosion and fatigue behavior of steel surfaces HVOF coated by Inconel 625 thermally sprayed. The authors found that the fatigue strength decreases as the period of coating exposure to corrosive environment increases which agrees with the current study findings.

The current research study and work completed by Al-Fadhli et al [38, 200] concluded different observations and findings regarding the coating performance onto welded steel surfaces. This could be justified due to that the current specimens were welded through the entire center and specimen thickness adding material strength to the specimen. While Al-Fadhli et al [200] used different weld methodology which is spot welding joining two pieces. Apparently, coating deposition onto welded surfaces behave differently depending on the welding geometry and joining process. Therefore, it is recommended that further investigation and experimental work to be performed examining weld geometry and process on the coating performance and corrosion resistance.

As indicated earlier, the minor variations in the plastic region could be due experimental errors resulting instability setting in at displacements of about 0.25 mm to 0.30 mm. In conclusion, beyond displacements of 0.30 mm results show minor instability becoming less important. Overall, there are always variations observed in the experimental results even when repeated several times. Such variations anticipated to be due to material inconsistency and experimental errors within  $\pm 10\%$  or more. These errors and variations may explain obtained un-expected trends were noticed from the generated plots.

#### 4.11 SUMMARY

The distinction in the yield strength for all the HVOF coated tested specimens including both welded and non-welded specimens is believed to be due to microstructural differences and in particular related to preferential attack along the inter-particle (splat) boundaries of the coating. Selected HVOF coated specimens including welded and non-welded coated specimens demonstrated porosity within the coating and poor bonding between the coating and the substrate. Apparently, the corrosive solution penetrated through coating pores and through the present observed gap/ discontinuity between coating and substrate causing early failure for those specimens. This porosity and delamination effects could be due to the impact of few un-melted powder particles causing residual stress local zones, particularly at the coating-substrate material interface. Additionally, poor bonding between coating and the substrate contributes to early failure and lower yield strength. These anticipated imperfection zones are considered stress

creators resulting in sub-surface and surface crack introduction and spread.

The fatigue failure life of stainless steel (304L SS) specimens and carbon steel HVOF coated and welded were examined prior and post static corrosion exposure.

Experimental tests concluded that exposure to static corrosion reduces fatigue life for those coated non welded specimens. Similar observation was found for those coated welded specimens when compared their fatigue life in the as received condition with no exposure to static corrosion and for those coated welded specimens exposed to three weeks static corrosion. Overall, it is concluded that static corrosion exposure reduces fatigue life for coated specimens either welded or non-welded. On the other hand, it is concluded that coated welded specimens demonstrate shorter fatigue life compared to the non welded coated specimens in both scenarios with corrosion exposure and without corrosion exposure. Additionally, it is concluded that increased weld size also shorten the fatigue life of the coated welded specimens in both cases exposed and non exposed specimens.

It is obvious from the plots that the tensile tests are completed if either the coating or the specimen material fails. The elastic deformation of the exposed specimens and non-exposed specimens showed similar behavior with negligible variations. Moreover, the elastic phenomenon for the welded-coated exposed specimen's tested with and without corrosion exposure is similar. However, in the region of initiation in the plastic zone there is a considerable difference. In this case a coated specimen (no weld) exposed to three weeks of static corrosion fails at a lower load than the non-exposed specimen. It is clearly observed that from the plots that the elastic modulus of the coating and the substrate varies introducing cracking mechanisms and transmission. During shear mode, the coating cracks due to tensile loadings leading to total coating cracking and propagation. This increases with tensile load causing the elastic flow of substrate material and plastic flow of the coating led to conformity of interface. Increasing tensile load further causes the coating to flow in the plastic region and the substrate material can no longer support the coating resulting in the cracking of the coating. Once this stage is

reached de-lamination failure and spalling occurs due to the extensive crack propagation along the subsurface and to the interface defects. Spalling is therefore triggered at the boundaries of the microstructural defects in the coating.

In the plastic region, selective coated specimens exposed to one week corrosion demonstrated early complete plastic deformation while the those coated specimens in the as received condition with no exposure showed improved plastic deformation. The coating porosity and poor bonding contributed in lowering the adhesion strength between the coating and the substrate. Moreover, coated specimens with three weeks exposure deformed plastically to total deformation showing lower plastic stress level compared to other coated specimens with one week exposure and in the as received condition. The elastic regions for the welded coated specimen with no exposure exhibited improved elastic properties. The weld presence influences the plastic behavior to early permanent total plastic deformation.

It is clearly observed that from the plots that the elastic modulus of the coating and the substrate varies introducing cracking mechanisms and transmission. The increased weld size of the HVOF coated specimens does not influence elastic properties compared to the coated non-welded steel surfaces with negligible variations. Exposure period of the coated and weld-coated specimens is not linear and occasionally influenced by exposure period. Increasing tensile load further causes the coating to flow in the plastic region and the substrate material can no longer support the coating. This results in the cracking of the coating. Once this stage is reached, de-lamination failure and spalling occurs due to the extensive crack propagation along the subsurface and to the interface defects. Spalling is therefore triggered at the boundaries of the microstructural defects in the coating. Due to spalling and de-lamination of the coating film from the substrate prior to tensile tests and post corrosion test which could have been due to surface preparation with leftover foreign materials and un-melted particles, it was visually and microscopically observed the initiation and propagation of localized corrosion due to the formation of pits, the presence of crevices or a breakdown of the oxide film. The corrosion effects represented by early coating failure also subjected to the start and

evolution of local pitting or crevice corrosion attack at the surface of the material being tested. These results show that coatings were prepared with low levels of porosity. Another factor influencing elevated improved tensile strength was the highly melted powder during the spraying process as a result of high combustion temperature giving a lamella type microstructure with oxide stringers. From previous SEM examinations for nickel based alloy coatings deposited onto 304 stainless-steel substrates, it was concluded that the microstructure obtained appeared to consist predominately of well stacked, partially deformed particles. This microstructure type suggests the powder particles were at a lower temperature on impact with the substrate, possibly below their melting point, when sprayed using the HVOF spraying facility. The earlier obtained SEM examinations showed that the smaller powder size range (15 to 45  $\mu\text{m}$ ) produced coatings with a slightly lower porosity. Likewise to be said, the oxide level in each coating type was dependent on the powder size range, with the smaller size producing conspicuously elevated oxide content in the prepared coatings.

The microstructures of the nickel alloy coatings deposited by the HVOF spraying system, exhibited a lamella type appearance with many oxide stringers. The coating microstructures obtained for the coatings sprayed showed to consist mainly of well stacked partially deformed particles. These coatings also demonstrated a clear layered structure, with the layers parallel to the substrate separated by a darker contrast phase supposed to be oxide. Each layer is believed to represent one pass of the spray gun over the surface.

Overall, the demonstrated tensile strengths for all the tested coatings prior and post exposure including welded specimens were excellent and reliable. The observed failures usually occurred at the coating to substrate boundary. For all the tests, the coatings showed excellent coating adhesion onto the plain and welded steel surfaces reflecting the fact that a superior adhesion was attained provided the tensile strength was not influenced by weld presence.

---

# APPENDIX A

---

## **(1) Tensile tested round solid bars ASTM: C633-01 specimens:**

A collection of round solid bars specimens of carbon steel and stainless (304 SS) steel materials were HVOF coated with a coating powder similar to Inconel 625. All the coated specimens were exposed to brine solution complete immersion for static corrosion testing. The exposure period was selected to be one (1) week, two (2) weeks and three (3) weeks for both types of specimens. Optical microscopy and Scanning Electron Microscopy examinations (Figure A122 to Figure A135) were made for the exposed tested specimens. The examinations were made for each tested specimens to show and observe the following:

- To observe Coating to substrate interface.
- To determine bonding between the coating adhesion to base metal.
- Coating porosity level.
- Coating adherence onto the specimen.
- Coating crack sites.
- Coating defects.

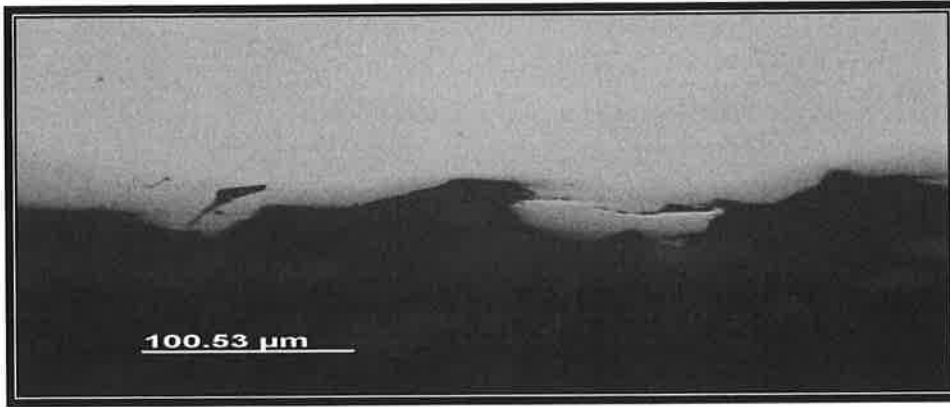


Figure A122: Round solid bar: Original coating surface cross section; Stainless steel after three (3) weeks exposure to brine solution tensile tested.

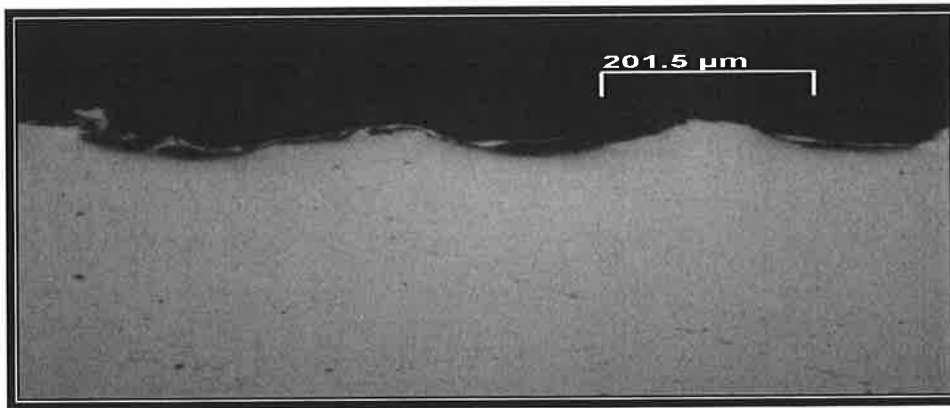


Figure A123: Round solid bar: Original coating surface cross section; Stainless steel after two (2) weeks exposure to brine solution tensile tested.



Figure A124: Round solid bar: Original coating surface cross section; Stainless Steel after two (2) weeks exposure to brine solution exposure tensile tested Center focus.



Figure A125: Round solid bar: Original coating surface cross section; Stainless Steel after two (2) weeks exposure tensile tested side focus.

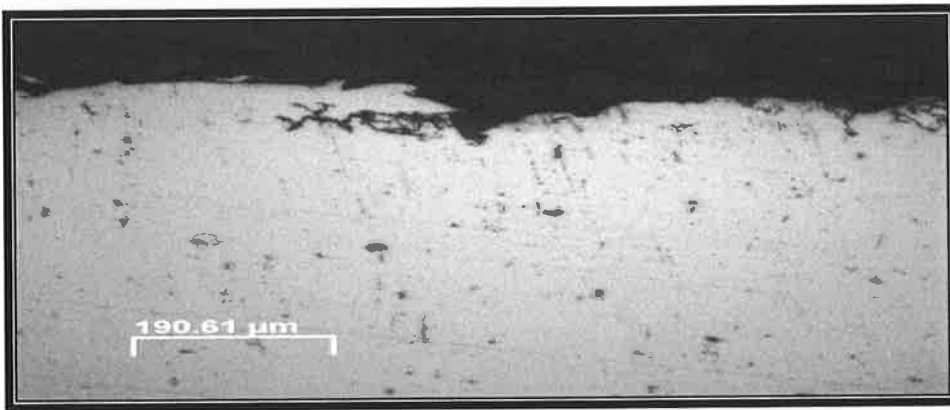


Figure A126: Round solid bar: Original coating surface cross section; Carbon steel after three (3) weeks exposure to brine solution tensile tested cross section.

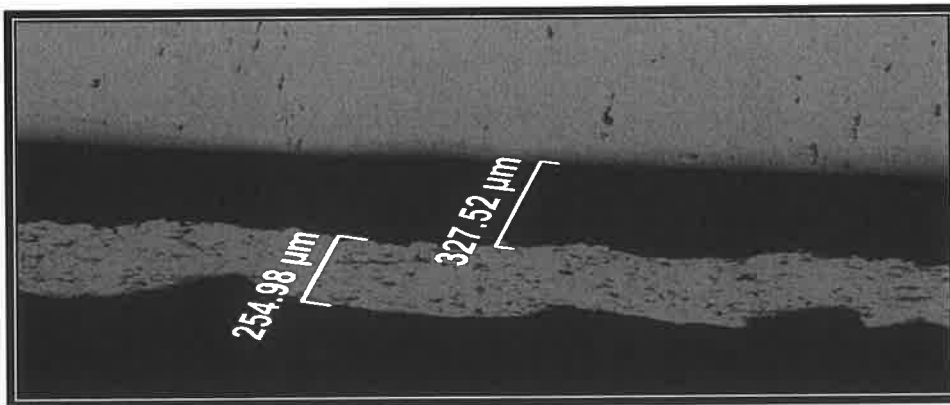


Figure A127: Round solid bar: Dummy specimen coating surface cross section; Carbon steel after three (3) weeks exposure to brine solution tensile tested cross section.

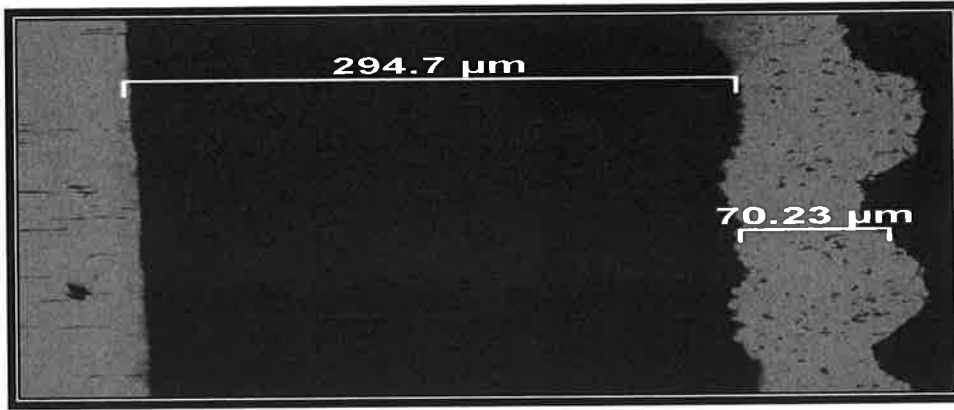


Figure A128: Round solid bar: Dummy specimen coating surface cross section; Stainless steel after two (2) weeks exposure tensile tested cross section.

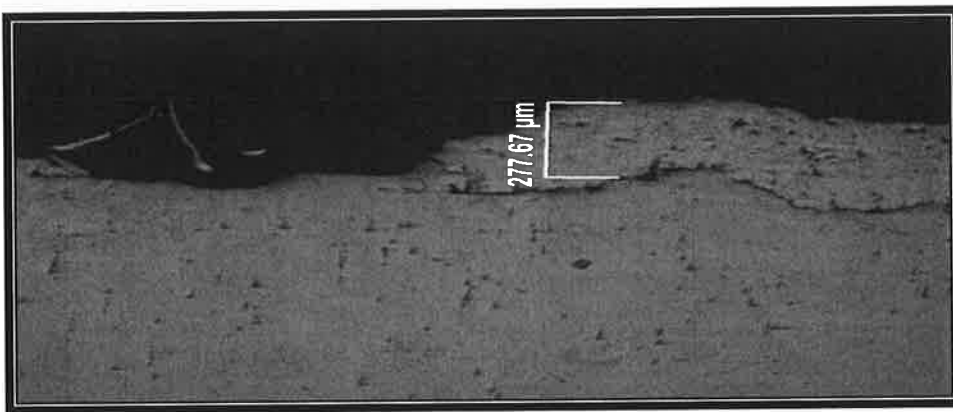


Figure A129: Round solid bar: Original specimen coating surface cross section; Carbon steel after two (2) weeks exposure to brine solution tensile tested cross section.

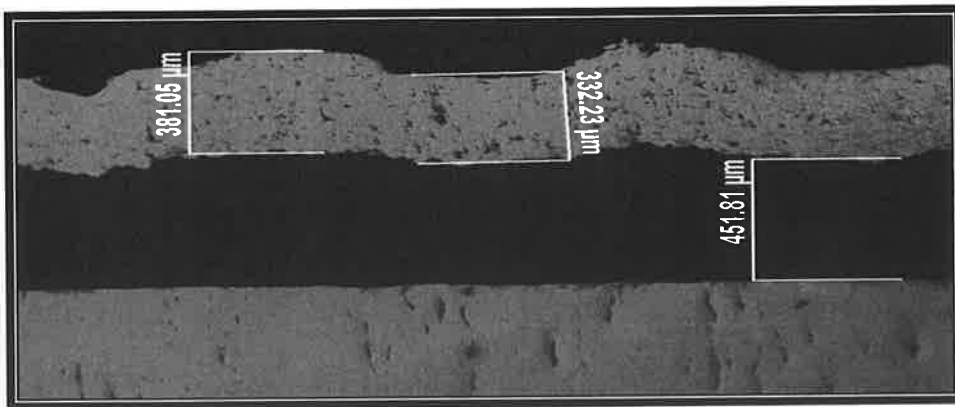


Figure A130: Round solid bar: Dummy specimen coating surface cross section; Carbon steel after two (2) weeks exposure to brine solution tensile tested cross section.

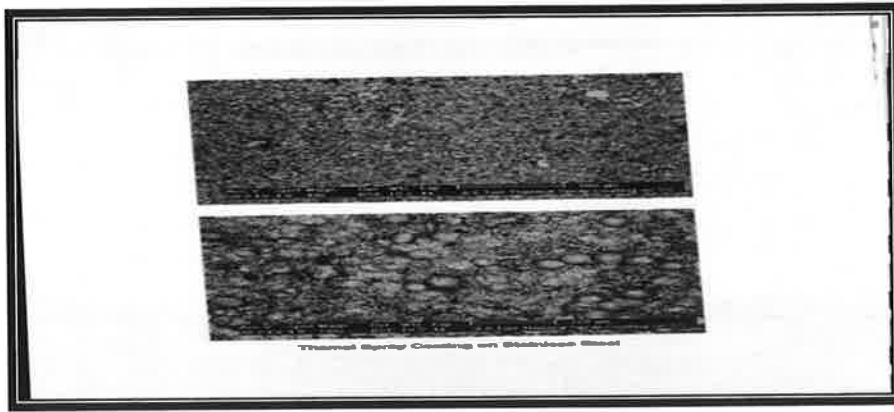


Figure A131: Micrograph showing coating deposited onto stainless steel surface.

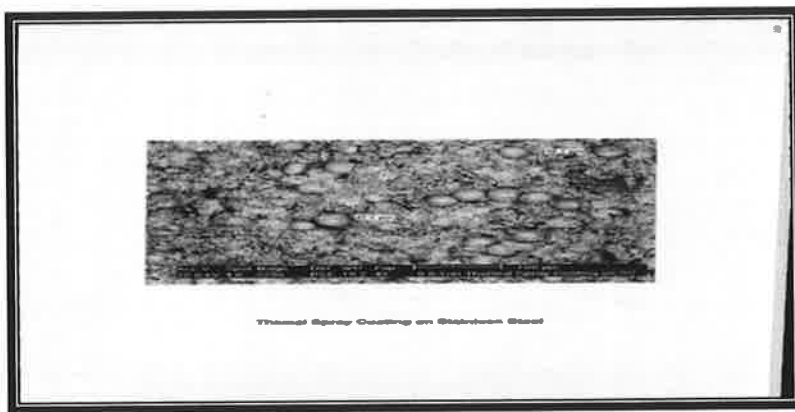


Figure A132: Micrograph showing coating deposited onto stainless steel surface.

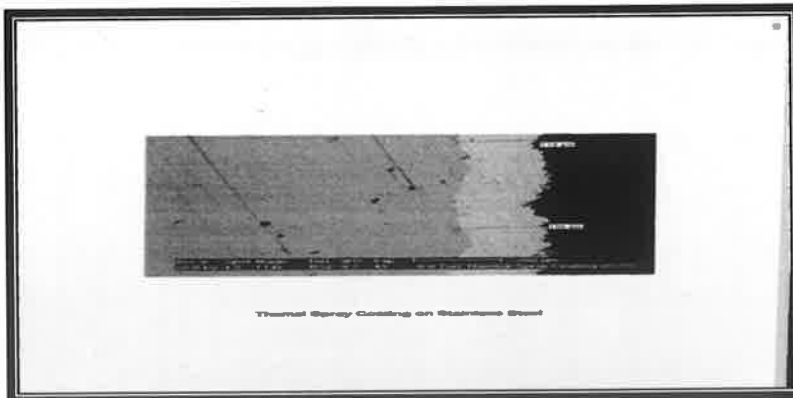


Figure A133: Micrograph showing coating deposited onto carbon steel surface.

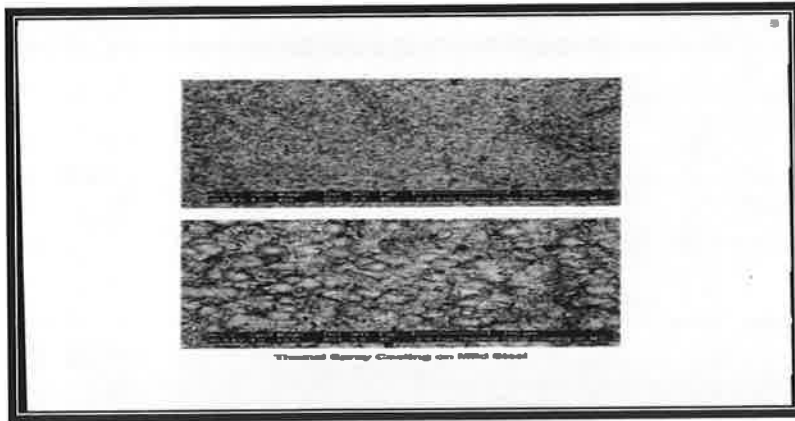


Figure A134: Micrograph showing coating deposited onto carbon steel surface.

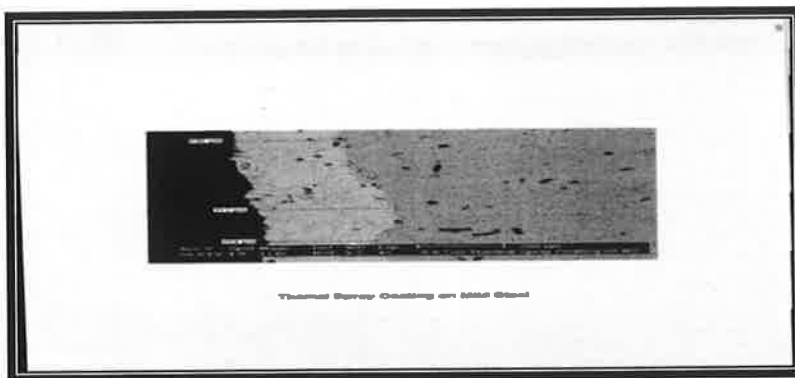


Figure A135: Micrograph showing coating deposited onto carbon steel surface.

## **(2) Fatigue and Tensile tested flat sheet specimens:**

A collection of flat sheets specimens of carbon steel and stainless (304L SS) steel materials were HVOF coated with a coating powder similar to Inconel 625. All the coated specimens were exposed to brine solution complete immersion for static corrosion testing. The exposure period was selected to be one (1) week and three (3) weeks for both types of specimens. Optical microscopy examinations at two magnifications both 50X and 200X were made to the exposed tested specimens. The examinations were made for each tested specimens to show and observe the following:

- To observe Coating to substrate interface.
- To determine bonding between the coating adhesion to base metal.
- Coating porosity level.
- Coating adherence onto the specimen.
- Coating crack sites.
- Coating defects.

The images show different coating cross-sections and give indication of the coating integrity. Selected images show that low porosity level is observed. Other images indicate coating dis-integrity from the substrate. Generally, there are no cracks observed in the coating it self. The following below figures (Figure A1 to Figure A121) are obtained from the optical microscopy examinations for total of twelve (12) coated specimens.

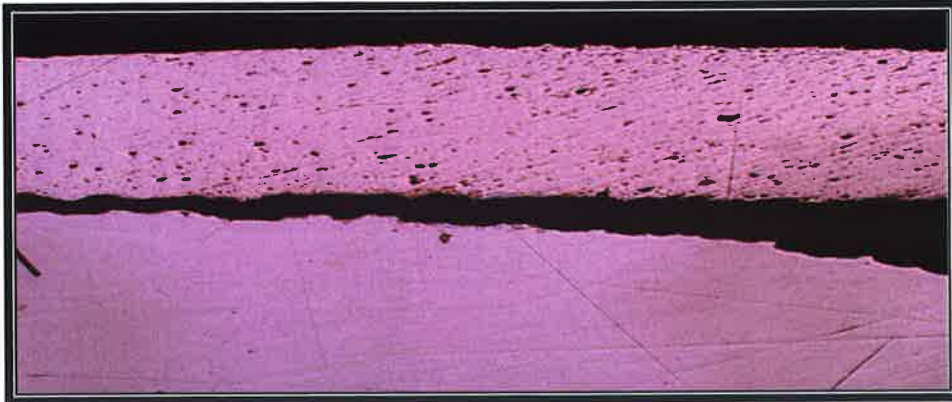


Figure A1: Carbon Steel after one (1) week exposure to brine solution and tensile tested.

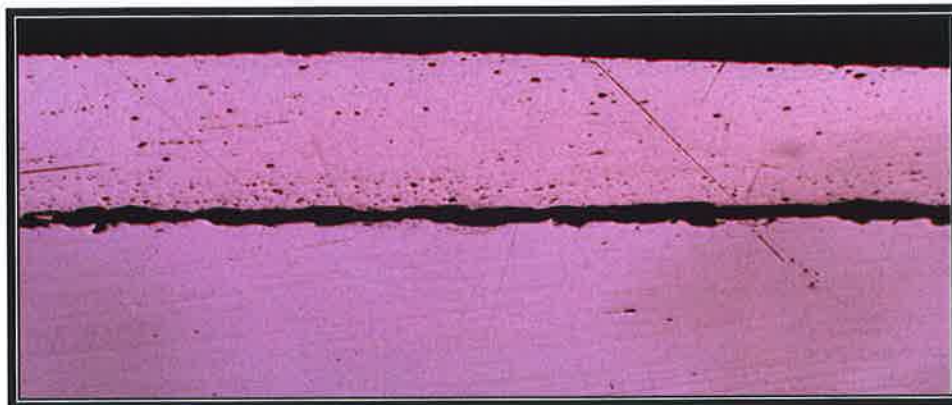


Figure A2: Carbon Steel after one (1) week exposure to brine solution and tensile tested.

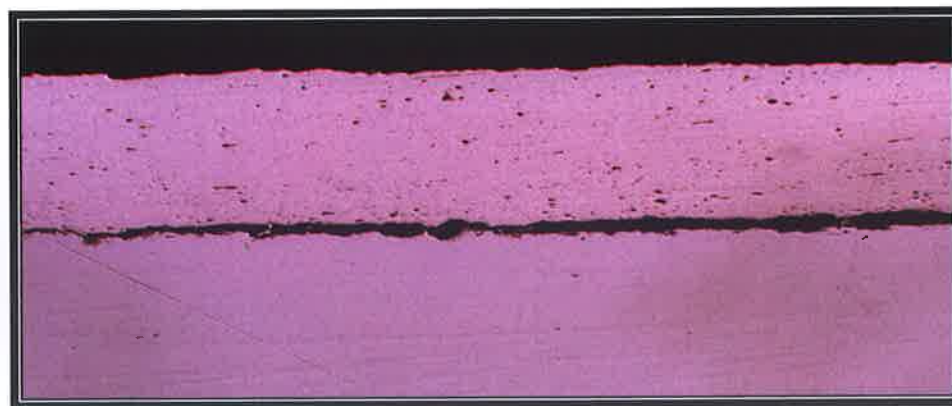


Figure A3: Carbon Steel after one (1) week exposure to brine solution and tensile tested.

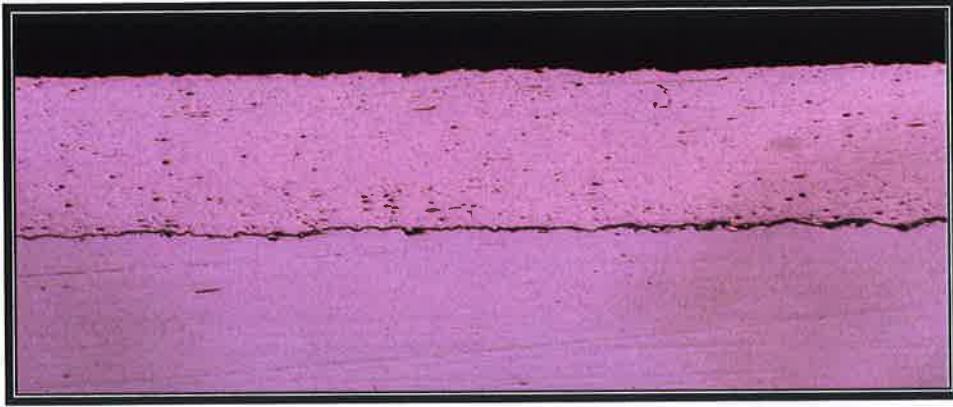


Figure A4: Carbon Steel after one (1) week exposure to brine solution and tensile tested.

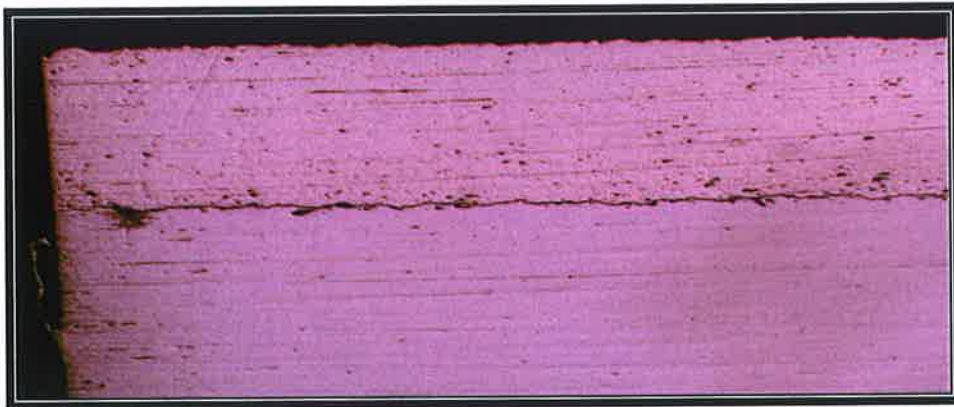


Figure A5: Carbon Steel after one (1) week exposure to brine solution and tensile tested.



Figure A6: Carbon Steel after one (1) week exposure to brine solution and tensile tested.

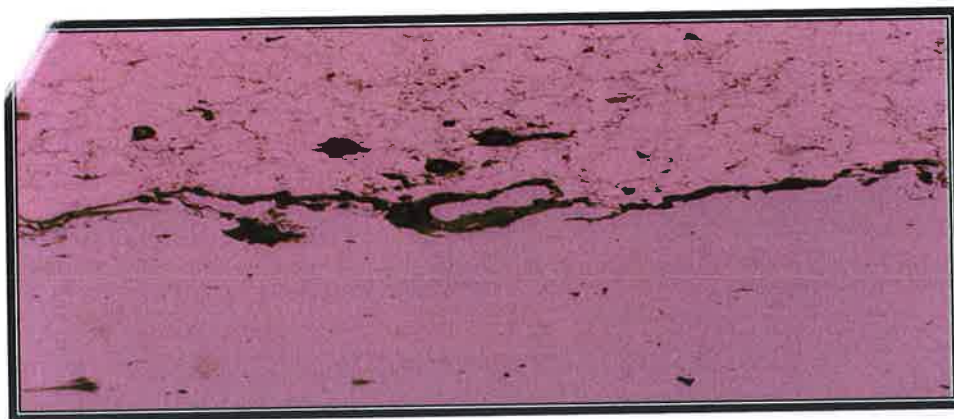


Figure A7: Carbon Steel after one (1) week exposure to brine solution and tensile tested.

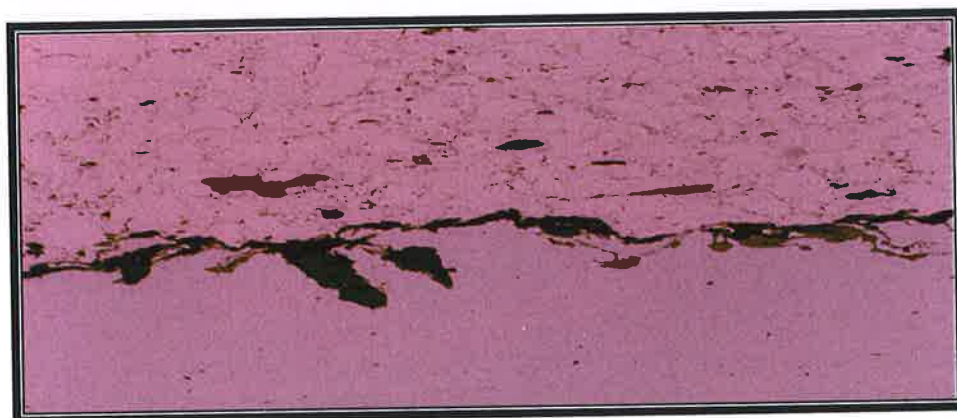


Figure A8: Carbon Steel after one (1) week exposure to brine solution and tensile tested.

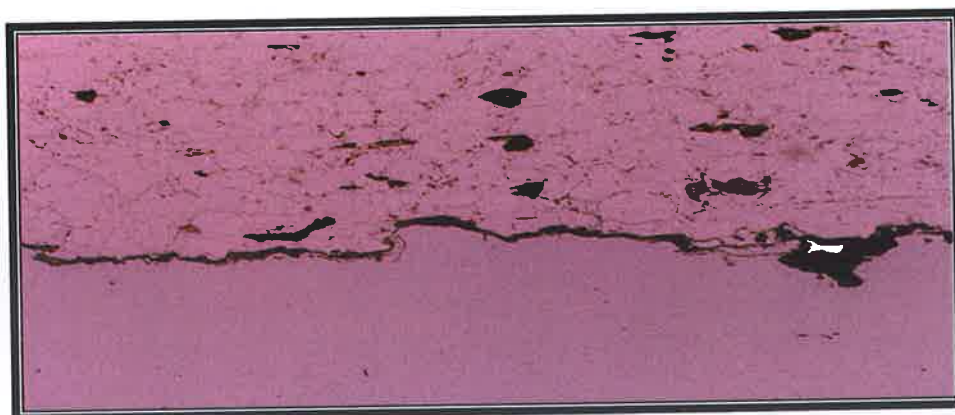


Figure A9: Carbon Steel after one (1) week exposure to brine solution and tensile tested.

Figure A12: Stainless Steel after one (1) week exposure to brine solution tensile tested.

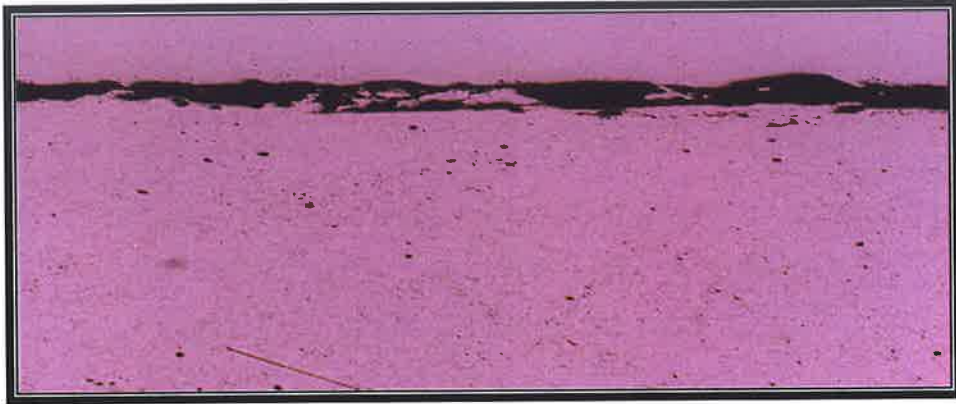


Figure A11: Stainless Steel after one (1) week exposure to brine solution tensile tested.

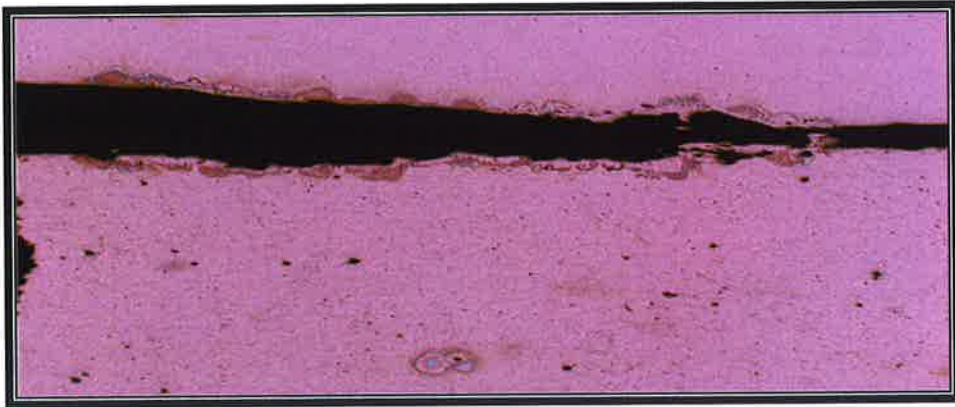
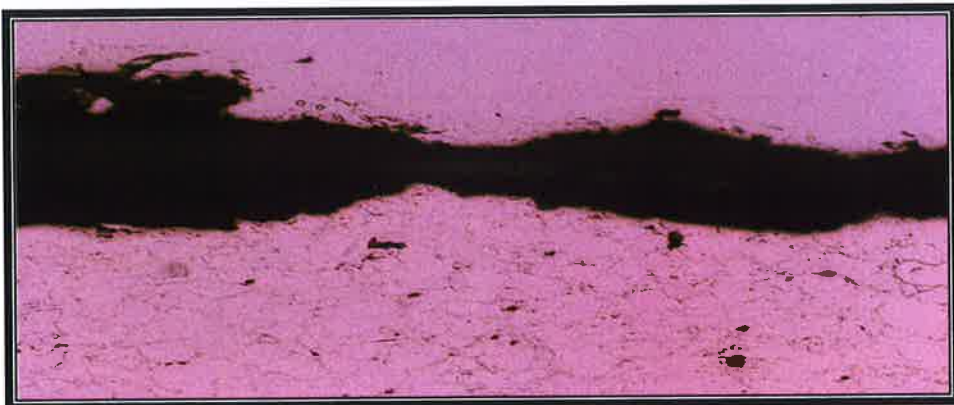


Figure A10: Carbon Steel after one (1) week exposure to brine solution and tensile tested.



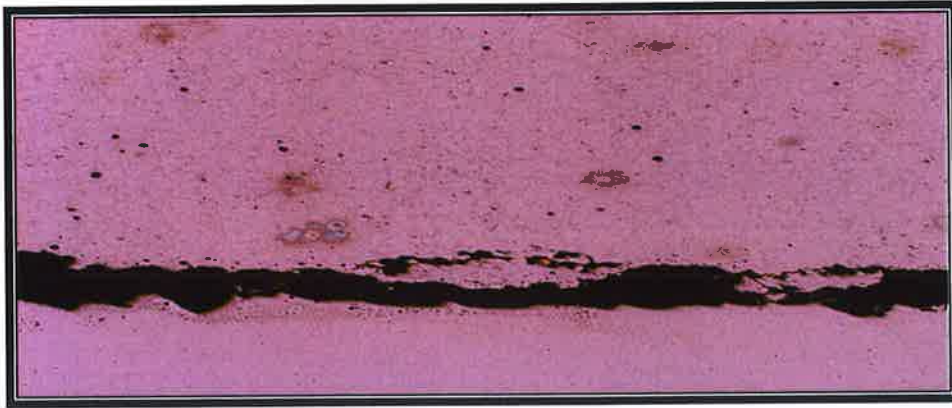


Figure A13: Stainless Steel after one (1) week exposure to brine solution tensile tested.

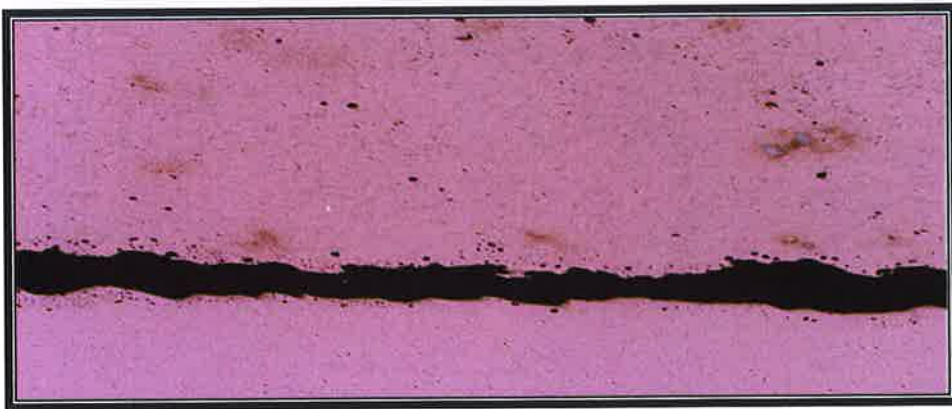


Figure A14: Stainless Steel after one (1) week exposure to brine solution tensile tested.

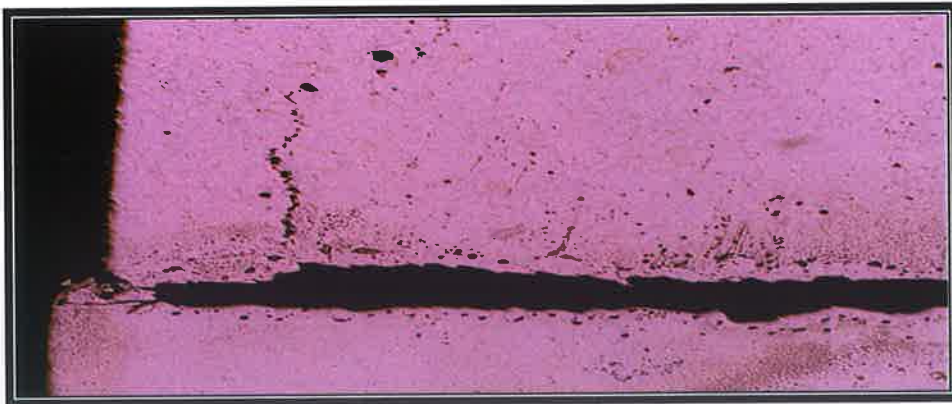


Figure A15: Stainless Steel after one (1) week exposure to brine solution tensile tested.

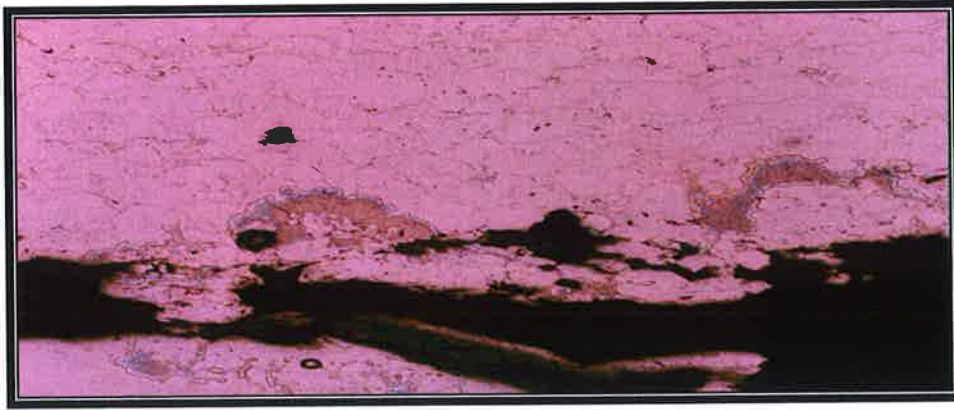


Figure A16: Stainless Steel after one (1) week exposure to brine solution tensile tested.



Figure A17: Stainless Steel after one (1) week exposure to brine solution tensile tested.

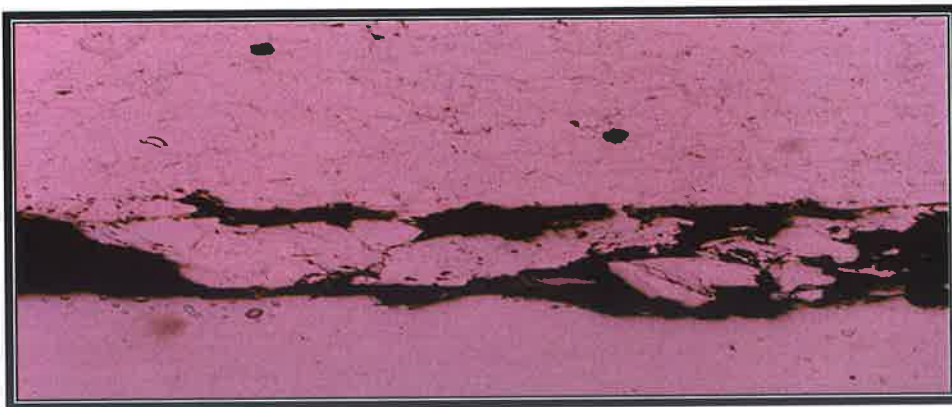


Figure A18: Stainless Steel after one (1) week exposure to brine solution tensile tested.



Figure A19: Stainless Steel after one (1) week exposure to brine solution tensile tested.

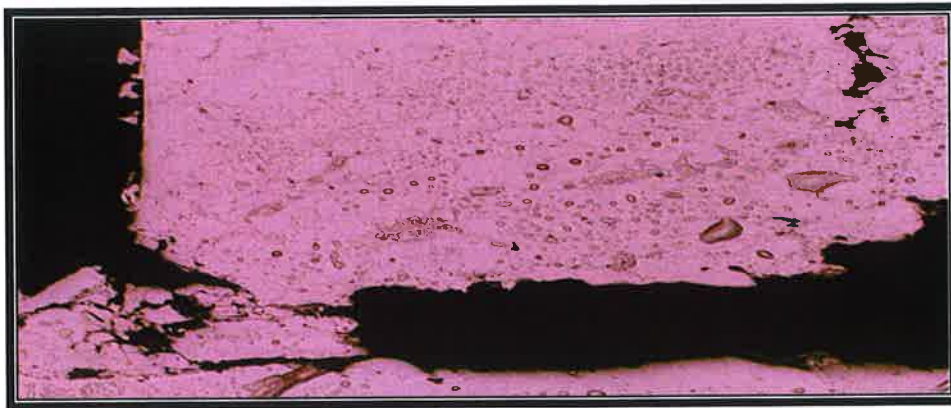


Figure A20: Stainless Steel after one (1) week exposure to brine solution tensile tested.

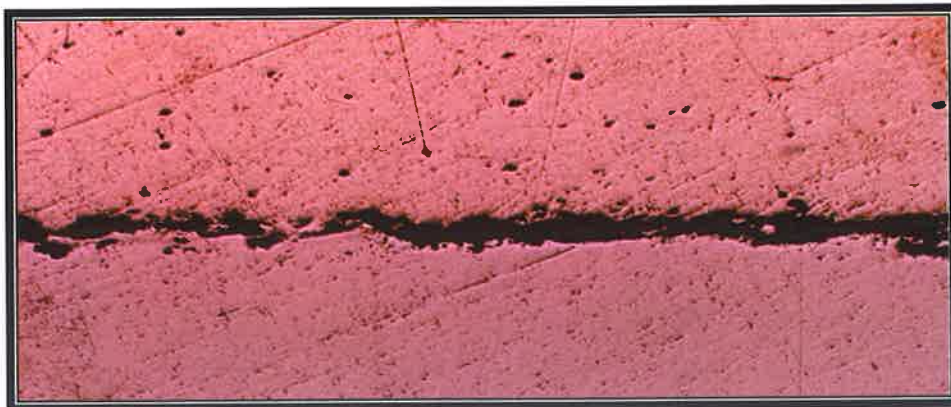


Figure A21: Carbon Steel after one (1) week exposure to brine solution tensile tested.



Figure A22: Carbon Steel after one (1) week exposure to brine solution tensile tested.

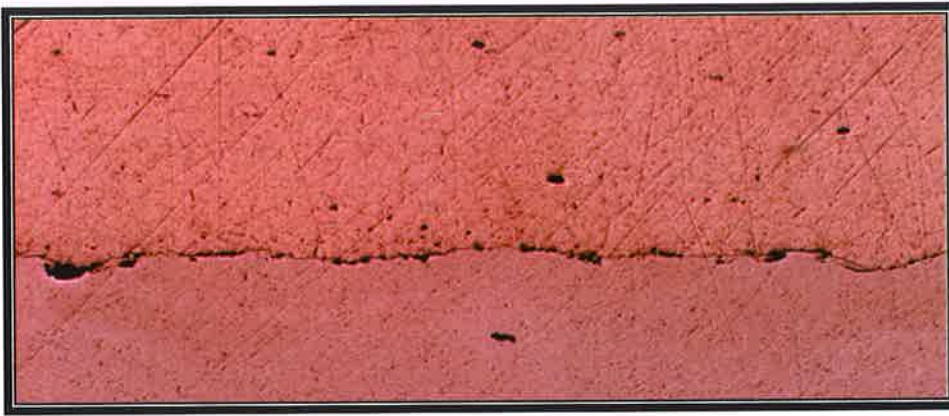


Figure A23: Carbon Steel after one (1) week exposure to brine solution tensile tested.

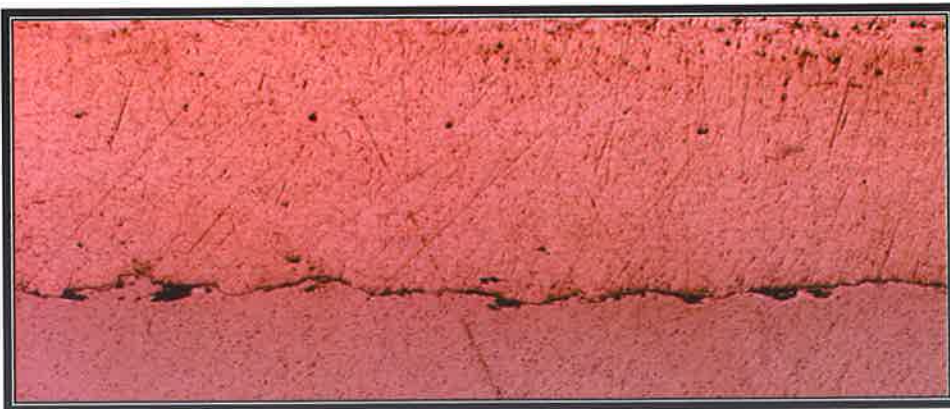


Figure A24: Carbon Steel after one (1) week exposure to brine solution tensile tested.

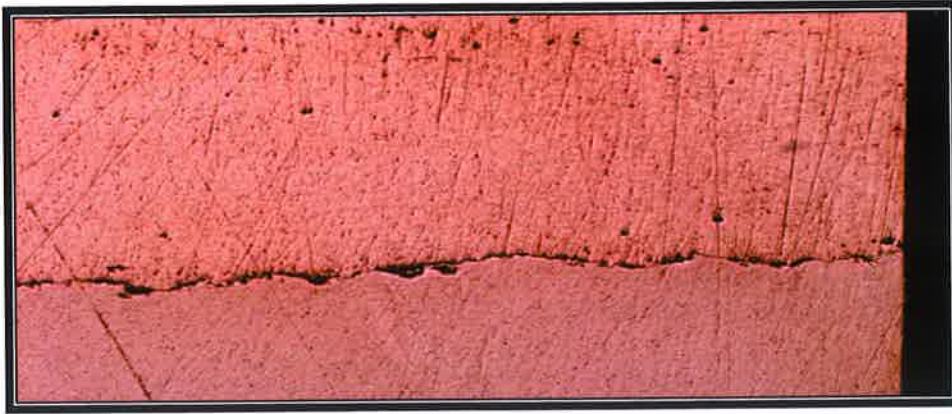


Figure A25: Carbon Steel after one (1) week exposure to brine solution tensile tested.

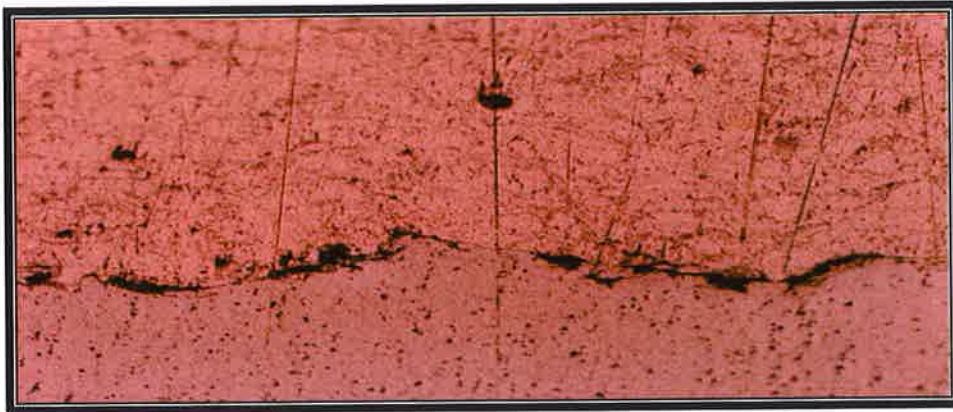


Figure A26: Carbon Steel after one (1) week exposure to brine solution tensile tested.

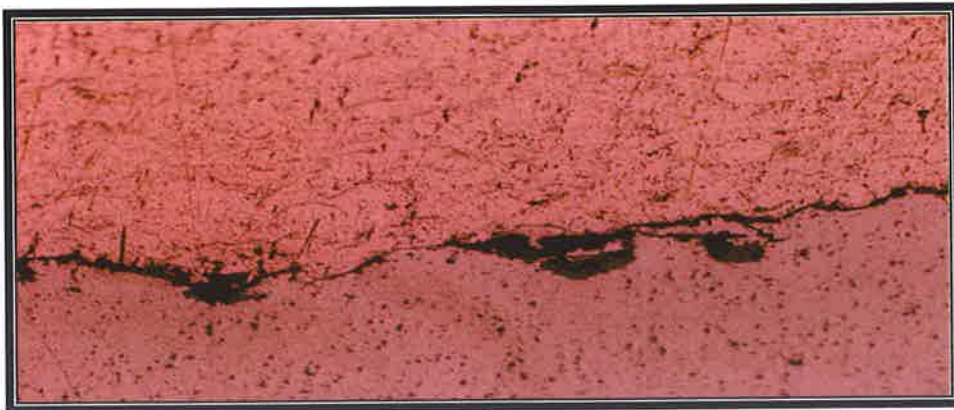


Figure A27: Carbon Steel after one (1) week exposure to brine solution tensile tested.

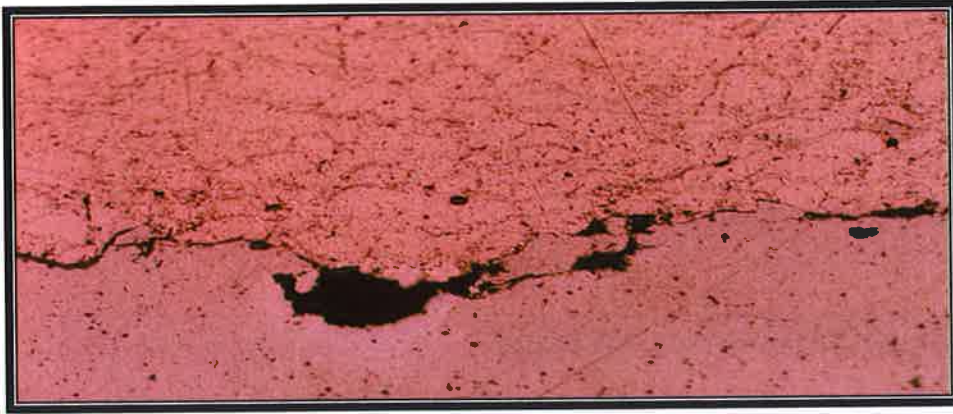


Figure A28: Carbon Steel after one (1) week exposure to brine solution tensile tested.

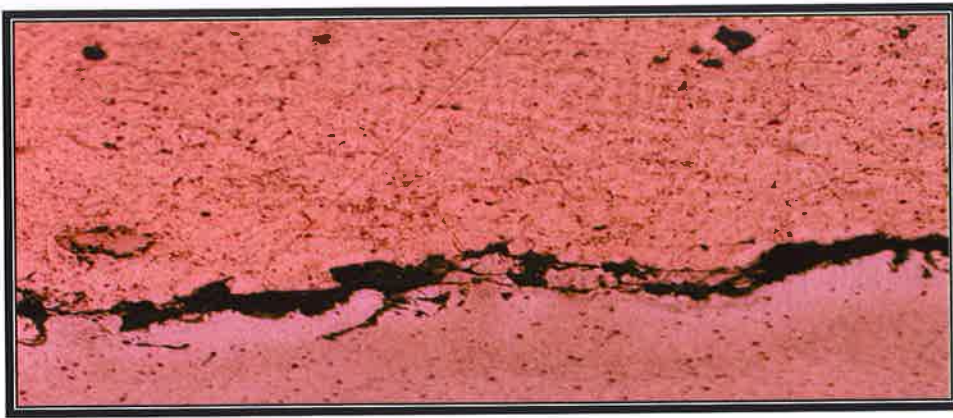


Figure A29: Carbon Steel after one (1) week exposure to brine solution tensile tested.

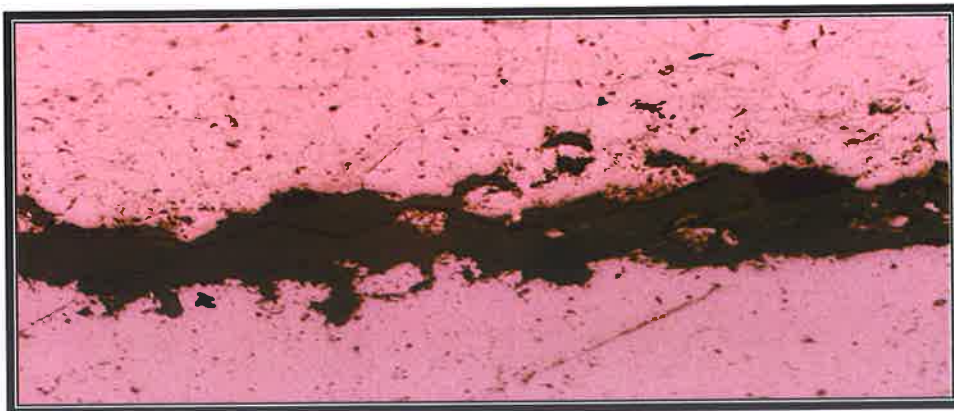


Figure A30: Carbon Steel after one (1) week exposure to brine solution tensile tested.

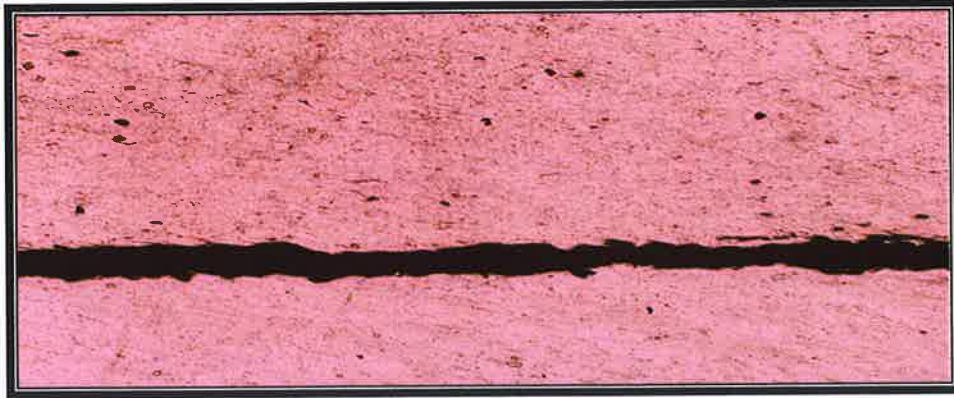


Figure A31: Stainless Steel after three (3) weeks exposure to brine solution tensile tested.

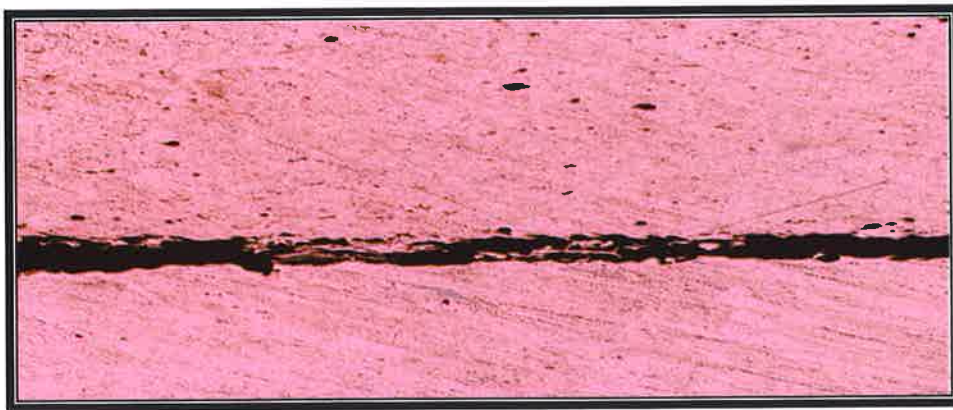


Figure A32: Stainless Steel after three (3) weeks exposure to brine solution tensile tested.



Figure A33: Stainless Steel after three (3) weeks exposure to brine solution tensile tested.

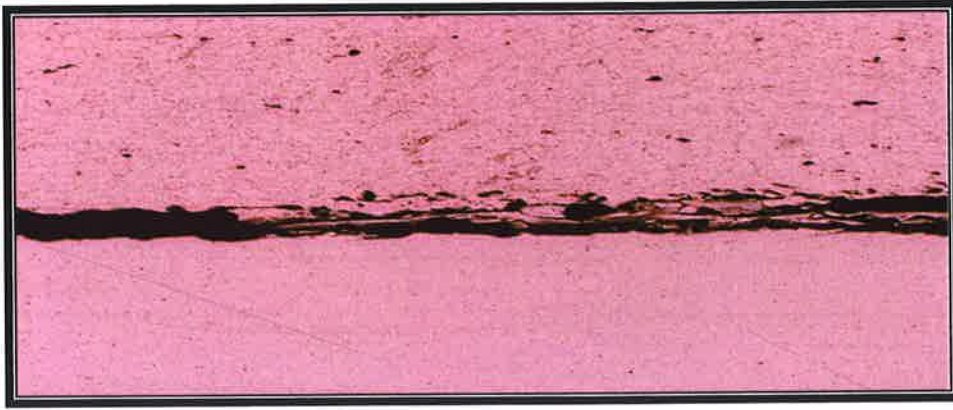


Figure A34: Stainless Steel after three (3) weeks exposure to brine solution tensile tested.

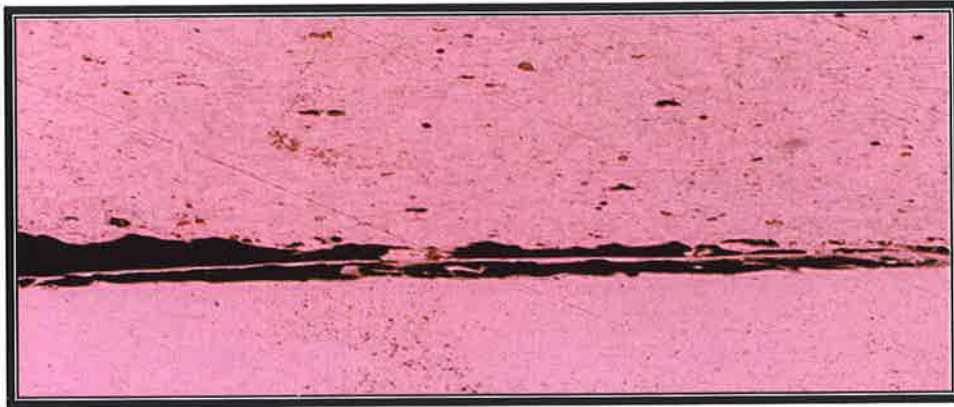


Figure A35: Stainless Steel after three (3) weeks exposure to brine solution tensile tested.

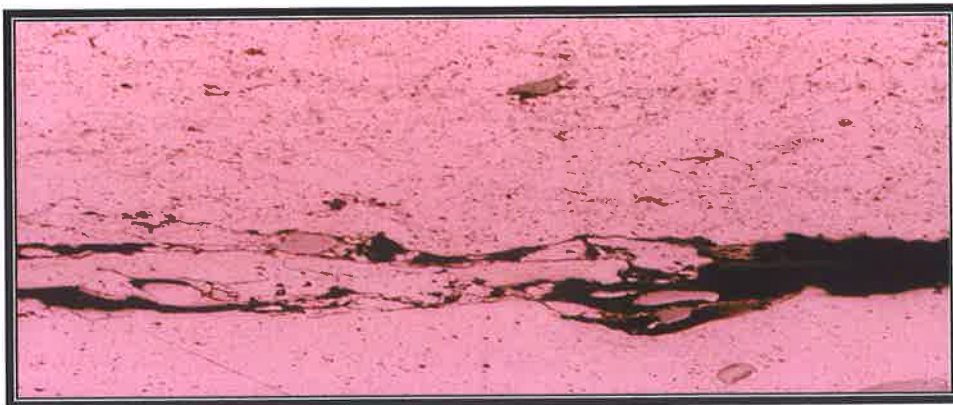


Figure A36: Stainless Steel after three (3) weeks exposure to brine solution tensile tested.

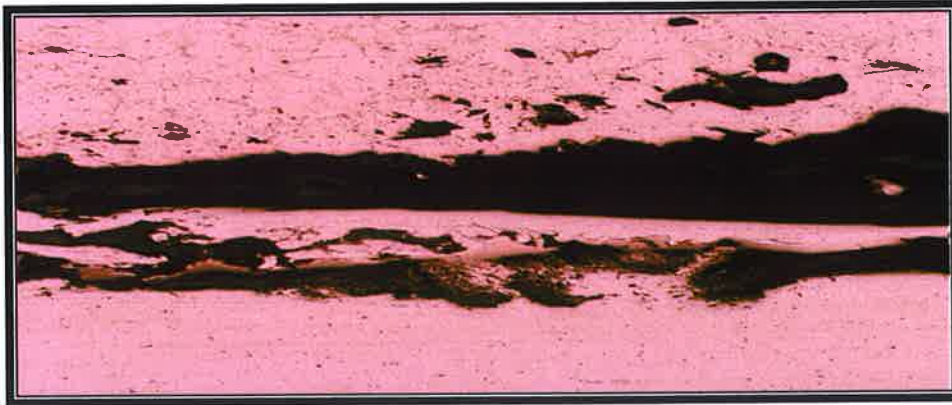


Figure A37: Stainless Steel after three (3) weeks exposure to brine solution tensile tested.

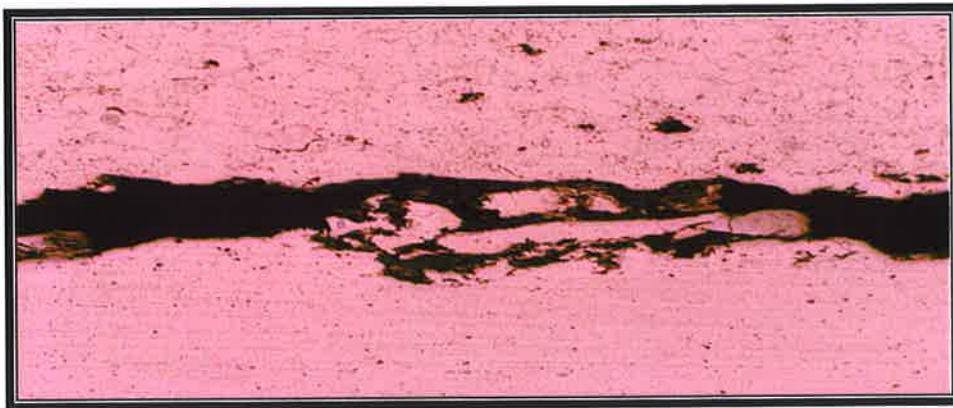


Figure A38: Stainless Steel after three (3) weeks exposure to brine solution tensile tested.

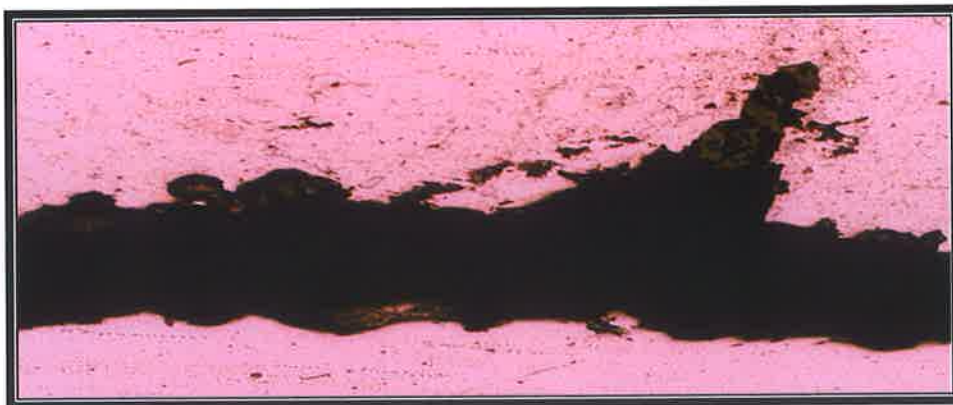


Figure A39: Stainless Steel after three (3) weeks exposure to brine solution tensile tested.

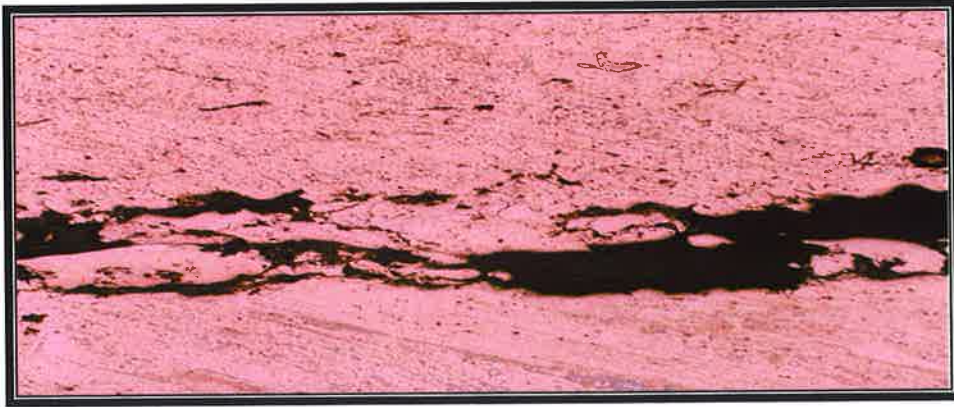


Figure A40: Stainless Steel after three (3) weeks exposure to brine solution tensile tested.

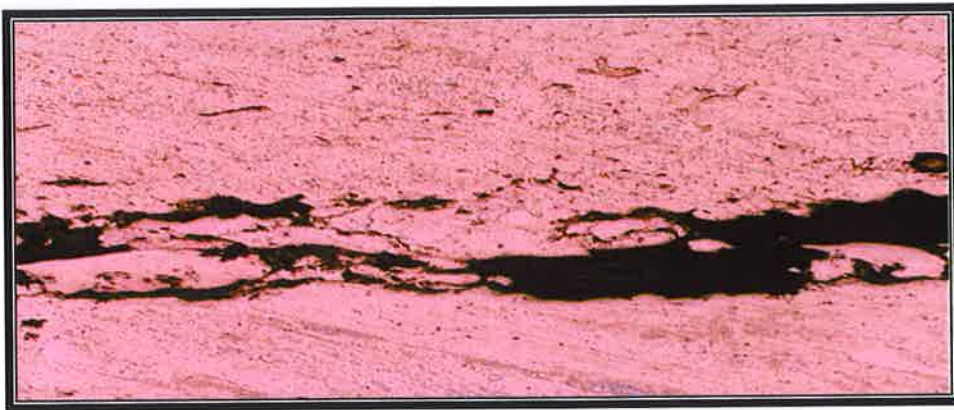


Figure A41: Stainless Steel after three (3) weeks exposure to brine solution tensile tested.

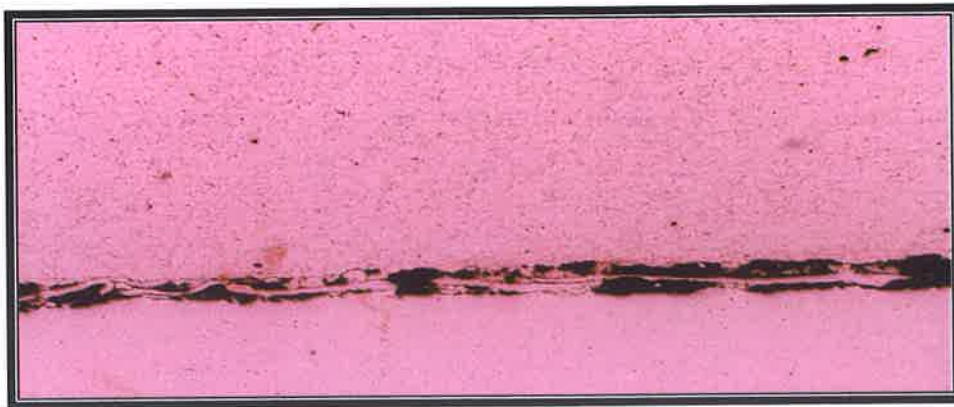


Figure A42: Stainless Steel after one (1) week exposure to brine solution tensile tested.

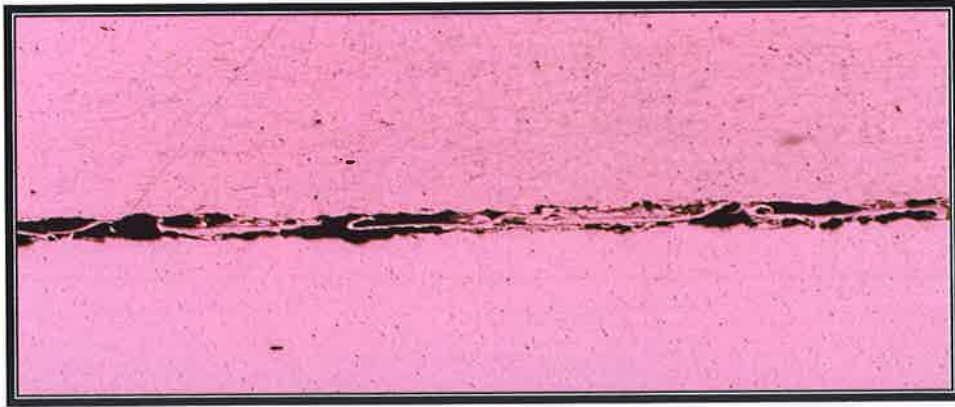


Figure A43: Stainless Steel after one (1) week exposure to brine solution tensile tested.

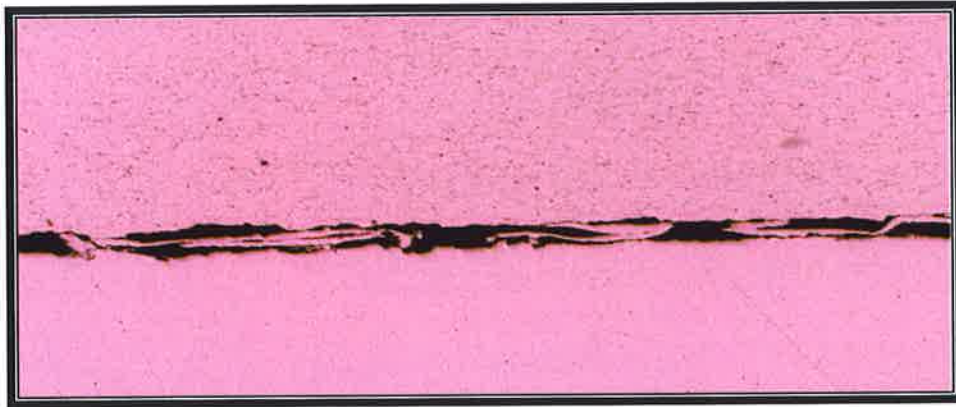


Figure A44: Stainless Steel after one (1) week exposure to brine solution tensile tested.

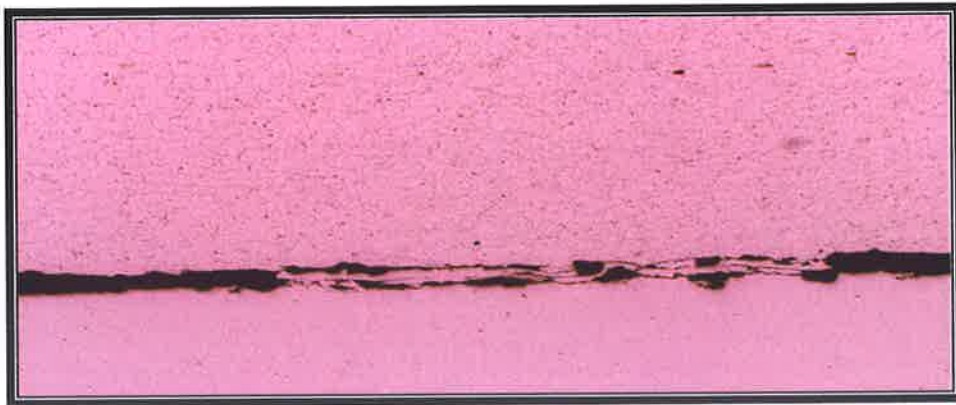


Figure A45: Stainless Steel after one (1) week exposure to brine solution tensile tested.

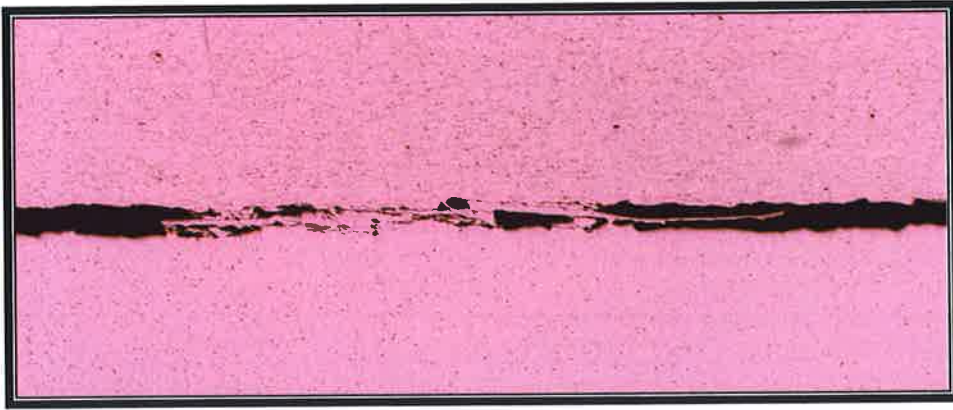


Figure A46: Stainless Steel after one (1) week exposure to brine solution tensile tested.

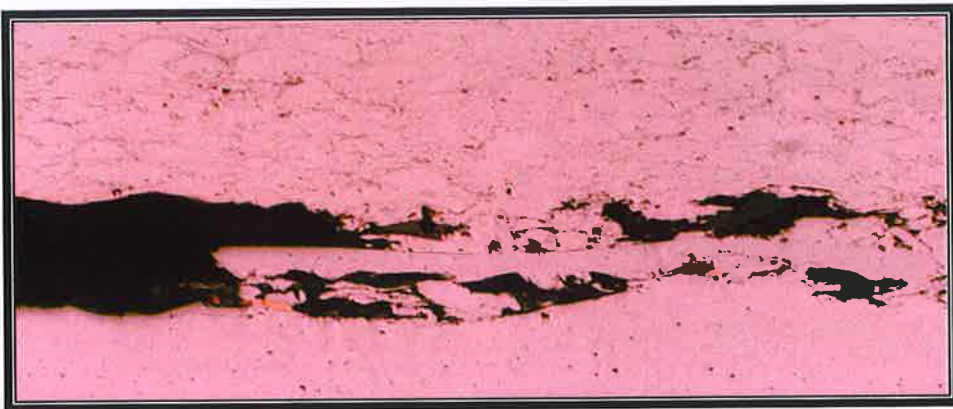


Figure A47: Stainless Steel after one (1) week exposure to brine solution tensile tested.

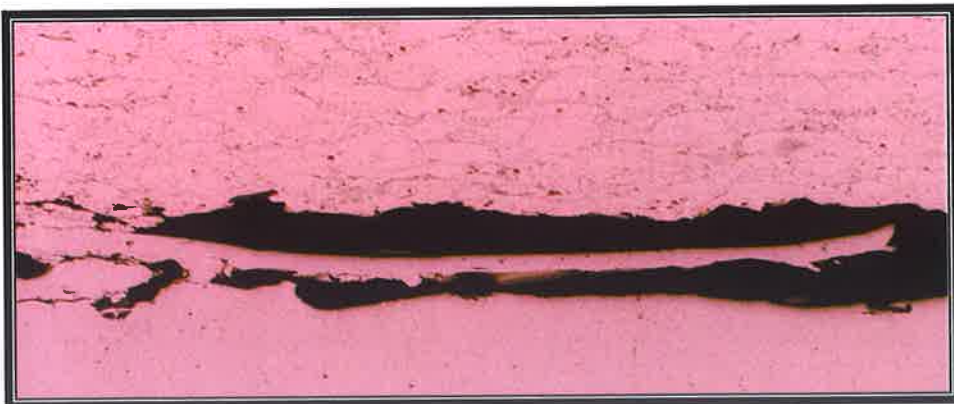


Figure A48: Stainless Steel after one (1) week exposure to brine solution tensile tested.

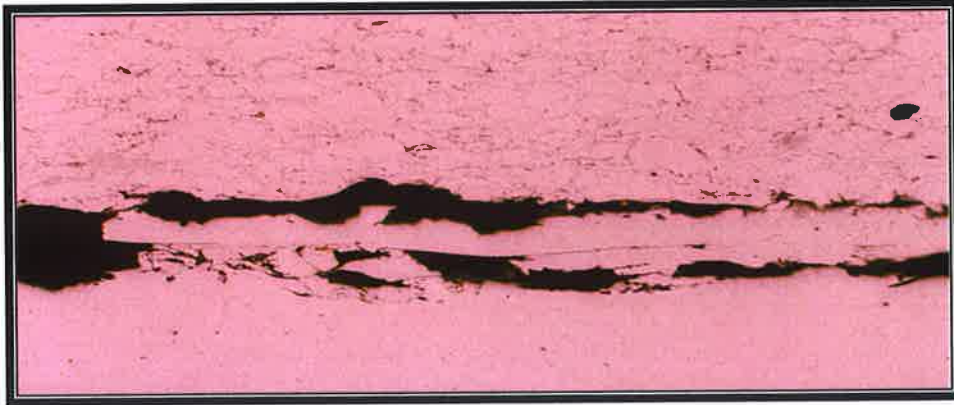


Figure A49: Stainless Steel after one (1) week exposure to brine solution tensile tested.

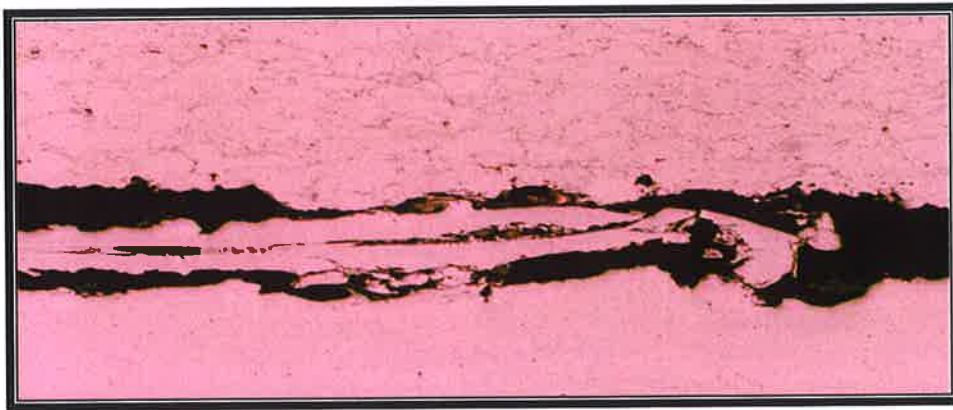


Figure A50: Stainless Steel after one (1) week exposure to brine solution tensile tested.



Figure A51: Stainless Steel after one (1) week exposure to brine solution tensile tested.

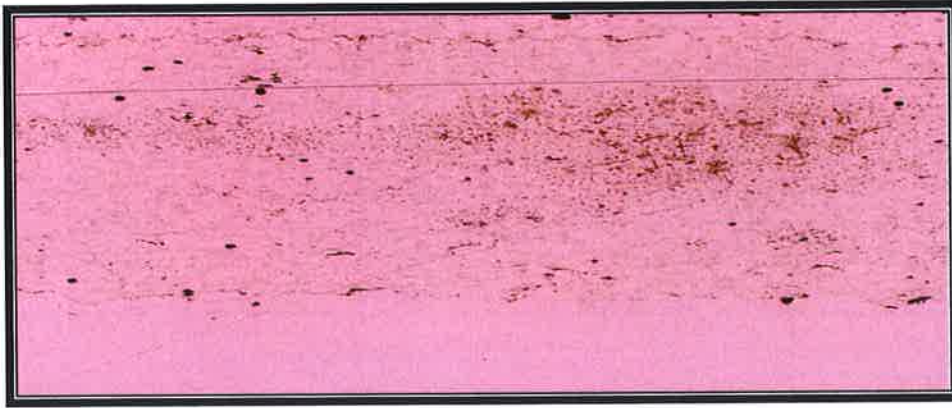


Figure A52: Stainless Steel after one (1) week exposure to brine solution fatigue tested.

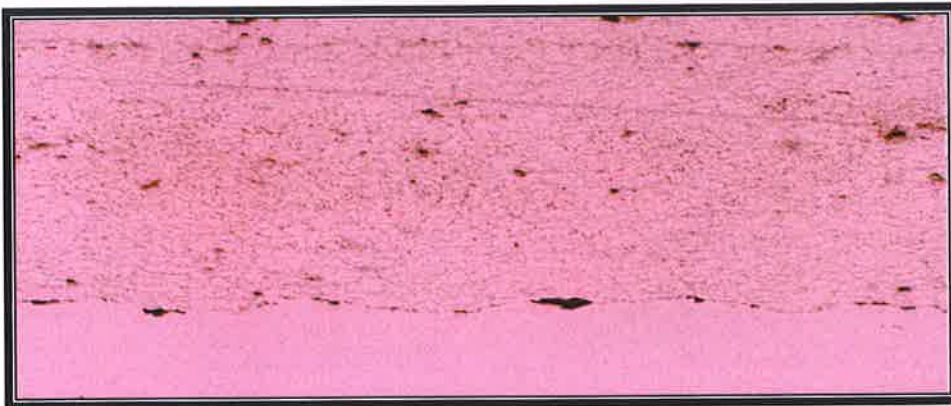


Figure A53: Stainless Steel after one (1) week exposure to brine solution fatigue tested.

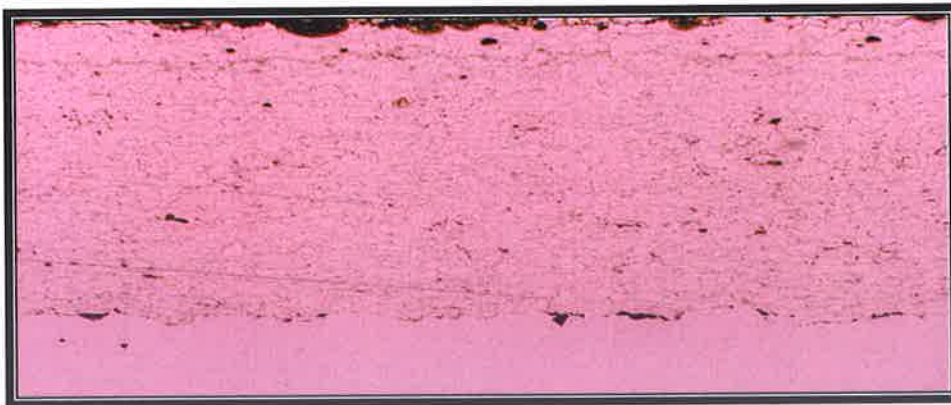


Figure A54: Stainless Steel after one (1) week exposure to brine solution fatigue tested.

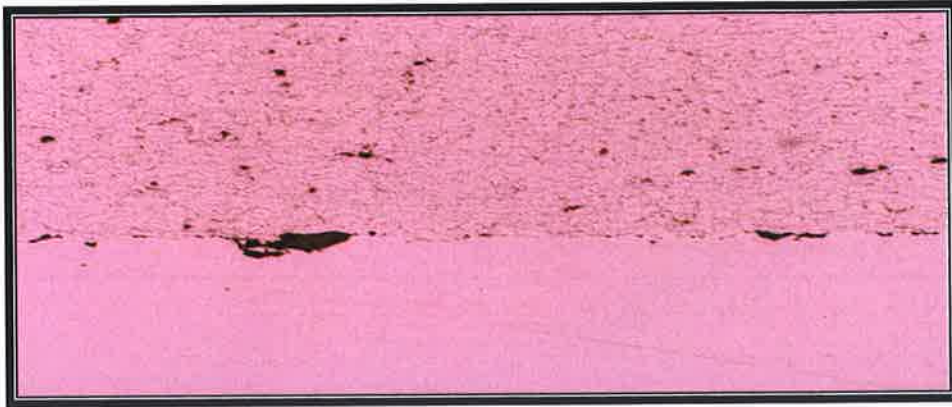


Figure A55: Stainless Steel after one (1) week exposure to brine solution fatigue tested.

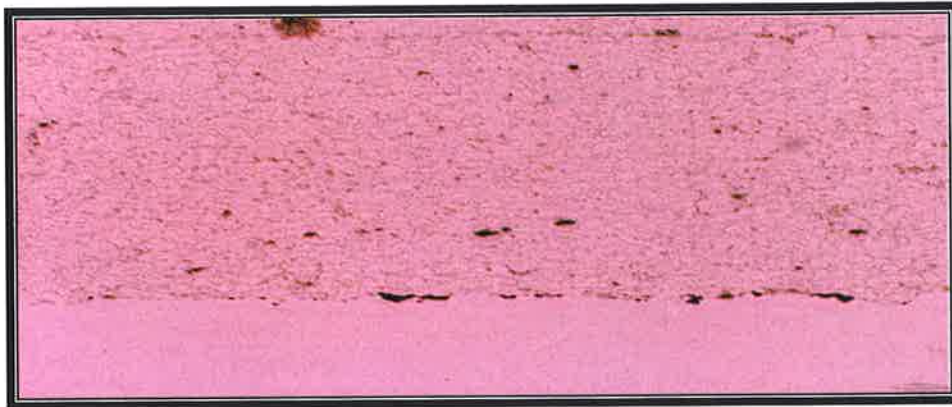


Figure A56: Stainless Steel after one (1) week exposure to brine solution fatigue tested.

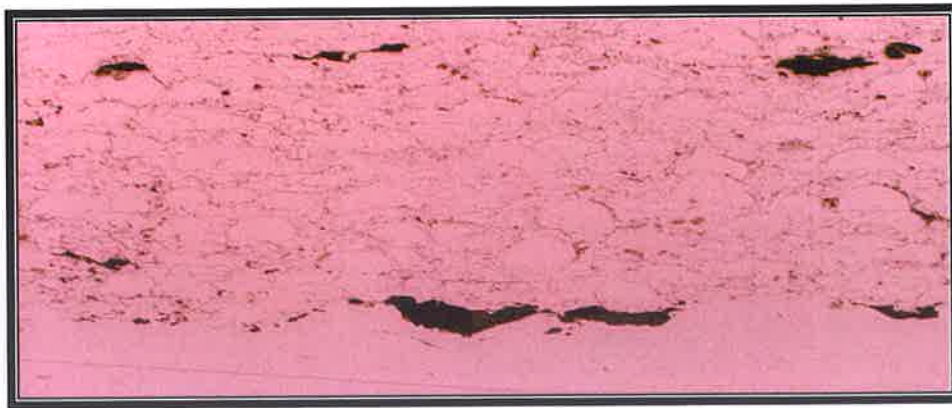


Figure A57: Stainless Steel after one (1) week exposure to brine solution fatigue tested.



Figure A58: Stainless Steel after one (1) week exposure to brine solution fatigue tested.

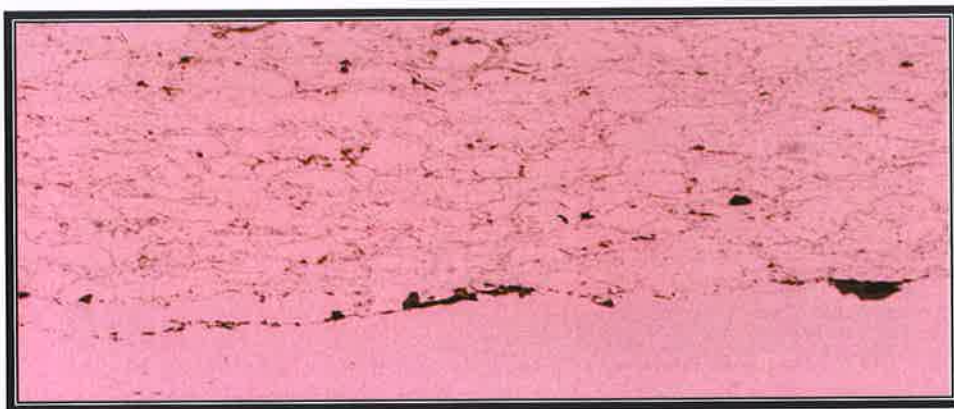


Figure A59: Stainless Steel after one (1) week exposure to brine solution fatigue tested.

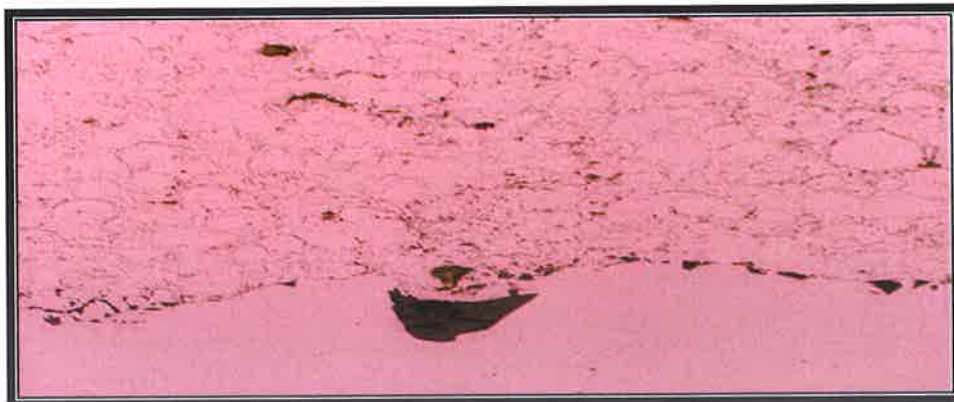


Figure A60: Stainless Steel after one (1) week exposure to brine solution fatigue tested.

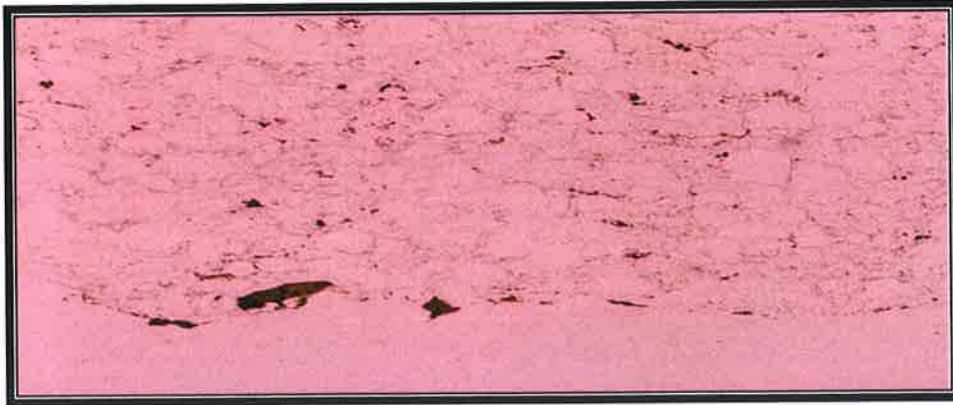


Figure A61: Stainless Steel after one (1) week exposure to brine solution fatigue tested.

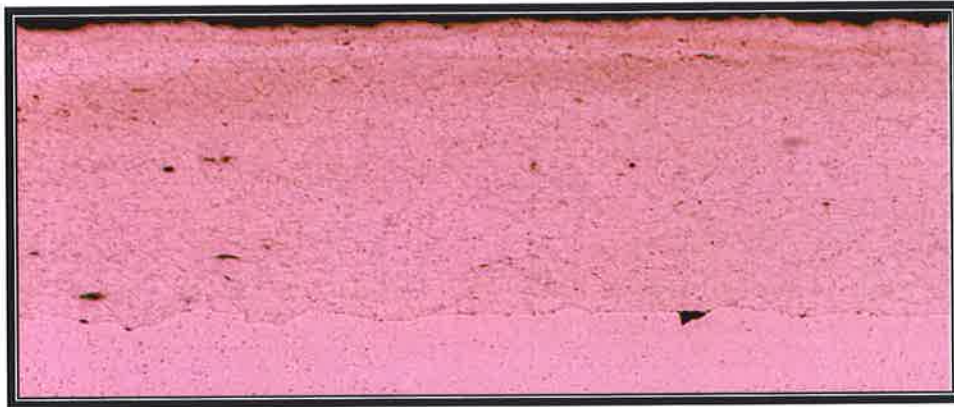


Figure A62: Stainless Steel after three (3) week exposure to brine solution fatigue tested.



Figure A63: Stainless Steel after three (3) week exposure to brine solution fatigue tested.

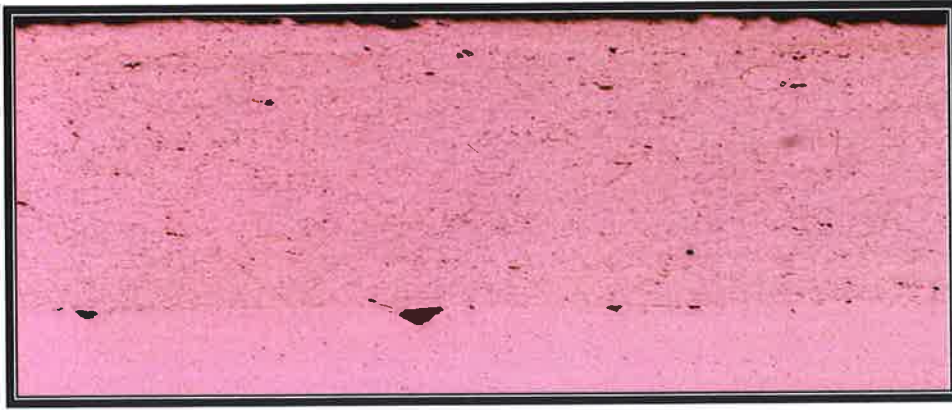


Figure A64: Stainless Steel after three (3) week exposure to brine solution fatigue tested.

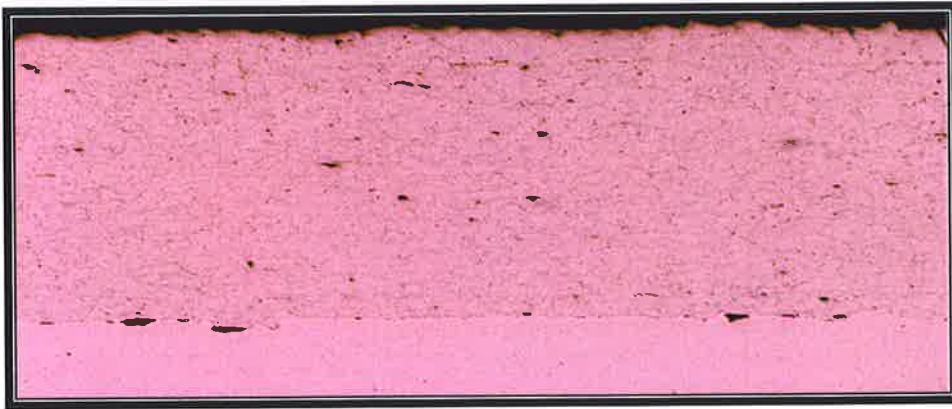


Figure A65: Stainless Steel after three (3) week exposure to brine solution fatigue tested.



Figure A66: Stainless Steel after three (3) week exposure to brine solution fatigue tested.

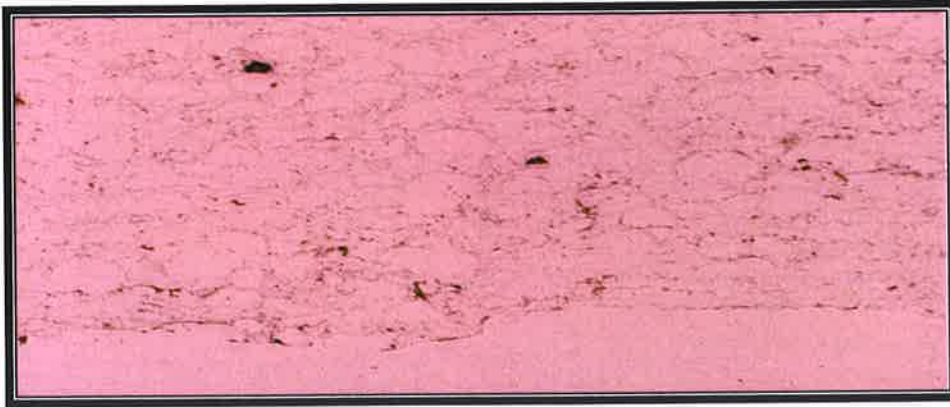


Figure A67: Stainless Steel after three (3) week exposure to brine solution fatigue tested.



Figure A68: Stainless Steel after three (3) week exposure to brine solution fatigue tested.

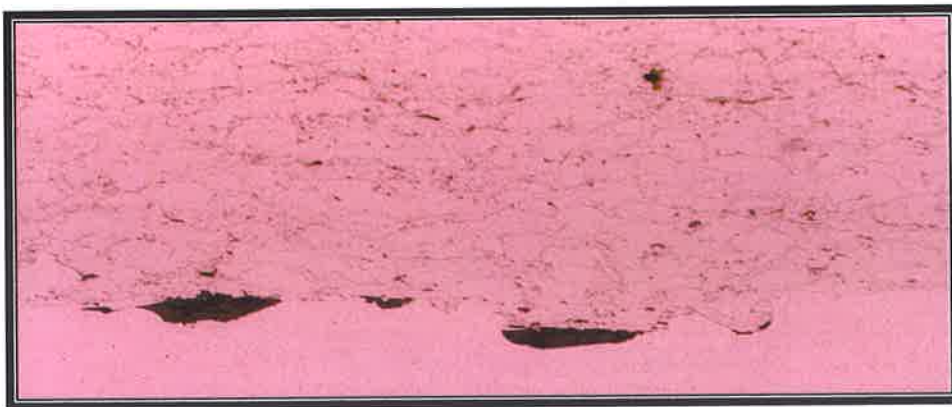


Figure A69: Stainless Steel after three (3) week exposure to brine solution fatigue tested.

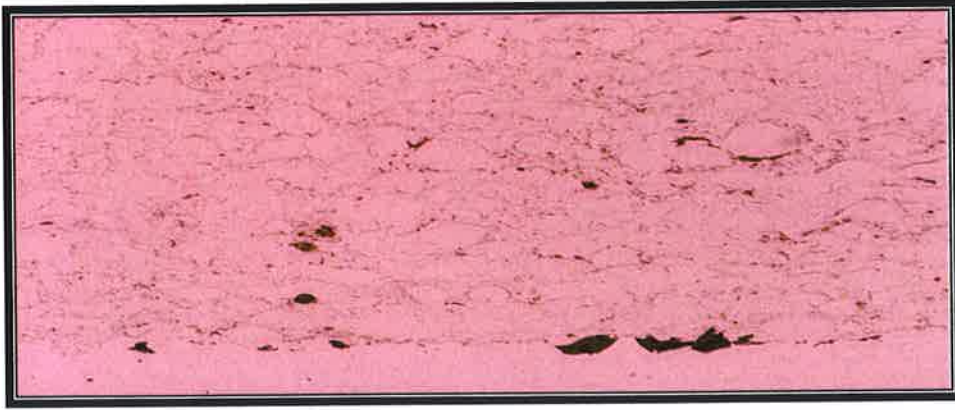


Figure A70: Stainless Steel after three (3) week exposure to brine solution fatigue tested.



Figure A71: Stainless Steel after three (3) week exposure to brine solution fatigue tested.



Figure A72: Carbon Steel after one (1) week exposure to brine solution tensile tested.

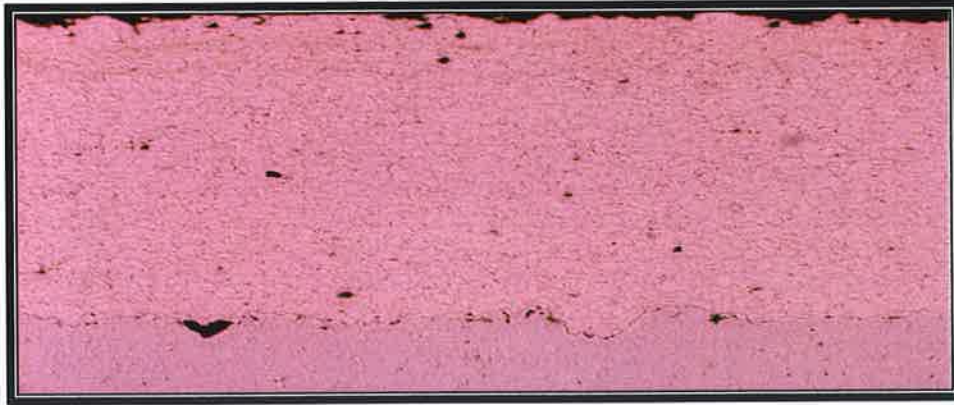


Figure A73: Carbon Steel after one (1) week exposure to brine solution tensile tested.



Figure A74: Carbon Steel after one (1) week exposure to brine solution tensile tested.



Figure A75: Carbon Steel after one (1) week exposure to brine solution tensile tested.

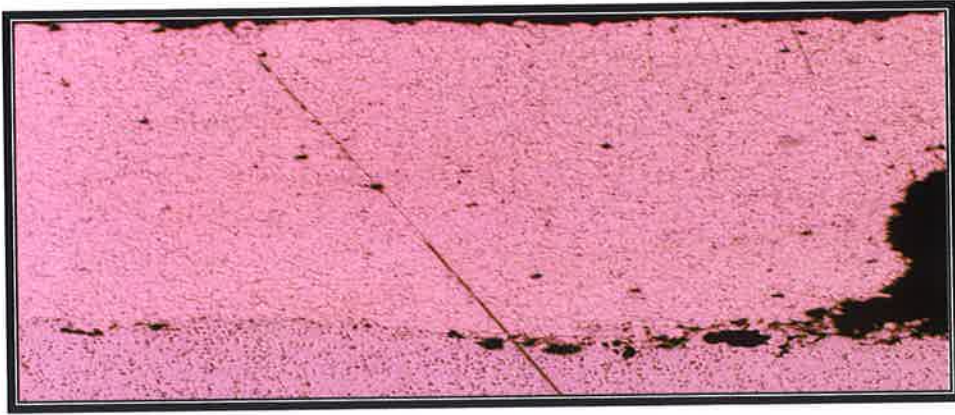


Figure A76: Carbon Steel after one (1) week exposure to brine solution tensile tested.



Figure A77: Carbon Steel after one (1) week exposure to brine solution tensile tested.



Figure A78: Carbon Steel after one (1) week exposure to brine solution tensile tested.



Figure A79: Carbon Steel after one (1) week exposure to brine solution tensile tested.

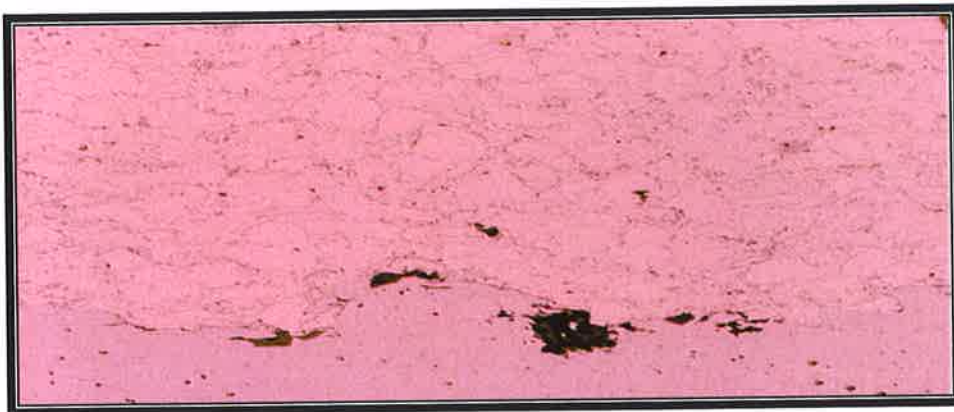


Figure A80: Carbon Steel after one (1) week exposure to brine solution tensile tested.



Figure A81: Carbon Steel after one (1) week exposure to brine solution tensile tested.

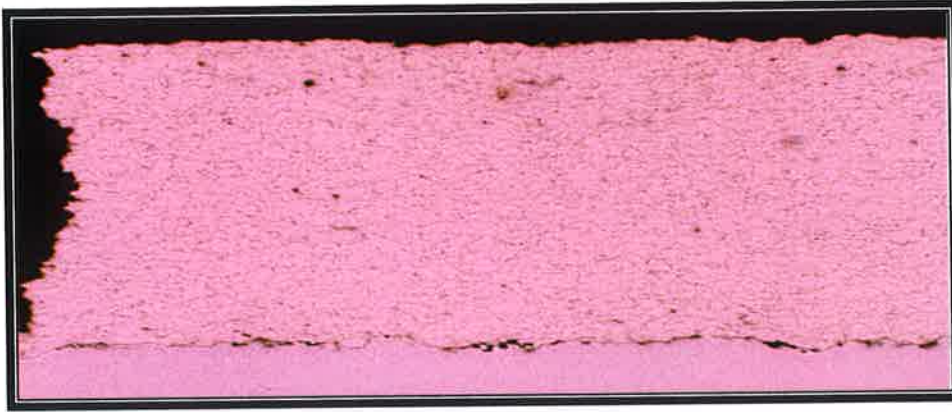


Figure A82: Carbon Steel after one (1) week exposure to brine solution fatigue tested.

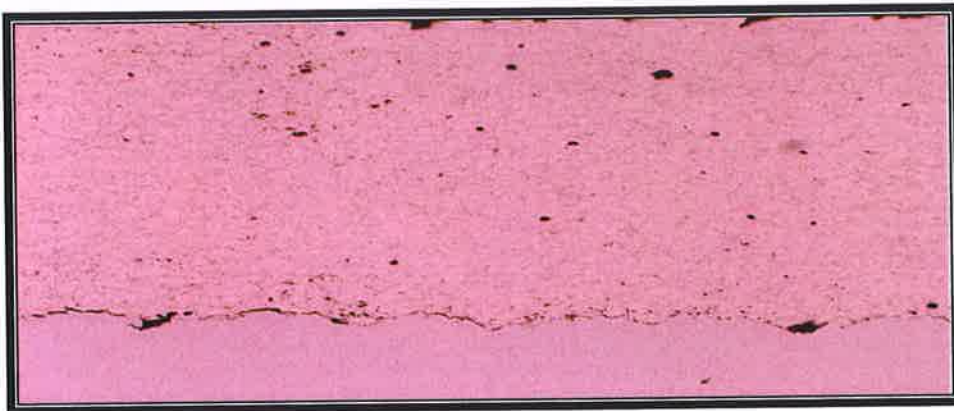


Figure A83: Carbon Steel after one (1) week exposure to brine solution fatigue tested.

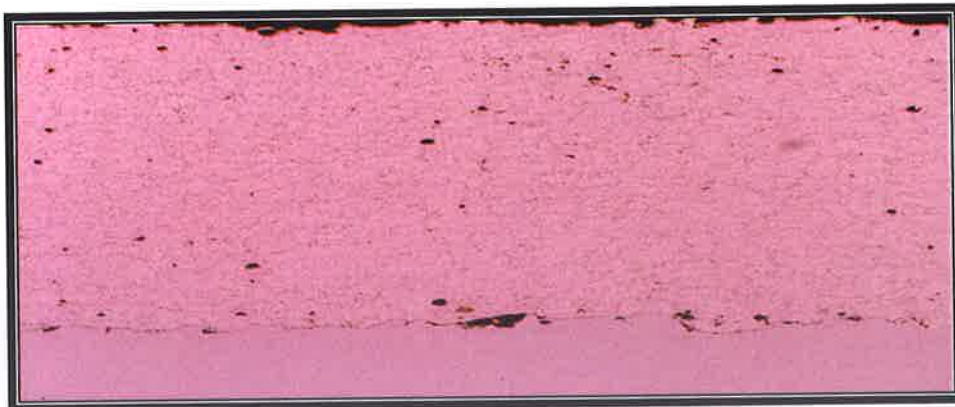


Figure A84: Carbon Steel after one (1) week exposure to brine solution fatigue tested.

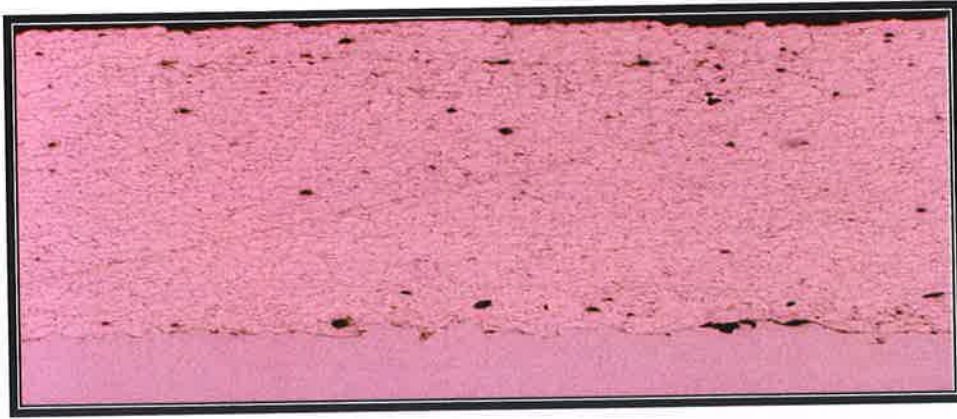


Figure A85: Carbon Steel after one (1) week exposure to brine solution fatigue tested.

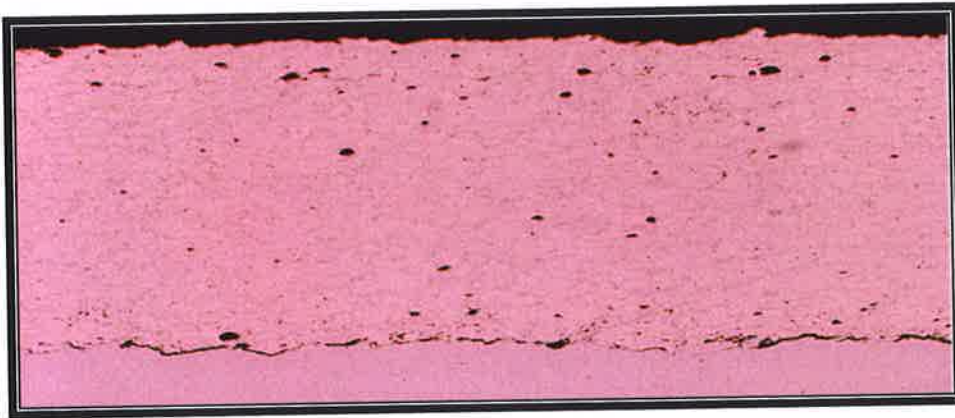


Figure A86: Carbon Steel after one (1) week exposure to brine solution fatigue tested.

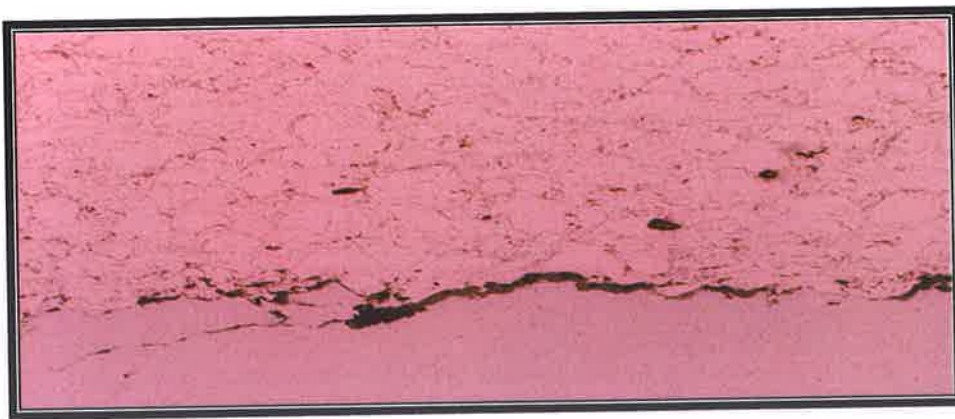


Figure A87: Carbon Steel after one (1) week exposure to brine solution fatigue tested.



Figure A88: Carbon Steel after one (1) week exposure to brine solution fatigue tested.

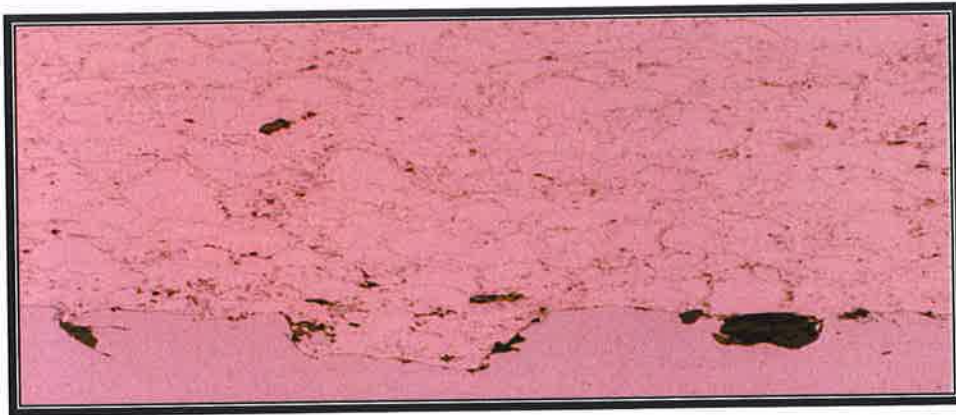


Figure A89: Carbon Steel after one (1) week exposure to brine solution fatigue tested.



Figure A90: Carbon Steel after one (1) week exposure to brine solution fatigue tested.

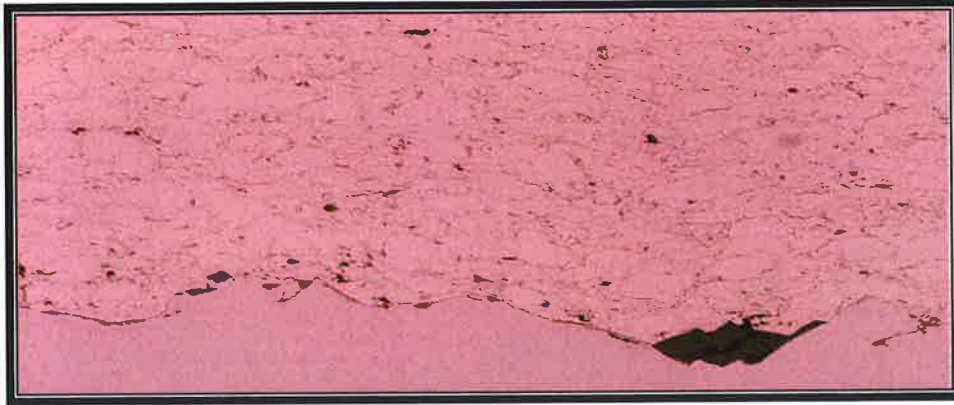


Figure A91: Carbon Steel after one (1) week exposure to brine solution fatigue tested.

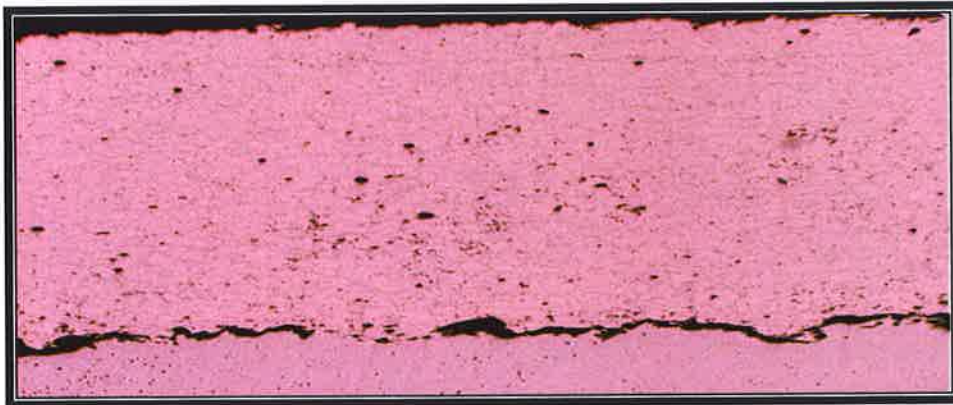


Figure A92: Carbon Steel after three (3) weeks exposure to brine solution fatigue tested.

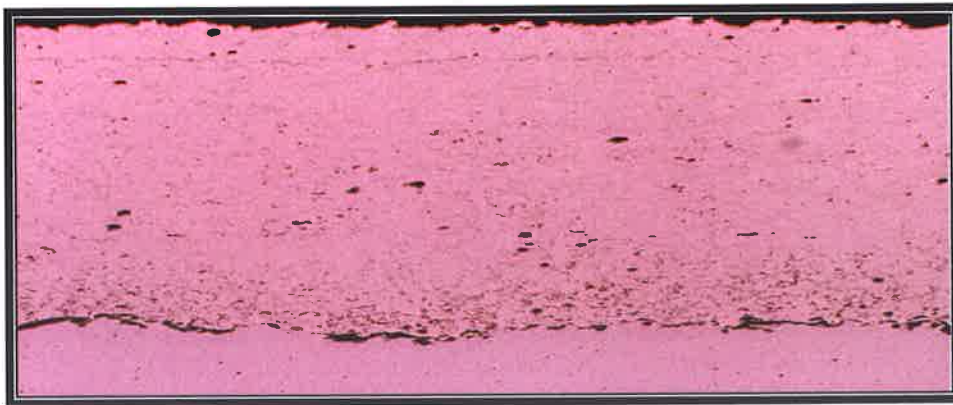


Figure A93: Carbon Steel after three (3) weeks exposure to brine solution fatigue tested.

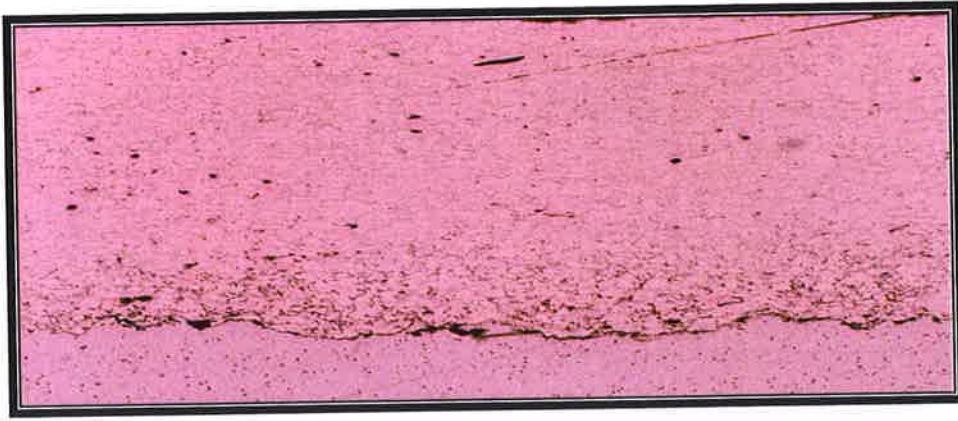


Figure A94: Carbon Steel after three (3) weeks exposure to brine solution fatigue tested.

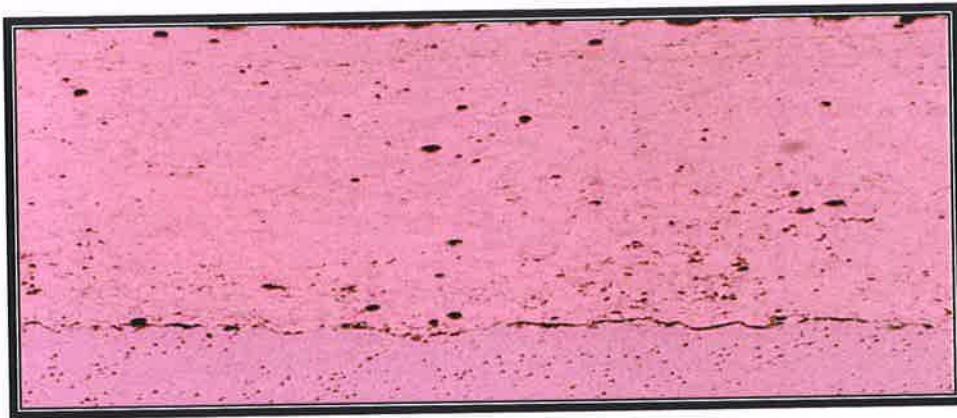


Figure A95: Carbon Steel after three (3) weeks exposure to brine solution fatigue tested.

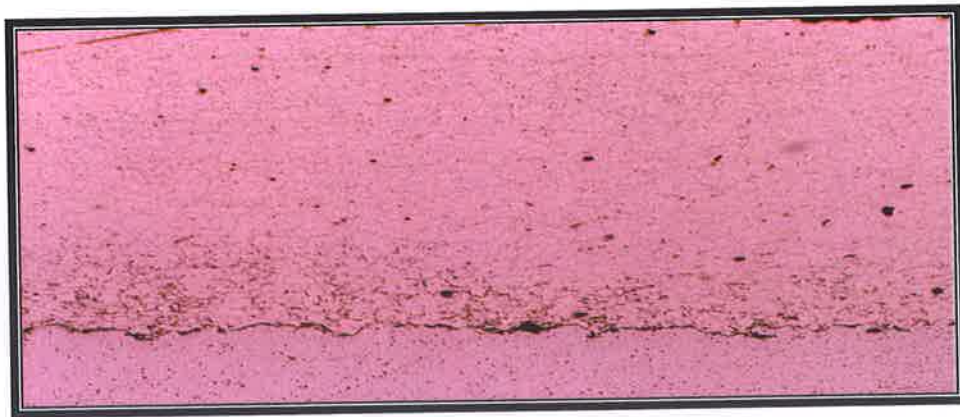


Figure A96: Carbon Steel after three (3) weeks exposure to brine solution fatigue tested.

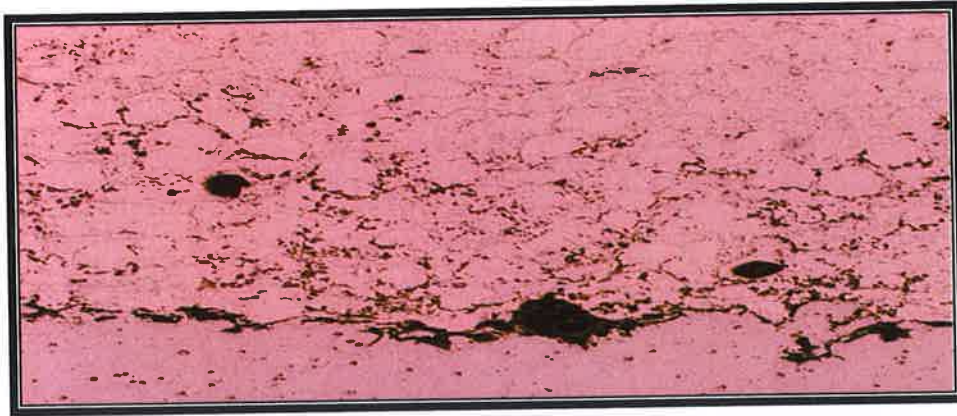


Figure A97: Carbon Steel after three (3) weeks exposure to brine solution fatigue tested.

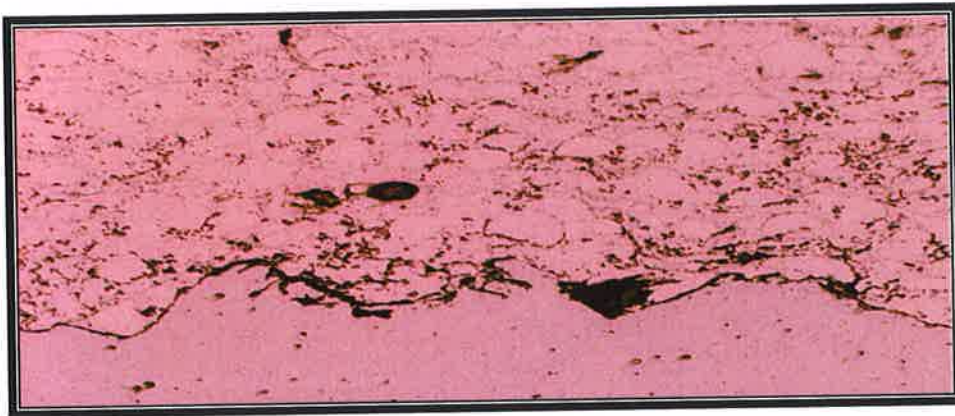


Figure A98: Carbon Steel after three (3) weeks exposure to brine solution fatigue tested.

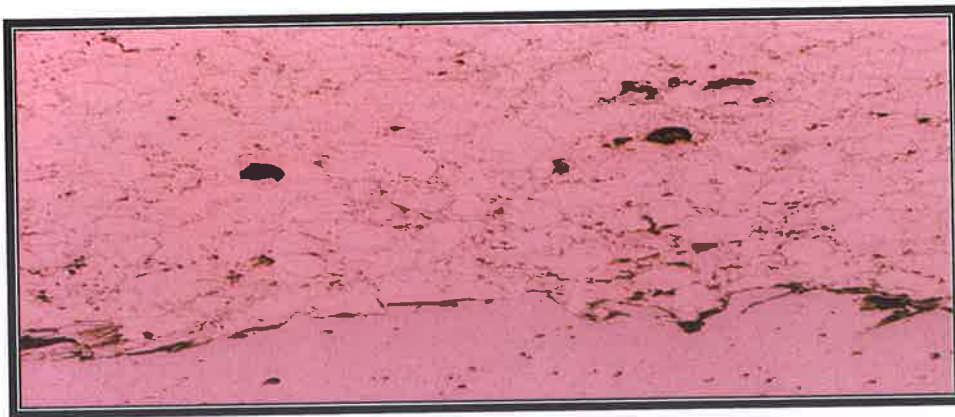


Figure A99: Carbon Steel after three (3) weeks exposure to brine solution fatigue tested.

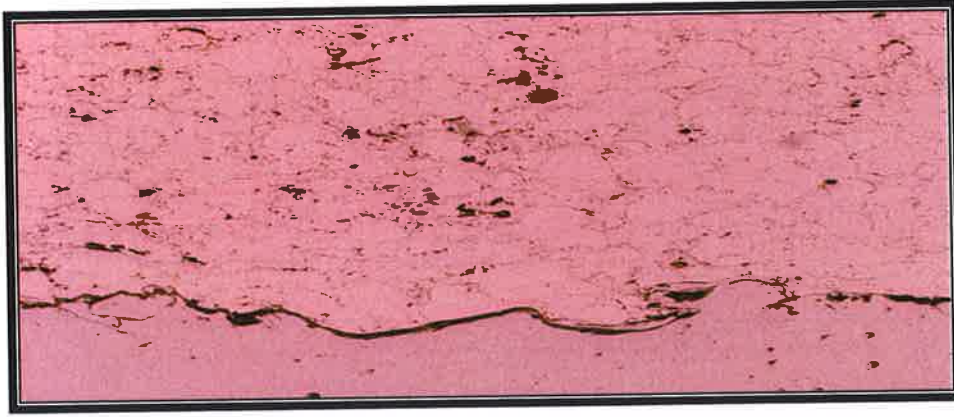


Figure A100: Carbon Steel after three (3) weeks exposure to brine solution fatigue tested.

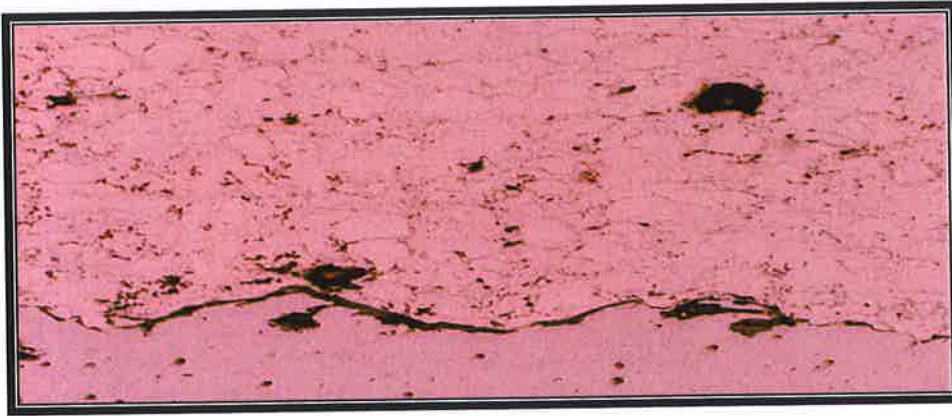


Figure A101: Carbon Steel after three (3) weeks exposure to brine solution fatigue tested.

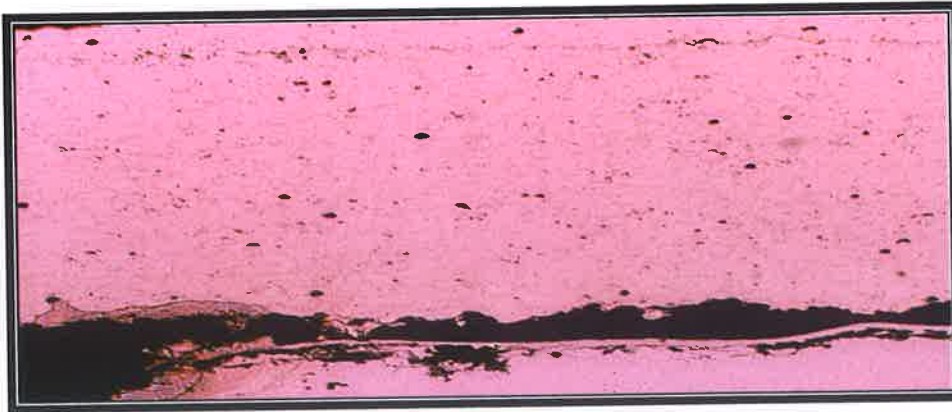


Figure A102: Carbon Steel after three (3) weeks exposure to brine solution tensile tested.

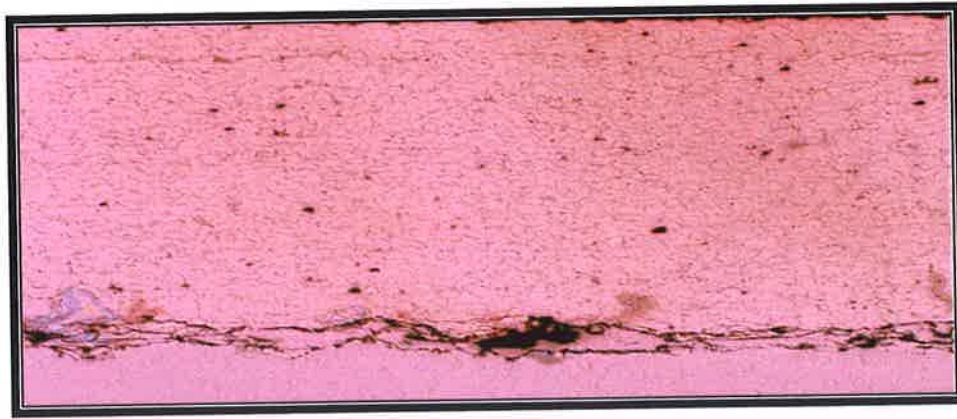


Figure A103: Carbon Steel after three (3) weeks exposure to brine solution tensile tested.

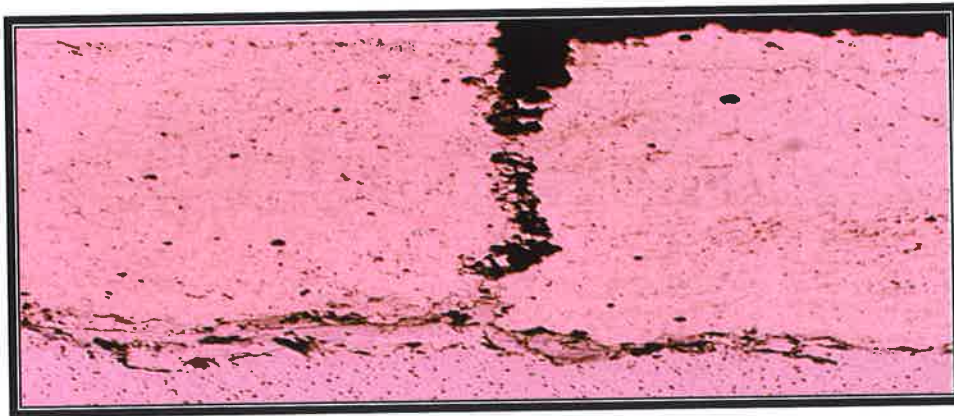


Figure A104: Carbon Steel after three (3) weeks exposure to brine solution tensile tested.



Figure A105: Carbon Steel after three (3) weeks exposure to brine solution tensile tested.



Figure A106: Carbon Steel after three (3) weeks exposure to brine solution tensile tested.



Figure A107: Carbon Steel after three (3) weeks exposure to brine solution tensile tested.



Figure A108: Carbon Steel after three (3) weeks exposure to brine solution tensile tested.

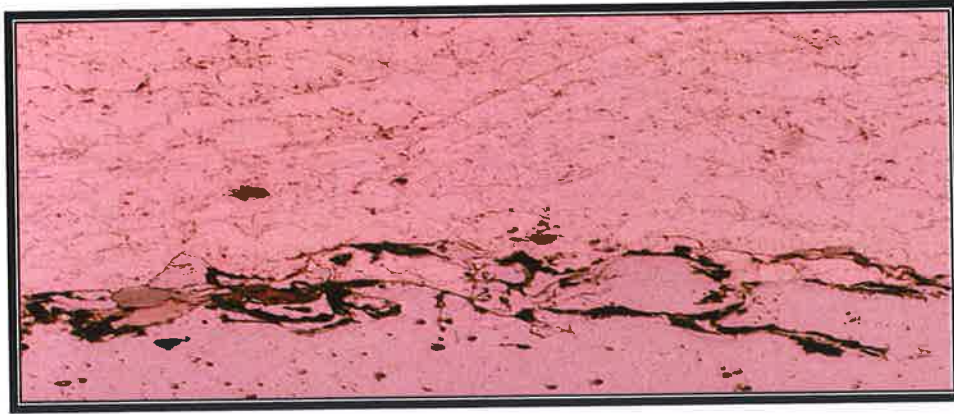


Figure A109: Carbon Steel after three (3) weeks exposure to brine solution tensile tested.

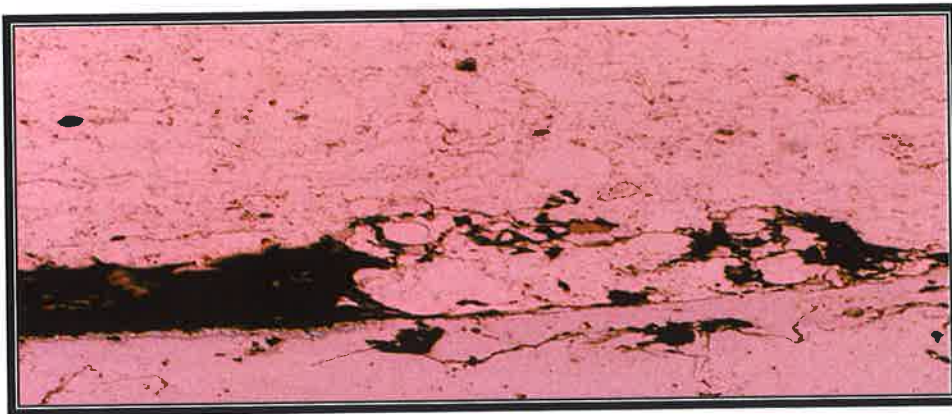


Figure A110: Carbon Steel after three (3) weeks exposure to brine solution tensile tested.

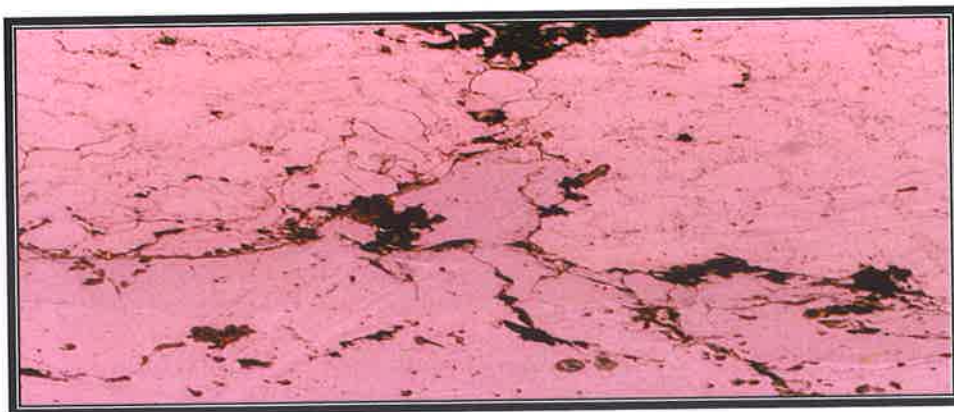


Figure A111: Carbon Steel after three (3) weeks exposure to brine solution tensile tested.

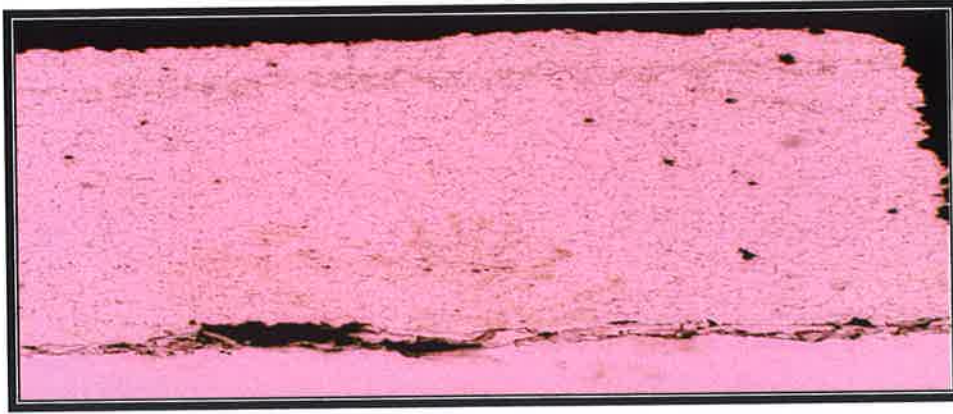


Figure A112: Stainless Steel after one (1) week exposure to brine solution tensile tested.

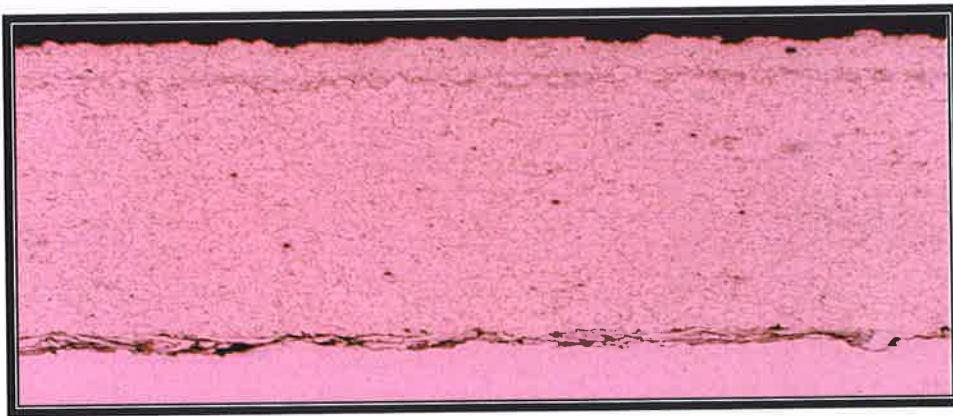


Figure A113: Stainless Steel after one (1) week exposure to brine solution tensile tested.

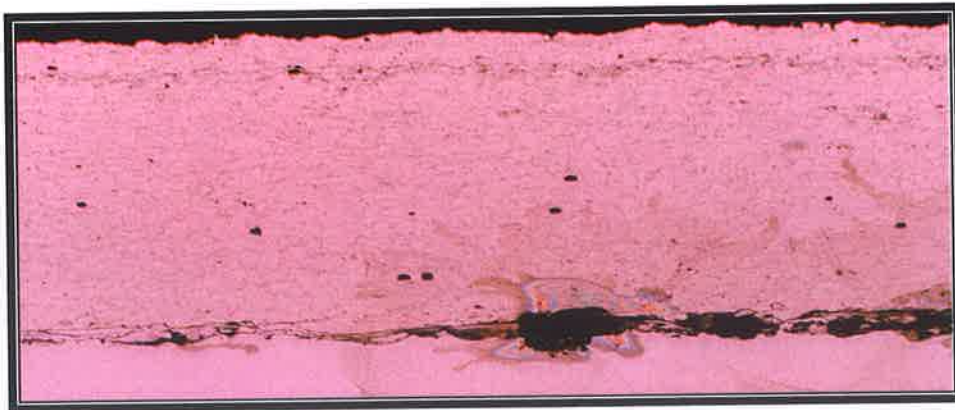


Figure A114: Stainless Steel after one (1) week exposure to brine solution tensile tested.

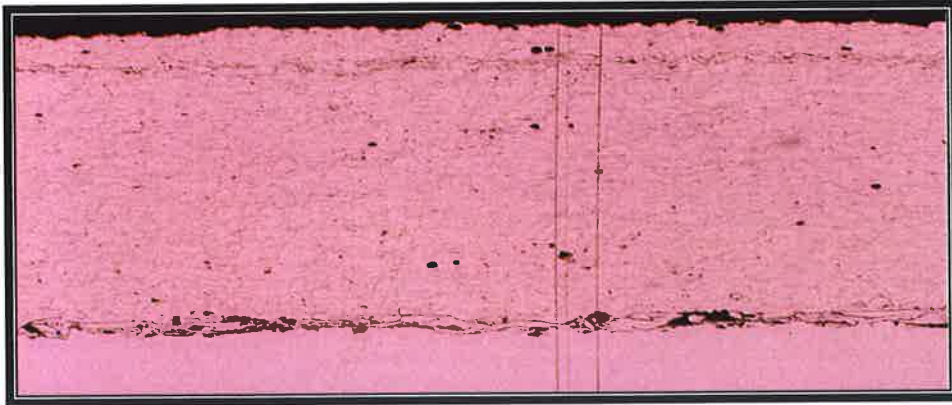


Figure A115: Stainless Steel after one (1) week exposure to brine solution tensile tested.

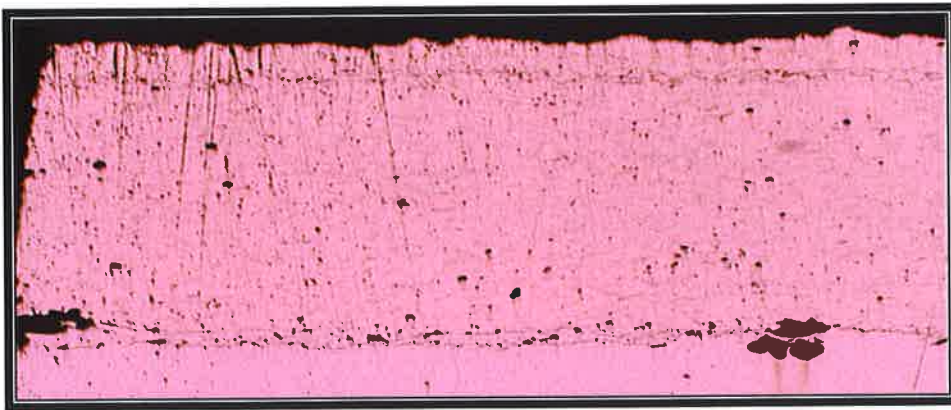


Figure A116: Stainless Steel after one (1) week exposure to brine solution tensile tested.

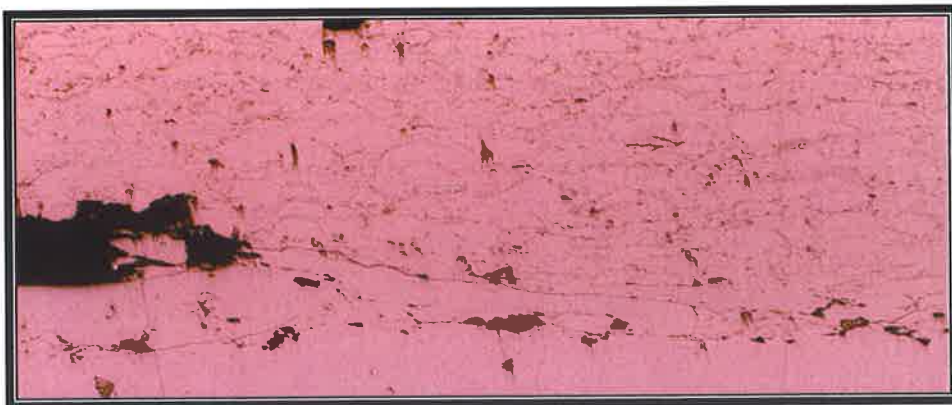


Figure A117: Stainless Steel after one (1) week exposure to brine solution tensile tested.



Figure A118: Stainless Steel after one (1) week exposure to brine solution tensile tested.

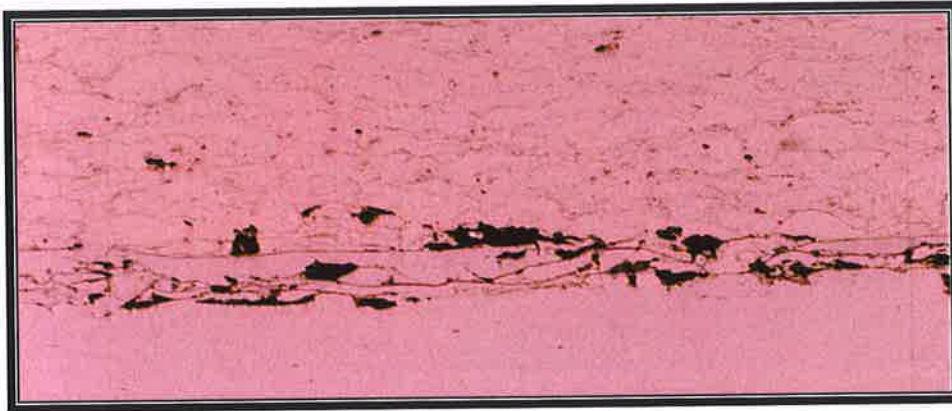


Figure A119: Stainless Steel after one (1) week exposure to brine solution tensile tested.

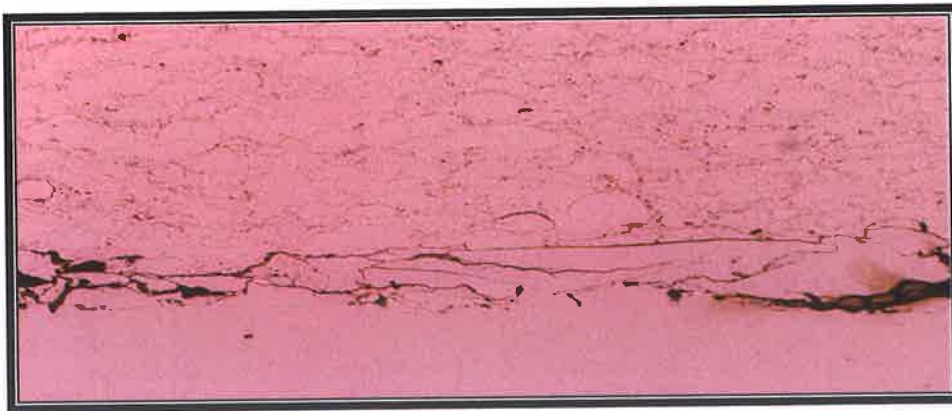


Figure A120: Stainless Steel after one (1) week exposure to brine solution tensile tested.



Figure A121: Stainless Steel after one (1) week exposure to brine solution tensile tested.



---

## APPENDIX B

---

### **Fatigue and Tensile tested flat sheet and round solid bar specimens:**

A collection of flat sheets specimens of carbon steel and stainless (304 SS) steel materials were HVOF coated with a coating powder similar to Inconel 625. All the coated specimens were exposed to brine solution complete immersion for static corrosion testing. The exposure period was selected to be one (1) week and three (3) weeks for both types of specimens. Optical microscopy examinations at two magnifications both 50X and 200X were made to the exposed tested specimens. The examinations were made for each tested specimens to show and observe the following:

- To observe Coating to substrate interface.
- To determine bonding between the coating adhesion to base metal.
- Coating porosity level.
- Coating adherence onto the specimen.
- Coating crack sites.
- Coating defects.

The images show different coating cross-sections and give indication of the coating integrity. Selected images show that low porosity level is observed. Other images indicate coating dis-integrity from the substrate. Generally, there are no cracks observed in the coating it self. The following below figures (Figure B1 to Figure B85) are obtained from the optical microscopy examinations for total of twelve (12) coated specimens.

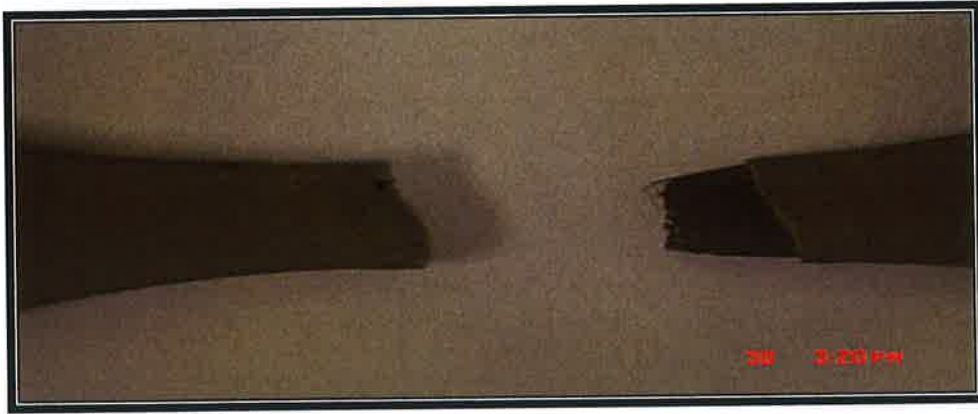


Figure B1: One week exposure to brine solution tensile tested.



Figure B2: One week exposure to brine solution tensile tested.



Figure B3: Carbon Steel round solid specimen tensile tested post brine solution exposure: Side view.

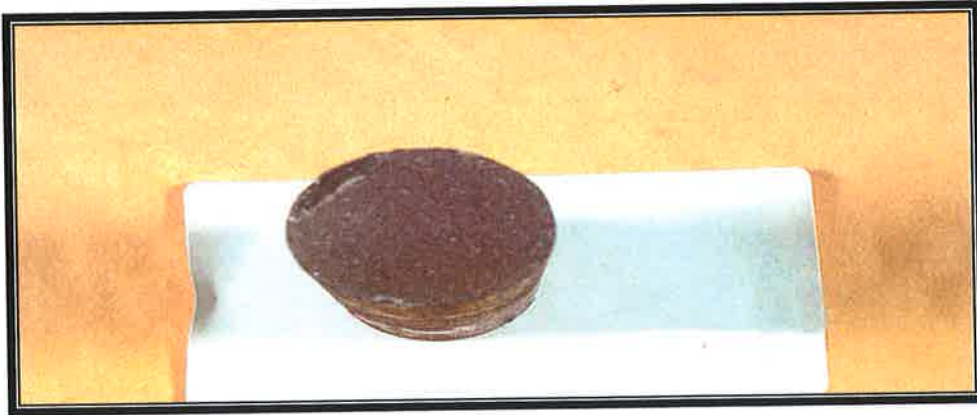


Figure B4: Carbon Steel round solid specimen tensile tested post brine solution exposure: Top view.

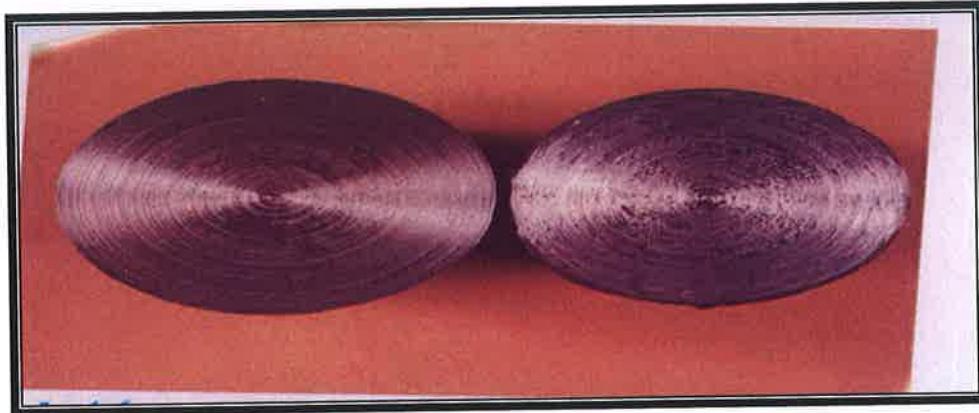


Figure B5: Stainless Steel round solid specimen exposed to brine solution and tensile tested: Top view.



Figure B6: Stainless Steel round solid specimen after two (2) weeks exposure to brine solution tensile tested: Top view.



Figure B7: Stainless Steel round solid specimen after three (3) weeks exposure to brine solution tensile tested: Top view.

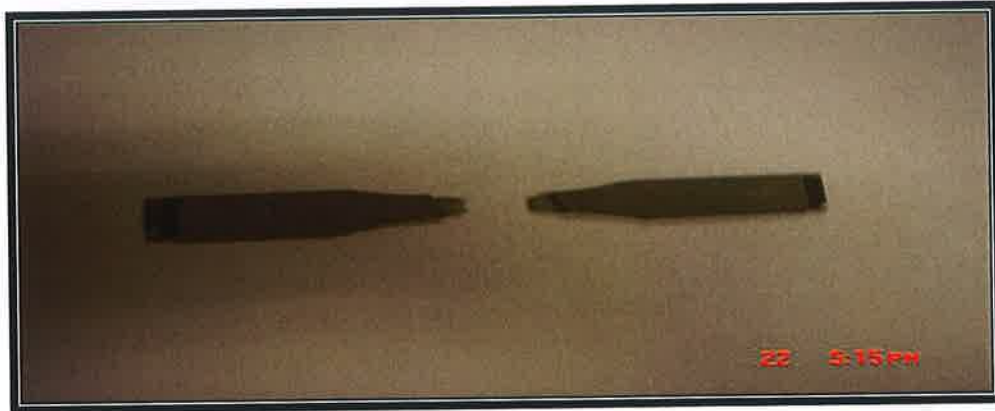


Figure B8: Tensile tested specimen.

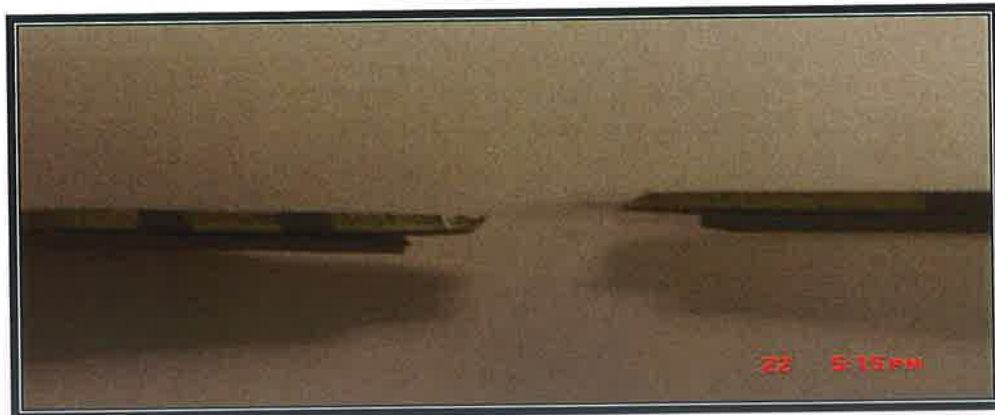


Figure B9: Tensile tested specimen



Figure B10: Carbon Steel specimen after one (1) week exposure to brine solution tensile tested.



Figure B11: Stainless Steel specimen after one (1) week exposure to brine solution tensile tested.



Figure B12: Stainless Steel specimen after one (1) week exposure to brine solution tensile tested.



Figure B13: Carbon Steel specimen after one (1) week exposure tensile tested.

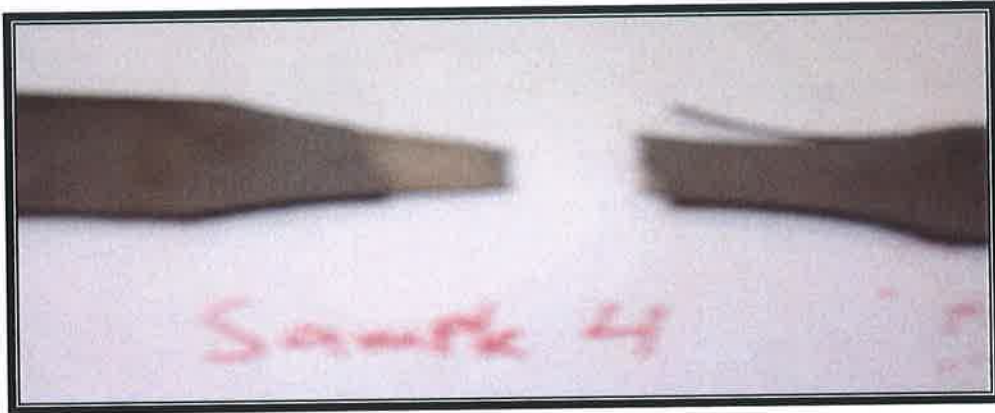


Figure B14: Stainless Steel specimen after three (3) weeks exposure to brine solution tensile tested.



Figure B15: Carbon Steel Specimen after one (1) week exposure to brine solution tensile tested.

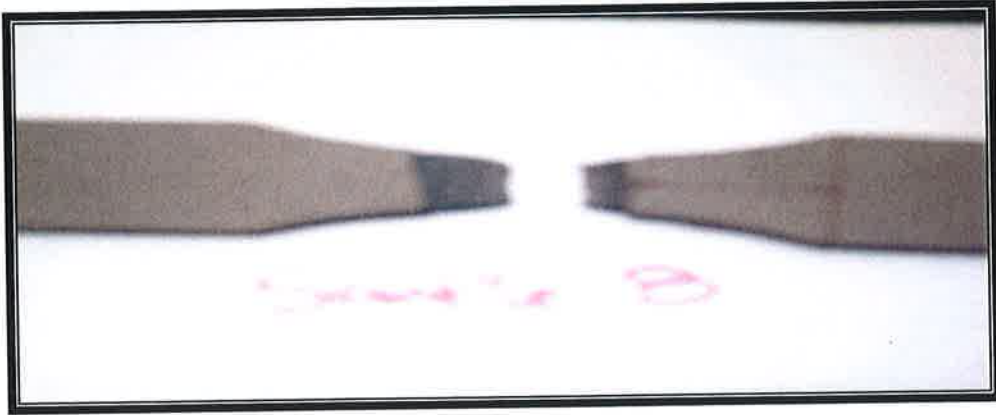


Figure B16: Carbon Steel Specimen after one (1) week exposure to brine solution tensile tested.



Figure B17: Carbon Steel Specimen after one (1) week exposure to brine solution tensile tested.



Figure B18: Carbon Steel Specimen after one (1) week exposure to brine solution tensile tested.

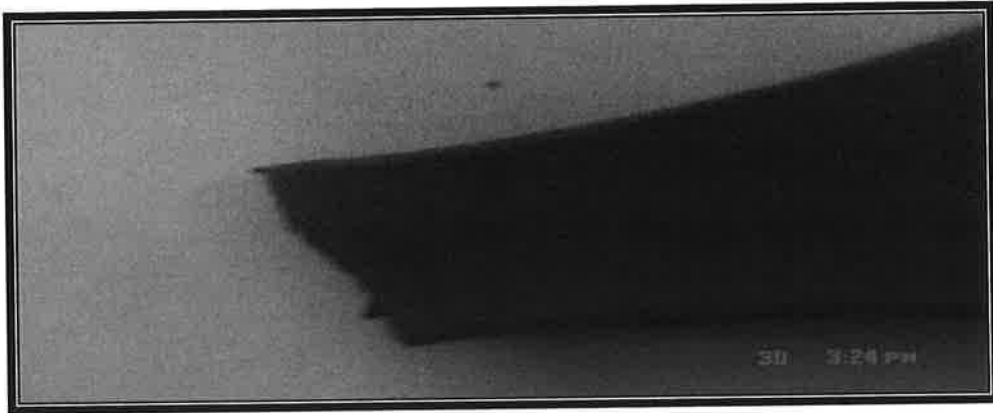


Figure B19: Carbon Steel Specimen after one (1) week exposure to brine solution tensile tested.

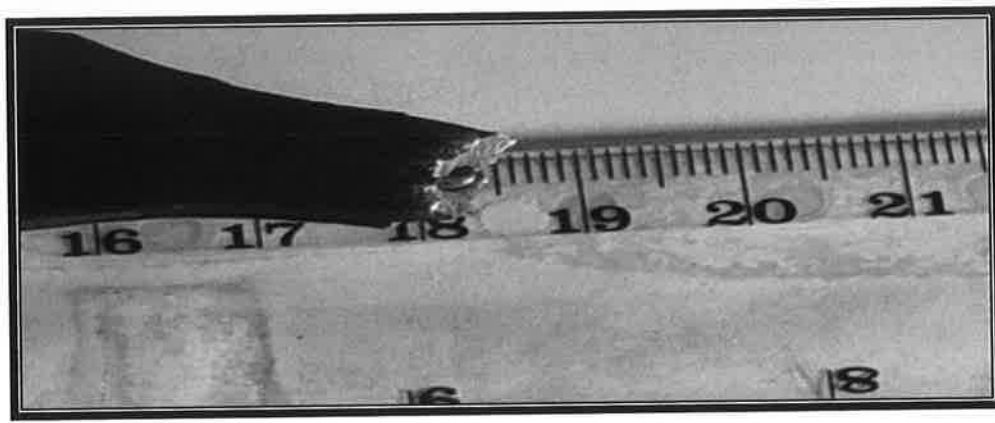


Figure B20: Welded Stainless Steel of 2 mm size after three weeks exposure to brine solution tensile tested.

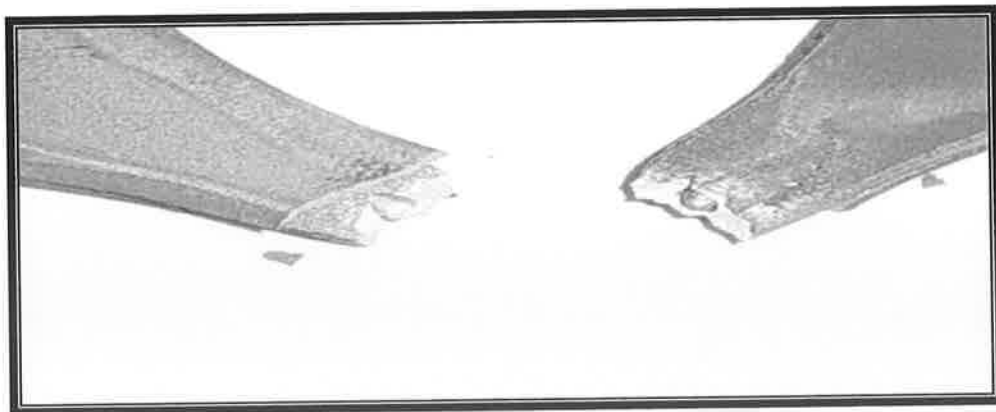


Figure B21: Welded Stainless Steel of 2 mm size after three weeks exposure to brine solution tensile tested.



Figure B22: Welded stainless steel 3 mm size after three (3) weeks exposure to brine solution tensile tested.

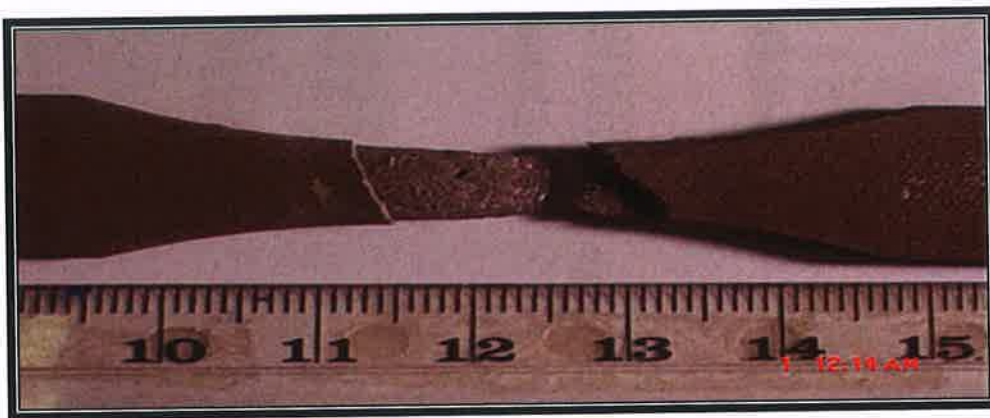


Figure B23: Welded stainless steel 5 mm size after one (1) week exposure to brine solution tensile tested.

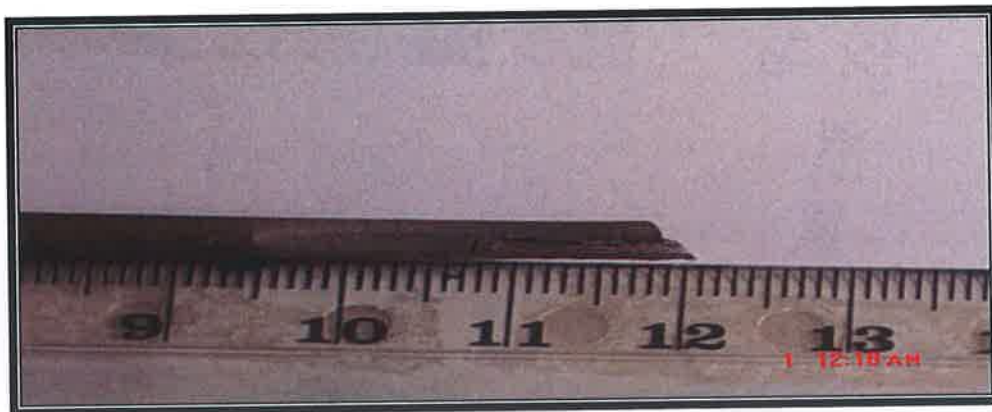


Figure B24: Welded stainless steel 5 mm size after one (1) week exposure to brine solution tensile tested.

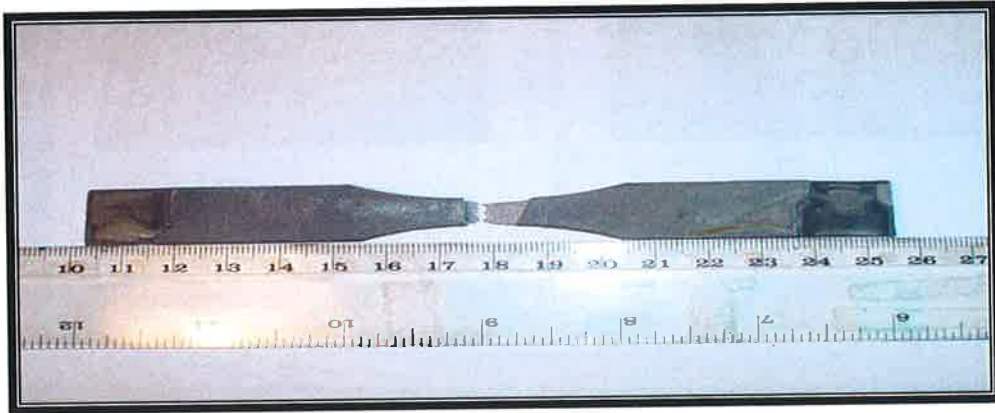


Figure B25: Welded stainless steel 5 mm size after three (3) week exposure to brine solution tensile tested.

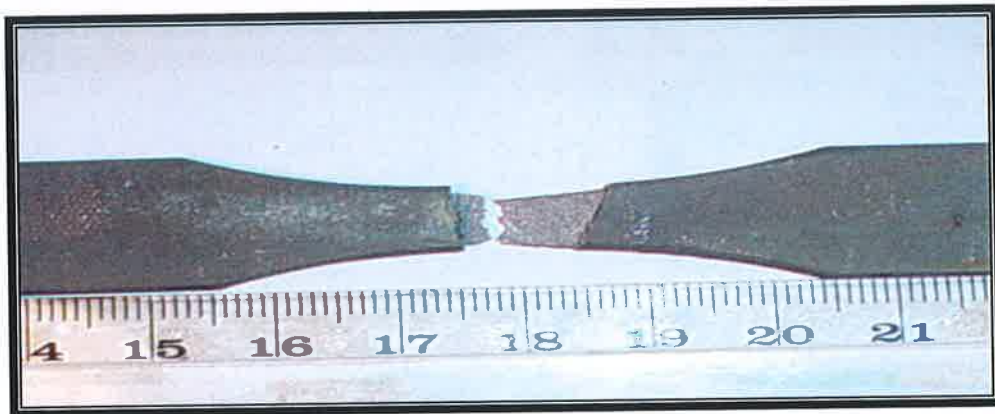


Figure B26: Welded stainless steel 5 mm size after three (3) week exposure to brine solution tensile tested.



Figure B27: Welded stainless steel 5 mm size after three (3) week exposure to brine solution tensile tested.



Figure B28: Welded stainless steel 5 mm size after three (3) week exposure to brine solution tensile tested.



Figure B29: Welded stainless steel 5 mm in as received condition (no exposure) tensile tested.

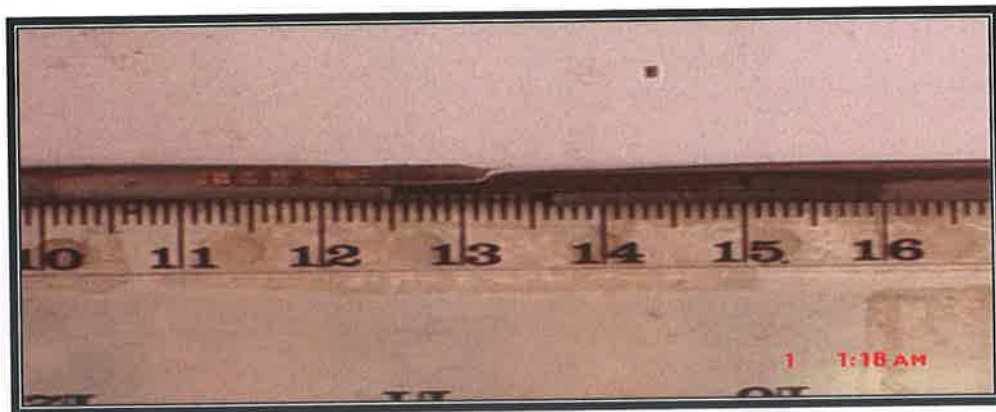


Figure B30: Welded stainless steel 5 mm in as received condition (no exposure) tensile tested.

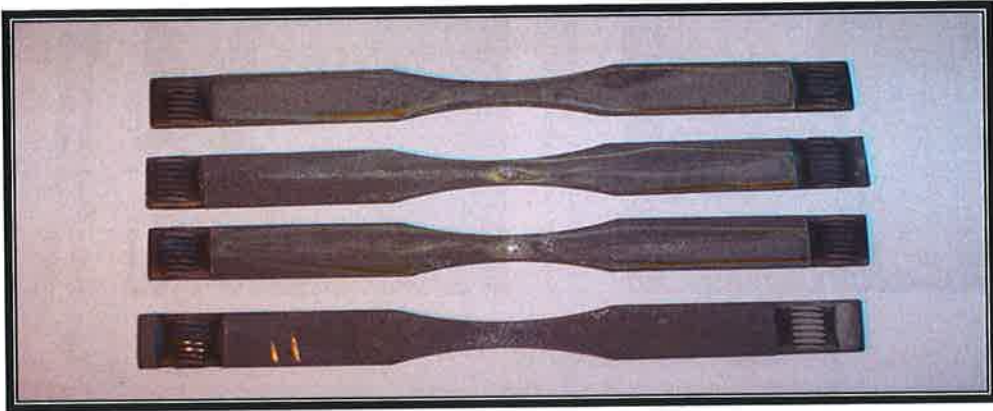


Figure B31: Welded stainless steel specimens after three (3) weeks exposure to brine solution prior to mechanical testing.

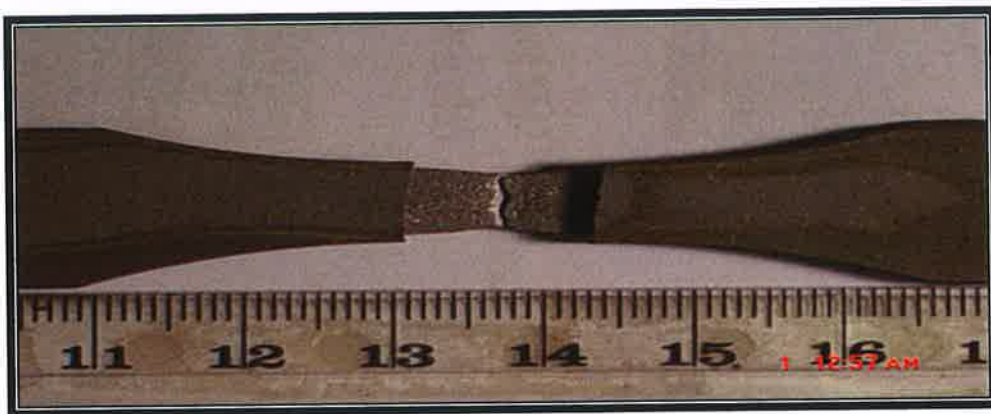


Figure B32: Stainless steel specimen after one (1) week exposure to brine solution tensile tested.



Figure B33: Stainless steel specimen after three (3) weeks exposure to brine solution tensile tested.

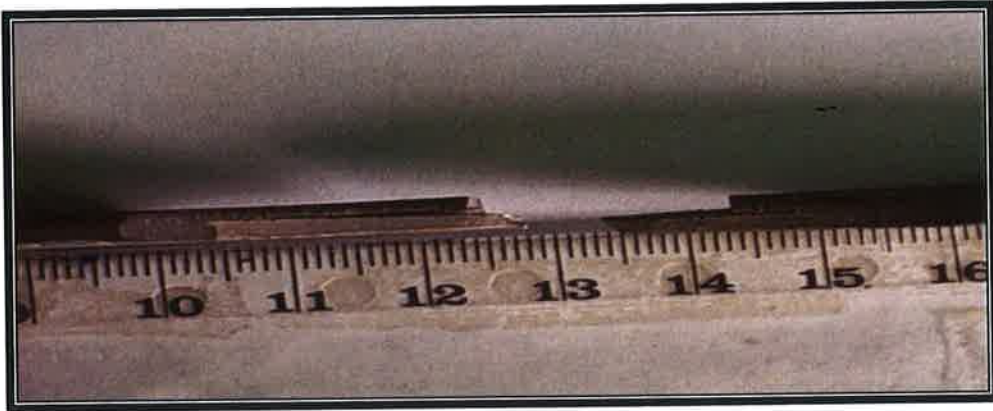


Figure B34: Stainless steel specimen after three (3) weeks exposure to brine solution tensile tested.

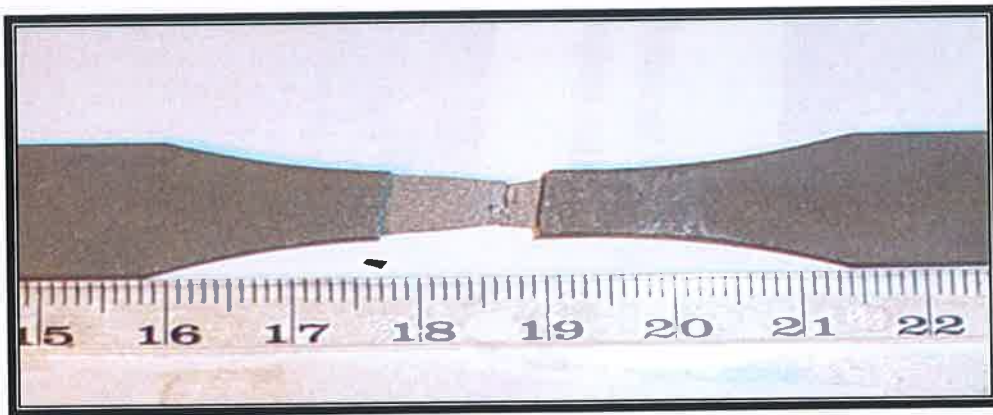


Figure B35: Stainless steel specimen after three (3) weeks exposure to brine solution tensile tested.



Figure B36: Stainless steel specimen after three (3) weeks exposure to brine solution tensile tested.

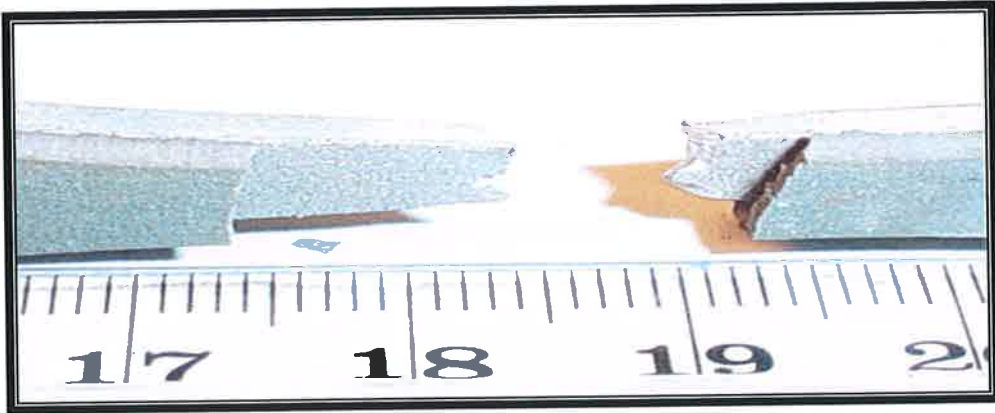


Figure B37: Stainless steel specimen after three (3) weeks exposure to brine solution tensile tested.

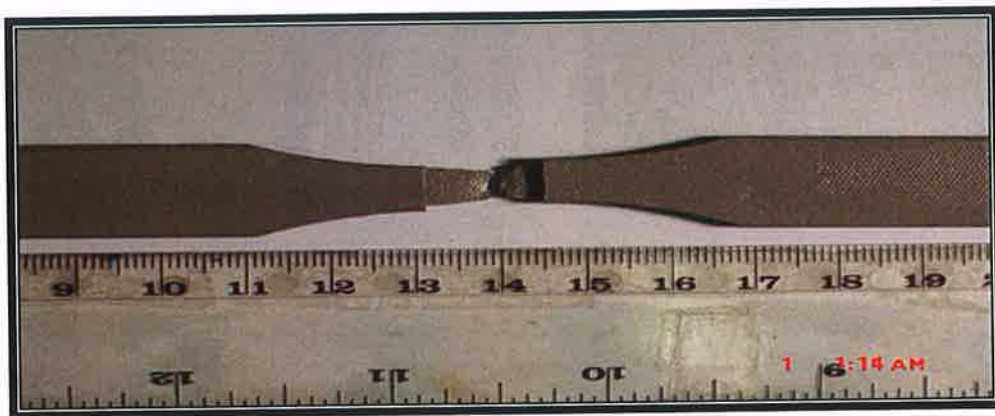


Figure B38: Stainless steel specimen in as received condition (no exposure) tensile tested.



Figure B39: Stainless steel specimens after one (1) week exposure to brine solution tensile tested.

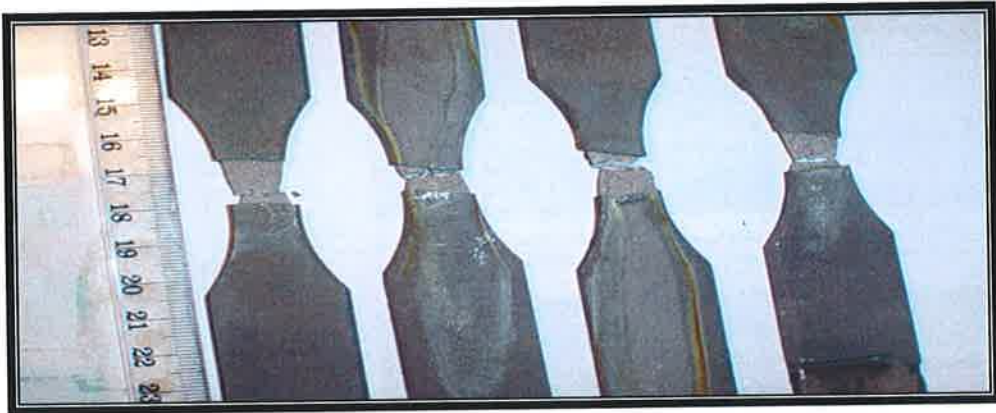


Figure B40: Stainless steel specimens after three (3) weeks exposure to brine solution tensile tested.

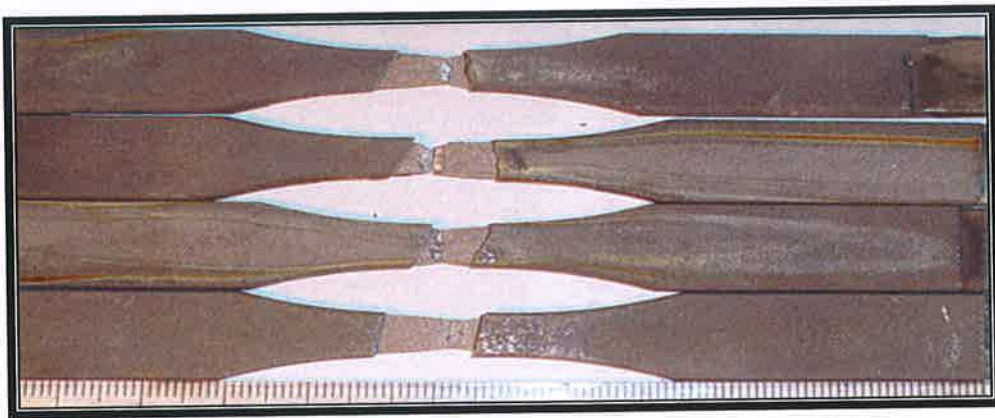


Figure B41: Stainless steel specimens after three (3) weeks exposure to brine solution tensile tested.



Figure B42: Welded Carbon steel specimen 2.5 mm size after three (3) weeks exposure to brine solution prior to mechanical testing.

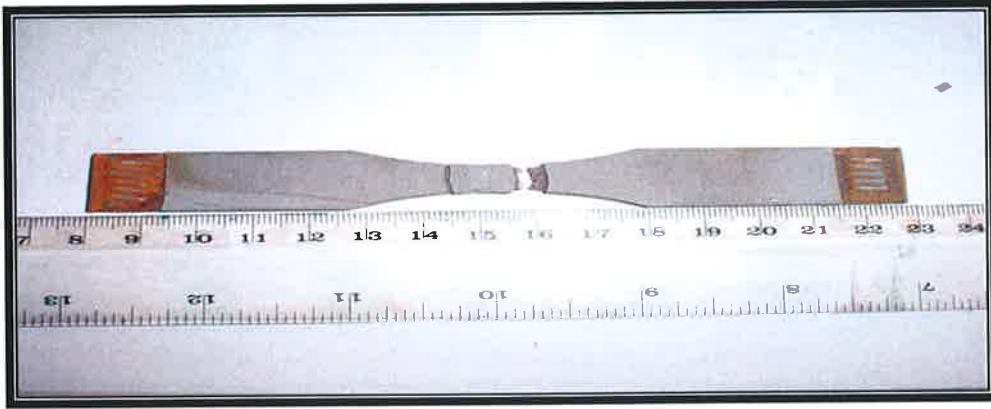


Figure B43: Welded Carbon steel specimen 5 mm size after one (1) week exposure to brine solution tensile tested.

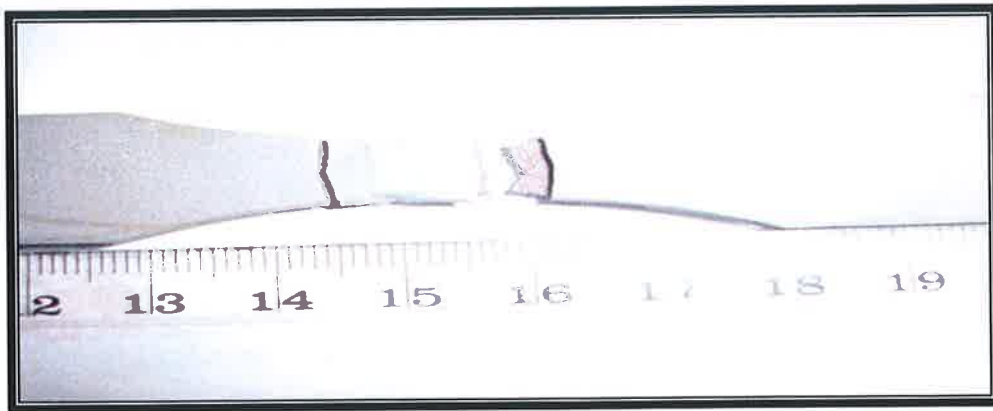


Figure B44: Welded Carbon steel specimen 5 mm size after one (1) week exposure to brine solution tensile tested.



Figure B45: Welded Carbon steel specimen 5 mm size after one (1) week exposure to brine solution tensile tested.

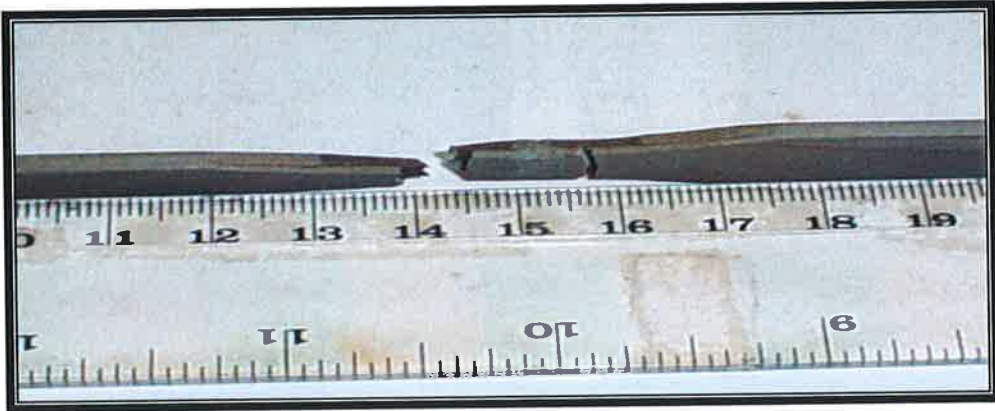


Figure B46: Welded Carbon steel specimen 5 mm size after one (1) week exposure to brine solution tensile tested.

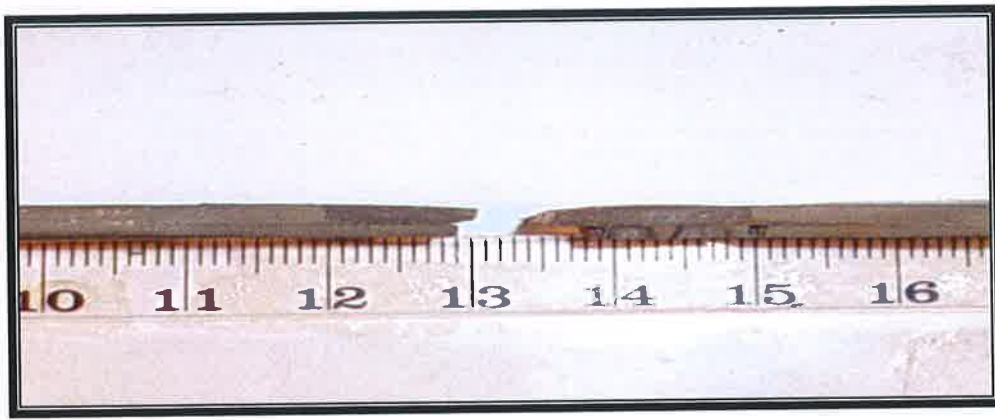


Figure B47: Welded Carbon steel specimen 5 mm size after three (3) week exposure to brine solution tensile tested.



Figure B48: Welded Carbon steel specimen 5 mm size after three (3) weeks exposure to brine solution prior to mechanical testing.



Figure B49: Welded Carbon steel specimen 5 mm size in as received (no exposure) condition tensile tested.

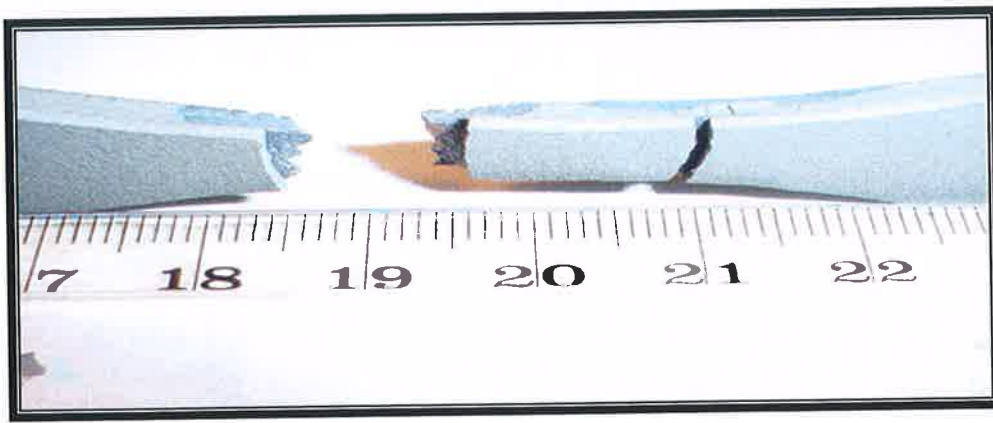


Figure B50: Welded Carbon steel 5 mm specimen in as received (no exposure) condition tensile tested.

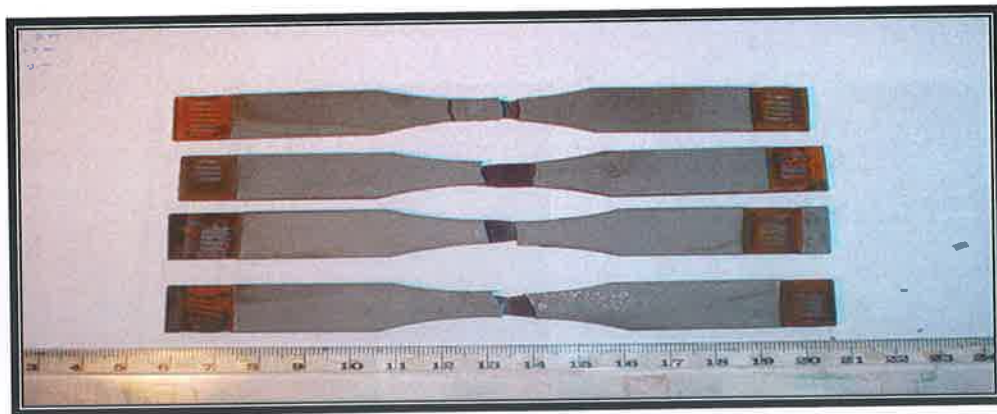


Figure B51: Carbon steel specimens after one (1) week exposure to brine solution tensile tested.



Figure B52: Carbon steel specimens after one (1) week exposure to brine solution tensile tested.

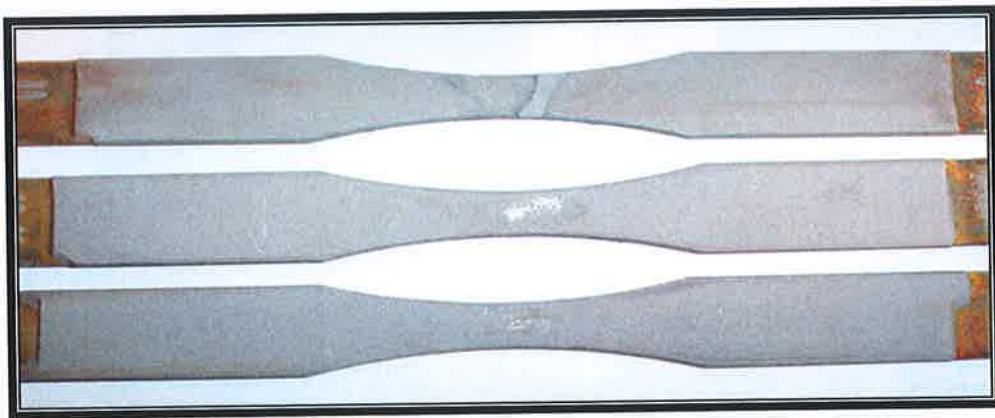


Figure B53: Carbon steel specimens after three (3) weeks exposure to brine solution prior to mechanical testing.



Figure B54: Carbon steel specimens after three (3) weeks exposure to brine solution tensile tested.

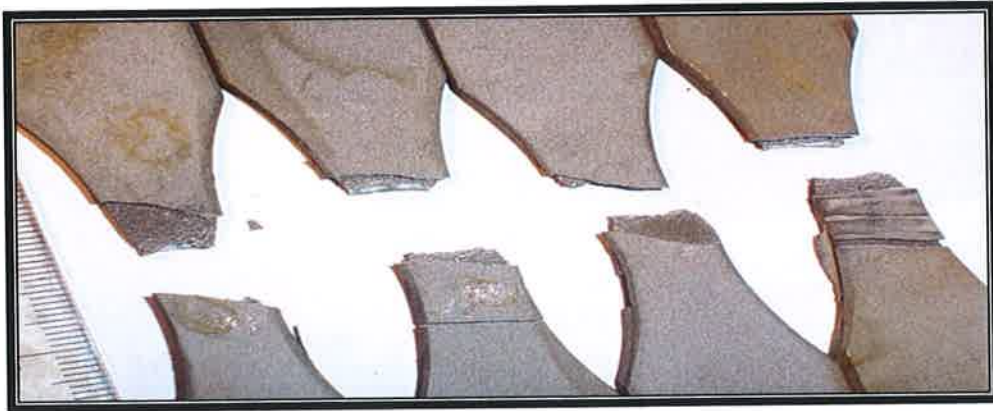


Figure B55: Carbon steel specimens after three (3) weeks exposure to brine solution tensile tested.

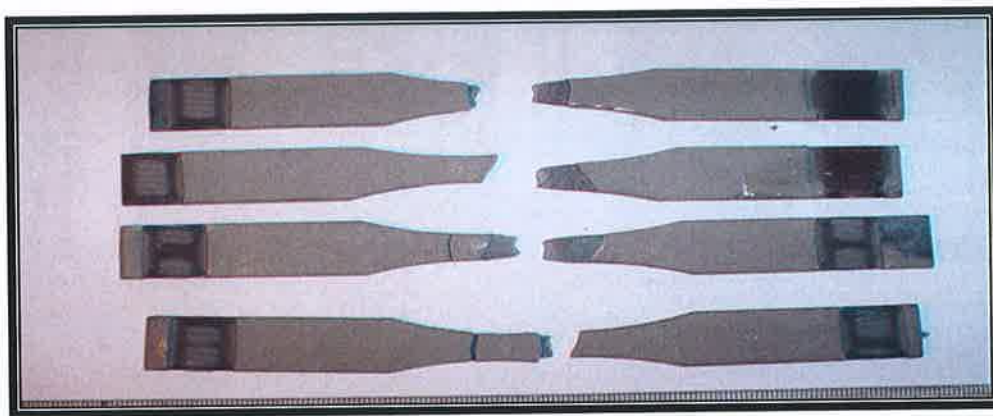


Figure B56: Carbon steel specimens in as received condition (no exposure) tensile tested.



Figure B57: Carbon steel specimen after one (1) week exposure to brine solution tensile tested.

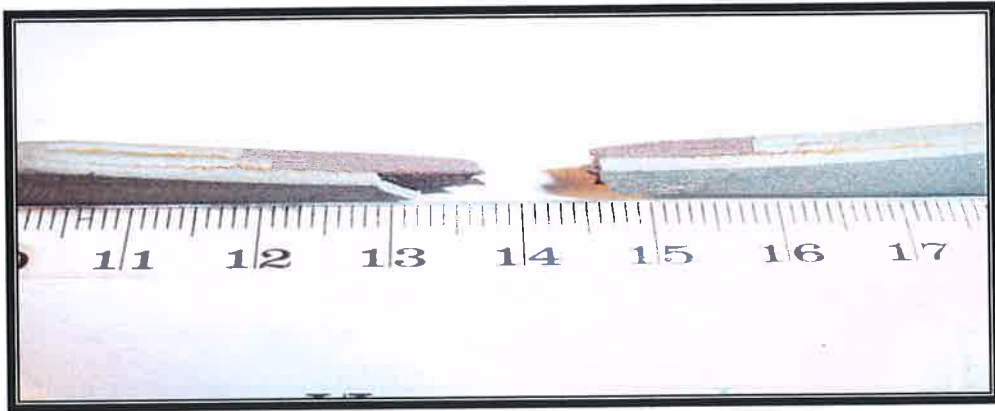


Figure B58: Carbon steel specimen after one (1) week exposure to brine solution tensile tested.



Figure B59: Carbon steel specimen after three (3) weeks exposure to brine solution tensile tested.



Figure B60: Carbon steel specimen after three (3) weeks exposure to brine solution tensile tested.

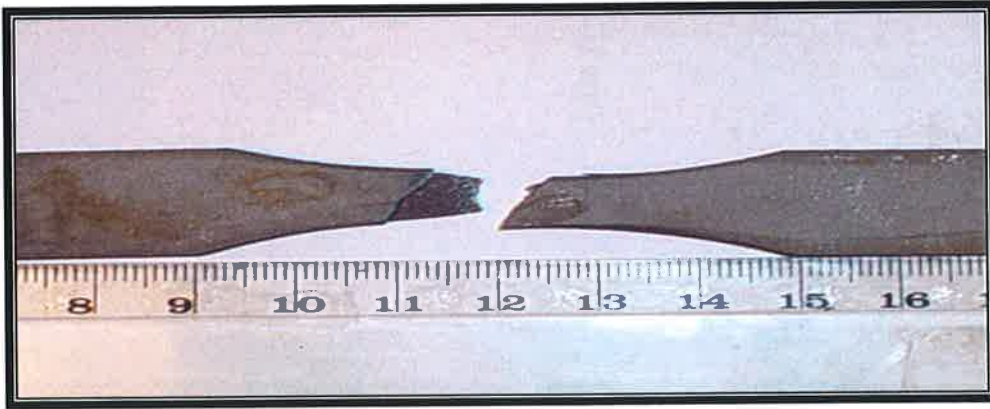


Figure B61: Carbon steel specimen after one (1) week exposure to brine solution tensile tested.

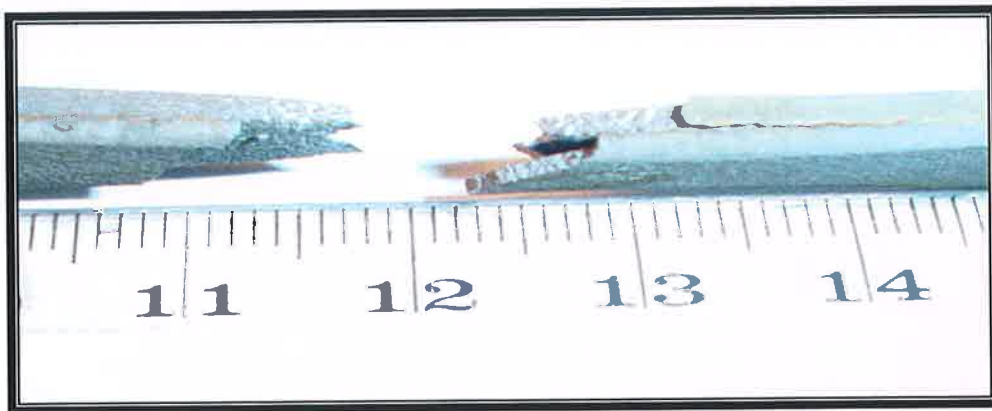


Figure B62: Carbon steel specimen after three (3) weeks exposure to brine solution tensile tested.

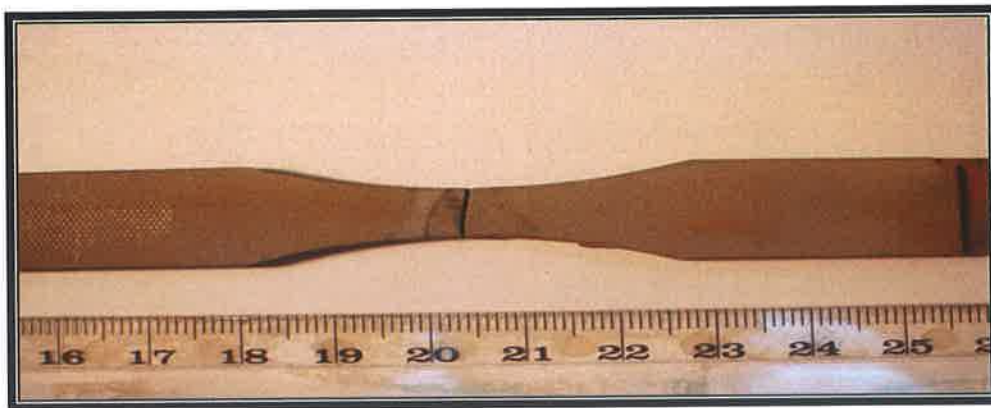


Figure B63: Welded Carbon steel specimen 5 mm size after three (3) weeks exposure to brine solution fatigue tested.

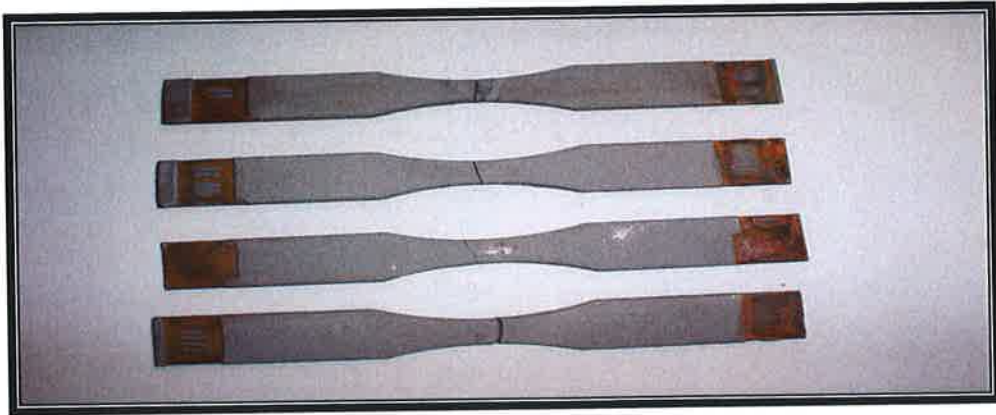


Figure B64: Carbon steel specimens after three (3) weeks exposure to brine solution fatigue tested.

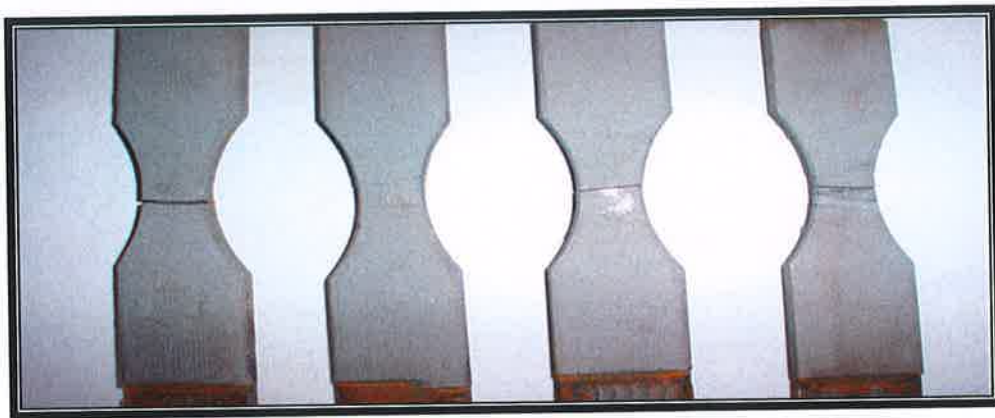


Figure B65: Carbon steel specimens after three (3) weeks exposure to brine solution fatigue tested.

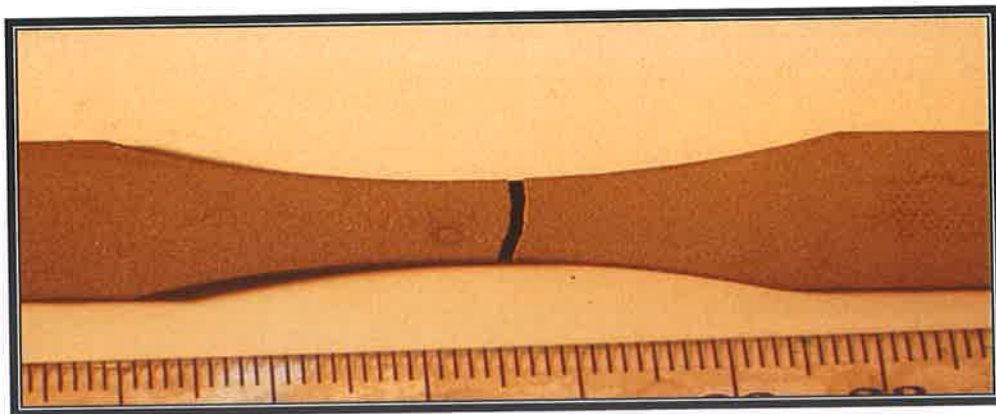


Figure B66: Carbon steel specimen after three (3) weeks exposure to brine solution fatigue tested.

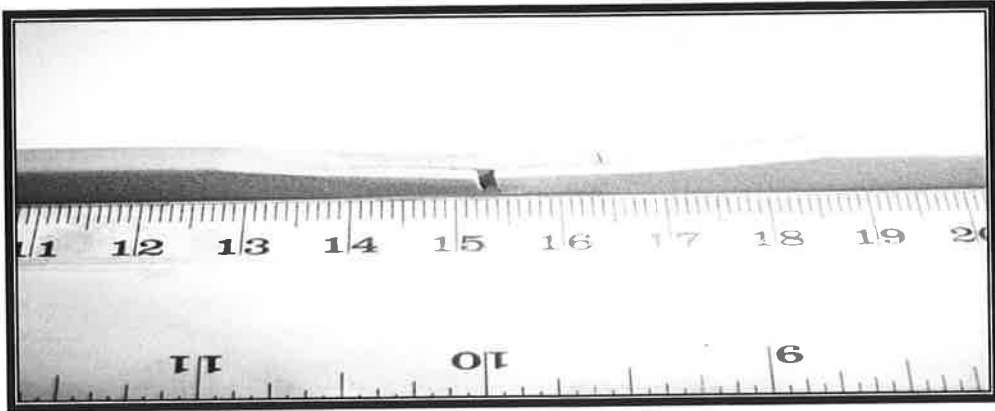


Figure B67: Welded Carbon steel specimen 5 mm size in as received condition (no exposure) fatigue tested.



Figure B68: Welded Carbon steel specimen 5 mm size in as received condition (no exposure) fatigue tested.

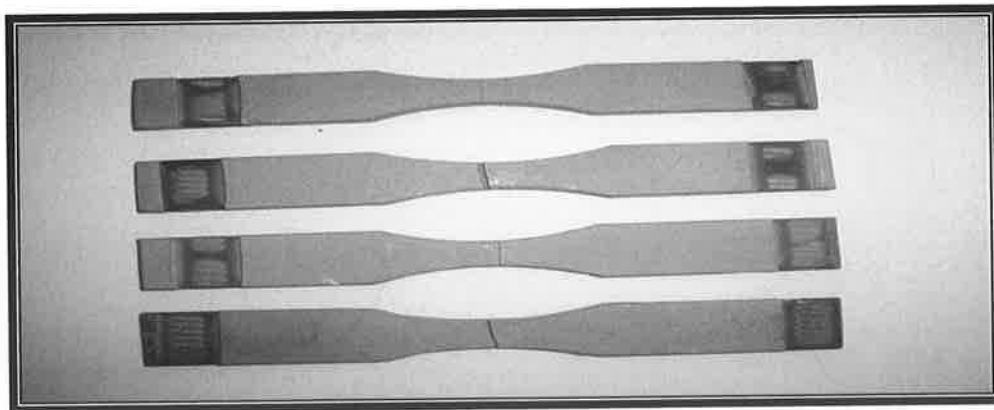


Figure B69: Carbon steel specimens in as received condition (no exposure) fatigue tested.

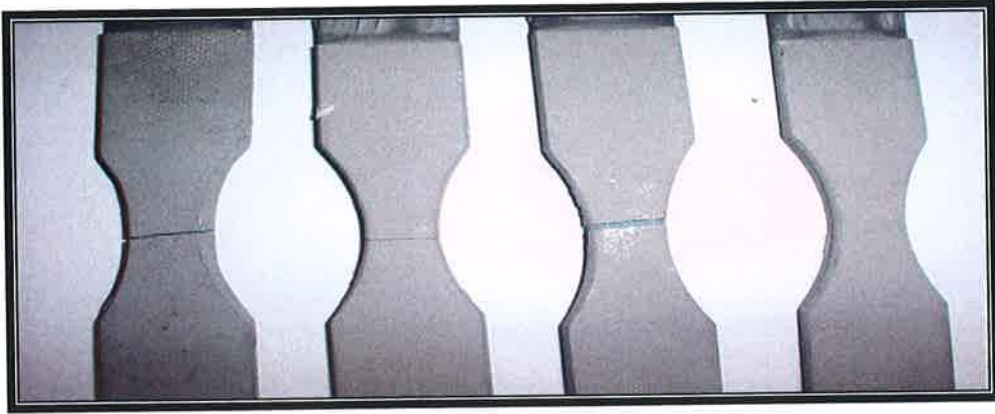


Figure B70: Carbon steel specimens in as received condition (no exposure) fatigue tested.

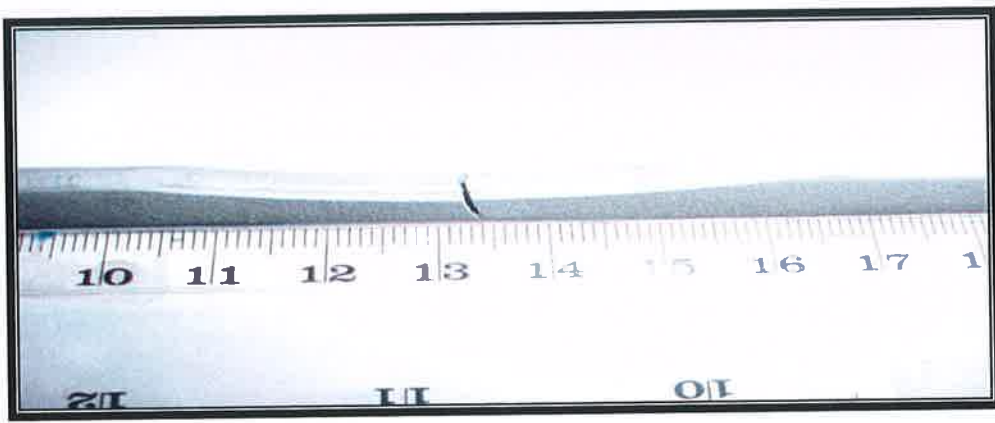


Figure B71: Carbon steel specimen in as received condition (no exposure) fatigue tested.



Figure B72: Carbon steel specimen in as received condition (no exposure) fatigue tested.

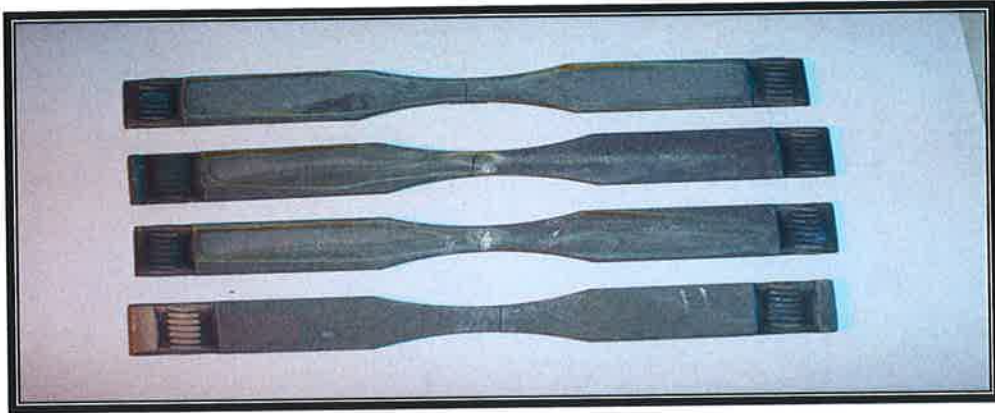


Figure B73: Stainless steel specimens after three (3) weeks exposure to brine solution fatigue tested.

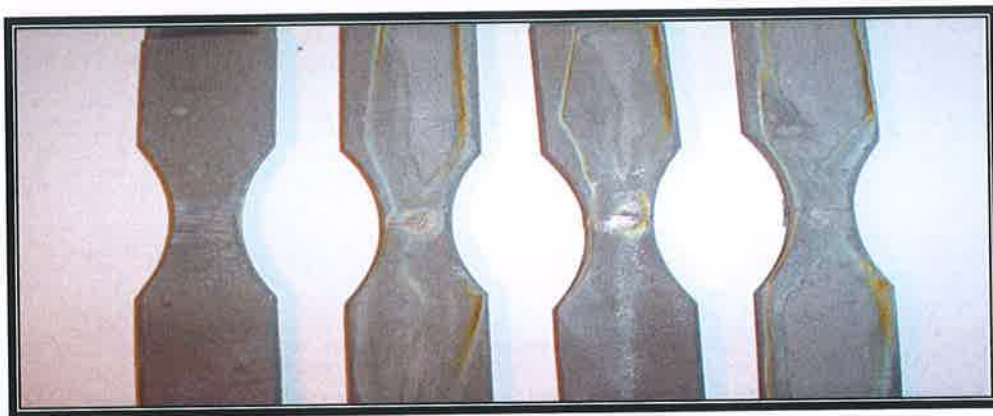


Figure B74: Welded Stainless steel specimens after three (3) weeks exposure to brine solution fatigue tested.

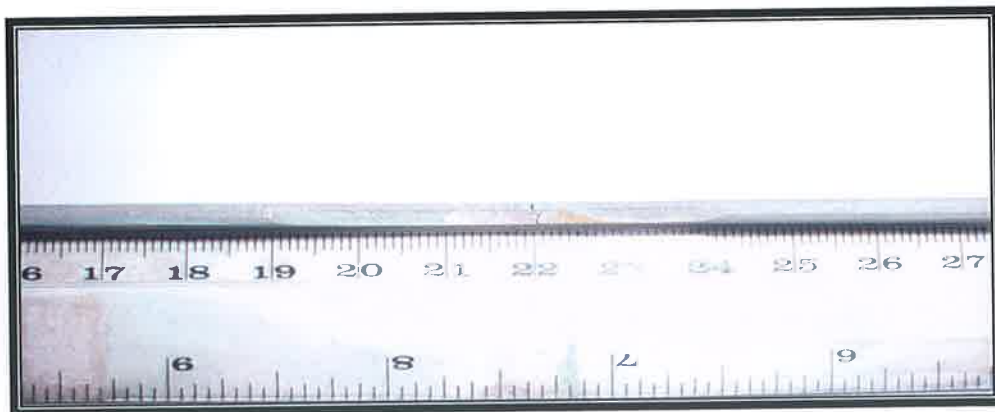


Figure B75: Stainless steel specimen after three (3) weeks exposure to brine solution fatigue tested.



Figure B76: Stainless steel specimen after three (3) weeks exposure to brine solution fatigue tested.

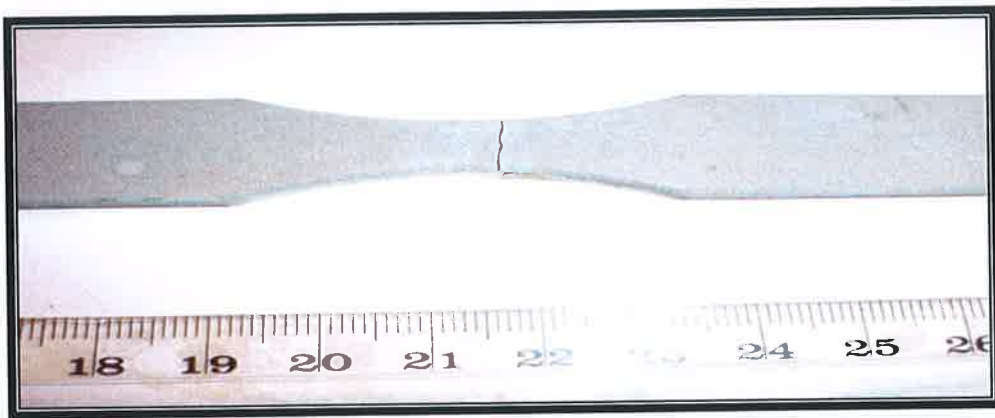


Figure B77: Stainless steel specimen after three (3) weeks exposure to brine solution fatigue tested.

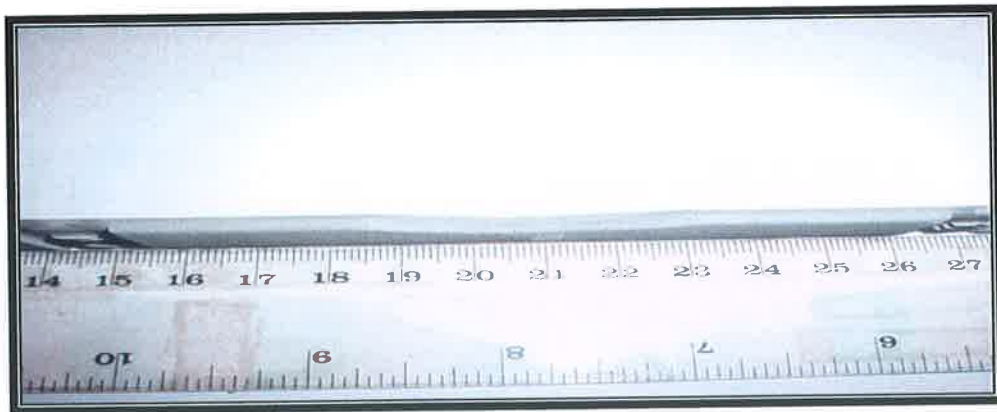


Figure B78: Welded Stainless steel specimen 5 mm in as received condition (no exposure) fatigue tested.

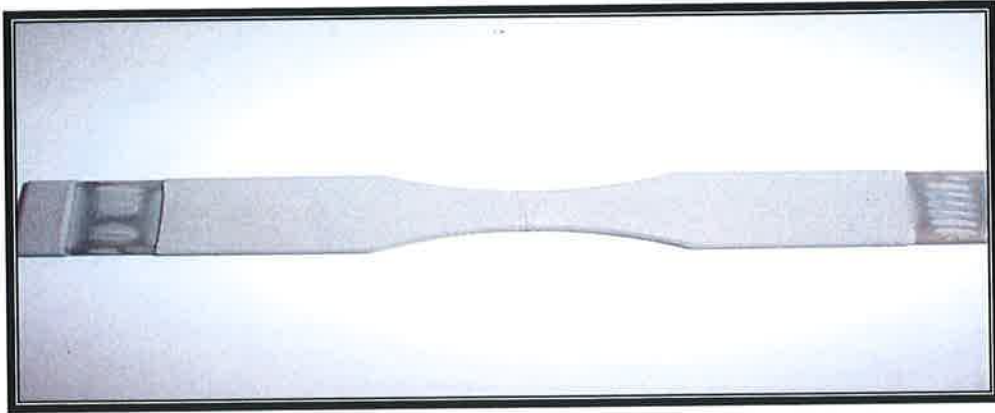


Figure B79: Welded Stainless steel specimen 5 mm size in as received condition (no Exposure) fatigue tested.

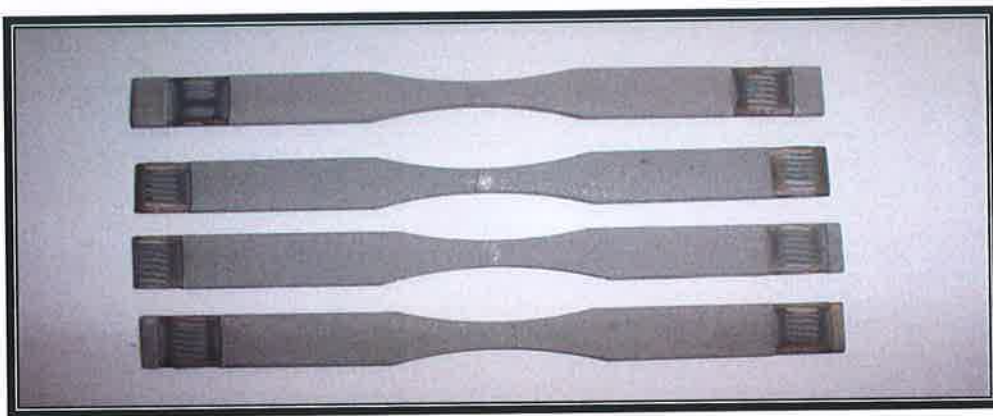


Figure B80: Stainless steel specimens in as received condition (no exposure) fatigue tested.

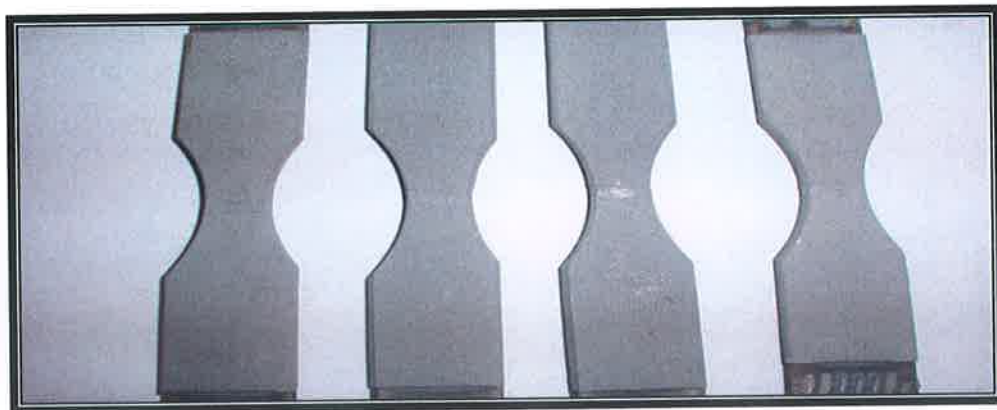


Figure B81: Stainless steel specimens in as received condition (no exposure) fatigue tested.

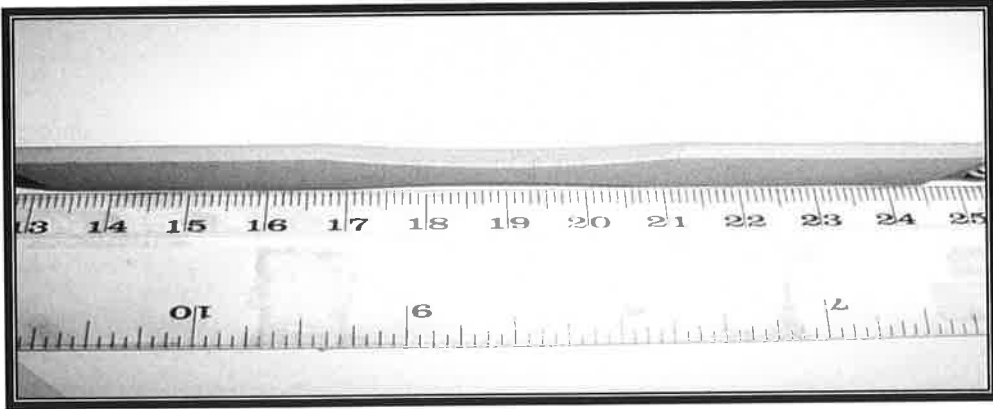


Figure B82: Stainless steel specimen in as received condition (no exposure) fatigue tested.

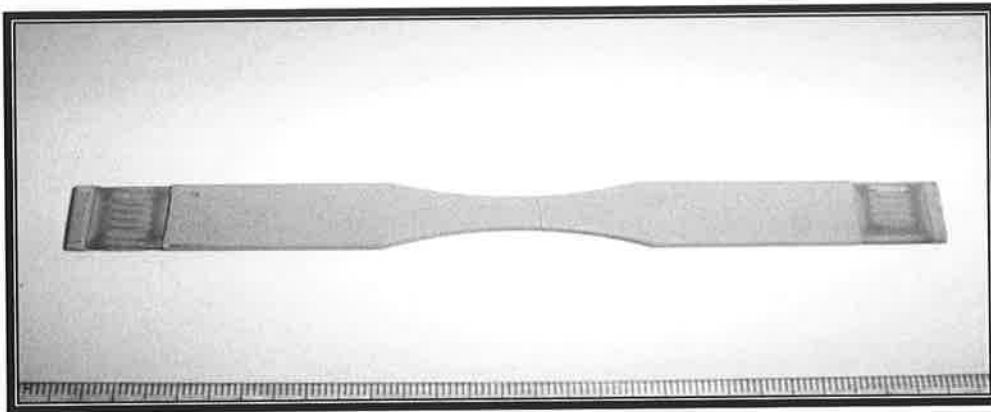


Figure B83: Stainless steel specimen in as received condition (no exposure) fatigue tested.

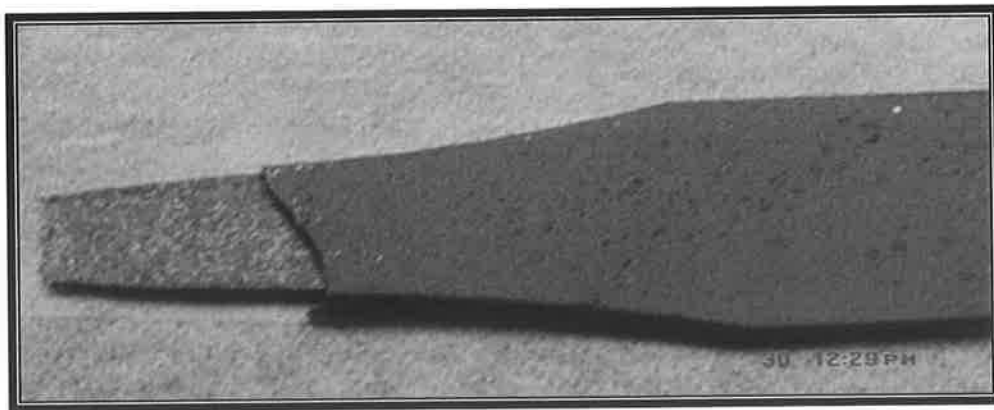


Figure B84: Stainless steel specimen after one (1) week exposure to brine solution tensile tested.

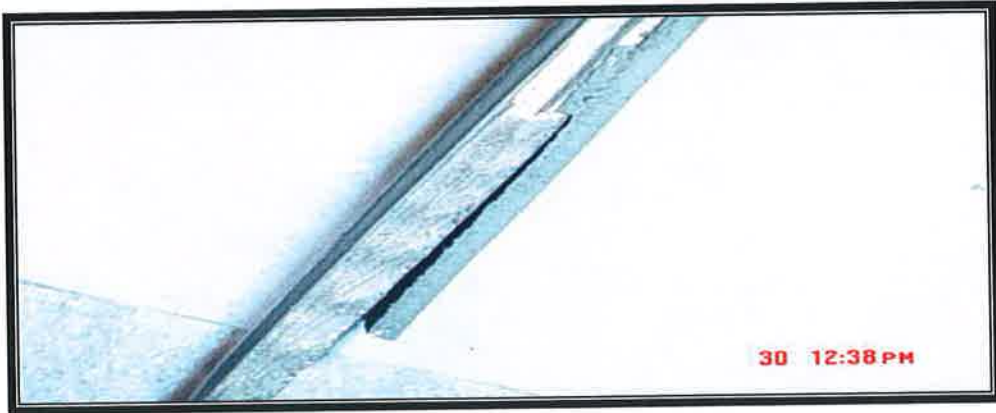


Figure B85: Stainless steel specimen after one (1) week exposure tensile tested.

---

## CONCLUSIONS AND RECOMMENDATIONS

---

### 5.1 CONCLUSION

In this research, the mechanical properties and static corrosion behavior of the High Velocity Oxy-Fuel (HVOF) thermal spray coatings powders of Inconel 625 commercially known as Diamalloy 1005 deposited onto steel surfaces were evaluated. Analytical characterizations were implemented studying coating and welds microstructures. The mechanical response of the coating deposited onto welded surfaces and exposed to static corrosion environment was analyzed by tensile and fatigue tests. The influence of the corrosion exposure periods on the coating mechanical properties performance was examined. The study covered performance comparison of both welded and non welded carbon steel and stainless steels specimens due to the application of Inconel 625 coatings deposited using HVOF process. The influence of weld size on the mechanical properties prior and post corrosion exposure were evaluated.

Investigation of the HVOF coating performance deposited onto welded steel surfaces received very limited attention. Consequently, the current research study becomes a unique in exploring this topic further in details. Deposition of metal coatings onto metallurgically affected surfaces is a very common phenomenon in industrial components requiring a careful study to provide improved understanding how these coatings behave onto welded surfaces. The response of the deposited coating in corrosive environments and subjected to tensile and fatigue external loadings was found to depend on a variety of factors which influence the coating adherence to the substrate. Tensile bonding strength of the coatings was comprehensively evaluated by performing repeated tensile tests examining influence of static corrosion exposure and weld size.

The specific conclusions derived from the investigation are listed as follows:

- Coating microstructures comprising well stacked partially deformed particles was found to exhibit improved corrosion resistance.
- Improper substrate surface preparation reduced coating adhesion.
- Iron-oxide presence in the coatings reduced the bonding strength.
- Surface roughness was found to directly influence coating mechanical interlocking with surface asperities.
- The coating porosity was observed to be in the range of 1.5% to 4.5% influencing corrosion rate.
- Tensile tests are terminated if either the coating or the substrate material fails.
- Un-melted powder particles impacting the surface create residual stresses sites that could lead to early coating cracking.
- Fatigue induced stresses do not have undue influence on the coating microstructure.
- The tensile strengths of coated surfaces and welded-coated surfaces were different.
- The corrosion resistance of the welded-coated specimens showed improvement compared to the non-welded-coated specimen.
- Weld presence enhances coating-substrate adhesion and bonding.
- Coatings showed excellent coating adhesion onto the plain and welded steel surfaces.
- The application of sealants material around the coating-substrate interface may significantly minimize corrosion attack of the coatings.
- Stainless steel coated specimens demonstrated excellent fatigue life resistance as opposed to coated carbon steel specimens.

## 5.2 Contributions

The specific contributions achieved from the current research work include the following:

- The effect of the weld size and weld size related heat affected zone on the tensile properties of the specimens is more pronounced for carbon steel specimens. For coated non-welded carbon steel specimens, the plastic stress level is affected and influenced more to longer exposure than shorter period or no exposure to static corrosion. The coated welded carbon steel specimens are influenced more by larger weld sizes specimens for 3 weeks exposure to static corrosion.
- The weld size and the related heat affected zone influence the plastic behavior of the specimens. Improved corrosion resistance was observed for the coated welded stainless steel specimens. The presence of HAZ enhanced corrosion resistance.
- Corrosion exposure increased duration reduces coating resistance to fatigue. Presence of weld beneath coating decreases the coating fatigue life. Stainless steel coated specimens demonstrated excellent fatigue life resistance as opposed to coated carbon steel specimens.
- High velocity impacting of splats onto specimens enhanced the hardness of the coating surface. This, in turn, improved fatigue properties at the interface. Progressive oxidation of the metal surface degrades coating adhesion.

### 5.3 RECOMMENDATIONS FOR FUTURE WORK

The results generated and presented in this research were significant. However, recommendations for future work are as follows:

- Surface preparation methods to be further developed to provide improved coating adherence to surface.
- The coating process should be carried in an inert atmosphere and the process parameters should be optimized to minimize oxidation of Cr and Nb during the coating process.
- Work could extend to evaluating other coating material adherence to welded and heat affected zones. The adherence of deposited coatings on heat treated surfaces may result in extending the working life of degraded components.
- Modeling different issues and cases related to the HVOF deposited coatings, would provide a consistent approach and enhanced understanding the HVOF coatings. Modeling and investigation might include, the prediction of the working life of HVOF coatings under fatigue cycle loadings, the failure of HVOF coating under tensile loading, adherence uniformity of the coating onto steel surfaces, adherence of the HVOF coatings to welded zones and heat affected areas, adherence and mechanical properties prediction of HVOF coatings deposited onto heat treated surfaces, and finally modeling the spraying process as it impacts both mechanical properties and coat integrity.
- One promising method to improve HVOF deposited coating performance for alloy 625 may be by applying laser treatment to the coating eliminating any coating porosity and resulting in a metallurgical bond. The high heat input from the laser operation may however produce a heat affected zone (HAZ) on the base-metal. This is similar to that experienced with any welded process. The laser process has more variables to model a physical situation. This includes preheat, inter-pass temperature, and the expansion rates of both the base metal and coating.

---

## PUBLICATIONS RESULTING FROM THE PRESENT THESIS

---

1. Boudi, A. A; Hashmi, M. S. J; Yilbas, B. S., "HVOF Coating of Inconel 625 onto Stainless And Carbon Steel Surfaces: Corrosion And Bond Testing", J. Materials Processing Technology, Vol 155/156, pp. 2051-2055, 2004.
2. Boudi, A. A; Hashmi, M. S. J; Yilbas, B. S., "Tensile Properties of HVOF Sprayed Inconel 625 Coating Subjected Aqueous Corrosion Environment", J. Industrial Lubrication and Tribology, accepted for publication to appear in 2006.
3. Boudi, A. A; Hashmi, M. S. J; Yilbas, B. S., "Fatigue Testing of Inconel-625 coatings on Carbon and Stainless Steel after 1 and 3 weeks of exposure to aqueous electrolytic solution", J. Industrial Lubrication and Tribology, in review, 2005.
4. Boudi, A. A; Hashmi, M. S. J; Yilbas, B. S., "ESEM Evaluation of Inconel-625 Thermal Spray Coating (HVOF) onto Stainless Steel and Carbon Steel Post Brine Exposure after Tensile Tests", J. Materials Processing Technology, accepted for publication, 2005.

---

## REFERENCES

---

- [1] C.C Brendt and W.J Lenling, "Handbook of Thermal Spray Technology", ASM International, 1<sup>st</sup> edition, September 2004.
- [2] F.J. Hermanek, "Thermal Spray Terminology and Company Origins", ASM International, 1<sup>st</sup> Edition, January 2001.
- [3] The Welding Institute (TWI), "Thermal spraying processes - a guide to best practice-Section 1", UK, <http://www.twi.co.uk>, December 1<sup>st</sup>, 2006.
- [4] International Thermal Spray Association (ITSA), <http://www.thermalspray.org>, November 1<sup>st</sup>, 2006.
- [5] D.J. Wulpi, "Understanding How Components Fail", ASM International, 2<sup>nd</sup> Edition, November 1999.
- [6] A.J. Sturgeon, "High velocity oxy-fuel spraying", Transactions of the Institute of Metal Finishing, v 72, n pt 4, Nov, 1994, pp 139-140.
- [7] O. Brandt "The influence of HVOF parameters on microstructure and wear resistance of typical WC-Coatings", 17th international SAMPE Europe Conference: Success of Materials by Combination, Basel, CH, 1996. pp 391-401.
- [8] S. Shrestha.; T. Hodgkiess, A. Neville, "Erosion-corrosion behavior of high-velocity oxy-fuel Ni-Cr-Mo-Si-B coatings under high-velocity seawater jet impingement", Wear, v 259, 2005, pp 208-218.
- [9] Sulzer Metco, "<http://www.sulzermetco.com/eprise/Sulzermetco/Sites>", Switzerland. November 2nd, 2006.

- [10] P. McIntyre, Proceedings of the Marine Corrosion Club Meeting, Aberdeen, April 1999.
- [11] C. J. Li; Y.Y. Wang; T. Wu; G.C. Ji; A. Ohmori, "Effect of types of ceramic materials in aggregated powder on the adhesive strength of high velocity oxy-fuel sprayed cermet coatings", Surface and Coatings Technology, v 145, n 1-3, Aug 1, 2001, pp 113-120.
- [12] Materials Australia, Vol. 32, no. 6, pp 14, November/December 2000.
- [13] S.V. Joshi and R. Sivakumar., "Particle behavior during high velocity oxy-fuel spraying", Surface and Coatings Technology, v 50, 1991, pp 67-74.
- [14] O.C. Brandt, "Mechanical properties of HVOF coatings", Journal of Thermal Spray Technology, v 4, n 2, Jun, 1995, pp 147-152.
- [15] B. D. Sartwell, P. M. Natishan, I. L. Singer, Naval Research Laboratory, Washington, DC; K. O. Legg, Rowan Catalyst, Inc., Libertyville, IL; J. D. Schell, GE Aircraft Engines, Cincinnati, OH; J. P. Sauer, Metcut Research Inc., Cincinnati, OH. "Replacement of Chromium Electroplating Using HVOF Thermal Spray Coatings": <http://www.hcat.org/documents/AESF%20Plating%20Forum%20Mar1998.pdf>. January 1<sup>st</sup>, 2004.
- [16] J. Kawakita; S. Kuroda; T. Fukushima; T. Kodama, "Development of dense corrosion resistant coatings by an improved HVOF spraying process", Science and Technology of Advanced Materials, v 4, n 4, Jul 1, 2003, pp 281-289.
- [17] S. Sampath; X. Y. Jiang; J. Matejicek; L. Prchlik; A. Kulkarni; A. Vaidya, "Role of thermal spray processing method on the microstructure, residual stress and properties of coatings: An integrated study of Ni-5 wt. % Al bond coats", Materials Science and Engineering A, v 364, n 1-2, Jan 15, 2004, pp 216-231.

- [18] P. E. Arvidsson; "Plasma and HVOF sprayed coatings of alloy 625 and 718", Proceedings of the National Thermal Spray Conference, Thermal Spray Coatings: Properties, Processes and Applications, 1992, pp 295.
- [19] B. D. Sartwell, Naval Research Laboratory, Code 6170, Washington, DC, K. Legg, Rowan Catalyst, Inc., Libertyville, IL, B. Bodger, Sulzer-Metco (US) Inc., Westbury, NY, " HVOF Thermal Spray Coatings as an Alternative To Hard Chrome Plating on Military and Commercial Aircraft".
- [20] D.J. Varacalle, Jr.; M. G. Ortiz; A. J. Rotollco; J. Nerz, J.; T. J. Steeper; W. L. Riggs II., "HVOF combustion spraying of nickel-aluminum powder", American Society of Mechanical Engineers, Heat Transfer Division, (Publication) HTD, v 196, Transport Phenomena in Materials Processing and Manufacturing, 1992, pp 119-123.
- [21] C. J. Li; Y. Y. Wang; G. J. Yang; A. Ohmori; K. A. Khor; "Effect of solid carbide particle size on deposition behavior, microstructure and wear performance of HVOF cermet coatings", Materials Science & Technology, Sep 2004, Vol. 20 Issue 9, pp1087-1096.
- [22] H. Du; W. Hua; J. Liu; J. Gong; S. Chao; W. Lishi, " Influence of process variables on the qualities of detonation gun sprayed WC-Co coatings", Materials Science & Engineering: A, Nov2005, Vol. 408 Issue 1/2, pp 202-210.
- [23] S. K. Chaudhury; A.K Singh; C.S. Sivaramakrishnan; S.C. Panigrahi, "Effect of processing parameters on physical properties of spray formed and stir cast Al-2Mg-TiO<sub>2</sub> composites", Materials Science & Engineering: A, Feb2005, Vol. 393 Issue 1/2, pp196-203.
- [24] S. Shrestha and A. Sturgeon, Cambridge/ UK, T. Hodgkiess, Glasgow/ UK, A. Neville, Edinburgh/ UK.; "The corrosion behavior of high velocity oxy-fuel (HVOF) sprayed Ni-Cr-Si-B coatings", Paper 95 presented at ITSC 2002 International Thermal Spray Conference, 4-6 March 2002, Essen, Germany.

- [25] ASM Metals Reference Book, ASM International, 3<sup>rd</sup> Edition, August 1999.
- [26] H. Li; K. A. Khor; P. Cheang, "Properties of heat-treated calcium phosphate coatings deposited by high-velocity oxy-fuel (HVOF) spray", *Biomaterials*, v 23, n 10, 2002, p 2105-2112.
- [27] B. H. Kim, D. S. Suhr; "Characteristics of spray-dried WC-17 mass%Co composite powder. Part 1: Effect of heating", *Materials Transactions*, v 42, n 3, 2001, p 491-495.
- [28] B. H. Kim and D. S. Suhr, "Characteristics of HVOF sprayed Cr<sub>3</sub>C<sub>2</sub> (20 mass % NiCr) coatings Part 2: Effect of heat treatment of the coatings", *Materials Transactions*, Vol.42 (5), 2001, 870-875.
- [29] C. H. Lee and K. O. Min, "Effects of heat treatment on the microstructure and properties of HVOF-sprayed Ni-Cr-W-Mo-B alloy coatings", *Surface and Coatings Technology*, v 132, n 1, Oct, 2000, p 49-57.
- [30] M. Rodriguez; M. Staia; L. Gil; F. Arenas; A. Scagni, "Effect of heat treatment on properties of nickel hard surface alloy deposited by HVOF", *Surface Engineering*, v 16, n 5, 2000, p 415-420.
- [31] D. A. Stewart; P. H. Shipway; D. G. McCartney, "Influence of heat treatment on the abrasive wear behavior of HVOF sprayed WC-Co coatings", *Surface & Coatings Technology*, v 105, n 1-2, Jun 5, 1998, p 13-24.
- [32] S. Shrestha; A. Neville; T. Hodgkiess, T., "The effect of post-treatment of a high-velocity oxy-fuel Ni-Cr-Mo-Si-B coating Part I: Microstructure/corrosion behavior relationships", *Journal of Thermal Spray Technology*, v 10, n 3, September, 2001, p 470-479.
- [33] S. Shrestha; T. Hodgkiess; A. Neville, "The effect of post-treatment of a high-velocity oxy-fuel Ni-Cr-Mo-Si-B coating part 2: Erosion-corrosion

- behavior", *Journal of Thermal Spray Technology*, v 10, n 4, December, 2001, p 656-665.
- [34] Y. Itoh; M. Saitoh; M. Tamura, "Characteristics of MCrAlY Coatings Sprayed by High Velocity Oxygen-Fuel Spraying System", *Journal of Engineering for gas turbines and Power*, v 122, 2000, p 43-49.
- [35] L. Gil; M. A. Prato; M. H. Staia, "Effect of post-heat treatment on the corrosion resistance of NiWCrBSi HVOF coatings in chloride solution", *Journal of Thermal Spray Technology*, v 11, n 1, March, 2002, pp 95-99.
- [36] S. K. ASI; M. H. Sohi; K. Hokamoto; M. Uemura, "Effect of heat treatment on wear behavior of HVOF thermally sprayed WC-Co coatings", *Wear*, v 260, 2006, pp 1203-1208.
- [37] E. S. Puchi-Cabrera; M. H. Staia; J. Lesage; D. Chicot; J. G. La Barbera; E. A. Ochoa-Perez; "Fatigue performance of a SAE 1045 steel coated with a Colmonoy 88 alloy deposited by HVOF thermal spraying", *Surface Coatings & Technology*, v 201, June 2006, pp 2038-2045.
- [38] H. Y. Al-Fadhli; J. Stokes; M.S.J. Hashmi; B. S. Yilbas, "HVOF coating of welded surfaces: Fatigue and corrosion behavior of stainless steel coated with Inconel-625 alloy", *Surface Coatings & Technology*, v 200, 2006, pp 4904-4908.
- [39] O. C. Brandt, "Mechanical properties of HVOF coatings", *Journal of Thermal Spray Technology*, v 4, n 2, Jun, 1995, pp 147-152.
- [40] R.C. Souza; M. P. Nascimento; H. J. C. Voorwald; W. L. Pigatin, "The effect of WC-17Co thermal spray coating by HVOF and hard chromium electroplating on the fatigue life and abrasive wear resistance of AISI 4340 high strength steel", *Corrosion Reviews*, v 21, n 1, 2003, pp 75-96.
- [41] K. Padilla; A. Velasquez; J. A. Berrios; E. S. Puchi Cabrera, "Fatigue behavior of a 4140 steel coated with a NiMoAl deposit applied by HVOF

- thermal spray", *Surface and Coatings Technology*, v 150, n 2, Feb 15, 2002, pp 151-162.
- [42] R. T. R. McGrann; D. J. Greving; J. R. Shadley; E. F. Rybicki; B. E. Bodger; D. A. Somerville; "Effect of residual stress in HVOF tungsten carbide coatings on the fatigue life in bending of thermal spray coated aluminum", *Journal of Thermal Spray Technology*, v 7, n 4, Dec, 1998, pp 546-552.
- [43] M. P. Nascimento; R. C. Souza; W. L. Pigatin; H. J. C. Voorwald; "Effect of surface treatment on the fatigue strength of AISI 4340 aeronautical steel", *International Journal of Fatigue*, v 23, 2001, pp 607-618.
- [44] H. J. C. Voorwald; R. C. Souza; W. L. Pigatin; M. O. H. Cioffi; "Evaluation of WC-17Co and WC-10Co-4Cr thermal spray coatings by HVOF on the fatigue and corrosion strength of AISI 4340 steel", *Surface and Coatings Technology*, v 190, 2005, pp 155-164.
- [45] R. Ahmed and M. Hadfield, "Mechanisms of fatigue failure in thermal spray coatings", *Journal of Thermal Spray Technology*, v 11, n 3, September, 2002, pp 333-349.
- [46] R. Ahmed, R.; "Contact fatigue failure modes of HVOF coatings", *Wear*, vol 253, 2002, 473-487.
- [47] Stewart, S.; Ahmed, R., "Contact fatigue failure modes in hot isostatically pressed WC-12%Co coatings", *Surface and Coatings Technology*, v 172, n 2-3, Jul 29, 2003, pp 204-216.
- [48] A. Tipton, "The effect of HVOF thermal spray on the elevated temperature high cycle fatigue behavior of a martensitic stainless steel", Dresser-Rand, Wellsville, N.Y., USA.
- [49] A. J. Sturgeon, "The Corrosion Behavior of HVOF Sprayed Stainless Steel and Nickel Alloy Coatings in Artificial Seawater", the Welding Institute, Cambridge, CBI 6AL, UK.

- [50] A. H. Dent; A. J. Horlock; D. G. McCartney; S. J. Harris, "The corrosion behavior and microstructure of high-velocity oxy-fuel sprayed nickel-base amorphous/nanocrystalline coatings", *Journal of Thermal Spray Technology*, v 8, n 3, Sep, 1999, pp 399-404.
- [51] F. Tang; L. Ajdelsztajn; J. M. Schoenung, "Characterization of oxide scales formed on HVOF NiCrAlY coatings with various oxygen contents introduced during thermal spraying", *Scripta Materialia*, v 51, n 1, July, 2004, pp 25-29.
- [52] J. M. Guilemany; J. Fernandez; J. Delgado; A. V. Benedetti; F. Climent, "Effects of thickness coating on the electrochemical behavior of thermal spray Cr<sub>3</sub>C<sub>2</sub>-NiCr coatings", *Surface and Coatings Technology*, v 153, n 2-3, Apr 15, 2002, pp 107-113.
- [53] L. Zhao; M. Maurer; E. Lugscheider, " Thermal spraying of a Nitrogen alloyed austenitic steel", *Thin Solid Films*, v 424, n 2, Jan 31, 2003, pp 213-218.
- [54] K. M. El-Khatib; M. O. Abou Helal; A. A. El-Moneim; H. Tawfik, "Corrosion stability of SUS316L HVOF sprayed coatings as lightweight bipolar plate materials in PEM fuel cells", *Anti-Corrosion Methods and Materials*, v 51, n 2, 2004, pp 136-142.
- [55] J. Kawakita; T. Fukushima; S. Kuroda; T. Kodama, "Corrosion behavior of HVOF sprayed SUS316L stainless steel in seawater", *Corrosion Science*, v 44, n 11, November, 2002, pp 2561-2581.
- [56] R. Hofman; M. P. W. Vreijling; G. M. Ferrari; J. H. W. de Wit., "Electrochemical methods for characterization of thermal spray corrosion resistant stainless steel coatings", *Materials Science Forum*, v 289-292, n pt 2, 1998, pp 641-654.

- [57] A. Neville and T. Hodgkiess, "Corrosion behavior and microstructure of two thermal spray coatings", *Surface Engineering*, v 12, n 4, 1996, pp 303-312.
- [58] S. Kuroda; J. Kawakita; T. Fukushima; S. Tobe, " Importance of the adhesion of HVOF sprayed coatings for aqueous corrosion resistance", *Materials Transactions*, v 44, n 3, March, 2003, pp 381-388.
- [59] C. Monticelli; A. Frignani; F. Zucchi, "Investigation on the corrosion process of carbon steel coated by HVOF WC/Co cermets in neutral solution", *Corrosion Science*, v 46, n 5, May, 2004, pp 1225-1237.
- [60] W. M. Zhao; Y. Wang; T. Han; K. Y. Wu; J. Xue, "Electrochemical evaluation of corrosion resistance of NiCrBSi coatings deposited by HVOF", *Surface and Coatings Technology*, v 183, n 1, May 1, 2004, pp 118-125.
- [61] N. F. AK; C. Tekmen; I. Ozdemir; H. S. Soykan; E. Celik; "NiCr coatings on stainless steel by HVOF technique", *Surface and Coatings Technology*, v 174-175, September/October, 2003, pp 1070-1073.
- [62] M. A. Uusitalo; P. M. J. Vuoristo, T. A. Mantyla, "High temperature corrosion of coatings and boiler steels below chlorine-containing salt deposits", *Corrosion Science*, v 46, n 6, June, 2004, pp 1311-1331.
- [63] J. A. Hearley; C. Liu; J. A. Little; A. J. Sturgeon, "Corrosion of Ni-Al high velocity oxyfuel (HVOF) thermal spray coating by fly ash and synthetic biomass ash deposits", *British Corrosion Journal*, v 36, n 2, 2001, pp 111-120.
- [64] T. S. Sidhu; S. Prakash; R. D. Agrawal, "Hot corrosion studies of HVOF NiCrBSi and Stellite-6 on a Ni-based superalloy in an actual industrial environment of a coal fired boiler", *Surface & Coatings Technology*, 2006, Vol. 201, pp 1602-1612.

- [65] T. S. Sidhu; R. D. Agrawal, S. Prakash, "Hot corrosion of some superalloys and role of high -velocity oxy-fuel spray coatings-a review", *Surface Coatings & Technology*, v 198, 2005, pp 441-446.
- [66] T. S. Sidhu; S. Prakash; R. D. Agrawal, "Characterization of HVOF sprayed NiCrBSi coatings on Ni-and Fe-based superalloys and evaluation of cyclic oxidation behavior of some Ni-based superalloys in molten salt environment", *Surface Coatings & Technology*, v 515, January 2006, pp 95-105.
- [67] W. M. Zhao; Y. Wang; L. X. Young; L. X. Dong; K. Y. Wu; J. Xue, "Corrosion mechanism of NiCrBSi coatings deposited by HVOF", *Surface Coatings & Technology*, v 190, 2005, pp 293-298.
- [68] D. Chidambaram; C. R. Clayton; M. R. Dorfman; "Evaluation of the electrochemical behavior of HVOF-sprayed alloy coatings-II", *Surface Coatings & Technology*, v 192, 2005, pp 278-283.
- [69] P. Jokinen; K. Korpiola; A. Mahiout, "Duplex coating of electroless nickel and HVOF (high-velocity oxygen fuel) sprayed WC-Co", *Journal of Thermal Spray Technology*, v 9, n 2, Jun, 2000, pp 241-244.
- [70] J. Kawakita; S. Kuroda; T. Fukushima; T. Kodama, "Development of dense corrosion resistant coatings by an improved HVOF spraying process", *Science and Technology of Advanced Materials*, v 4, n 4, Jul 1, 2003, pp 281-289.
- [71] P. H. Suegama; C. S. Fugivara; A. V. Benedetti, J. M. Guilemany; J. Fernandez; J. Delgado; "The influence of gun transverse speed on electrochemical behavior of thermally sprayed Cr<sub>3</sub>C<sub>2</sub>-NiCr coatings in 0.5 M H<sub>2</sub>SO<sub>4</sub> solution", *Electrochimica Acta*, v 49, n 4, Feb 15, 2004, pp 627-634.

- [72] A. Neville; J. M. Perry; T. Hodgkiess; H. P. Chua, "Wrought and High-velocity Oxy Fuel Sprayed Inconel 625—examination of Corrosion Aspects" Proceedings of the Institution of Mechanical Engineers -- Part L -- Journal of Materials: Design & Applications, 2000, Vol. 214 Issue 1, pp 41-48.
- [73] R. C. Tucker Jr.; A. A. Ashary; "Advanced thermal spray coatings for corrosion and wear resistance", TMS Annual Meeting, Advances in Coatings Technologies for Corrosion and Wear Resistant Coatings, 1995, pp 89-98.
- [74] D. Zhang; S. J. Harris; D. G. McCartney, "An investigation of the corrosion behavior of Ni-and Co-based alloys sprayed with gas and liquid fuel HVOF guns", Nottingham, UK.
- [75] K. S. Tan; R. J. K. Wood; J. A. Wharton; K. R. Stokes, "Corrosion Monitoring of High Velocity Oxy-Fuel (HVOF) Sprayed Aluminum Bronze Coatings". Surface Engineering and Tribology Group, School of Engineering Science, University of Southampton, Highfield, Southampton. SO17 1BJ.
- [76] C. Reignier; C. A. Sturgeon; D. Lee; D. D. Wet; "HVOF sprayed WC-Co-Cr as a generic coating type for replacement of hard chrome plating".
- [77] K. S. Tan; J. A. Wharton; R. J. K. Wood, "Solid particle erosion-corrosion behavior of a novel HVOF nickel aluminum bronze coating for marine applications –correlation between mass loss and electrochemical measurements", Wear, v 258, 2005, pp 629-640.
- [78] S. Dallaire, "Hard Arc-Sprayed Coating with Enhanced Erosion and Abrasion Wear Resistance", Proceedings of the International Thermal Spray Conference, 2000, pp 575-582.
- [79] A. Hjornhede; I. Olefjord, "Erosion corrosion of thermally sprayed Fe<sub>12</sub>Cr and Cr<sub>3</sub>C<sub>2</sub>-NiCr coatings", Materials Science Forum, v 369-372, n I, 2001, pp 507-514.

- [80] Y. Wang; W. Chen; L. Wang; "Micro-indentation and erosion properties of thermal sprayed NiAl intermetallic-based alloy coatings", *Wear*, v 254, n 3-4, February, 2003, pp 350-355.
- [81] B. Wang and S. W. Lee, "Erosion-corrosion behavior of HVOF NiAl-Al<sub>2</sub>O<sub>3</sub> intermetallic-ceramic coating", *Wear*, v 239, n 1, Apr, 2000, pp 83-90.
- [82] R. J. K. Wood and A. J. Speyer, "Erosion-corrosion of candidate HVOF aluminum-based marine coatings", *Wear*, v 256, n 5, March, 2004, pp 545-556.
- [83] S. W. Lee and B. Q. Wang, "Erosion phenomena of the low carbon steel and thermal sprayed coatings at low elevated temperature", *American Society of Mechanical Engineers, Fluids Engineering Division (Publication) FED*, v 236, n 1, 1996, pp 767-772.
- [84] B. Q. Wang and A. Verstak, "Elevated temperature erosion of HVOF Cr<sub>3</sub>C<sub>2</sub>/TiC-NiCrMo cermet coating", *Wear*, v 233-235, Dec, 1999, pp 342-351.
- [85] B. Q. Wang and K. Luer, " Erosion-oxidation behavior of HVOF Cr<sub>3</sub>C<sub>2</sub>-NiCr cermet coating", *Wear*, v 174, n 1-2, May, 1994, pp 177-185.
- [86] A. Scrivani; S. Ianelli; A. Rossi; R. Groppetti; F. Casadei; G. Rizzi, "A contribution to the surface analysis and characterization of HVOF coatings for petrochemical application", *Wear*, v 250-251, n PART 1, October, 2001, pp 107-113.
- [87] N. Y. Sari; M. Yilmaz, "Investigation of abrasive + erosive wear behavior of surface hardening methods applied to AISI 1050 steel", *Materials & Design*, v. 27, 2006, pp 470-478.

- [88] A. H. Dent; A. J. Horlock; S. J. Harris; D. G. McCartney; "Enhanced wear resistant nickel-based alloy coatings produced by high velocity oxy-fuel spraying", Transactions of the Institute of Metal Finishing, v 77, n pt 2, Mar, 1999, pp 60-63.
- [89] B. R. Marple and J. Voyer; "Improved wear performance by the incorporation of solid lubricants during thermal spraying", Journal of Thermal Spray Technology, v 10, n 4, December, 2001, pp 626-636.
- [90] Y. Liu; Y. Qiao; J. He; E. J. Lavernia; T. E. Fischer, "Near-nanostructured WC-18 pct Co coatings with low amounts of non-WC carbide phase: Part II. Hardness and resistance to sliding and abrasive wear", Metallurgical and Materials Transactions A: Physical Metallurgy and Materials Science, v 33, n 1, January, 2002, pp 159-164.
- [91] M. Mohanty; R. W. Smith; M. De Bonte; J. P. Celis; E. Lugscheider, "Sliding wear behavior of thermally sprayed 75/25 Cr<sub>3</sub>C<sub>2</sub>/NiCr wear resistant coatings", Wear, v 198, n 1-2, Oct, 1996, pp 251-266.
- [92] M. H. Staia; T. Valente; C. Bartuli; D. B. Lewis; C. P. Constable; A. Roman; J. Lesage; D. Chicot; G. Mesmacque; "Part II: Tribological performance of Cr<sub>3</sub>C<sub>2</sub>-25% NiCr reactive plasma sprayed coatings deposited at different pressures" Surface and Coatings Technology, v 146-147, Sept/Oct, 2001, pp 563-570.
- [93] X. M. Li; Y. Y. Yang; T. M. Shao; Y. S. Jin; G. Barbezat, "Impact wear performances of Cr<sub>3</sub>C<sub>2</sub>-NiCr coatings by plasma and HVOF spraying", Wear, v 202, n 2, Jan, 1997, pp 208-214.
- [94] V. Stoica; R. Ahmed; M. Golshan; S. Tobe, "Sliding Wear Evaluation of Hot Isostatically Pressed Thermal Spray Cermet Coatings", Journal of Thermal Spray Technology, v 13, March 2004, pp93-107.

- [95] D. Toma; W. Brandl; G. Marginean, "Wear and corrosion behavior of thermally sprayed cermet coatings", *Surface and Coatings Technology*, v 138, n 2-3, Apr 16, 2001, pp 149-158.
- [96] C. J. Li and W. Y. Li, "Effect of sprayed powder particle size on the oxidation behavior of MCrAlY materials during high velocity oxygen-fuel deposition" *Surface and Coatings Technology*, v 162, n 1, Jan 1, 2002, pp 31-41.
- [97] H. Edris; D. G. McCartney; A. J. Sturgeon, "Microstructural characterization of high velocity oxy-fuel sprayed coatings of Inconel 625", *Journal of Materials Science*, v 32, n 4, Feb 15, 1997, pp 863-872.
- [98] J. M. Guilemany; J. Nutting; J. R. Miguel; Z. Dong, "Microstructure formation of HVOF sprayed WC-Ni coatings deposited on low alloy steel", *Materials and Manufacturing Processes*, v 12, n 5, Sep, 1997, pp 901-909.
- [99] C. Verdon; A. Karimi; J. L. Martin, "Study of high velocity oxy-fuel thermally sprayed tungsten carbide based coatings. Part 1: microstructures", *Materials Science & Engineering A: Structural Materials: Properties, Microstructure and Processing*, v A246, n 1-2, May 15, 1998, pp 11-24.
- [100] M. L. Lau and E. J. Lavernia; "Microstructural evolution and oxidation behavior of nanocrystalline 316-stainless steel coatings produced by high-velocity oxygen fuel spraying", *Materials Science and Engineering A: Structural Materials: Properties, Microstructure and Processing*, v 272, n 1, Nov, 1999, pp 222-229.
- [101] I. Natali-Sora; F. Mor; G. M. La Vecchia; M. Zocchi; "Structural changes in high velocity oxy-fuel sprayed Cr<sub>3</sub>C<sub>2</sub>/NiCr 75/25 coatings after annealing treatments", *Materials Science Forum*, v 278-281, n pt 2, 1998, pp 520-525.
- [102] A. H. Dent; A. J. Horlock; D. G. McCartney; S. J. Harris; "Microstructural characterization of a Ni-Cr-B-C based alloy coating produced by high

- velocity oxy-fuel thermal spraying", *Surface and Coatings Technology*, v 139, n 2-3, May 15, 2001, pp 244-250
- [103] J. He; M. Ice; E. Lavernia, " Particle melting behavior during high-velocity oxygen fuel thermal spraying", *Journal of Thermal Spray Technology*, v 10, n 1, March, 2001, pp 83-93.
- [104] J. He; M. Ice; S. Dallek; E. J. Lavernia, "Synthesis of nanostructured WC-12 pct Co coating using mechanical milling and high velocity oxygen fuel thermal spraying", *Metallurgical and Materials Transactions A: Physical Metallurgy and Materials Science*, v 31A, n 2, Feb, 2000, pp 541-553.
- [105] A. J. Horlock; D.G. McCartney; P. H. Shipway; J. V. Wood; " Thermally sprayed Ni(Cr)-TiB<sub>2</sub> coatings using powder produced by self-propagating high temperature synthesis: Microstructure and abrasive wear behavior", *Materials Science and Engineering A*, v 336, n 1-2, Oct 25, 2002, pp 88-98.
- [106] S. Tuurna; P. Vuoristo; S. Ahmaniemi; T. Mantyla; J. Takeuchi, " MCrAlY coatings sprayed with HVOF and VPS processes", *VTT Symposium (Valtion Teknillinen Tutkimuskeskus)*, n 211, 2001, pp 163-172.
- [107] R. N. Wright and T. C. Totemeier; "Microstructure and Properties of Iron Aluminide Coatings", *Idaho National Engineering and Environment Laboratory*.
- [108] K. Hamashima; Y. Shinozaki; M. Sasaki, "Thermal spraying of Mo<sub>2</sub>NiB<sub>2</sub>-Ni cermet", *Advances in Powder Metallurgy and Particulate Materials*, v 1, 1997, pp 2-43-2-49.
- [109] J. Ilavsky; J. Pisacka; N. Margadant; S. Siegmann; W. Wagner; P. Fiala; G. Barbezat; P. Chraska; "Microstructure-Wear and Corrosion Relationships for Thermally Sprayed Metallic Deposits", *1<sup>st</sup> International Thermal Spray Conference-Thermal Spray: Surface Engineering via Applied Research*, Quebec, Canada, 2000, pp 449-454.

- [110] R. Schwetzke and H. Kreye, "Microstructure and properties of tungsten carbide coatings sprayed with various high-velocity oxygen fuel spray systems", *Journal of Thermal Spray Technology*, v 8, n 3, Sep, 1999, pp 433-439.
- [111] V. V. Sobolev; J. M. Guilemany; J. A. Calero, "Development of coating structure and adhesion during high velocity oxygen-fuel spraying of WC-Co powder on a copper substrate", *Journal of Thermal Spray Technology*, v 9, n 1, Mar, 2000, pp 100-106.
- [112] D. Zhang; S. J. Harris; D. G. McCartney, " Microstructure formation and corrosion behavior in HVOF-sprayed Inconel 625 coatings", *Materials Science and Engineering A*, v 344, n 1-2, Mar 15, 2003, pp 45-56.
- [113] G. C. Ji; C. J. Li; Y. Y. Wang; Li W. Y. "Microstructural characterization and abrasive wear performance of HVOF sprayed  $\text{Cr}_3\text{C}_2\text{-NiCr}$  coating", *Surface Coatings & Technology*, v 200, 2006, pp 6749-6757.
- [114] Y. Wang and W. Chen, "Microstructures, properties and high-temperature carburization resistances of HVOF thermal sprayed NiAl intermetallic-based alloy coatings", *Surface and Coatings Technology*, v 183, n 1, May 1, 2004, pp 18-28.
- [115] S. Sampath; X. Y. Jiang; J. Matejicek; L. Prchlik; A. Kulkarni; A. Vaidya, "Role of thermal spray processing method on the microstructure, residual stress and properties of coatings: An integrated study of Ni-5 wt. % Al bond coats", *Materials Science and Engineering A*, v 364, n 1-2, Jan 15, 2004, pp 216-231.
- [116] L. Gil; and M. H. Staia, "Microstructure and properties of HVOF thermal sprayed NiWCrBSi coatings", *Surface and Coatings Technology*, v 120-121, Nov, 1999, pp 423-429.

- [117] L. Zhao; J. Zwick; E. Lugscheider, "HVOF spraying of Al<sub>2</sub>O<sub>3</sub>-dispersion-strengthened NiCr powders", *Surface and Coatings Technology*, v 182, n 1, Apr 1, 2004, pp 72-77.
- [118] V. V. Sobolev; J. M. Guilemany; I. R. Miguel; J. A. Calero, "Investigation of the development of coating structure during high velocity oxy-fuel (HVOF) spraying of WC-Ni powder particles", *Surface & Coatings Technology*, v 82, n 1-2, Jul, 1996, pp 114-120.
- [119] H. Li; K. A. Khor; P. Cheang, "Impact formation and microstructure characterization of thermal sprayed hydroxyapatite/titania composite coatings", *Biomaterials*, v 24, n 6, March, 2003, pp 949-957.
- [120] E. Lugscheider; C. Herbst; L. Zhao, "Parameter studies on high-velocity oxy-fuel spraying of MCrAlY coatings", *Surface & Coatings Technology*, v 108-109, n 1-3, Oct 10, 1998, pp 16-23.
- [121] D. J. Varacalle Jr.; M. G. Ortiz; A. J. Rotollo; J. Nerz; T. J. Steeper; W. L. II Riggs; "HVOF combustion spraying of nickel-aluminum powder", *American Society of Mechanical Engineers, Heat Transfer Division, (Publication) HTD*, v 196, *Transport Phenomena in Materials Processing and Manufacturing*, 1992, pp 119-123.
- [122] P. E. Arvidsson, "Plasma and HVOF sprayed coatings of alloy 625 and 718", *Proceedings of the National Thermal Spray Conference, Thermal Spray Coatings: Properties, Processes and Applications*, 1992, pp 295-301.
- [123] Y. Y. Wang; C. J. Li; A. Ohmori, "Examination of factors influencing the bond strength of high velocity oxy-fuel sprayed coatings", *Surface Coatings & Technology*, v 200, 2006, pp 2923-2928.
- [124] ITSC 2000, "Thermal Spray Technology", *Advanced Materials & Processes*, August 2000, pp45-48.

- [125] R. Thorpe; H. Kopech; N. Gagne, "HVOF Thermal Spray Technology", *Advanced Materials & Processes*, April 2000, pp 27-29.
- [126] D. Parker and G. Kutner, "HVOF Thermal Spray Upgrades Power Turbines", *Welding Design & Fabrication*, December 94, pp 20-23.
- [127] A. J. Sturgeon, "High velocity oxy-fuel spraying", *Transactions of the Institute of Metal Finishing*, v 72, n pt 4, Nov, 1994, pp 139-140.
- [128] L. Zhao; and E. Lugscheider, " High velocity oxy-fuel spraying of a NiCoCrAlY and an intermetallic NiAl-TaCr alloy", *Surface and Coatings Technology*, v 149, n 2-3, Jan 15, 2002, pp 231-235.
- [129] P. H. Suegama; C. S. Fugivara; A. V. Benedetti; J. M. Guilemany; J. Fernandez; J. Delgado, "The influence of gun transverse speed on electrochemical behavior of thermally sprayed  $\text{Cr}_3\text{C}_2$ -NiCr coatings in 0.5 M  $\text{H}_2\text{SO}_4$  solution", *Electrochimica Acta*, v 49, n 4, Feb 15, 2004, pp 627-634.
- [130] M. P. Planche; B. Normand; H. Liao; G. Rannou; C. Coddet, "Influence of HVOF spraying parameters on in-flight characteristics of Inconel 718 particles and correlation with the electrochemical behavior of the coating", *Surface and Coatings Technology*, v 157, n 2-3, Aug 22, 2002, pp 247-256.
- [131] B. H. Kim and D. S. Suhr, "Influence of fuel/oxygen ratio in HVOF spraying on the deposition of  $\text{Cr}_3\text{C}_2$  coatings", *Materials Transactions, JIM*, v 41, n 12, Dec, 2000, pp 1657-1662.
- [132] J. A. Hearley; J. A. Little; A. J. Sturgeon, "The effect of spray parameters on the properties of high velocity oxy-fuel NiAl intermetallic coatings", *Surface and Coatings Technology*, v 123, n 2-3, Jan, 2000, pp 210-218.
- [133] V. Higuera; F. J. Belzunce; A. Carriles; S. Poveda, "Influence of the thermal-spray procedure on the properties of a nickel-chromium coating", *Journal of Materials Science*, v 37, n 3, Feb 1, 2002, pp 649-654.

- [134] H. D. Steffens and K. Nassenstein, "Influence of the spray velocity on arc-sprayed coating structures", *Journal of Thermal Spray Technology*, v 8, n 3, Sep, 1999, pp 454-460.
- [135] C. J. Li; K. Sonoya; G. C. Ji; Y. Y. Wang, "Effect of spray conditions on the properties of HVOF Cr<sub>3</sub>C<sub>2</sub>-NiCr coatings", *Welding in the World, Le Soudage Dans Le Monde*, v 41, n 2, Mar-Apr, 1998, pp 77-87.
- [136] O. Brandt, "The influence of HVOF parameters on microstructure and wear resistance of typical WC-Coatings", 17th international SAMPE Europe Conference: Success of Materials by Combination, Basel, CH, 1996. pp 391-401.
- [137] J. Kawakita and S. Kuroda, "Oxidation Restriction of In-flight Particles upon GS-HVOF Spraying by Nitrogen Addition to Combustion Gas", *Materials Transactions*, v 45, n 2, February, 2004, pp 346-349.
- [138] K. Dobler; H. Kreye; R. Schwetzke, "Oxidation of stainless steel in the high velocity oxy-fuel process", *Journal of Thermal Spray Technology*, v 9, n 3, Sep, 2000, pp 407-413.
- [139] T. C. Hanson; C. M. Hackett; G. S. Settles, "Independent control of HVOF particle velocity and temperature", *Journal of Thermal Spray Technology*, v 11, n 1, March, 2002, pp 75-85.
- [140] W. C. Lih; S. H. Yang; C. Y. Su; S. C. Huang; I. C. Hsu; M. S. Leu, "Effects of process parameters on molten particle speed and surface temperature and the properties of HVOF CrC/NiCr coatings", *Surface and Coatings Technology*, v 133-134, Nov, 2000, pp 54-60.
- [141] G. Fillon, "Applying Nickel-Based Alloys by HVOF", *Welding Journal*, October 1995, pp 45-47.

- [142] M. L. Lau; V. V. Gupta; E. J. Lavernia, "Particle behavior of nanocrystalline 316-stainless steel during high velocity oxy-fuel thermal spray", *Nanostructured Materials*, v 12, n 1, 1999, pp 319-322.
- [143] S. V. Joshi and R. Sivakumar, "Particle behavior during high velocity oxy-fuel spraying", *Surface & Coatings Technology*, v 50, n 1, Dec 16, 1991, pp 67-74.
- [144] N. Ait-Messaoudene and A. A. El-Hadj, "Effect of the substrate and of thermophoresis on the acceleration and heating of particles during HVOF spraying", *Surface & Coatings Technology*, v 106, n 2-3, Aug 4, 1998, pp 140-144.
- [145] R. Ghafouri-Azar; J. Mostaghimi; S. Chandra, "Modeling development of residual stresses in thermal spray coatings", *Computational Materials Science*, v 35, 2006, pp 13-26.
- [146] M. Li; D. Shi; P. D. Christofides; "Modeling and control of HVOF thermal spray processing of WC-Co coatings", *Powder Technology*, v. 156m 2005, pp 177-194.
- [147] V. V. Sobolev; J. M. Guilemany; J. A. Calero, "Dynamic processes during in-flight motion of  $\text{Cr}_3\text{C}_2\text{-NiCr}$  powder particles in high velocity oxy-fuel (HVOF) spraying", *Journal of Engineering and Applied Science*, v 4, n 1, Jul, 1995, pp 25-39.
- [148] S. H. Chang and R. L. Moore, "Numerical Simulation of Gs and Particle Flow in a High-Velocity Oxygen-Fuel (HVOF) Torch", *Journal of Thermal Spray Technology*, December 1995, v 4, pp358-366.
- [149] M. Buchmann; R. Gadow; D. Lopez; M. Wenzelburger, "Process Modeling and Simulation of Plasma and HVOF Sprayed Cylinder Liner Coatings", University of Stuttgart, Institute for Manufacturing Technologies of Ceramic Components and Composites IMTCCC, Germany.

- [150] M. L. Lau; V. V. Gupta; E. J. Lavernia, "Mathematical Modeling of Particle Behavior of Nanocrystalline Ni During High Velocity Oxy-Fuel Thermal Spray", *Nanostructured Materials*, 1998, v 10, pp 715-722.
- [151] C. Bartuli; E. Cipri; T. Valente; N. Verdone, "CFD simulation of an HVOF process for the optimization of WC-Co protective coatings", Department of Chemical and Materials engineering, University "La Sapienza", Rome, Italy.
- [152] T. Grosdidier; H. Liao; A. Tidu, "X-rays and TEM characterization of nanocrystalline iron aluminide coatings prepared by HVOF thermal spraying", *Thermal Spray: Surface Engineering via Applied Research* Ed. C.C. Berndt, Pub. ASM International, Materials Park, OH, USA, 2000, 1383+pages, (Montreal) pp 1341-1344.
- [153] B. Wielage; A. Wank; H. Pokhmurska; T. Grund; C. Rupprecht; G. Reisel; E. Friesen; "Development and trends in HVOF spraying technology", *Surface Coatings & Technology*, v 201; 2006, pp 2032-2037.
- [154] D. Zhu; L. Ghosn; R. Miller, "Effect of Layer-Graded Bond Coats on Edge Stress Concentration and Oxidation Behavior of Thermal Barrier Coatings", *Symposium on High Temperature Corrosion and Materials Chemistry*, May 1998, pp 1-21.
- [155] J. C. Tan; L. Looney; M. S. J. Hashmi, "Component repair using HVOF thermal spraying", *Journal of Materials Processing Technology*, v 92-93, Aug, 1999, pp 203-208.
- [156] H. Gassot; T. Junquera; V. Ji; M. Jeandin; V. Guipont; C. Coddet; C. Verdy; L. Grandsire; "Comparative study of mechanical properties and residual stress distributions of copper coatings obtained by different thermal spray processes", *Surface Engineering*, v 17, n 4, 2001, pp 317-322.
- [157] T. C. Totemeier; R. N. Wright; W. D. Swank, "Residual Stresses in High – Velocity Oxy-Fuel Metallic Coatings", *Journal of Metallurgical and Materials Transactions A*, v 35A, June 2004, pp 1807.

- [158] M. Watanabe; K. Yokoyama; S. Kuroda; Y. Gotoh, "Evaluation of Adhesion Strength and Residual Stress of HVOF Sprayed Metallic Coatings", International Thermal Spray Conference & Exposition, May 2006.
- [159] J. Stokes; L. Looney; "Residual stress in HVOF thermally sprayed thick deposits", Surface and Coatings Technology, v 177-178, Jan 30, 2004, pp 18-23.
- [160] T. C. Totemeier and J. K. Wright, "Residual stress determination in thermally sprayed coatings-a comparison of curvature models and X-ray techniques", Surface & Coatings Technology, v 200, 2006, pp-3955-3962.
- [161] M. Wenzelburger; D. Lopez; R. Gadow; "Methods and applications of residual stress analysis on thermally sprayed and layer composites", Surface & Coatings Technology, v 201, 2006, pp-1995-2001.
- [162] C. R. C. Lima; J. Nin; J. M. Guilemany, "Evaluation of residual stresses of thermal barrier coating with HVOF thermally sprayed bond coats using the Modified Layer Removal Method (MLRM)", Surface Coatings & Technology, v 200, 2006, pp 5963-5972.
- [163] Y. Y. Santana; J. G. La Barbera; M. H. Staia; J. Lesage; E. S. Puch-Cabrera; D. Chicot; E. Bemporad, "Measurement of residual stress in thermal spray coatings by the incremental hole drilling method", Surface Coatings & Technology, v 201, June 2006, pp 2092-2098.
- [164] J. Stokes and L. Looney, "Properties of WC-Co Components Produced Using the HVOF Thermal Spray Process", Proceedings of the 1st International Thermal Spray Conference (ITSC 2000), Montreal, Canada, 8-11 May 2000, pp. 263-271.

- [165] J. Stokes and L. Looney, "HVOF System Definition to Maximize the Thickness of Formed Components", *Journal of Surface and Coatings Technology*, Vol. 148(1), (2001), pp. 18-24.
- [166] J. Tuominen; P. Vuoristo; T. Mantyla; J. Latokartano; J. Vihinen; P. H. Andersson; "Microstructure and corrosion behavior of high power diode laser deposited Inconel 626 coatings", *Journal of Laser Applications*, v 15, n 1, February, 2003, pp 55-61.
- [167] P. Serra; J. M. Miguel; J. L. Morenza; J. M. Guilemany, " Structural characterization of laser-treated Cr<sub>3</sub>C<sub>2</sub>-NiCr coatings", *Journal of Materials Research*, v 16, No. 12, December 2001, pp 3416-3422.
- [168] H. Hamatani and Y. Miyazaki; "Optimization of an electron beam remelting of HVOF sprayed alloys and carbides", *Surface and Coatings Technology*, v 154, 2002, pp 176-181.
- [169] R. Potzl, "Laser Remelting of HVOF coatings", *Materials Science Forum*, vols. 163-165, 1994, pp 595-602.
- [170] J. Tuominen; P. Vuoristo; T. Mantyla; M. Kylmalahti; J. Vihinen; P. H. Andersson; " Improving Corrosion Properties of High-Velocity Oxy-Fuel Sprayed Inconel 625 by Using a High-Power Continuous Wave Neodymium-Doped Yttrium Aluminum Garnet Laser", *Journal of Thermal Spray Technology*, v 9, December 2000, pp 513-519.
- [171] E. Lugscheider; J. Wilden; D. Hofmann; Huber, "Influence of laser treatment on the coating properties of mcraly-alloys", *Laser-5*.
- [172] J. Tuominen; P. Vuoristo; T. Mantyla; S. Ahmaniemi; J. Vihinen; P. H. Andersson; " Corrosion Behavior of HVOF-Sprayed and Nd-YAG Laser-Remelted High-Chromium, Nickel-Chromium Coatings", *Journal of Thermal Spray Technology*, v 11, June 2002, pp 233-243.

- [173] A. F. M. Arif and B. S. Yilbas, "Three-point bend testing of HVOF Inconel 625 coating: FEM simulation and experimental investigation", *Surface Coatings & Technology*, v 201, June 2006, pp 1873-1879.
- [174] T. C. Totemeier; R. N. Wright; W. D. Swank, "Mechanical and physical properties of high-velocity oxy-fuel-sprayed iron aluminide coatings", *Metallurgical and Materials Transactions A: Physical Metallurgy and Materials Science*, v 34 A, n 10, October, 2003, pp 2223-2231.
- [175] J. P. Banks; S. Osgerby; S. R. J. Saunders, "Test methods for evaluating the mechanical properties of coatings". *Proceedings of the Sixth International Conference in the Series "Engineering the Surface"*, 23-25, September 1997, pp 225-232. Edinburgh Conference Center. Edinburgh, UK.
- [176] T. Sundararajan; S. Kuroda; F. Abe; S. Sodeoka, "Effect of thermal cycling on the adhesive strength of Ni-Cr coatings", *Surface Coatings & Technology*, v 194, 2005, pp 290-299.
- [177] Y. Y. Wang; C. J. Li; A. Ohmori, "Influence of substrate roughness on the bonding mechanism of high velocity oxy-fuel sprayed coatings", *Thin Solid Films*, v 485, 2005, pp 141-147.
- [178] R. S. Lima and B. R. Marple "Enhanced ductility in thermally sprayed titania coating synthesized using a nanostructured feedstock", *Materials Science & Engineering A*, v 395, (2005), 269-280.
- [179] E. Celik; O. Culha; B. Uyulgan; N. F. Azem; O. I. Ak; A. Turk, "Assessment of microstructural and mechanical properties of HVOF sprayed WC-based cermet coatings for a roller cylinder", *Surface Coatings & Technology*, v 200, 2006, pp 4320-4328.
- [180] H. J. Jang; D. H. Park; Y. G. Jung; J. C. Jang; S. C. Choi; U. Paik, "Mechanical characterization and thermal behavior of HVOF-sprayed bond coat in thermal barrier coating (TBCs)", *Surface Coatings & Technology*, v 200, 2006, pp 4355-4362.

- [181] J. Y. Kwon; J. H. Lee; J. H. Kim; Y. G. Jung; U. Paik; K. S. Lee "Effect of thermal fatigue on mechanical characteristics and contact damage of Zirconia-based thermal barrier coatings with HVOF-sprayed bond coat", *Materials Science and Engineering A* v. 429, May 2006, pp 173-180.
- [182] Sidhu, T. S.; Prakash, S.; Agrawal, R.D.; "Studies of the metallurgical and mechanical properties of high velocity oxy-fuel sprayed satellite-6 coatings on Ni-and Fe-based superalloys", *Surface Coatings & Technology*, v 201, January 2006, pp 273-281.
- [183] C. J. Li; Y. Y. Wang; T. Wu; G. C. Ji; A. Ohmori, "Effect of types of ceramic materials in aggregated powder on the adhesive strength of high velocity oxy-fuel sprayed cermet coatings", *Surface and Coatings Technology*, v 145, n 1-3, Aug 1, 2001, pp 113-120.
- [183] T. C. Totemeier; R. N. Wright; W. D. Swank, "Mechanical and physical properties of high-velocity oxy-fuel-sprayed iron aluminide coatings", *Metallurgical and Materials Transactions A: Physical Metallurgy and Materials Science*, v 34 A, n 10, October, 2003, pp 2223-2231.
- [184] F. Otsubo; H. Era; T. Uchida; K. Kishitake, "Properties of Cr<sub>3</sub>C<sub>2</sub>-NiCr cermet coating sprayed by high power plasma and high velocity oxy-fuel processes", *Journal of Thermal Spray Technology*, v 9, n 4, Dec, 2000, pp 499-504.
- [185] H. Y. Al-Fadhli; J. Stokes; M. S. J. Hashmi; B. S. Yilbas, "Post Test Analysis of Inconel-625 (HVOF) Coating Using SEM and EDS after exposure to erosion-Corrosion Test", *M&M 2005*, Hawaii, USA.
- [186] H. Y. Al-Fadhli; B. S. Yilbas; M. S. J. Hashmi, "HVOF-Coating of Metallic Surfaces: Coating Response to Corrosion and Bending", *Proceeding of the International Thermal Spray Conference*, Basel, Switzerland, May 2-4, 2005, pp. 695-699.

- [187] H. Y. Al-Fadhli; J. Stokes; M. S. J. Hashmi; B. S. Yilbas, "The erosion-corrosion behavior of high velocity oxy-fuel (HVOF) thermally sprayed inconel-625 coatings on different metallic surfaces", *Surface & Coatings Technology*, 2006, pp. 5782-5788.
- [188] ASTM C 633-01, "Standard Test Method for Adhesion or Cohesive Strength of Thermal Spray Coatings", American Society of Testing Materials.
- [189] ASTM E 466-96, "Standard Practice for Conducting Force Controlled Constant Amplitude Axial Fatigue Tests of Metallic Materials", American Society of Testing Materials.
- [190] Empire Abrasive Equipment Company, <http://www.empire-airblast.com>, 2101 West Cabot Boulevard, Langhorne, PA 19047 USA.
- [191] Sulzer Metco, "<http://www.sulzermetco.com>", Sulzer Metco (US) Inc., 1101 Prospect Avenue, Westbury, New York 11590-0201, U.S.A.
- [192] Raytek, "<http://www.raytek.com>", Raytek Corporation, 1201 Shaffer Road Santa Cruz, CA 95061-1820 USA.
- [193] Lab-Line Instruments, <http://www.labline.com>, Barnstead International 2555 Kerper Boulevard, Dubuque, Iowa USA 52001-1478.
- [194] Instron Structural Testing System, "<http://www.instron.us>", Instron Corporate Headquarters, 825 University Ave., Norwood, MA 02062-264, USA.
- [195] BUEHLER, "<http://www.buehlerltd.com>", 41 Waukegan Rd. P.O. Box 1 Lake Bluff, IL 60044-1699 • USA.
- [196] Leica Microsystems, "<http://www.leica-microsystems.com>", Leica Microsystems Inc. 2345 Waukegan Road Bannockburn, IL 60015 USA.

- [197] FEI Company, "<http://www.fei.com>", North America NanoPort, 5350 NE Dawson Creek Drive, Hillsboro, Oregon 97124 USA.
- [198] Master Bond, "<http://www.masterbond.com>", 154 Hobart Street Hackensack, NJ 07601 USA.
- [199] ASTM E1920-03, "Standard Guide for Metallographic Preparation of Thermal Sprayed Coatings", American Society of Testing Materials.
- [200] H. Y. Al Fadhli, "Analysis of the effect of bending, fatigue, erosion-corrosion and tensile stresses on HVOF coating of metallic surfaces". Thesis (PhD) -- Dublin City University, 2006.